ACTIVE CONTROL OF A COUPLED PLATE-CYLINDER SYSTEM

by

Eric Toffin

Thesis submitted to the Faculty of

Virginia Polytechnic Institute and State University

in partial fulfillment of the requirements for the degree of

MASTER OF SCIENCE

in

Mechanical Engineering

APPROVED

Dr. C. R. Fuller, Chairman

Dr. R. A. Burdisso

Dr. A.L. Wicks

April 1994

Blacksburg, Virginia

ACTIVE CONTROL OF A COUPLED PLATE-CYLINDER SYSTEM

by

Eric Toffin

Committee Chairman : Chris R. Fuller, Mechanical Engineering

(ABSTRACT)

An analytical expression for the sound pressure radiated into the far-field by a coupled plate-cylinder system is derived. The system is composed of a rigid plate mounted inside a finite length simply-supported cylindrical shell via a fixed number of active-passive mounts. A harmonic point-force disturbance is applied to the plate.

Various active control approaches are applied to minimize the acoustic pressure radiated by the coupled system. The Active Structural Acoustic Control (ASAC) approaches include the control of the acoustic pressure in one or several directions of radiation, the control of the total radiated power, the control of the power radiated in a sector and the control of selected components associated with circumferential cylinder modes. The Active Vibration Control (AVC) approach is the control of the radial vibration at the points of attachment of the mounts on the cylinder.

Numerical calculations show that the radiated pressure can be controlled using active-passive mounts for all these approaches. However, comparisons in terms of control efficiency and control effort show that ASAC yield better results than AVC. Moreover, ASAC enables directional control of sound and AVC does not.

Opposed and parallel active-passive mount configurations are compared. The results show that the first arrangement requires much larger control forces on-resonance, but the two methods show similar performance off-resonance.

Acknowledgments

I would like to thank my advisor Chris for giving me the opportunity to work on this project. I am not only grateful for the degree I obtained and for all the material I learned from this experience, but also for the opportunity to study abroad he offered me and for the freedom he gave me to conduct this research.

Thanks to all the people in the Acoustics Lab who provided me with technical support and useful advice, and who helped me writing and proofing this thesis.

I am very grateful to all the persons who made this period in Blacksburg possible : Mrs Nicole Jaffrin at the University of Compiegne, Dr. J. R. Mahan at Virginia Tech and my parents for their encouragement.

Anne, Anne-Claire, Benoit, thank you for all the fun in the good times and for your support in times that were less good...

Margarita, without your encouragement and your culinary support this work would never have been completed.

Table of contents

List of figures

List of tables

List of symbols

$\dot{}$	derivation with respect to time operator
$\tilde{}$	wavenumber transform operator
T	transpose operator
α	angle between the radial component of the force f on the cylinder and the vertical direction
β	thickness ratio of the cylinder
Δ	control effort
δ	Dirac operator
ε_n	constant, $\varepsilon_0 = 1$, $\varepsilon_{n\neq 0} = 2$
ϕ	angular coordinate in the cylindrical coordinate system
ϕ_0	angular coordinate of the point force f applied to the cylinder
ϕ_a	circumferential coordinate of the point of attachment of the mount number a on the cylinder
Λ	cost function
γ	variable in the wavenumber domain
μ	underdetermined system parameter
ν_c	Poisson's ratio of the cylinder material
ν_p	Poisson's coefficient of the plate
ω	angular frequency of the disturbance
Ω	non-dimensional frequency
Ω_{mn}	non-dimensional resonance frequency of the mode m, n
ψ_{mn}	ϕ dependent part of the modal amplitude of the radial displacement of the cylinder
Π	total power radiated in the half-plane
Π_{sec}	power radiated in a sector of the half-plane
ρ_0	density of the fluid surrounding the system (air)
ρ_c	density of the cylinder material
ρ_p	density of the plate
θ_x	angular coordinate of the plate around the x-axis
θ_y	angular coordinate of the plate around the y-axis

ξ_{mn} z dependent part of the modal amplitude of the radial displacement of the cylinder

a index of the number of active isolators

c_0 speed of sound in the surrounding fluid (air)

c index of the number of control forces

C_a Damping coefficient in the mount number a

C_{mn} modal coefficient of the pressure developed into series

c_p extensional phase speed of the cylinder material

e_a contribution of the force in the passive isolator number a to the radiation in the far-field

E_c Young's modulus of the cylinder material

$\overline{E}_c$ complex Young's modulus (accounts for the structural damping)

E_k kinetic energy in the rigid plate

E_p Young's modulus of the plate

f point force excitation applied to the cylinder

f_a excitation of the mount number a on the cylinder

f^v circumferential component of the force f on the cylinder

f^w radial component of the force f on the cylinder

F_a force in active mount number a

F_c control force

F_d disturbance applied to the rigid plate

F_c^I imaginary part of the control force F_c

F_c^R real part of the control force F_c

F_{mn}^v circumferential modal excitation

F_{mn}^w radial modal excitation

g_c contribution of the control force number c to the radiation in the far-field

$H_n^{(1)}$ Hankel function of first kind

$H_{mn}^{(1)}, H_{mn}^{(2)}$ modal amplitudes of the radial displacement of the cylinder

h_c thickness of the cylinder

J_n Bessel function of first kind

J_x moment of inertia of the plate around the x-axis

J_y moment of inertia of the plate around the y-axis

k_0 acoustic wavenumber

K_a	spring constant of the active isolator number a
$\overline{K}_a$	complex constant : stiffness and damping of the active isolator number a
k_m	longitudinal wave number
L_c	half length of the cylinder
L_x	length of the plate in the x direction
L_y	length of the plate in the y-direction
L_z	length of the plate in the z direction
m	longitudinal mode number
m_p	mass of the plate
M_x	bending moment in the cylinder
M_a^x	moment around the x-axis created by the displacement of the active isolator number a
M_a^y	moment around the y-axis created by the displacement of the active isolator number a
M_d^x	moment around the x-axis created by the disturbance
M_d^y	moment around the y-axis created by the disturbance
n	circumferential mode number
N_a	number of active isolators
N_c	number of control forces
N_x	longitudinal membrane force in the cylinder
$O(\Omega_{mn})$	$O(\Omega_{mn}) = \left(\Omega^2 - {\Omega^1_{mn}}^2\right)\left(\Omega^2 - {\Omega^2_{mn}}^2\right)\left(\Omega^2 - {\Omega^3_{mn}}^2\right)$
p	acoustic pressure
p_0^v	circumferential excitation on the cylinder
p_0^w	radial excitation on the cylinder
R	Radial coordinate in the spherical coordinate system
r_c	mean radius of the cylinder
R_{mn}	r dependent part of the pressure
u	longitudinal (axial) displacement of the cylinder
U_{mn}	longitudinal modal amplitude of the cylinder displacement
v	torsional (circumferential) displacement of the cylinder
V_{mn}	circumferential modal amplitude of the cylinder displacement
w	flexural (radial) cylinder displacement
W_{mn}	radial modal amplitude of the cylinder displacement

x_a coordinate of the point of attachment of the mount number a on the plate along the x-axis

x_c coordinate of the point of application of the control force number c on the plate along the x-axis

x_d coordinate of the point of application of the disturbance on the plate along the x-axis

y_a coordinate of the point of attachment of the mount number a on the plate along the y-axis

y_c coordinate of the point of application of the control force number c on the plate along the y-axis

y_d coordinate of the point of application of the disturbance on the plate along the y-axis

Y_n Bessel function of second kind

z_0 longitudinal coordinate of the point force f applied to the cylinder

z_a longitudinal coordinate of the point of attachment of the mount number a on the cylinder

z_a^c displacement of the point of attachment of the active isolator number a on the cylinder

z_a^p displacement of the point of attachment of the active isolators number a to the plate

z_G^p displacement of the center of mass of the rigid plate

$\{\Gamma\}$ vector of the excitation of the cylinder

$\{A\}$ matrix of the contribution of the forces in the mounts to the pressure in the far-field

$\left[A_{mn}^{(1)}\right]$, $\left[A_{mn}^{(2)}\right]$ mode shape matrices for the mode m,n

$[C]$ matrix of the contribution of the control forces to the pressure in the far-field

$\left[C_w\right]$ matrix of the contribution of the control forces to the displacement of the cylinder

$\{X\}$ matrix of the contribution of the disturbance to the pressure in the far-field

$[D]$ matrix of the contribution of the disturbance to the pressure in the far-field

$\left[D_w\right]$ matrix of the contribution of the disturbance to the displacement of the cylinder

$\{D_G\}$ vector of the displacement of the center of mass of the plate (3×1)

$\{E\}$ vector of the contribution of the control forces to the radiation of the system

$\{F\}$ vector of the excitation of the cylinder

$\{F_a\}$ vector of the forces in the active-isolators $(N_a \times 1)$

$\{\overline{F_c}\}$ set of optimal control forces

$\{F_c\}$ vector of the control forces $(N_c \times 1)$

$\{F_d\}$ vector of the disturbance (3×1)

$\{G\}$ vector of the contribution of the forces in the passive mounts to the radiation of the system

$[H_a]$ transfer matrix between the forces in the active-isolators and the displacement of their extremities attached to the cylinder $(N_a \times N_a)$

$[H_c]$ transfer matrix between the control forces the displacement of the extremities of the active- isolators attached to the cylinder $(N_a \times N_c)$

$[I]$ identity matrix $(N_c \times N_c)$

$[I_w]$ identity matrix

$[M]$ transfer matrix between the forces in the active-isolators and the displacement of their extremities attached to the plate $(N_a \times N_a)$

$[R_a]$ stiffness matrix of the mounts $(3 \times N_a)$

$[R_c]$ matrix of transfer between the displacement of the center of gravity of the plate and the point of application of the control forces on the plate $(3 \times N_c)$

$[R_G]$ dynamic matrix of the plate (3×3)

$[S_{mn}^{(1)}], [S_{mn}^{(2)}]$ characteristic matrices for the mode m, n

$[{}_aT_c]$ transfer matrix between the control forces and the forces in the mounts

$[{}_aT_d]$ transfer matrix between the disturbance and the forces in the mounts

$\{U_{mn}^{(1)}\}, \{U_{mn}^{(2)}\}$ displacement vectors for the mode m, n

$[V]$ matrix of transfer between the displacement of the center of gravity of the plate and the extremities of the passive-isolators attached to the plate $(N_a \times 3)$

$\{w_a\}$ vector of the displacement of the extremity of the active-isolators attached to the cylinder $(N_a \times 1)$

$\{z^c\}$ vector of the displacement of the extremity of the active-isolators attached to the cylinder $(N_a \times 1)$

$\{z^p\}$ vector of the displacement of the extremity of the active-isolators attached to the plate $(N_a \times 1)$

Chapter I

Introduction

Noise radiation from structures is a major concern in many industrial and military applications. In the first case, noise is a nuisance as for example in cars, or aircraft interiors. In the latter, noise radiation from aircraft, ships or submarines can be a crucial issue in terms of detection. Therefore, noise reduction is an important topic. In aeronautics and naval applications, many structures and sub-structures can be modeled as cylindrical shells. Thus the noise radiation of cylinders in the far-field as well as the interior noise of cylinders have been the subject of extensive studies. In a submarine, the vibrations transmitted by auxiliary machines to the surrounding cylindrical shell through the floor contribute very significantly to the noise radiated outside the structure. A rigid plate mounted inside a finite cylindrical shell and coupled to it via a selected number of mounts is a simple model to study the influence of the vibration transmission.

Reduction of the structural noise level can be achieved by different means: a) reducing the input force; b) adding mass, stiffness or damping, or even modifying the structure itself (for example by introducing discontinuities); and c) lowering the radiation efficiency by applying active control. Extensive work has been carried out on the first two methods revealing several drawbacks : a) they add a significant amount of mass to the structure, which is a major concern in many applications such as aircraft; b) they are inefficient at low frequencies; and c) they require that either the structure or the input force be modified by the addition of dampers. Due to above limitations, the active control of sound has been a topic of major interest in the last decade. It has shown very good

practical results when applied to the minimization of radiated noise from structures. It is a good alternative to conventional passive methods, especially at low frequencies.

Active control has successfully been applied to vibration isolation and to structurally radiated noise from cylindrical shells. However, no analytical study has been presented on the control of the sound pressure radiated from a coupled plate-cylinder system. It is noted that Pan and Hansen [1] studied passive control of the power flow in a similar system and showed potential for applying active control techniques. Their study is presented in section 1.4. and some of their results are contrasted to those of this work.

The purpose of this research is to derive an analytical model for the acoustic radiation in the far-field of a coupled plate-cylinder system where the plate is supported in the cylindrical shell by a set of active-passive control mounts. Several control approaches will then be compared to reduce the sound pressure radiated from the cylinder when a disturbance is applied to the plate.

The next section will present an overview of previous work in the fields of active control, vibration and radiation of cylindrical shells, and vibration isolation. Then, the scope of this work will be presented.

1. Previous work

This section first presents an overview of the historical development of Active Noise Control along with a scope of the work done in its various domains. Then, we will focus on the topics related to the work presented in this thesis : Active Structural Acoustic Control, vibration and radiation of cylindrical shells and finally active isolation of vibrations.

1.1. Active Noise Control

The work in the domain of active control has been reviewed by Warnaka [2], [3], Ffowcs-Williams [4] and Chaplin [5]. The active control of sound is based on Young's principle of superposition which states that two waves of same amplitude but 180° out-of-phase will cancel and therefore result in silence. Another formulation is that of Huygens, indicating that the sound produced by a primary source at any point within a closed surface can be reproduced by a set of secondary sources distributed over the surface. Setting these secondary sources 180° out-of-phase with the disturbance (primary source) will therefore produce a "zone of silence" within the surface. Practically, a finite number of secondary sources spread over the surface will produce an attenuation of the sound level without modifying the primary noise source. The main issue of the problem is to set the correct amplitude and phase of the secondary sources so as to produce an attenuation of the sound field.

The active noise control (A.N.C.) movement started in 1936 with a US. patent by Paul Lueg [6], showing the principle for noise cancellation in a one-dimensional duct using a loudspeaker as a secondary source. In 1953, Olson and May [7] published an article about an "electronic sound absorber" that presented noise cancellation of the sound recorded by a microphone close to the secondary source, therefore creating a local zone of quiet. However, these results were not used in practical applications. In 1956, Conover [8], [9] developed a feed-forward control of radiated noise from transformers. The controller achieved local noise control but also amplified the sound field in other regions. It was never used in industrial applications. Then, the practical study of noise control lost its momentum until developments in the areas of electronics and fast

computing facilitated further investigation. The noise cancellation process requires that the secondary and primary sound fields match with a very close precision in order to achieve destructive interference. With new developments in computer technology, in 1968, in Japan, Kido [10] first applied digital techniques to noise control, showing that additional sound sources could reduce transformers noise within a certain angle from the horizontal plane. The work that followed was mostly theoretical, epitomized by that of Jessel and Mangiante[11].

Then, active noise control developed rapidly with industrial and military applications in different fields. The active control techniques enabled performance of tasks that conventional approaches could not achieve, such as low-frequency noise reduction, directional noise control, and control of selected frequency components.

Warnaka [3] sorted the different applications of active control into four categories :

- duct noise
- personal hearing protection
- interior noise or radiated noise within an enclosed space
- noise radiated into 3-dimensional space

The first two categories have successfully achieved practical application because of the relative simplicity of the problems. Below certain frequencies, duct noises deal with one-dimensional field noises which can be modeled as plane waves. In that case, the control problem is far easier than that of three-dimensional sound fields. The personal hearing protection is a problem of local noise control. The error signal (from a miniature microphone) and the control signal are collocated and the secondary source can easily cancel the noise reaching the ear. Recent developments have produced ear protection devices able to filter the speech and the sounds giving information while cancelling the unwanted noises. More research is now directed to the fields of enclosed space or three-

dimensional space noise control. Elliott and Nelson [12], [13] studied the active control of the noise inside cars and aircraft cabins where sound is produced by the engine and has mostly low-frequency components. Using a feed-forward controller, they experimentally achieved significant reduction of the sound pressure level in both cases.

1.2. Active Structural Acoustic Control

Fuller and Jones [14], [15], [16] studied the reduction of the interior noise in an aircraft fuselage both analytically and experimentally. They showed that the active control of the sound field could be achieved by directly applying forces on the structure itself, thereby modifying its response, instead of using acoustic secondary sources. The cylindrical model was excited by a set of external acoustic monopoles and the control applied by means of shakers. The spatially averaged internal noise dropped by 30 dB with control, although the vibrational energy in the cylindrical shell was increased. This method allows control of the modes that contribute the most to the radiation and thus to reduce the noise globally.

Later, Fuller [17] demonstrated that the radiation control from structures in the far-field could be achieved by the same method, now called Active Structural Acoustic Control since it controls the acoustic radiation by applying forces on the structure itself. He showed that high attenuation of the sound pressure radiated in the far-field by a baffled circular clamped plate could be highly reduced by applying point forces on the plate itself. Guigou and Fuller [18] developed an analytical model for a simply-supported beam.

Pan et al [19] developed an analytical model for the control of the far-field sound radiated by a rectangular panel. The model was verified experimentally for minimization of either the local sound pressure or the total radiated power. Results yielded a reduction of

the total radiated power of up to 13 dB with vibration control secondary sources (shakers) and 15 dB with acoustic control sources (horn drives).

Fuller and Burdisso [20] showed that the control could be achieved in the wavenumber domain by evaluating the pressure in the sound field using the wavenumber transform. Thus, minimizing selected wavenumber components associated with a particular angle of radiation provides a means to control the radiation in specific directions of space without the use of an error microphone in the radiation far-field. Clark and Fuller [21] experimentally demonstrated the efficiency of this method by applying it to the Active Structural Acoustic Control of a simply-supported plate with adaptive structures by implementing the cost function in the wavenumber domain. Results showed a reduction in the supersonic range of the wavenumber spectrum after control.

More recently, shakers used to apply the control forces have been replaced by piezoelectric actuators, which have the advantage of being light and compact. Clark and Fuller [21] [22], [23], studied the active control of sound with actuators bonded on the radiating structure. They showed that those actuators provided an effective means of controlling the radiation in the far-field either by global mode attenuation or by modal restructuring. They also showed how polyvinylidene fluoride (PVDF) sensors applied to the structure could, to some extent, replace the use of microphones in the far-field. They compared the performances of microphones and shaped PVDF sensors to provide the error signal to the controller. The use of PVDF sensors yielded a 10 dB reduction of the pressure field. Lefebvre [24] used these actuators for the active control of interior noise in a fuselage. The fuselage was modeled as the cylindrical shell excited by an external loudspeaker. Error sensors were provided by microphones inside the cylinder. Secondary sources consisted of piezoceramic actuators bonded to the surface of the cylinder.

1.3. Vibration and radiation of cylinders :

The vibration of cylinders has been studied extensively and has been reviewed by Leissa [25]. Control of the noise radiated from the vibration of elastic cylinders was studied by Abler and Silcox [26] and Bullmore et al [27]. Radiation control of cylinders in the far-field using piezoelectric actuators was experimentally studied by Clark and Fuller [28] and by Sumali [29]. Clark and Fuller demonstrated that control using polyvinylidene fluoride (PVDF) sensors could achieve significant global reduction of the sound pressure field : 25 dB on-resonance and 15 dB off-resonance. Sumali showed that Active Structural Acoustic Control could reduce the sound pressure level by 29 dB in the reverberant field.

Regarding the enclosed space problem, Lester and Fuller [30] developed a model for the control of sound inside a flexible cylinder (modeling an aircraft interior) excited by external sources. The secondary sources were provided by acoustic monopoles inside the cylinder. The active control of the interior sound pressure yielded a reduction of 20 to 25 dB in some areas of the cylinder cross-section. Silcox et al [31] investigated the use of four secondary sources placed at ninety degrees increments around the cylindrical shell and found that the pressure field could significantly be reduced over a large area of the cross section inside the cylinder. Increasing the number of control sources improved the control efficiency. Bullmore et al [27] investigated alternative secondary source placement and showed that good reduction of the sound field could be achieved even when the secondary sources were not placed close to the primary source, provided that they couple efficiently to the dominant modes of the primary noise field.

The sound transmission into an aircraft fuselage and the influence of a floor laid in the fuselage was studied both analytically by Fuller [32] and experimentally by Fuller and Jones [33]. Using a simplified analytical model, Fuller showed that the floor has little

influence on the transmission of the acoustic energy into the interior at low frequencies. At higher frequencies, however, it altered significantly the interior sound field. Experiments by Fuller and Jones demonstrated that the floor significantly altered the acoustic field inside the fuselage, but also that a reduction of the shell response was not a guarantee of a reduction in the sound level. The floor altered the sound field by modification of the interior acoustic mode shape rather than by structural modification of the lattice floor support.

1.4. Active isolation of vibrations :

When a structure is composed of several parts, vibrations of one part of the structure is transmitted to the others. One example is the problem of rotating machines mounted on supporting structures. Isolation of the vibrations transmitted from the vibrating structure to the receiving structure is generally solved by using passive approach, i.e. by placing damping elements between the two structures. However, passive methods are very inefficient at low frequencies. Lately, active techniques applied to vibration isolation have been investigated.

Von Flotow [34] presented a general overview of active techniques applied to vibration isolation including recent developments. Active control can be implemented in this type of problem by associating a set of secondary forces to the passive isolators. Control forces are usually applied to the structures either in parallel or in series with the passive isolators. Nelson et al. [35] studied both analytically and experimentally the active control of vibration transmission through active mounts, for which a control force was placed either in parallel or in opposition with the passive component of the mount. They obtained a good agreement between the theoretical development and the experiments. A

15 dB reduction of the vibrational energy in the receiving structure was achieved on-resonance. They demonstrated that the opposed configuration required much larger secondary control forces (but yielded smaller displacements of the system) than the parallel configuration on-resonance, but that the two approaches compared well off-resonance. Lefebvre et al [36] studied active isolation in a system composed of two parallel plates separated by active-passive mounts. Error signals were provided by PVDF sensors. The control forces (coil magnet devices) were in parallel with the passive mounts. The control yielded 32 dB reduction in the vibration level on-resonance, but the off-resonance case was difficult to control globally because of the large number of modes contributing to the vibration of the structure. Guigou et al [37] studied active isolation on a system composed of two plates using adaptive structures (PVDF films). The secondary control forces were provided by piezoceramic actuators bonded to the surface of the receiving plate. These actuators were configured in such a way as to control selected modes of vibration in the plate. thus this technique is control by modal reduction. On-resonance, the first three modes were controlled with reduction in the vibration level of the receiving plate up to 18 dB. However, when the plate was excited off-resonance, the control of the vibration was rather inefficient and yielded only a 4 dB reduction.

Pan and Hansen developed an analytical model for the power flow transmitted through multiple elastic mounts from a rigid body to a flexible panel [38]. They demonstrated that passive mounts could not significantly reduce the power flow to the receiving structure at low frequencies, but that the reduction of the power flow increased as the frequency increased. Then, they developed a similar model with two active isolators [39]. They experimentally verified this model and showed that active control forces would drop the power flow to the receiving structure by 3 to 10 dB. They also demonstrated that passive isolators alone increase the power flow to the flexible panel at the resonance

frequency of the rigid body-mount subsystem. More recently, Pan and Hansen presented a model for the power transmission from a rigid body to a flexible cylinder through an intermediate flexible panel and multiple connected isolators [1]. Passive isolators were used in numerical simulations. These simulations showed that softer actuators yielded more reduction of the power flow transmitted to the cylinder but also that the transmitted power was relatively insensitive to the damping factor in the passive mounts. However, at higher frequencies, using passive isolators resulted in an increase of the vibration transmission.

2. Outline

The main purpose of this work is to show that active control of the sound radiated by a coupled plate-cylinder system is feasible by using active-passive mounts between the plate and the cylinder. It aims also to investigate different control approaches and to compare their performances.

In chapter I, an expression is derived for the response the coupled raft-system composed of a plate (modeling a floor) mounted inside a cylindrical shell of finite length by means of a set of active-passive mounts. The displacement of the cylindrical is calculated as a function of the disturbance applied to the coupled plate and of the control forces in the active-passive mounts supporting the plate. Then, the far-field radiation of the cylindrical shell in response to a point force applied to the plate is calculated and expressed in terms of the disturbance and the control forces.

Different control approaches will be discussed at this point. These approaches fall into two categories : Active Vibration Control and Active Structural Acoustic Control. Active

Vibration Control minimizes the displacement at selected locations on the cylindrical shell using the active components (control forces) of the mounts. Active Structural Acoustic Control minimizes an acoustic quantity using the control forces. The acoustic quantity can take many forms such as the pressure at selected point of the sound field, the total acoustic power radiated from the cylinder, or the power radiated in a selected region of the sound field.

In chapter II, numerical calculations are performed to simulate the radiation of the system in the far-field. A first set of results will discuss the influence of the coupling parameters on the radiation of the system. These parameters are the number of active-passive mounts, the location of the mounts on the transmitting structure (plate) as well as on the receiving structure (cylinder), and the location of the disturbance on the plate. A second set of results will present the influence of the characteristics of the three components in the system : the plate, the cylinder and the passive mounts. A third set of simulations will present and discuss the results obtained for the different approaches of active control. These approaches will be compared in terms of the control efficiency as well as the amplitude of the control forces needed to perform the control. Two active-passive mount configurations will be discussed and their performances will be compared.

Chapter II

Analytical Study

This part presents first the analysis of the coupled raft-system under consideration. Then the radiation of the system in the far-field is derived. Finally, different methods of active control are applied to the structure and the performance is compared.

1. System

The system under consideration is shown on Figure 1. It is composed of a rigid plate (the raft) mounted inside an elastic baffled cylinder. The two structures are coupled via a set of active-passive mounts. These active-passive mounts, defined in section 1.3., support the raft inside the cylinder as well as transmit the vibrations from one structure to the other. The rigid plate is excited by a harmonic disturbance F_d. The active-passive mounts transmit the energy to the cylinder. The coupling considered is only structural, through the active-passive mounts. The acoustic coupling between the sound radiated by the plate and the cylindrical shell is assumed negligible when modeling the dynamics of the structure.

This section presents the characteristics of the different components of the coupled raft-cylinder system.

1.1. Rigid plate

The plate is assumed to be rigid. Its specifications are shown in Table 1. It is excited by the disturbance (F_d) and by the forces in the passive-active isolators(F_a, as defined in section 1.3.).

The following assumptions will be made concerning the plate displacement:

- All the forces applied to the cylinder are "vertical", i.e. directed along the z-axis.
- The displacements are small and only along the z-axis; no displacement is considered along the x- and y-axes.
- No rotation is considered around the z-axis.

These assumptions imply that the plate behaves as a three-degree of freedom system, since it has one displacement along the z-axis (z) and two rotations around the x-axis (θ_x) and y-axis (θ_y). This means that the rigid plate will have three resonant frequencies and three modes of vibrations : one translational mode along the z-axis, and two rotational modes around θ_x and θ_y.

The coordinate system for the plate is show in Figure 2. The origin is taken at the center of mass of the plate. The angle θ_x is such that for the half of the plate corresponding to $y>0$, increasing θ_x will increase z, and the angle θ_y such that increasing θ_y will increase z for the half-plate corresponding to $x>0$.

The signs of the moments are such that a positive force which is directed toward the positive z and which increases the angle θ_x will give a positive moment M^x.

1.2. Cylinder

The cylinder under consideration is elastic and therefore its excitation will result in acoustic radiation. Its specifications are given in the Table 2 and its cylindrical coordinate system is shown on the Figure 3 (note that it is different from the coordinate system of the plate). The cylinder is simply-supported at both ends. It is assumed that the cylinder is baffled and radiates only in the upper (positive z) semi-space. The displacements are assumed small compared to the shell thickness. The cylinder is a thin shell which means its thickness to radius ratio (h_c / r_c) is typically less than approximately 0.05 (as defined in Leissa [25]). The cylinder structure is excited by the forces transmitted through the passive-active isolators (passive isolators and control forces).

1.3. Active-passive isolators

Each active mount can be represented by an ideal spring-damper system (passive isolator) combined with a control force (active isolator). One of the ends of the active isolator is attached to the plate and the other to the cylinder. It is assumed that the forces applied by the active-passive mounts to the cylinder lie in a cross-section of the cylinder (within a plane parallel to the x-y-plane of Figure 3) so that they do not result in applying moments on the structure.

The active mounts can be configured in two different ways : the active isolator can be either in parallel or in opposition (as defined in [35]) with the passive isolator. In the first case, each active mount (passive isolator and active isolator) applies two forces of equal amplitude but opposite direction on the plate and on the cylinder respectively. In the case of the opposed configuration, the passive isolator still applies two forces of equal

amplitude but opposite direction on the plate and on the cylinder; whereas the active isolator acts only on the cylinder and not on the plate. The two systems are shown in Figure 4. Except for the section III.3.5. where the two systems performances will be compared , the parallel active mounts will be used for all the simulations.

The amplitudes of the forces in the passive-active isolators depend on the relative displacement between the two structures and on the physical properties of the mounts, i.e. the stiffness of each mount K_a and its damping coefficient C_a.

Let z_a^p be the displacement of the end of the active isolator number a attached to the plate and z_a^c the corresponding displacement on the cylinder. Then the force in this mount is:

$$F_a = (K_a + j\omega C_a)(z_a^p - z_a^c) = \overline{K}_a(z_a^p - z_a^c) \tag{1}$$

where $\overline{K}_a = (K_a + j\omega C_a)$.

The forces applied on the cylinder are, as seen previously, in a direction parallel to the z-axis. In cylindrical coordinates, they are split into two components: a radial component (f^v) and a circumferential component (f^w) as shown on Figure 5. Let α be the angle between the radial component and the vertical line. This angle can be deducted from ϕ which is the angular coordinate of the point of attachment of the active isolator on the cylinder. Once α is obtained, any force f can be decomposed into components along the circumferential and radial coordinate axes :

$$\begin{cases} f^v = f\sin\alpha \\ f^w = f\cos\alpha \end{cases} \tag{2}$$

2. Vibration of the rigid plate (raft)

The previous section has presented the different components of the system and their specifications, as well as the equation describing the behavior of the active-passive mounts. Now, the behavior of the rigid plate and of the elastic cylinder will be studied. This section presents the response of the rigid plate excited by a disturbance, a set of passive mounts and a set of control forces.

The force applied to the plate (F_d) is a harmonic excitation and therefore the analysis of the system will be performed in the frequency domain.

2.1. System with parallel active mounts

Using the energy method, the displacement of any point on the plate can be obtained as a function of the external forces applied to it : the disturbance forces (F_d), the forces in the passive isolators (F_a), and the control forces (F_c).

The kinetic energy is [40], [41]

$$\mathrm{E}_k = \frac{1}{2} m_p (\dot{z}_G^p)^2 + \frac{1}{2} J_x (\dot{\theta}_x)^2 + \frac{1}{2} J_y (\dot{\theta}_y)^2 \tag{3}$$

where z_G^p is the displacement along the z-axis of the center of mass of the plate, θ_x and θ_y are the angular displacements around the x- and y-axes (see Figure 2) and the moments of inertia are given by :

$$J_x = \frac{m_p}{2}(L_y^2 + L_z^2) \text{ and } J_y = \frac{m_p}{2}(L_x^2 + L_z^2) \tag{4}$$

The external forces are :

active isolator number a	$\hat{F}_a = F_a e^{i\omega t} = \overline{K}_a (z_a^p - z_a^c) e^{i\omega t}$
disturbance	$\hat{F}_d = F_d e^{i\omega t}$
control forces	$\hat{F}_c = F_c e^{i\omega t}$

where $\hat{F}_d$ is the disturbance force (magnitude and phase) and F_d is its magnitude. This notation is applied to all the time-dependent quantities.

The external moments :

active isolator number a	$\hat{M}_a^x = \hat{F}_a x_a$, $\hat{M}_a^y = \hat{F}_a y_a$
disturbance	$\hat{M}_d^x = \hat{F}_d x_d$, $\hat{M}_d^y = \hat{F}_d y_d$
control forces	$\hat{M}_c^x = \hat{F}_c x_c$, $\hat{M}_c^y = \hat{F}_c y_c$

Now, the energy method gives :

$$\begin{cases} m_p \ddot{\hat{z}}_G^p = \hat{F}_d - \sum_{a=1}^{N_a} \hat{F}_a - \sum_{c=1}^{N_c} \hat{F}_c \\ J_x \ddot{\hat{\theta}}_x = \hat{F}_d y_d - \sum_{a=1}^{N_a} \hat{F}_a y_a - \sum_{c=1}^{N_c} \hat{F}_c y_c \\ J_y \ddot{\hat{\theta}}_y = \hat{F}_d x_d - \sum_{a=1}^{N_a} \hat{F}_a x_a - \sum_{c=1}^{N_c} \hat{F}_c x_c \end{cases} \tag{5}$$

Substituting the expression for the forces in the passive mounts given by Equation (1),

$$\begin{cases} m_p \ddot{\hat{z}}_G^p = \hat{F}_d - \sum_{a=1}^{N_a} \overline{K}_a \left[\left(\hat{z}_G^p + x_a \sin(\hat{\theta}_y) + y_a \sin(\hat{\theta}_x) \right) - \hat{z}_a^c \right] - \sum_{c=1}^{N_c} \hat{F}_c \\ J_x \ddot{\hat{\theta}}_x = \hat{F}_d \hat{y}_d - \sum_{a=1}^{N_a} \overline{K}_a y_a \left[\left(\hat{z}_G^p + x_a \sin(\hat{\theta}_y) + y_a \sin(\hat{\theta}_x) \right) - \hat{z}_a^c \right] - \sum_{c=1}^{N_c} \hat{F}_c y_c \\ J_y \ddot{\hat{\theta}}_y = \hat{F}_d x_d - \sum_{a=1}^{N_a} \overline{K}_a x_a \left[\left(\hat{z}_G^p + x_a \sin(\hat{\theta}_y) + y_a \sin(\hat{\theta}_x) \right) - \hat{z}_a^c \right] - \sum_{c=1}^{N_c} \hat{F}_c x_c \end{cases} \quad (6)$$

Assuming that the angles θ_x and θ_y are small, $\sin(\theta_x)$ can be approximated by θ_x giving :

$$\begin{cases} m_p \ddot{\hat{z}}_G^p + \sum_{a=1}^{N_a} (\overline{K}_a) \hat{z}_G^p + \sum_{a=1}^{N_a} (\overline{K}_a x_a) \hat{\theta}_y + \sum_{a=1}^{N_a} (\overline{K}_a y_a) \hat{\theta}_x \\ \qquad = \hat{F}_d + \sum_{a=1}^{N_a} (\overline{K}_a \hat{z}_a^c) - \sum_{c=1}^{N_c} \hat{F}_c \\ J_x \ddot{\hat{\theta}}_x + \sum_{a=1}^{N_a} (\overline{K}_a y_a) \hat{z}_G^p + \sum_{a=1}^{N_a} (\overline{K}_a x_a y_a) \hat{\theta}_y + \sum_{a=1}^{N_a} (\overline{K}_a y_a^2) \hat{\theta}_x \\ \qquad = \hat{F}_d y_d + \sum_{a=1}^{N_a} (\overline{K}_a y_a \hat{z}_a^c) - \sum_{c=1}^{N_c} \hat{F}_c y_c \\ J_y \ddot{\hat{\theta}}_y + \sum_{a=1}^{N_a} (\overline{K}_a x_a) \hat{z}_G^p + \sum_{a=1}^{N_a} (\overline{K}_a x_a^2) \hat{\theta}_y + \sum_{a=1}^{N_a} (\overline{K}_a x_a y_a) \hat{\theta}_x \\ \qquad = \hat{F}_d x_d + \sum_{a=1}^{N_a} (\overline{K}_a x_a \hat{z}_a^c) - \sum_{c=1}^{N_c} \hat{F}_c x_c \end{cases} \quad (7)$$

Assuming small displacements, the motion is considered to be harmonic and the system is linear:

$$\hat{z}_G^p = z_G^p e^{i\omega t} \,,\ \hat{\theta}_x = \theta_x e^{i\omega t} \quad (8)$$

therefore the response of the system can be written in the matrix form:

$$\begin{bmatrix} m_p & 0 & 0 \\ 0 & J_x & 0 \\ 0 & 0 & J_y \end{bmatrix} \begin{Bmatrix} \ddot{z}_G^p \\ \ddot{\theta}_x \\ \ddot{\theta}_y \end{Bmatrix} e^{i\omega t} + \begin{bmatrix} \sum_{a=1}^{N_a} \overline{K}_a & \sum_{a=1}^{N_a} \overline{K}_a y_a & \sum_{a=1}^{N_a} \overline{K}_a x_a \\ \sum_{a=1}^{N_a} \overline{K}_a y_a & \sum_{a=1}^{N_a} \overline{K}_a y_a^2 & \sum_{a=1}^{N_a} \overline{K}_a x_a y_a \\ \sum_{a=1}^{N_a} \overline{K}_a x_a & \sum_{a=1}^{N_a} \overline{K}_a x_a y_a & \sum_{a=1}^{N_a} \overline{K}_a x_a^2 \end{bmatrix} \begin{Bmatrix} z_G^p \\ \theta_x \\ \theta_y \end{Bmatrix} e^{i\omega t}$$

$$= \begin{Bmatrix} 1 \\ y_d \\ x_d \end{Bmatrix} F_d e^{i\omega t} + \sum_{a=1}^{N_a} \left(\begin{Bmatrix} \overline{K}_a \\ \overline{K}_a y_a \\ \overline{K}_a x_a \end{Bmatrix} z_a^c e^{i\omega t} \right) - \sum_{c=1}^{N_c} \left(\begin{Bmatrix} 1 \\ y_c \\ x_c \end{Bmatrix} F_c e^{i\omega t} \right) \tag{9}$$

We now define :

$$\begin{Bmatrix} D_G \end{Bmatrix} = \begin{Bmatrix} z_G^p \\ \theta_x \\ \theta_y \end{Bmatrix} \tag{10}$$

where $\{D_G\}$ is the vector of the displacement of the center of mass of the plate.

$$[R_G] = \begin{bmatrix} -\omega^2 m_p + \sum_{a=1}^{N_a} \overline{K}_a & \sum_{a=1}^{N_a} \overline{K}_a y_a & \sum_{a=1}^{N_a} \overline{K}_a x_a \\ \sum_{a=1}^{N_a} \overline{K}_a y_a & -\omega^2 J_x + \sum_{a=1}^{N_a} \overline{K}_a y_a^2 & \sum_{a=1}^{N_a} \overline{K}_a x_a y_a \\ \sum_{a=1}^{N_a} \overline{K}_a x_a & \sum_{a=1}^{N_a} \overline{K}_a x_a y_a & -\omega^2 J_y + \sum_{a=1}^{N_a} \overline{K}_a x_a^2 \end{bmatrix} \tag{11}$$

$[R_G]$ is the dynamic matrix of the plate.

$$[R_a]=\begin{bmatrix} \overline{K}_1 & \overline{K}_2 & \overline{K}_3 & \cdots & \overline{K}_{N_a} \\ \overline{K}_1 y_1 & \overline{K}_2 y_2 & \overline{K}_3 y_3 & \cdots & \overline{K}_{N_a} y_{N_a} \\ K_1 x_1 & \overline{K}_2 x_2 & \overline{K}_3 x_3 & \cdots & \overline{K}_{N_a} x_{N_a} \end{bmatrix}, \quad \{z^c\}=\begin{Bmatrix} z_1^c \\ z_2^c \\ \vdots \\ z_{N_a}^c \end{Bmatrix}, \quad \{F_d\}=\begin{Bmatrix} 1 \\ x_d \\ y_d \end{Bmatrix} F_d \qquad (12)$$

where $\{z^c\}$ is the vector of the cylinder displacement at the points of attachment of the mounts and $[R_a]$ is the stiffness matrix of the mounts.

$$[V]=\begin{bmatrix} 1 & y_1 & x_1 \\ 1 & y_2 & x_2 \\ \vdots & \vdots & \vdots \\ 1 & y_{N_a} & x_{N_a} \end{bmatrix}, \quad \{z^p\}=[V]\{D_G\} \qquad (13)$$

$[V]$ is the transfer matrix between the displacement of the plate at the attachment points of the mounts and the displacement of the center of mass of the plate.

$$[R_c]=\begin{bmatrix} 1 & y_1 & x_1 \\ 1 & y_2 & x_2 \\ \vdots & \vdots & \vdots \\ 1 & y_{N_c} & x_{N_c} \end{bmatrix} \qquad (14)$$

$[R_c]$ is the transfer matrix between the displacement of the plate at the points of application of the control forces and the displacement of the center of mass of the plate.

Now, $e^{i\omega t}$ can be eliminated on both sides of the equation to give:

$$[R_G]\{D_G\}=\{F_d\}+[R_a]\{z^c\}-[R_c]\{F_c\} \qquad (15)$$

which is the displacement of the center of mass of the plate as a function of the disturbance, the displacement of the cylinder and the control forces.

2.2. System with opposed active mounts

The difference with the previous sections is that the control forces do not excite the plate in the case of opposed active mounts as can be seen on Figure 4. The control forces will not be applied on the transmitting structure (plate) but only on the receiving structure (cylinder). The derivation of the displacement of the plate is the same as in section 2.1, but the external forces are the disturbance applied on the plate (F_d) and the forces in the passive isolators (F_a) only.

Equation (15) now becomes

$$[R_G]\{D_G\} = \{F_d\} + [R_a]\{z^c\} \tag{16}$$

3. Vibration of the cylinder

In this section, the free vibration and the resonance frequencies of the cylinder are first presented. Then its response to a point force is derived. Finally, using the principle of superposition, the result is generalized for a multiple-forces excitation, which models the cylinder in the system excited by the forces in the passive mounts and the control forces.

The cylinder under consideration has characteristics given by Table 2 and its coordinate system is shown on the Figure 3. The displacement of the shell is derived in cylindrical coordinates.

Let u, v and w be the longitudinal, circumferential and radial displacements of the cylinder respectively.

We will use the Kennard simplified equations as given in Leissa [25]:

$$\begin{cases} \dfrac{\partial^2 u}{\partial z^2}+\dfrac{1-\nu_c}{2r_c^{\,2}}\dfrac{\partial^2 u}{\partial \phi^2}+\dfrac{1+\nu_c}{2r_c}\dfrac{\partial^2 v}{\partial z\partial \phi}+\dfrac{\nu_c}{r_c}\dfrac{\partial w}{\partial z}-\dfrac{\ddot{u}}{c_p^2}=0 \\ \dfrac{1+\nu_c}{2r_c}\dfrac{\partial^2 u}{\partial z\partial \phi}+\dfrac{1-\nu_c}{2}\dfrac{\partial^2 v}{\partial z^2}+\dfrac{1}{r_c^{\,2}}\dfrac{\partial^2 v}{\partial \phi^2}+\dfrac{1}{r_c^{\,2}}\dfrac{\partial w}{\partial \phi}+\dfrac{3}{2r_c^{\,2}}\beta^2\dfrac{\nu_c}{1-\nu_c}\left(\dfrac{\partial^3 w}{\partial \phi^3}+\dfrac{\partial w}{\partial \phi}\right) \\ \qquad -\dfrac{\ddot{v}}{c_p^2}=\dfrac{p_0^v(1-\nu_c^{\,2})}{E_c h_c} \\ \dfrac{\nu_c}{r_c}\dfrac{\partial u}{\partial z}+\dfrac{1}{r_c^{\,2}}\dfrac{\partial v}{\partial \phi}+\dfrac{w}{r_c^{\,2}}+\beta^2\left(r_c^{\,2}\dfrac{\partial^4 w}{\partial z^4}+2\dfrac{\partial^4 w}{\partial z^2\partial \phi^2}+\dfrac{1}{r_c^{\,2}}\dfrac{\partial^4 w}{\partial \phi^4}\right) \\ +\beta^2\left(\dfrac{4-\nu_c}{2(1-\nu_c)}\dfrac{1}{r_c^{\,2}}\dfrac{\partial^2 w}{\partial \phi^2}+\dfrac{2+\nu_c}{2(1-\nu_c)}\dfrac{1}{r_c^{\,2}}w\right)+\dfrac{\ddot{w}}{c_p^2}=\dfrac{p_0^w(1-\nu_c^{\,2})}{E_c h_c} \end{cases} \tag{17}$$

where $\beta=\sqrt{h_c^{\,2}/\left(12r_c^{\,2}\right)}$, r_c is the mean radius of the shell and h_c is the thickness of the shell. E_c is the Young's modulus, ν_c is the Poisson's ratio and $c_p=\sqrt{E_c/\rho_c\left(1-\nu_c^{\,2}\right)}$ is the extensional phase speed of the cylinder material. The density of the cylinder material is ρ_c.

Equation (17) is based on the following assumptions :

- the transverse shear stress is negligible

- the rotary inertia effects in the shell are ignored

Moreover, the cylinder is a thin shell, which implies that :

- its thickness to radius ratio (h_c / r_c) is smaller than 0.05 (Leissa [25])
- the displacement of the shell is small in comparison with the shell thickness.
- the transverse normal stress acting on planes parallel to the shell middle surface is negligible

The circumferential (p_0^v) and radial (p_0^w) excitation on the cylinder have the dimension of a pressure. They are related to the actual point force excitation f by the following relationship:

$$p = f \frac{\delta(\phi - \phi_0)}{r_c} \delta(z - z_0) \tag{18}$$

where $\delta(z - z_0)$ has the dimension of the inverse of a length, and therefore p has the dimension of a force divided by a surface, i.e. a pressure.

The cylinder considered is of finite length ($2L_c$) and is simply supported at its ends which means that it satisfies the following boundary conditions :

$w = v = 0$ and $\vec{M}_x = \vec{N}_x = \vec{0}$ at $z = -L_c, L_c$

where $\vec{M}_x$ is the bending moment and $\vec{N}_x$ is the longitudinal membrane force. These boundary conditions are also called "shear diagram" in [25].

It can be show that the set of equations :

$$\begin{cases} u(\phi,z)=\sum_{m=1}^{\infty}\sum_{n=0}^{\infty}\{U_{mn}^{(1)}\cos(n\phi)+U_{mn}^{(2)}\sin(n\phi)\}\cos\left[k_m(z+L_c)\right] \\ v(\phi,z)=\sum_{m=1}^{\infty}\sum_{n=0}^{\infty}\{V_{mn}^{(1)}\sin(n\phi)+V_{mn}^{(2)}\cos(n\phi)\}\sin\left[k_m(z+L_c)\right] \\ w(\phi,z)=\sum_{m=1}^{\infty}\sum_{n=0}^{\infty}\{W_{mn}^{(1)}\cos(n\phi)+W_{mn}^{(2)}\sin(n\phi)\}\sin\left[k_m(z+L_c)\right] \end{cases} \quad (19)$$

describing the displacement of the shell satisfies these boundary conditions for the coordinate system shown in Figure 3. The ϕ dependency splits into a sine and a cosine part so as to include contribution from all possible modes. In this section, the superscript $^{(1)}$ indicates the quantities associated with $U_{mn}^{(1)}$, $V_{mn}^{(1)}$ and $W_{mn}^{(1)}$, and the superscript $^{(2)}$ the quantities associated with $U_{mn}^{(2)}$, $V_{mn}^{(2)}$ and $W_{mn}^{(2)}$.

In Equation (19), the longitudinal and circumferential mode numbers are m and n respectively ; $U_{mn}^{(1)}$, $V_{mn}^{(2)}$ and $W_{mn}^{(1)}$ are the modal amplitudes of the cylinder displacement associated with $\cos(n\phi)$ and $U_{mn}^{(2)}$, $V_{mn}^{(1)}$ and $W_{mn}^{(2)}$ are the modal amplitudes of the cylinder displacement associated with $\sin(n\phi)$. The longitudinal wave number is $k_m = m\pi / 2L_c$ with $m = 1..M$ for the simply-supported boundary conditions and the coordinate system chosen (see Figure 3).

Substituting u, v and w as given in Equation (19) in Equation (17) and simplifying, we get the non-homogeneous shell system equation

$$\sum_{m=1}^{\infty}\sum_{n=0}^{\infty}\left([A_{mn}^{(1)}][S_{mn}^{(1)}]\{U_{mn}^{(1)}\}+[A_{mn}^{(2)}][S_{mn}^{(2)}]\{U_{mn}^{(2)}\}\right)=\{\Gamma\} \quad (20)$$

where

$$[A_{mn}^{(1)}]=\begin{bmatrix}\cos(n\phi)\cos\left[k_m(z+L_c)\right] & 0 & 0\\ 0 & \sin(n\phi)\sin\left[k_m(z+L_c)\right] & 0\\ 0 & 0 & \cos(n\phi)\sin\left[k_m(z+L_c)\right]\end{bmatrix} \quad (21)$$

$$[A_{mn}^{(2)}]=\begin{bmatrix}\sin(n\phi)\cos\left[k_m(z+L_c)\right] & 0 & 0\\ 0 & \cos(n\phi)\sin\left[k_m(z+L_c)\right] & 0\\ 0 & 0 & \sin(n\phi)\sin\left[k_m(z+L_c)\right]\end{bmatrix} \quad (22)$$

$$\{\Gamma\}=\begin{Bmatrix}0\\ f_c^{v}\dfrac{(1-\nu^2)r_c}{E_c h_c}\delta(\phi-\phi_0)\delta(z-z_0)\\ f_c^{w}\dfrac{(1-\nu^2)r_c}{E_c h_c}\delta(\phi-\phi_0)\delta(z-z_0)\end{Bmatrix} \quad (23)$$

and

$$\left[S_{mn}^{(1)}\right]=\begin{bmatrix}S_{mn}^{11} & S_{mn}^{12} & S_{mn}^{13}\\ S_{mn}^{21} & S_{mn}^{22} & S_{mn}^{23}\\ S_{mn}^{31} & S_{mn}^{32} & S_{mn}^{33}\end{bmatrix},\quad \left[S_{mn}^{(2)}\right]=\begin{bmatrix}S_{mn}^{11} & -S_{mn}^{12} & S_{mn}^{13}\\ -S_{mn}^{21} & S_{mn}^{22} & -S_{mn}^{23}\\ S_{mn}^{31} & -S_{mn}^{32} & S_{mn}^{33}\end{bmatrix} \quad (24)$$

$$S_{mn}^{11}=-{k_m}^2{r_c}^2-\frac{1}{2}(1-\nu_c)n^2+\Omega^2 \qquad S_{mn}^{12}=\frac{1}{2}(1+\nu_c)nk_m r_c$$

$$S_{mn}^{21}=\frac{1}{2}(1+\nu_c)nk_m r_c \qquad S_{mn}^{22}=-\frac{1}{2}(1-\nu_c){k_m}^2{r_c}^2-n^2+\Omega^2$$

$$S_{mn}^{31}=-\nu_c k_m r \qquad S_{mn}^{32}=n$$

$$
\begin{aligned}
S_{mn}^{13} &= \nu_c k_m r_c \\
S_{mn}^{23} &= -n + \frac{3}{2}\beta^2\left(\frac{\nu_c}{1-\nu_c}\left(n-n^3\right)\right) \\
S_{mn}^{33} &= 1+\beta^2\left(k_m{}^2 r_c{}^2 + n^2\right)^2 - \beta^2\left[\frac{4-\nu_c}{2(1-\nu_c)}n^2 - \frac{2+\nu_c}{2(1-\nu_c)}\right] - \Omega^2
\end{aligned}
\tag{25}
$$

Solving the homogeneous system

$$
\sum_{m=1}^{\infty}\sum_{n=0}^{\infty}\left(\left[A_{mn}^{(1)}\right]\left[S_{mn}^{(1)}\right]\left\{U_{mn}^{(1)}\right\} + \left[A_{mn}^{(2)}\right]\left[S_{mn}^{(2)}\right]\left\{U_{mn}^{(2)}\right\}\right) = 0 \tag{26}
$$

gives the eigenvalues Ω_{mn} which are the non-dimensional natural frequencies of the mode m,n. They are given as a function of the angular frequency ω by: $\Omega = \omega r_c / c_p$. It can be noted that the $\Omega = \omega/(2\pi f_r)$ and the quantity $f_r = c_p/(2\pi r_c)$ is called the ring frequency of the cylinder. At this particular frequency, the wavelength is equal to the circumference of the cylinder.

The system of Equation (20) can be written in the form of a cubic equation in Ω_{mn}^2 and therefore there are three solutions for each mode m,n, which are the natural frequencies for the longitudinal ($\Omega_{mn}^{(1)}$), circumferential ($\Omega_{mn}^{(2)}$) and radial ($\Omega_{mn}^{(3)}$) modes respectively. Tables 3 and 4 gives the natural frequencies of the cylinder under consideration. In this work, and particularly in section III, we will consider that the resonance frequency and the natural frequency are very close since the damping in the structure is low.

Now, we derive the response of the cylinder to a point force.

The point force f lies in a cross-section (x-y plane) of the cylinder, i.e. it has no longitudinal component. It is applied at a point of coordinates (ϕ_0, z_0). It splits into a radial and circumferential components as shown in Equation (2) of section 1.3.

Note that the excitation $\{\Gamma\}$ has the dimension of a length in Equation (23).

We now multiply each side of Equation (20) by $[A_{pq}^{(1)}]$ and integrate with respect to z between $-L_c$ and L_c and ϕ between $-\pi$ and π.

$$\begin{aligned}\int_{-L_c}^{L_c}\int_{-\pi}^{\pi}\left[A_{pq}^{(1)}\right]\sum_{m=1}^{\infty}\sum_{n=0}^{\infty}\left(\left[A_{mn}^{(1)}\right]\left[S_{mn}^{(1)}\right]\left\{U_{mn}^{(1)}\right\}+\left[A_{mn}^{(2)}\right]\left[S_{mn}^{(2)}\right]\left\{U_{mn}^{(2)}\right\}\right)dzd\phi \\ =\int_{-L_c}^{L_c}\int_{-\pi}^{\pi}\left[A_{pq}^{(1)}\right]\{\Gamma\}dzd\phi\end{aligned} \tag{27}$$

The cases $n \neq 0$ and $n = 0$ need here to be separately derived.

- case $n \neq 0$:

We now apply the orthogonality conditions (see Appendix 1) to get the matrix form of the non-homogeneous system equation:

$$\begin{bmatrix}\frac{2\pi L_c}{\varepsilon_n} & 0 & 0\\ 0 & \pi L_c & 0\\ 0 & 0 & \frac{2\pi L_c}{\varepsilon_n}\end{bmatrix}\begin{bmatrix}\ddots & & \iddots\\ & S_{mn}^{(1)} & \\ \iddots & & \ddots\end{bmatrix}\begin{Bmatrix}U_{mn}^{(1)}\\ V_{mn}^{(1)}\\ W_{mn}^{(1)}\end{Bmatrix}=\begin{Bmatrix}0\\ \Gamma_{mn}^{v,(1)}\\ \Gamma_{mn}^{w,(1)}\end{Bmatrix} \tag{28}$$

with

$$\begin{aligned}\Gamma_{mn}^{v,(1)} &= \frac{1}{r_c}\frac{1-\nu_c^{\,2}}{E_c h} f_c^{v}\sin(n\phi_0)\sin\left[k_m(z_0+L_c)\right]\\ \Gamma_{mn}^{w,(1)} &= \frac{1}{r_c}\frac{1-\nu_c^{\,2}}{E_c h} f_c^{w}\cos(n\phi_0)\sin\left[k_m(z_0+L_c)\right]\end{aligned} \tag{29}$$

giving:

$$\begin{bmatrix} \ddots & & \iddots \\ & S_{mn}^{(1)} & \\ \iddots & & \ddots \end{bmatrix} \begin{Bmatrix} U_{mn}^{(1)} \\ V_{mn}^{(1)} \\ W_{mn}^{(1)} \end{Bmatrix} = \begin{Bmatrix} 0 \\ \frac{1}{\pi L_c} \Gamma_{mn}^{v,(1)} \\ \frac{\varepsilon_n}{2\pi L_c} \Gamma_{mn}^{w,(1)} \end{Bmatrix} \tag{30}$$

As will be shown in the next section, the radiation of the cylinder depends only on its radial displacement w [42]. Therefore only W_{mn} needs to be calculated.

Using Cramer's rule:

$$W_{mn}^{(1)} = \frac{\begin{bmatrix} S_{mn}^{11} & S_{mn}^{12} & 0 \\ S_{mn}^{21} & S_{mn}^{22} & \frac{1}{\pi L_c} \Gamma_{mn}^{v,(1)} \\ S_{mn}^{31} & S_{mn}^{32} & \frac{\varepsilon_n}{2\pi L_c} \Gamma_{mn}^{w,(1)} \end{bmatrix}^{(1)}}{\begin{bmatrix} S_{mn}^{11} & S_{mn}^{12} & S_{mn}^{13} \\ S_{mn}^{21} & S_{mn}^{22} & S_{mn}^{23} \\ S_{mn}^{31} & S_{mn}^{32} & S_{mn}^{33} \end{bmatrix}^{(1)}} \tag{31}$$

$$W_{mn}^{(1)} = \frac{\frac{1}{\pi L_c} \Gamma_{mn}^{v} \left[S_{mn}^{31} S_{mn}^{12} - S_{mn}^{11} S_{mn}^{32} \right] + \frac{\varepsilon_n}{2\pi L_c} \Gamma_{mn}^{w} \left[S_{mn}^{11} S_{mn}^{22} - S_{mn}^{12} S_{mn}^{21} \right]}{\left(\Omega^2 - \left(\Omega_{mn}^{(1)} \right)^2 \right) \left(\Omega^2 - \left(\Omega_{mn}^{(2)} \right)^2 \right) \left(\Omega^2 - \left(\Omega_{mn}^{(3)} \right)^2 \right)} \tag{32}$$

$$W_{mn}^{(1)} = \frac{1}{r_c}\frac{1-\nu_c^{\,2}}{E_c h_c}\frac{\sin\left[k_m(z_0+L_c)\right]}{O^{(1)}(\Omega_{mn})}\left\{\frac{1}{\pi L_c}\sin(n\phi_0)\left[S_{mn}^{31}S_{mn}^{12}-S_{mn}^{11}S_{mn}^{32}\right]^{(1)} f_c^{\nu}\right. \\ \left. +\frac{\varepsilon_n}{2\pi L_c}\cos(n\phi_0)\left[S_{mn}^{11}S_{mn}^{22}-S_{mn}^{12}S_{mn}^{21}\right]^{(1)} f_c^{w}\right\} \tag{33}$$

where

$$O^{(1)}(\Omega_{mn}) = \left(\Omega^2-\left(\Omega_{mn}^{(1)}\right)^2\right)\left(\Omega^2-\left(\Omega_{mn}^{(2)}\right)^2\right)\left(\Omega^2-\left(\Omega_{mn}^{(3)}\right)^2\right) \tag{34}$$

repeating the orthogonality conditions, but multiplying by $[A_{mn}^{(2)}]$ to get:

$$W_{mn}^{(2)} = \frac{1}{r_c}\frac{1-\nu_c^{\,2}}{E_c h_c}\frac{\sin\left[k_m(z_0+L_c)\right]}{O^{(2)}(\Omega_{mn})}\left\{\frac{\varepsilon_n}{2\pi L_c}\cos(n\phi_0)\left[S_{mn}^{31}S_{mn}^{12}-S_{mn}^{11}S_{mn}^{32}\right]^{(2)} f_c^{\nu}\right. \\ \left. +\frac{1}{\pi L_c}\sin(n\phi_0)\left[S_{mn}^{11}S_{mn}^{22}-S_{mn}^{12}S_{mn}^{21}\right]^{(2)} f_c^{w}\right\} \tag{35}$$

- case $n=0$:

The orthogonality conditions yield

$$W_{m0}^{(1)} = \frac{1}{r_c}\frac{1-\nu_c^{\,2}}{E_c h_c}\frac{\sin\left[k_m(z_0+L_c)\right]}{O^{(1)}(\Omega_{m0})}\frac{\varepsilon_0}{2\pi L_c}\left[S_{m0}^{11}S_{m0}^{22}-S_{m0}^{12}S_{m0}^{21}\right]^{(1)} f_c^{w} \tag{36}$$

and $W_{m0}^{(2)}$ is not defined (its contribution will be zero since multiplied by $\sin(0\times\phi)$).

Now,

$$O^{(1)}(\Omega_{mn}) = O^{(2)}(\Omega_{mn})$$

since $O^{(1)}(\Omega_{mn})$ depends only on the natural frequencies and on the frequency of excitation.

It can also be shown that,

$$\left[S_{mn}^{31}S_{mn}^{12} - S_{mn}^{11}S_{mn}^{32}\right]^{(2)} = -\left[S_{mn}^{31}S_{mn}^{12} - S_{mn}^{11}S_{mn}^{32}\right]^{(1)}$$

$$\left[S_{mn}^{11}S_{mn}^{22} - S_{mn}^{12}S_{mn}^{21}\right]^{(2)} = \left[S_{mn}^{11}S_{mn}^{22} - S_{mn}^{12}S_{mn}^{21}\right]^{(1)}$$

by replacing the following quantities by their expression in Equation (25).

Now, it can be noted that the general expression used for $n \neq 0$ is also suitable for the case $n = 0$. Therefore, using the previous relations, a general expression for $w(\phi, z, t)$ is

$$w(\phi,z,t) = \frac{1-\nu_c^{\,2}}{r_c E_c h_c \pi L_c} f \sum_{m=1}^{\infty}\sum_{n=0}^{\infty} \frac{\sin\left[k_m(z_0+L_c)\right]}{O^{(1)}(\Omega_{mn})} \left\{ \sin\left[n(\phi-\phi_0)\right] \left[S_{mn}^{31}S_{mn}^{12} - S_{mn}^{11}S_{mn}^{32}\right]^{(1)} \cos\alpha + \frac{\varepsilon_n}{2} \cos\left[n(\phi-\phi_0)\right] \left[S_{mn}^{11}S_{mn}^{22} - S_{mn}^{12}S_{mn}^{21}\right]^{(1)} \sin\alpha \right\} \sin\left[k_m(z+L_c)\right] \tag{37}$$

or

$$w(\phi,z) = f \sum_{m=1}^{\infty}\sum_{n=0}^{\infty} \left\{ H_{mn}^{(1)} \sin\left[n(\phi-\phi_0)\right] + H_{mn}^{(2)} \cos\left[n(\phi-\phi_0)\right] \right\} \sin\left[k_m(z+L_c)\right] \tag{38}$$

where

$$H_{mn}^{(1)} = \frac{1-\nu_c^{\,2}}{r_c E_c h_c \pi L_c} \frac{\sin\left[k_m(z_0+L_c)\right]}{O^{(1)}(\Omega_{mn})} \sin\left[n(\phi-\phi_0)\right]\left[S_{mn}^{31}S_{mn}^{12} - S_{mn}^{11}S_{mn}^{32}\right]^{(1)} \cos\alpha$$
$$H_{mn}^{(2)} = \frac{1-\nu_c^{\,2}}{r_c E_c h_c \pi L_c} \frac{\sin\left[k_m(z_0+L_c)\right]}{O^{(1)}(\Omega_{mn})} \frac{\varepsilon_n}{2} \cos\left[n(\phi-\phi_0)\right]\left[S_{mn}^{11}S_{mn}^{22} - S_{mn}^{12}S_{mn}^{21}\right]^{(1)} \sin\alpha \quad (39)$$

$$w(\phi,z) = f\sum_{m=1}^{\infty}\sum_{n=0}^{\infty}\psi_{mn}(\phi)\xi_m(z) \quad (40)$$

where f_c^{ν} and f_c^{w} have been replaced by their expression as functions of f, the point force applied to the cylinder,

The response of the cylinder to a number a of point forces is the sum of the responses to those single forces:

$$w(\phi,z) = \sum_{a=1}^{N_a} f_a \sum_{m=1}^{\infty}\sum_{n=0}^{\infty}\psi_{mn}(\phi,\phi_a,z_a)\xi_m(z) \quad (41)$$

In our case, these forces are those transmitted by the passive isolators and the control forces.

4. Coupled system

In order to derive the response of the coupled system, i.e. the radiation of the cylinder due to a point force applied on the rigid plate, we need to calculate the forces applied by the plate on the cylinder. These forces are the forces transmitted by the passive isolators and by the control forces.

Equation (1) shows that we need to know the displacement of the points of attachment of the active-isolators to the cylinder in order to calculate the forces in the active isolators. Equation (41) gives the displacement of one point of the cylinder submitted to a set of forces. Now $\{z^c\}$ is the vector of the cylinder displacement at the points of attachment of the active-passive mounts and it can be written as

$$\{z^c\} = [H_a]\{F_a\} + [H_c]\{F_c\} \tag{42}$$

4.1. Parallel active mounts

Equations (1), (15) and (42) give a system of three equations and three unknowns:

$$\left.\begin{aligned} \{F_a\} &= [M](\{z^p\} - \{z^c\}) \\ [R_G]\{D_G\} &= \{F_d\} + [R_a]\{z^c\} + [R_c]\{F_c\} \\ \{z^c\} &= [H_a]\{F_a\} + [H_c]\{F_c\} \end{aligned}\right\} \tag{43}$$

Now, recalling Equation (13), we replace $\{F_a\}$ by its expression in Equation (43) to get

$$\left.\begin{aligned} \{w_a\} &= [H_a][M]([V]\{D_G\} - \{w_a\}) + [H_c]\{F_c\} \\ [R_G]\{D_G\} &= \{F_d\} + [R_a]\{w_a\} + [R_c]\{F_c\} \end{aligned}\right\} \tag{44}$$

$$\left.\begin{aligned} ([I_w] + [H_a][M])\{w_a\} - [H_a][M][V]\{D_G\} &= [H_c]\{F_c\} \\ [R_a]\{w_a\} - [R_G]\{D_G\} &= -\{F_d\} - [R_c]\{F_c\} \end{aligned}\right\} \tag{45}$$

$$\left.\begin{aligned}&([I_w]+[H_a][M])\{w_a\}-[H_a][M][V][R_G]^{-1}(\{F_d\}+[R_c]\{F_c\}-[R_a]\{w_a\})=[H_c]\{F_c\}\\&\{D_G\}=[R_G]^{-1}(\{F_d\}+[R_c]\{F_c\}-[R_a]\{w_a\})\end{aligned}\right\}(46)$$

$$\left.\begin{aligned}\{w_a\}&=\frac{[H_a][M][V][R_G]^{-1}\{F_d\}+([H_a][M][V][R_G]^{-1}[R_c]+[H_c])\{F_c\}}{([I]+[H_a][M]-[H_a][M][V][R_G]^{-1}[R_a])}\\\{D_G\}&=[R_G]^{-1}(\{F_d\}+[R_c]\{F_c\}-[R_a]\{w_a\})\end{aligned}\right\}\qquad(47)$$

and now, we can rewrite the forces in the passive spring-damper system as:

$$\begin{aligned}\{F_a\}&=[M][V]\{D_G\}-\{w_a\})\\&=[M][V][R_G]^{-1}(\{F_d\}+[R_c]\{F_c\}-[R_a]\{w_a\})-\{w_a\})\\&=[M]([V][R_G]^{-1}(\{F_d\}+[R_c]\{F_c\})-([V][R_G]^{-1}[R_a]+[I_w]))\{w_a\}\\&=[M][V][R_G]^{-1}(\{F_d\}+[R_c]\{F_c\})+\\&\quad[M]([V][R_G]^{-1}[R_a]+[I_w])\frac{[H_a][M][V][R_G]^{-1}\{F_d\}+([H_a][M][V][R_G]^{-1}[R_c]+[H_c])\{F_c\}}{([I_w]+[H_a][M]-[H_a][M][V][R_G]^{-1}[R_a])}\end{aligned}$$

(48)

which can be written as :

$$\{F_a\}=[{}_aT_d]\{F_d\}+[{}_aT_c]\{F_c\}\qquad(49)$$

where

$$[{}_aT_d]=[M][V][R_G]^{-1}+[M]\left([V][R_G]^{-1}[R_a]+[I_w]\right)+\frac{[H_a][M][V][R_G]^{-1}}{\left([I_w]+[H_a][M]-[H_a][M][V][R_G]^{-1}[R_a]\right)} \tag{50}$$

and $[{}_aT_d]$ indicates the contribution of the disturbance F_d to the force in the passive mount a.

$$[{}_aT_c]=[M][V][R_G]^{-1}[R_c]+\frac{\left([H_a][M][V][R_G]^{-1}[R_c]+[H_c]\right)}{\left([I_w]+[H_a][M]-[H_a][M][V][R_G]^{-1}[R_a]\right)} \tag{51}$$

and $[{}_aT_c]$ indicates the contribution of the control force F_c to the force in the passive mount a.

4.2. Opposed active mounts

For the system with opposed active mounts, the system of three equations becomes:

$$\begin{cases}\{F_a\}=[M]\left(\{z^p\}-\{z^c\}\right)\\ [R_G]\{D_G\}=\{F_d\}+[R_a]\{z^c\}\\ \{w_a\}=[H_a]\{F_a\}+[H_c]\{F_c\}\end{cases} \tag{52}$$

since the control forces are not applied on the plate. The derivation is the same as in the previous section except that the term related to the contribution of the control forces to

the displacement of the plate ($[R_c]\{F_c\}$) does not appear. The expression for the forces in the passive mounts is the same as in Equation (49). The contribution of the disturbance, $[{}_aT_d]$ is the same as for the parallel configuration (50), but the contribution of the control forces is different :

$$[{}_aT_c] = \frac{[H_c]}{\left([I]+[H_a][M]-[H_a][M][V][R_G]^{-1}[R_a]\right)} \tag{53}$$

5. Radiation of the system in the far-field

Now that the radial displacement of the cylindrical shell due to a disturbance on the rigid plate is known, the radiation of the vibrating system in the far-field can be derived from the analysis presented in Junger and Feit [42] using a wave number transform formulation.

5.1. Cylinder excited by one point force

Keeping the same cylindrical coordinate system as previously (Figure 3), the three-dimension Helmholtz equation is written in cylindrical coordinates :

$$\left(\frac{\partial^2}{\partial r^2}+\frac{1}{r}\frac{\partial}{\partial r}+k_0{}^2+\frac{1}{r^2}\frac{\partial^2}{\partial \phi^2}+\frac{\partial^2}{\partial z^2}\right)p(r,\phi,z)=0 \tag{54}$$

where k_0 is the wavenumber and $p(r,\phi,z)$ the acoustic pressure at an arbitrary point of coordinates r,θ and z. The Helmholtz equation governs the pressure of a three-dimensional wave propagating in the free-space, in a cylindrical coordinate system.

Now, the acoustic pressure is related to the acceleration distribution of the radiating structure $\ddot{W}(\phi,z)$ through the boundary conditions on its surface :

$$\rho\ddot{w}(\phi,z) = -\frac{\partial}{\partial r}p(r,\phi,z) \quad \text{at} \quad r = r_c \tag{55}$$

Define the wavenumber transform as

$$\tilde{f}(\gamma) = \int_{-\infty}^{\infty} f(z)e^{-j\gamma z}dz \tag{56}$$

and apply to the Helmoltz Equation (54) as well as the boundary condition (55) to get:

$$\begin{cases} \left(\frac{\partial^2}{\partial r^2} + \frac{1}{r}\frac{\partial}{\partial r} + {k_0}^2 - \gamma^2 + \frac{1}{r^2}\frac{\partial^2}{\partial \phi^2}\right)\tilde{p}(r,\phi,\gamma) = 0 \\ \rho\tilde{\ddot{w}}(\phi,\gamma) = -\frac{\partial}{\partial r}\tilde{p}(r,\phi,\gamma) \quad \text{at} \quad r = r_c \end{cases} \tag{57}$$

The wave equation is separable in cylindrical coordinates, which means that r,z and ϕ are independent variables. Then, the pressure can be expressed as a series,

$$\tilde{p}(r,\phi,\gamma) = \sum_{n=0}^{\infty} C_n \tilde{R}_n(r,\gamma)\cos(n\phi) \tag{58}$$

The second derivative of the pressure can now be written as

$$\frac{\partial^2}{\partial \phi^2}\tilde{p}(r,\phi,\gamma) = -n^2\tilde{p}(r,\phi,\gamma) \tag{59}$$

In the wavenumber domain, the Helmholtz equation now takes the form

$$\left(\frac{\partial^2}{\partial r^2}+\frac{1}{r}\frac{\partial}{\partial r}+{k_0}^2-\gamma^2-\frac{n^2}{r^2}\right)\tilde{p}(r,\gamma)=0 \tag{60}$$

This equation is Bessel's differential equation and it has a solution of the form

$$\tilde{p}(r,\phi,\gamma)=\sum_{n=0}^{\infty}C_n H_n^{(1)}\left[\left({k_0}^2-\gamma^2\right)^{\frac{1}{2}}r\right]\cos(n\phi) \tag{61}$$

where $H_n^{(1)}$ is Hankel's function of the first kind.

The boundary condition of Equation (57) becomes:

$$\rho_0\int_{-\infty}^{\infty}\ddot{w}(\phi,z)e^{-j\gamma z}dz=-\sum_{n=0}^{\infty}C_n\left({k_0}^2-\gamma^2\right)^{\frac{1}{2}}H_n^{(1)'}\left[\left({k_0}^2-\gamma^2\right)^{\frac{1}{2}}r_c\right]\cos(n\phi) \tag{62}$$

with

$$\ddot{w}(\phi,z)=-\omega^2 w(\phi,z) \tag{63}$$

and $W(\phi,z)$ defined in (40), leading to :

$$\begin{aligned}\rho_0\int_{-\infty}^{\infty}\ddot{w}(\phi,z)e^{-j\gamma z}dz &= -\rho_0\omega^2 f\int_{-\infty}^{\infty}\sum_{m=1}^{\infty}\sum_{n=0}^{\infty}\psi_{mn}(\phi)\xi_m(z)e^{-j\gamma z}dz \\ &= -\rho_0\omega^2 f\sum_{m=1}^{\infty}\sum_{n=0}^{\infty}\psi_{mn}(\phi)\int_{-\infty}^{\infty}\xi_m(z)e^{-j\gamma z}dz\end{aligned} \tag{64}$$

Now, the wave number transform of $\xi_m(z)$ is calculated :

$$\tilde{\xi}_m(\gamma) = \int_{-L_c}^{L_c} \xi_m(z) e^{j\gamma z} dz = \begin{cases} -\dfrac{2k_m \cos(\gamma L_c)}{(k_n^2 - \gamma^2)} & \text{for } m \text{ even} \\ \dfrac{2jk_m \sin(\gamma L_c)}{(k_n^2 - \gamma^2)} & \text{for } m \text{ odd} \end{cases} \quad \text{for } k_m \neq \gamma$$
$$= je^{j\gamma L_c} L_c \quad \text{for } k_m = \gamma \qquad (65)$$

Replacing this value in (64) and then in (62) ,

$$-\rho_0 \omega^2 f \sum_{m=1}^{\infty} \sum_{n=0}^{\infty} \psi_{mn}(\phi) \tilde{\xi}_m(\gamma) = -\sum_{n=0}^{\infty} C_n (k_0^2 - \gamma^2)^{\frac{1}{2}} H_n^{(1)'} \left[(k_0^2 - \gamma^2)^{\frac{1}{2}} r_c \right] \cos(n\phi) \qquad (66)$$

which gives a solution for the coefficients C_{mn} :

$$C_n = \frac{\rho_0 \omega^2 f \sum_{m=1}^{\infty} \psi_{mn}(\phi) \tilde{\xi}_m(\gamma)}{(k_0^2 - \gamma^2)^{\frac{1}{2}} H_n^{(1)'} \left[(k_0^2 - \gamma^2)^{\frac{1}{2}} r_c \right] \cos(n\phi)} \qquad (67)$$

Hence, inserting this result in Equation (61),

$$\tilde{p}(r, \phi, \gamma) = \sum_{n=0}^{\infty} \frac{\rho_0 \omega^2 \sum_{m=1}^{\infty} \psi_{mn}(\phi) \tilde{\xi}_m(\gamma)}{(k_0^2 - \gamma^2)^{\frac{1}{2}} H_n^{(1)'} \left[(k_0^2 - \gamma^2)^{\frac{1}{2}} r_c \right]} H_n^{(1)} \left[(k_0^2 - \gamma^2)^{\frac{1}{2}} r \right] \qquad (68)$$

To obtain the pressure field, the inverse wavenumber transform of Equation (68) is performed :

$$p(r,\phi,z)=\frac{1}{2\pi}\int_{-\infty}^{\infty}\tilde{p}(r,\phi,\gamma)e^{j\gamma z}d\gamma$$

$$=\frac{\rho_0\omega^2}{2\pi}f\sum_{m=1}^{\infty}\sum_{n=0}^{\infty}\psi_{mn}(\phi)\int_{-\infty}^{\infty}\frac{e^{j\gamma z}H_n^{(1)}\left[\left(k_0{}^2-\gamma^2\right)^{\frac{1}{2}}r\right]\tilde{\xi}_m(\gamma)}{\left(k_0{}^2-\gamma^2\right)^{\frac{1}{2}}H_n^{(1)'}\left[\left(k_0{}^2-\gamma^2\right)^{\frac{1}{2}}r_c\right]}d\gamma \tag{69}$$

In the far-field ($r\rangle\rangle r_c$) this integral can be approximated using the stationary-phase approach [43, 44].

For this method, the cylindrical coordinates are first transformed into spherical coordinates :

$$\begin{cases} r=R\sin\theta \\ z=R\cos\theta \end{cases} \tag{70}$$

The Hankel function is estimated using a large-argument asymptotic value (see Appendix 2).

$$H_n^{(1)}\left[\left(k_0{}^2-\gamma^2\right)^{\frac{1}{2}}r\right]=\left(\frac{2}{\left(k_0{}^2-\gamma^2\right)^{\frac{1}{2}}r}\right)^{\frac{1}{2}}(-j)^n e^{-j\frac{\pi}{4}}e^{j\left(k_0{}^2-\gamma^2\right)^{\frac{1}{2}}r} \tag{71}$$

Replacing in Equation (69),

$$p(R,\theta,\phi)=\frac{\rho_0\omega^2}{\left(2\pi^3 R\sin\theta\right)^{\frac{1}{2}}}f\sum_{m=1}^{\infty}\sum_{n=0}^{\infty}\psi_{mn}(\phi)(-j)^n e^{j\frac{\pi}{4}}\int_{-\infty}^{+\infty}\frac{e^{j\gamma R\cos\theta}e^{i\left(k_0{}^2-\gamma^2\right)^{\frac{1}{2}}R\sin\theta}\tilde{\xi}_n(\gamma)}{\left(k_0{}^2-\gamma^2\right)^{\frac{3}{4}}H_n^{(1)'}\left[\left(k_0{}^2-\gamma^2\right)^{\frac{1}{2}}r_c\right]}d\gamma \tag{72}$$

And the stationary phase approximation gives (see Appendix 3):

$$p(R,\theta,\phi)=\frac{\rho_0\omega^2 e^{jkR}}{\pi R k\sin\theta} f\sum_{m=1}^{\infty}\sum_{n=0}^{\infty}\psi_{mn}(\phi)(-j)^{n+1}\frac{\tilde{\xi}_n(k\cos\theta)}{H_n^{(1)'}[r_c k\sin\theta]} \tag{73}$$

which is the pressure radiated at the point of space of coordinates (R,θ,ϕ) for a single point-force excitation.

5.2. Cylinder excited by a set of forces

Now, we want to consider the multiple point-force excitation in the case of the coupled system. The cylinder is excited by the forces applied by the N_a mounts and also by the N_c control forces. The pressure is

$$\begin{aligned} p(R,\theta,\phi)=\frac{\rho_0\omega^2 e^{jkR}}{\pi R k\sin\theta}\Bigg(&\sum_{a=1}^{N_a}\sum_{m=1}^{\infty}\sum_{n=0}^{\infty} f_a\psi_{mn}(\phi,\phi_a)(-j)^{n+1}\frac{\tilde{\xi}_n(k\cos\theta,z_a)}{H_n^{(1)'}[r_c k\sin\theta]} \\ &+\sum_{c=1}^{N_c}\sum_{m=1}^{\infty}\sum_{n=0}^{\infty} f_c\psi_{mn}(\phi,\phi_c)(-j)^{n+1}\frac{\tilde{\xi}_n(k\cos\theta,z_c)}{H_n^{(1)'}[r_c k\sin\theta]}\Bigg) \end{aligned} \tag{74}$$

This can be put in a matrix form

$$\begin{aligned} p(R,\theta,\phi)&=\begin{Bmatrix} e_1 & e_2 & \cdots & e_{N_a}\end{Bmatrix}\begin{Bmatrix} F_1\\ F_2\\ \vdots\\ F_{N_a}\end{Bmatrix}+\begin{Bmatrix} g_1 & g_2 & \cdots & g_{N_c}\end{Bmatrix}\begin{Bmatrix} F_1\\ F_2\\ \vdots\\ F_{N_c}\end{Bmatrix} \\ &=\{E\}\{F_a\}+\{G\}\{F_c\} \end{aligned} \tag{75}$$

where e_a represents, for example, the contribution of the force in the passive isolator number a to the radiation in the far-field, and g_c the contribution of the control force number c.

Now, using the result of Equation (49), the pressure radiated by the system can be expressed only as a function of the disturbance and of the control forces by replacing the amplitude of the forces in the mount by their expression as a function of $\{F_d\}$ and $\{F_c\}$.

$$\begin{aligned} p(R,\theta,\phi) &= \{\Pi_a\}\left([{}_aT_d]\{F_d\}+[{}_aT_c]\{F_c\}\right)+\{\Pi_c\}\{F_c\} \\ &= \{\Pi_a\}[{}_aT_d]\{F_d\}+\left(\{\Pi_a\}[{}_aT_c]+\{\Pi_c\}\right)\{F_c\} \\ &= [D]\{F_d\}+[C]\{F_c\} \end{aligned} \tag{76}$$

This expression of the sound pressure at an arbitrary point in the far field is now independent of the forces in the passive mounts which are forces internal to the system. It can thus be used to compute the control of the radiation from the system.

6. Control

In this part, several methods are proposed to minimize the radiation from the system excited by a disturbance. The linear quadratic optimal control will first be explained, then several control approaches will be presented.

6.1. Optimal quadratic feedforward control

The optimal control is characterized by a cost function which is the quantity to be minimized and by two vectors of forces which are the disturbance force $\{F_d\}$ (or primary

source) and the control forces $\{F_c\}$ (or secondary sources). The quantity to be minimized is a linear function of these two vectors of forces. It is moreover a quadratic function of the control forces. For a given location of the forces and a given amplitude of the disturbance, the cost function has a unique minimum. This minimum is obtained for a set of control forces defined as the optimal control forces.

As long as it is a quadratic function of the control forces, the cost function can take many forms. The cost function can be chosen among the followings and are described in sections 6.2. to 6.6. :

- the sound pressure at a discrete number of points in the half plane. The cost function is then the sum of the square pressure moduli at these points.
- the total power radiated by the structure which leads to global control of the radiation over the outer half plane.
- the power radiated in a particular sector of the outer half-plane.
- the sound pressure at a discrete number of points in the half plane evaluated by taking in account only radiating components. These radiating components are associated with the circumferential modes of the cylinder.
- the radial displacement at some location on the radiating structure. These location can coincide with the location of the active-passive mounts or they can be any particular point on the surface of the cylinder.

The first four methods are Active Structural Acoustic Control approaches (ASAC) since the cost function is an acoustic quantity (sound pressure) and the control forces are applied directly to the radiating structure. The last method is an Active Vibration Control approach (AVC) since the cost function is the displacement of the structure. Therefore it does not aim to control the radiation of the structure, but its vibration.

For all forms of the cost function, Λ is written as a quadratic function of $\{F_c\}$ and $\{F_d\}$:

$$\begin{aligned}\Lambda &= \left|[D]\{F_d\}+[C]\{F_c\}\right|^2 \\ &= \left([D]\{F_d\}+[C]\{F_c\}\right)\left([D]\{F_d\}+[C]\{F_c\}\right)^{T^*} \\ &= \{F_d\}^T[D][D]^{T^*}\{F_d\}^* + \{F_d\}^T[D][C]^{T^*}\{F_c\}^* + \{F_c\}^T[C][D]^{T^*}\{F_d\}^* \\ &\quad +\{F_c\}^T[C][C]^{T^*}\{F_c\}^*\end{aligned} \tag{77}$$

where $[D]\{F_d\}$ is the contribution of the primary source, and $[C]\{F_c\}$ of the secondary source(s).

Nelson et al [45] developed a general solution giving the unique minimum of the cost function of Equation (77).The control forces must satisfy :

$$\frac{\partial \Lambda}{\partial F_c^R} + j\frac{\partial \Lambda}{\partial F_c^I} = 0 \tag{78}$$

where F_c^R and F_c^I are the real and imaginary part of F_c respectively. Setting the derivative of the cost function with respect to the real and imaginary part of the control forces to zero will give a relationship for the amplitude of the control forces. The control forces calculated will minimize of the cost function.

Then the optimal solution for the control forces is

$$\{\overline{F}_c\} = -\left([C]^T[C]\right)^{-1}[C]^T[D]\{F_d\} \tag{79}$$

and the unique minimum of the cost function is given as

$$\Lambda_{\min} = \{F_d\}^T \left([D] - \left([C]^T[C]\right)^{-1}[C]^T[D]\right)\{F_d\} \tag{80}$$

This general principle of the optimal control can now be applied to different control approaches.

6.2. Minimization of the acoustic pressure in one direction of radiation

In this section, the sound pressure radiated by the system is to be minimized at one (or several) point of the radiation half-space. The quadratic cost function is therefore defined as the square of the pressure at a particular point of coordinates (R, θ, ϕ).

Recalling Equation (76) giving the far-field radiated pressure, the cost function Λ is given by :

$$\begin{aligned}\Lambda &= \left|p(R,\theta,\phi)\right|^2 \\ &= \{F_d\}^T [D][D]^{T^*}\{F_d\}^* + \{F_d\}^T [D][C]^{T^*}\{F_c\}^* + \{F_c\}^T [C][D]^{T^*}\{F_d\}^* \\ &+ \{F_c\}^T [C][C]^{T^*}\{F_c\}^*\end{aligned} \tag{81}$$

The optimal control forces are given by Equation (79), and applying these forces will result in minimizing the pressure at the point of coordinates (R, θ, ϕ).

Now, the expression for the pressure in Equation (73) shows that the pressure field radiated at an angle θ depends only on the structural wavenumber component corresponding to the point of stationary phase [42] : $k_0 \cos\theta$ (see Appendix 3). Therefore, minimizing the pressure in the far-field at the point of coordinates (R, θ, ϕ) is equivalent to minimizing the wavenumber component $k = k_0 \cos\theta$ (associated with each circumferential mode n) in the wavenumber spectrum. Since the wavenumber transform is a transform

with respect to the longitudinal coordinate z (Equation (56)), and not with respect to the circumferential coordinate ϕ (in the cylindrical coordinate system), the wavenumber transform will have components associated with each circumferential mode n.

Fuller and Burdisso [20] theoretically showed that the radiated pressure could be minimized in a particular direction of space by applying the control in the wavenumber domain. Now, the control forces are independent of the radial coordinate R and the sound pressure will be minimized at the angle theta, independently of R, provided it is large enough to be in the far-field since the derivation of the pressure is valid only in this case. The control is therefore not local, but rather directional since it applies to a direction of radiation.

Minimizing the pressure in several directions follows exactly the same principle except that the cost function is now the sum of the squared pressure moduli at the respective radiation points. A given number of directions of minimization can be chosen so as to cover evenly the outer half-plane and therefore to give a global minimization of the radiated pressure over the whole space. In this latter case, the results are expected to be close to those obtained by minimizing the total radiated power.

It can be noted that performing the optimal control to totally minimize sound at all the observation points requires in this particular case as many control forces as there are directions of radiation to be controlled. If the number of control forces is not sufficient, optimal control can still be achieved, but the minimum cost function will not be zero after control.

On the contrary, if the number of control forces is larger than the number of radiation angle, then the system is underdetermined and the optimal control does not lead to a unique minimum. In this case, an alternative cost function strategy is required, that will be discussed in section 6.7.

6.3. Minimization of the radiated power in the far-field

To obtain a reduction of the sound pressure over the whole outer half-plane, the cost function is taken as the total power radiated from the structure.

The power radiated from the system in the far-field is obtained by integrating the acoustic intensity over a hemisphere corresponding to the radiation half-space

$$\Pi = \int_0^{2\pi} \int_0^{\pi/2} \frac{|p(r,\theta,\phi)|^2}{\rho_0 c_0} r^2 \sin\theta \, d\theta \, d\phi \tag{82}$$

Recalling Equation (81) giving $|p(r,\theta,\phi)|^2$ as a function of $[C]$ and $[D]$, we define the following matrices,

$$\left[\tilde{D}D\right] = \int_0^{2\pi} \int_0^{\pi/2} \frac{1}{\rho_0 c_0} [D][D]^{T^*} r^2 \sin\theta \, d\theta \, d\phi \tag{83}$$

$$\left[\tilde{D}C\right] = \left[\tilde{C}D\right]^{T^*} = \int_0^{2\pi} \int_0^{\pi/2} \frac{1}{\rho_0 c_0} [D][C]^{T^*} r^2 \sin\theta \, d\theta \, d\phi \tag{84}$$

$$\left[\tilde{C}C\right] = \int_0^{2\pi} \int_0^{\pi/2} \frac{1}{\rho_0 c_0} [C][C]^{T} r^2 \sin\theta \, d\theta \, d\phi \tag{85}$$

The radiated power can now be written as a quadratic function of the control forces

$$\Pi = \{F_d\}^T \left[\tilde{D}D\right]\{F_d\}^* + \{F_d\}^T \left[\tilde{D}C\right]\{F_c\}^* + \{F_c\}^T \left[\tilde{D}C\right]^T \{F_d\}^* + \{F_c\}^T \left[\tilde{C}C\right]\{F_c\}^* \tag{86}$$

Then, recalling Equation (79), the optimal control forces are

$$\{\overline{F_c}\} = -\left(\left[\tilde{C}C\right]^{-1}\right)^T \left[\tilde{D}C\right]^T \{F_d\} \tag{87}$$

and the minimum sound power radiated by the system after control is

$$\Lambda_{\min} = \{F_d\}^T \left(\left[\tilde{D}D\right] - \left[\tilde{D}C\right]\left[\tilde{C}C\right]^{-1}\left[\tilde{D}C\right]^{*T}\right)\{F_d\}^* \tag{88}$$

6.4. Minimization of the acoustic pressure in a sector

Instead of the total power radiated in the far-field, the power radiated in a certain part of the space can be minimized. This particular area of the semi-space will be defined by four angles : θ_1, θ_2, ϕ_1 and ϕ_2. As explained in section 6.2, the quantity minimized does not depend on the radius R and the control will result in minimizing the acoustic pressure in a sector defined by these four angles.

$$\Pi = \int_{\phi_1}^{\phi_2} \int_{\theta_1}^{\theta_2} \frac{|p(r,\theta,\phi)|^2}{\rho_0 c_0} r^2 \sin\theta \, d\theta \, d\phi \tag{89}$$

The matrices $\left[\tilde{D}D\right]$, $\left[\tilde{D}C\right]$ and $\left[\tilde{C}C\right]$ are calculated in the same way as in Equations (83) to (85), and the optimal control forces are calculated as in Equation (87).

6.5. Minimization of radiating components associated with circumferential modes

For a given frequency of excitation, only a certain number of modes (m,n) will significantly contribute to the structural response. Moreover, among these, some will have a low radiation efficiency and will contribute very little to the radiation from the structure in the far-field. Thus a small number of modes will significantly contribute to the sound pressure radiated. For global radiation control, if the cost function takes only the contribution of these modes to the pressure field into account, the control can be expected to be more efficient.

Since the radiating structure considered (cylinder) is finite in the longitudinal direction z, there is no cut-on frequency for the modes. All the modes will have wavenumber components in the supersonic range $[-k_0;k_0]$, where $k_0=\omega/c_0$ is the acoustic wavenumber. Therefore, the particular modes that will radiate the most cannot be predicted a priori. Only after the wavenumber transform is achieved can they be identified as the modes that have significant wavenumber components in the supersonic range.

The amplitude of the Hankel derivative of Equation (73) gives the relative weight of the circumferential mode n in the radiation. The smaller $H_n^{(1)'}[kr_c\sin\theta]$, the larger the influence of the circumferential mode n.

Finally, there are two conditions for a mode to contribute significantly to the sound pressure radiated :

- the mode (m,n) must contribute significantly to the structural response of the radiating structure
- the Hankel derivative of the corresponding circumferential mode n must be small.

Now, we define $p_n(R,\theta,\phi)$ as the contribution of the circumferential mode of order n to $p(R,\theta,\phi)$, the sound pressure at the point of coordinates (R,θ,ϕ). The total contribution of the radiating modes is

$$\begin{aligned} p_r(R,\theta,\phi) &= \sum_{\text{radiating } n\text{'s}} p_n(R,\theta,\phi) \\ &= [D_R]\{F_d\} + [C_R]\{F_c\} \end{aligned} \tag{90}$$

where $[C_R]$ and $[D_R]$ are respectively the contribution of the control forces and of the disturbance to the sound pressure evaluated with the contribution of the radiating modes only. The cost function is

$$\Lambda = \left| p_r(R,\theta,\phi) \right|^2 \tag{91}$$

The cost function defined here is very similar to that defined in section 6.2., except that it takes only selected circumferential modes into account. However, the pressure will still be minimized in the direction of radiation θ.

Now the derivation of the optimal control forces and of the minimum cost function is the same as in section 6.2., and

$$\{\overline{F_c}\} = -\left([C_R]^T[C_R]\right)^{-1}[C_R]^T[D_R]\{F_d\} \tag{92}$$

$$\Lambda_{\min} = \{F_d\}^T\left([D_R] - \left([C_R]^T[C_R]\right)^{-1}[C_R]^T[D_R]\right)\{F_d\} \tag{93}$$

6.6. Active vibration control

The principle of active vibration control is to minimize the radial displacement at some points of the radiating structure. The cost function is now,

$$\begin{aligned}\Lambda &= \left|w(\phi_{\min}, z_{\min})\right|^2 \\ &= \left([D_w]\{F_d\}+[C_w]\{F_c\}\right)\left([D_w]\{F_d\}+[C_w]\{F_c\}\right)^{T^*}\end{aligned} \tag{94}$$

Applying the control forces will result in minimizing the radial displacement of the cylinder at the point of coordinates $(\phi_{\min}, z_{\min})$. The optimal control forces have an expression similar to that of Equation (79).

The displacement can also be minimized at several locations on the structure, and the larger the number of points, the more the vibrations of the structure will be reduced. But minimizing the vibrations does not ensure that the radiated pressure will be reduced in the same proportions or will be reduced at all. The structure could vibrate less but radiate more efficiently.

In this particular case of the coupled system, a good way to ensure that the level of radiation will be reduced is to control the displacement at the locations of the active-passive mounts. The mounts being the only mean of transmitting the energy from the plate to the cylinder, this will result in controlling the displacement at the location of the disturbances applied to the cylinder. If the control forces are chosen of equal magnitude but opposed phase as the forces in the passive mounts, no overall force will be applied to the cylinder, and total radiation control will be achieved. This control approach should give results comparable to the minimization of the total radiated power, although its principle is different.

6.7. Control of underdetermined systems

When there are more control forces than quantities to be minimized, then the system becomes underdetermined, which means that there is no unique minimum for the cost function. The matrix $[C]^T[C]$ in Equation (79) is not full rank and therefore cannot be inverted.

One solution is to include in the cost function the amplitude of the control forces. This will result in the minimization of the quantity chosen (acoustic pressure, vibration of the structure, ...) but with the minimum control effort. The control effort is the sum of the square of the control forces moduli. This solution solves the problem since it adds as many quantities to be minimized as there are control forces to the system. The system has now more quantities to be minimized than control forces which implies that the cost function will not be zero after control.

Elliott et al [46] proposed a solution for the control of underdetermined system using the following cost function :

$$\Lambda = E^T E + \beta \{F_c\}^T \{F_c\} \tag{95}$$

where E is the quantity to be minimized and $\Delta = \{F_c\}^T \{F_c\}$ is the control effort. The parameter β acts as a balance between reducing E or reducing Δ.

Recalling Equation (77), the cost function becomes :

$$\begin{aligned}\Lambda &= \left([D]\{F_d\}+[C]\{F_c\}\right)\left([D]\{F_d\}+[C]\{F_c\}\right)^{T^*} \\ &= \{F_d\}^T[D][D]^{T^*}\{F_d\}^* + \{F_d\}^T[D][C]^{T^*}\{F_c\}^* + \{F_c\}^T[C][D]^{T^*}\{F_d\}^* \\ &+\{F_c\}^T\left[[C][C]^{T^*}+\beta[I]\right]\{F_c\}^*\end{aligned} \tag{96}$$

where $[I]$ is the identity matrix of dimensions $(N_c \times N_c)$.

The optimal control forces are now given by :

$$\{\overline{F}_c\} = \left[[C][C]^{T^*}+\beta[I]\right]^{-1}[C]^T[D]\{F_d\} \tag{97}$$

Figure 6 shows the influence of the parameter β on the control effort and on the control efficiency (pressure reduction). In that case, the pressure radiated by a 4-mount system at 242 Hz was reduced in the direction $\theta = 60°$. The graph shows the level of pressure reduction versus the control effort required to achieve this pressure drop for different values of the β. Small values of β tend to give a high level of control on the quantity E to be minimized (the pressure) but with a high control effort. Even smaller values yield to singular matrices and the results are not significant. Large values of β yield a smaller control effort, but achieve very little reduction of the pressure. Looking at the scales, it can be observed that a small variation of the control effort gives a considerable change in the control efficiency (pressure reduction). Therefore, β should be taken as small as possible to obtain a high control efficiency, but still large enough for the control matrix not to be singular. In the simulations performed in section III, the smallest value of the matrix $[C]^T[C]$ was first evaluated. Then, β was chosen such as to render $\left[[C][C]^{T^*}+\beta[I]\right]$ invertible considering that the smallest value that yield invertible matrices in Matlab [47] is 10^{-16}.

Chapter III

Simulations

This section presents simulations of the acoustic radiation of the system in the far-field which were performed using a program written in Matlab code [47]. This program computes the far-field pressure radiated from the cylindrical shell in response to a point-force excitation on the rigid plate. The sound pressure (in decibels) is shown in the half-plane corresponding to $\phi = 0$ and $\theta > 0$ (in the spherical coordinate system) at a distance $R = 10\,\mathrm{m}$. As seen in section II.5, the stationary-phase approximation requires that the pressure be expressed in a spherical coordinate system which is different from the cylindrical coordinate system of Figure 3.

We will first study the coupling between the plate and the cylinder, i.e. how the location of the disturbance on the plate, the number of active-passive mounts and the points of attachment of the active-passive mounts both on the plate and on the cylinder changes the forces transmitted from the receiving structure (the plate) to the radiating structure (the cylinder), and thus changes the pressure field radiated from the cylindrical shell. Then the influence of the characteristics of the plate, the cylinder and the active-passive mounts on the sound pressure radiated will be discussed. Finally, the different control approaches presented in sections II.6.2. to II.6.6. will be compared and discussed.

Except for section 3.5. where the parallel and opposed active-passive mounts configurations will be compared, the system has 8 active-passive mounts configured in parallel (see section II.1.3.). The points of attachment of the active-passive mounts on the cylinder and the plate are given in Tables 5 and 6 respectively. The specifications of the

plate, cylinder and passive mounts are given in Tables 1, 2 and 7 respectively. These are the parameters used for all the simulations except where notified. The disturbance F_d has an amplitude of 10N which yields a satisfactory level of radiation in the far-field. It is applied at the point of coordinates $(x = L_p/10, y = w_p/10)$ in the plate coordinate system of Figure 2. This point is close enough to the center of the plate to have a fair distribution of the energy in the mounts. However, the difference in the amplitude of the forces in the mounts will produce a dissymetrical radiation pattern.

1. Coupling

In this part, the influence of the coupling between the raft (rigid plate) and the cylinder on the cylinder radiation will be studied. The coupling of the raft alters the cylinder dynamics : the raft applies forces through the isolators and the damping in the passive components of the mounts changes the vibration of the cylinder.

The influence of the number of active-passive mounts, their locations on the transmitting and receiving structures, and the location of the disturbance on the transmitting structure will be discussed. The radiation of a cylinder excited by a point force will be compared to the radiation of the coupled plate-cylinder system with different layouts of mounts so as to understand how the coupling with the plate modifies the radiation of the cylinder.

1.1. Influence of the number of mounts

The position of the mounts on the raft of the coupled raft-cylinder system is shown in Figures 7, 8 and 9 for 4, 6 and 8 mounts, respectively, along with the raft coordinate system.

The acoustic radiation from the coupled raft-cylinder systems with 4, 6 and 8 mounts are shown in Figures 10, 12, and 14 respectively. For this study, the excitation at 242 Hz corresponds to the resonance frequency of the mode (2,2) of the cylindrical shell (see Tables 3 and 4). For a mode (m,n), the first index, m, refers to the longitudinal mode number and the second, n, to the circumferential mode number. The disturbance is located at the point of coordinates $\left(x = L_p / 3, y = w_p / 3\right)$ on the plate and has an amplitude of 10N.

The system with 8 mounts, Figure 10, has a maximum acoustic radiation level of 52 dB , whereas the systems with 4 mounts, Figure 14, and 6 mounts, Figure 12 have a maximum level of 63 dB.

Looking at the modal decomposition of the radiation in the direction $\theta = 70°$, it can be observed that the distribution of the energy among the modes is not the same for the different mount layouts. The dominant mode remains the (2,2) mode. As can be seen in Figures 15 for the 4-mount system, and Figure 13 for the 6-mount system, the (2,2) mode is 20 dB higher than the (2,3), (2,4) and (1,4) modes which resonates at 196.3 Hz, 279.8 Hz and 254.3 Hz, respectively. For the 8-mount system, Figure 11, the (2,4) mode is only 5 dB lower than the (2,2) mode. The modal decomposition for the 4-mount and 6-mount systems is typical of an excitation on-resonance since one mode contributes for the most part of the radiation. In the case of the 8-mount system, two modes contributes almost equally to the radiation, as if the excitation was off-resonance.

But as will be discussed in section 1.3., not only the number of mounts, but also the layout of the mounts has a significant influence on the level of the acoustic radiation and in the directivity pattern. Changing the number of mounts in the system implies that the points of attachment of the mounts on both the transmitting and receiving structure be modified. Therefore, the eigenproperties of the system will be changed.

1.2. Frequency response of the system

In this section, the sound pressure radiated from a cylinder excited by a point force (which will be referred to as the uncoupled cylinder) is compared to the radiation of the coupled plate-cylinder system when the plate is excited by a point force disturbance.

The uncoupled cylinder is excited by a point force of amplitude 10N directed along the z-axis of the plate (and therefore with both a radial and circumferential component, see section II.1.3.) and was located at the point of coordinates $(z = .62L_c, \phi = 126°)$. The coupled raft-system has 8 mounts and is excited by a point force disturbance of amplitude 10N at the point of coordinates $(x = L_p/3, y = w_p/3)$ on the plate.

Figures 16 and 17 present the pressure radiated form the uncoupled cylinder and the coupled raft-cylinder system respectively in the direction $\theta = 45°$ as a function of the frequency of excitation, i.e. the frequency response at $\theta = 45°$. Figures 18 and 19 show the frequency response at $\theta = 60°$, and Figures 20 and 21 at $\theta = 90°$. It is necessary to look at different directivity angles θ since some modes will have notches (minima) in the radiation pattern at particular angles therefore giving no information on their contribution to the radiation. For example, the modes with a longitudinal mode number (m) equal to 3 will have a notch in the direction $\theta = 60°$.

The amplitude of the response of the uncoupled cylinder and of the coupled raft-cylinder system cannot be compared since the excitations are different, but the relative amplitudes of the resonance peaks are a good clue to understand how the plate coupling affects the radiation of the cylindrical shell.

Comparing Figures 18 and 19, it appears that the resonances are less pronounced for the coupled raft-system. The uncoupled cylinder has high level peaks at its resonance and a low level of radiation off-resonance. On the contrary the coupled plate-cylinder system has a high level of radiation off-resonance. As mentioned in the previous section, the multiple excitation applied to the cylindrical shell in the case of the coupled plate-cylinder system enable to excite a larger number of modes than the uncoupled shell. The resonance peaks in the former case will not be as high as in the latter, but the radiation level off-resonance will be higher. Also, high damping in the coupled system at some modes will result in modal coupling.

Looking at the radiation of the coupled plate-cylinder system in Figures 21, 17 and 19 shows that the response of the low frequency modes is much higher than the high frequency modes. The amplitude drops dramatically after 300 Hz. The uncoupled cylinder, on the other hand, has modes at higher frequencies that still radiate at a level comparable to the low frequency modes. The mode (1,6) at 694 Hz, for example, is at a level comparable to the (2,3) mode at 196 Hz in the case of the cylinder, but it is 40 dB lower in the case of the coupled system.

The damping effect in the passive mounts is more efficient at higher frequencies since the energy dissipated in the dampers is proportional to the frequency. However, the modal density (number of mode in a given range of frequency) is much higher in the high frequency range as can be seen in Tables 3 and 4, and a large number of modes will contribute to the radiation of the coupled plate-system.

This has important consequences for the control of the radiation of the system. Since the radiation level at high frequencies is low, it is expected to be controlled more easily. On the other hand, the low frequency range will require more control effort to obtain satisfactory results.

1.3. Layout of the mounts

The layout of the mounts on the cylinder is very important and has a high influence on its radiation. Both the longitudinal (z) and the circumferential coordinate (ϕ) of the point of attachment of the mount on the cylindrical shell are critical parameters to the system radiation.

1.3.1. Longitudinal coordinate of the attachment point of the mounts on the cylinder

Figures 22 through 27 show the radiation of the system in the far-field and the modal decomposition of the sound pressure radiated by the coupled plate-cylinder system for different layouts of a system with 2 rows of 3 mounts symmetrical with respect to the (x,z)-plane of the cylinder. The layout of the mounts on the plate is shown on Figure 8.

The modal decomposition bar-graph shows the contribution of each mode (m,n) to the pressure radiated at the point of coordinates . Each box corresponds to a longitudinal mode number m. The circumferential mode number n is on the horizontal axis, and the pressure amplitude (in decibels) on the vertical axis.

The mounts are laid on the cylinder in the configurations shown in Table 8. The plate is excited by a point force located at coordinates $\left(x = L_p / 3, y = w_p / 3\right)$ at a frequency of 303 Hz which corresponds to the (3,3) mode resonance.

The modal decomposition shows that the system configuration A, Figure 23, does not allow excitation of the longitudinal mode $m = 3$ since the forces act at its nodes of vibration. On the contrary, the modal response of the system configurations B, Figure 25, and C, Figure 27, is mainly due to the vibration of the mode (3,3) with respectively 28 dB and 34 dB. The latter cases also give a higher radiation for the (4,3) and (4,4) modes with 20 dB compared to 10 dB in the former case.

The major implication of these results is that the longitudinal position of the mounts (position along the z-axis of the cylindrical shell) has a dramatic influence on the sound pressure radiated from the system. This enables excitation or cancellation of selected modes by placing the mounts on their nodes or on their anti-nodes of vibration. Canceling or reducing the contribution of the dominant mode does not necessarily yield a reduction of the sound pressure level as seen on Figures 22, 24 and 26 where the maximum pressure is 40 dB in all cases. However, the radiation in some directions of the radiating space can be favored (and therefore reduced in other directions) by placing the mounts so as to excite selected modes. For example, exciting even longitudinal modes ($m = 1, m = 3, \ldots$) will yield a minimum pressure level in the mid-plane directions whereas odd modes ($m = 2, m = 4, \ldots$) will have a maximum in this direction.

1.3.2. Circumferential coordinate of the mounts on the cylinder

Figures 28 through 31 show the radiation of the system with 8 mounts at different frequencies and for different layouts of mounts. The circumferential coordinate of the

point of attachment of the mounts on the cylinder is respectively $\phi = 120°$, $\phi = 135°$ and $\phi = 144°$. Changing this parameter does not only change the location of the forces applied to the structure, but also changes the relative amplitude of the radial and circumferential component of the force. The radiation of the cylinder is due to its radial displacement only, therefore, changing ϕ yields a change in both the radiation pattern and level. Since all the forces are directed along the z-axis of the plate (vertical direction), the smaller ϕ, the smaller the radial component, and therefore the smaller the radiation level. Moreover, the layout of the mounts will tend to favor the radiation of some particular modes. For example, two rows of mounts at $\phi = -120°$ and $\phi = 120°$ will tend to favor the excitation of modes of circumferential order $n = 3$ since the two maxima will be separated by an angle of 120°. Therefore, the modes with a circumferential mode number of $n = 3$ will prevail in the radiation. Two rows of mounts at $\phi = -135°$ and $\phi = 135°$ will make the system radiate like a quadrupole (modes of circumferential order $n = 4$); and at $\phi = -144°$ and $\phi = 144°$, the modes of circumferential order $n = 5$ will be excited.

In contrast to the longitudinal coordinate, there is no boundary condition on the circumferential coordinate. In the former case, some modes could be inhibited by placing forces on or close to their nodes of vibration ; in the latter case, the acoustic field will just be rotated, the maximum of vibration being at the location of the forces.

Figure 28 shows the radiation at 303 Hz, resonance frequency of the mode (3,3), for the three different angles ϕ. The radiation level is lower for $\phi = 120°$, than for $\phi = 135°$ and $\phi = 144°$ as expected. Also, the radiation patterns of the latter cases are very close whereas the radiation of the former has a deeper notch in the mid-plane direction and has side lobes of considerably smaller amplitude. Its radiation pattern is therefore more like a dipole type and receives a large contribution from the (2,4) mode which has a resonance at 280 Hz. Looking at the amplitude of the forces in the mounts reveals that they are not

significantly (1 to 2%) changed by the modification of ϕ. However, if the amplitude of the forces is not changed significantly when ϕ varies, the radial and circumferential contributions of theses forces change. This is why the sound pressure level is lower for $\phi = 120°$, for example.

Figure 29 displays the radiation of the 8-mount system at 242 Hz and shows only a variation in the level and not in the pattern for the different values of ϕ because no mode has a resonance close enough to 242 Hz to be excited.

The radiation at 516 Hz, resonance frequency of the mode (5,4) and (4,5) is a more interesting case since the three radiation patterns are very different (Figure 30). For $\phi = 120°$, it is characteristic of a longitudinal odd mode, with a lobe in the mid-plane direction and two notches at $\phi = 60°$ and $\phi = 120°$, therefore, the mode (5,4) contributes more to the radiation. When $\phi = 135°$, there is no lobe in the mid-plane direction, therefore indicating an even longitudinal mode, here the mode $m = 4$, and the mode (4,5) dominates over the mode (5,4). If $\phi = 144°$, the lobe in the mid-plane direction is present, although "shifted" from 90° to 93°, indicating that the mode (5,4) prevails.

The radiation off-resonance at 420 Hz, Figure 31, displays different patterns. Even though the lobes and the notches are at the same angles, the radiation occurs mainly around $\phi = 60°$ and $\phi = 120°$ for the mounts laid at $\phi = 120°$, and around $\phi = 90°$ for $\phi = 135°$ and $\phi = 144°$.

Although all show different results, what is apparent from these four simulations is that the layout of the mounts has a dramatic influence on the radiation pattern. If the disturbance, and particularly its amplitude, is known, the mounts can be laid in a way such as to favor the radiation of some modes versus the radiation of others.

1.4. Location of the disturbance on the plate

Figures 32 and 33 show the influence of the location of the disturbance on the plate at 242 Hz and 303 Hz respectively. The further the disturbance from the center of the plate, the larger the displacement of the plate, and therefore, the larger the forces transmitted by the passive components of the mounts. Also, the location of the disturbance on the plate has a significant influence on the radiation pattern since it will put larger forces on some mounts than on others and therefore favor the radiation in some particular direction of the acoustical field. Changing this location can, for example, slightly shift the angle of lobes and notches, or change the radiation level in some particular directions. As seen in Figure 33, the radiation pattern is different when the disturbance is at $x = -L_p / 3, y = w_p / 3$ and at $x = L_p / 3, y = w_p / 3$.

2. Plate, cylinder and mounts characteristics

This part aims to show the influence of the characteristics of the three sub-structures in the coupled raft-system : the rigid plate, the elastic cylinder and the passive components of the mounts.

2.1. Thickness of the raft

Figure 34 shows the influence of the thickness of the raft (rigid plate) on the acoustic radiation from the system excited at 280 Hz. This parameter does not have a significant influence on the directivity pattern, but rather on the radiation level. The thinner the plate, the more displacement is obtained for a given disturbance on the plate. A light plate will

have less inertia than a heavy plate and thus will be set into motion more easily. The forces in the mounts are larger in that case since they are proportional to the relative displacement between the raft and the cylinder. Thus the forces acting on the cylindrical shell will be larger for thin plates giving a larger radiation level from the structure.

2.2. Stiffness of the mounts

Changing the stiffness of the mounts, Figure 35 will change only the radiation amplitude. An increase of the stiffness will increase the forces in the mounts in the same proportion since those are proportional to the stiffness.

The resonance frequency of the plate-passive mounts system (35 Hz) is not high enough to have an influence on the coupling. The first resonance of the cylinder is that of mode (1,2) at 87 Hz. The coupled resonance is not in the range of interest, as far as the resonance of the radiating structure (cylindrical shell) is concerned. This means that the system will resonate at the resonance frequencies of the uncoupled cylindrical shell, and there will not be any coupled resonance frequency.

2.3. Damping ratio in the mounts

The damping ratio in the mounts is defined as $\eta = \omega C_a / K_a$ where C_a is the damping, ω the angular frequency and K_a the stiffness constant. Figure 36 shows the radiation at 242 Hz after dividing the assumed damping ratio by 2 or multiplying it by 5. The radiation increases as the damping ratio decreases. Less energy is dissipated in the mounts and therefore the forces acting on the radiating structure are larger. At 303 Hz, Figure 37, the radiation undergoes very little change when the damping ratio is reduced by a factor of 2.

For higher frequencies, however, the behavior of the system is different. Increasing the damping ratio will increase the radiation of the structure. By definition, the damping ratio is frequency dependent. Moreover, it is a linear function of the frequency. At high frequencies, the forces in the dampers overcome the forces in the springs. They no longer dissipate energy, but carry energy from the plate to the cylindrical shell. This results in a dramatic increase of the pressure level, as can be seen in Figure 38 where, at 1020 Hz, close to the resonance frequency of the mode (6,7), the level of the main lobes increases of 10 dB when the damping ratio is multiplied by 5, and the amplitude of the forces in the mounts is increased by a factor of 3. However, if on the contrary the damping ratio is decreased by a factor of two, the forces in the mounts undergo very little change (10% approximately) and the radiation is not consequently modified. Therefore, increasing the damping in the structure is not always a valid method to reduce the radiation of the system. These results show agreement with those of Pan and Hansen [1]. They developed a model for a coupled rigid body-intermediate flexible panel-flexible cylinder where the panel and the cylinder where coupled via passive isolators. They showed that the use of passive isolators result in an increase of the vibration transmission at high frequencies.

Off-resonance, at 220 Hz, Figure 39, increasing the damping in the passive mounts decreases the level of radiation from the coupled raft-cylinder system. However, the reduction of the pressure level is not uniform over the pressure field. The peak reduction, 8 dB, is close to the mid-plane direction ($\theta = 90°$). Over most of the pressure field, no reduction is achieved and the damping is an inefficient method to significantly reduce the radiation.

Results for off-resonance cases at higher frequencies are similar to the results for on-resonance case, i.e. an increase in the radiation level.

2.4. Thickness ratio of the cylinder

The thickness ratio of the cylinder is a very important parameter. Cylinders with a ratio smaller than 0.05 are considered as thin shells [25] and the method used to derive the expression for the vibration of the cylindrical structure is only valid for thin shells. The values considered here are all below this "critical value". Figure 40 shows that changing this value changes the radiation dramatically. The pattern is the same, but the relative amplitude of the lobes is different. Looking at the modal decomposition would show a dominant (2,4) mode at 40 dB in all cases. For $h_c / r_c = .03$, the modes (4,4) which resonates at 322 Hz, (5,4) at 418 Hz and (2,6) at 368 Hz contribute respectively for 10 dB, 7 dB and 20 dB to the radiation at 100°. These modes are absent from the radiation when $h_c / r_c = .04$ or .05. This shows that for thinner shells, modes whose resonance frequencies are as much as 100 Hz apart from the frequency of excitation can contribute significantly to the radiation. Only for $h_c / r_c = .05$ does the mode (3,3), which resonates at 303 Hz, contribute to the radiation at 100° with an amplitude of 20 dB.

When the thickness ratio changes, the contribution of the different modes to the structure is different. The resonance frequencies are not the same and the modes do not appear in the same order (although the modes (1,2) and (1,3) always appear first). The thinner shells have lower fundamental frequencies. In this particular case, they had a higher modal density around the frequency of excitation (303 Hz), which explains why the radiation patterns were more complex.

At higher frequencies, above 700 Hz, the resonance frequencies are very close for the three different thickness ratios and the radiation patterns are very similar.

3. Control

The aim of this section is to show how the radiation of the cylinder can be controlled using different active control methods. Different approaches have been presented and discussed in section II.6.2. through II.6.6.

Active Structural Acoustic Control techniques (as defined in section II.6.1.) will first be applied to the coupled plate-cylinder system. They use the control forces of the active-passive mounts in the system to control acoustic quantities such as the acoustic pressure in one or several directions (section II.6.2), the total acoustic power radiated from the structure (section II.6.3.), or the acoustic pressure evaluated with components associated with circumferential modes (section II.6.5.). Then Active Vibration Control (as defined in section II.6.1., and discussed in section II.6.6.) of the system will be discussed. This approach uses the active components of the mounts to minimize the radial displacement at selected locations on the radiating structure. Finally, two active-passive mounts configurations will be compared. The first configuration uses control forces in parallel with the passive components of the mounts and the second, control forces in opposition (as defined in section II.1.3.)

The different control approaches will be compared according to two criteria : the control efficiency and the control effort required. The control efficiency will be defined as the ability of the control approach to perform the control, i.e. to minimize the quantity used to evaluate the cost function. For example, if the pressure is to be minimized over the whole pressure field, a technique leading to a 5 dB global control will be considered more efficient than a technique yielding 20 dB reduction in one region of the sound field, and no reduction in other regions. If the cost function is defined as the pressure in a selected direction of radiation, a technique yielding total control in that particular direction will be

considered very efficient even though the pressure level is amplified in other directions of minimization. Another technique leading to global control but still having pressure radiated in the direction of minimization will be inefficient in this case. The control effort is defined as the square root of the squared amplitudes of the control forces applied to the system :

$$e = \sqrt{\left(\left(f_c^1\right)^2 + \left(f_c^2\right)^2 + \ldots + \left(f_c^{N_c}\right)^2\right)} \tag{98}$$

The control effort has the dimension of a force and is therefore expressed in Newtons. It evaluates the amount of force put into the active mounts to achieve the control. If two active control techniques yield the same control efficiency, i.e. have the same pressure after control, the approach that requires the less control effort is the more suitable.

3.1. Control of the radiation in one particular direction

In this section, active control of the pressure radiated by the coupled plate-cylinder system in one particular direction θ will be performed. This control approach is defined in section II.6.2.

First, the uncontrolled radiation of the coupled plate-cylinder system is performed. The only forces acting on the system are then : the disturbance F_d and the forces in the passive mounts F_a. The cost function is then calculated as the pressure at the point of coordinates $(R, \theta, \phi = 0)$ in the radiation half-plane. The angle ϕ is equal to zero since all the radiation plots are shown for this particular radiating plane. The distance R from the center of the coordinate system, Figure 3, is large enough to be in the far-field, $R = 10\text{m}$. The angle θ is the angle of minimization, i.e. the pressure after control will be minimized

in the particular direction $(\theta, \phi = 0)$ of the pressure field. The optimal control forces, $\overline{F}_c$, are calculated according to Equation (79). Now, the controlled radiation is performed with F_d, F_a and $\overline{F}_c$ acting on the system.

The plots in this section show both the uncontrolled and the controlled radiation of the coupled plate-system excited by a point-force disturbance of 10 N at the point of coordinates $(x = L_p/10, y = w_p/10)$ on the plate. The sound pressure amplitude is in decibels. The dash-dotted straight line indicates the direction of pressure minimization. The forces on the system are show before and after control. The index of the forces refers to the index on Figure 9, which is the number of the active-passive mounts. The forces in the mounts are shown for the uncontrolled case (u) and for the controlled case (c). The amplitude of the forces is in Newtons and the phase of the forces, in radians, is shown between parenthesis. The control effort, previously defined, is also in Newtons.

Figure 41 shows the radiation for the system with 8 active mounts at 242 Hz, resonance frequency of the mode (2,2), without and with control in the direction $\theta = 60°$. There is no radiation in this particular direction after control, giving a local 52 dB reduction. Overall, the radiation is reduced from 0 to up to 40 dB at $\theta = 30°$ and 150°. In the directions of radiation $\theta = 90°$ and 135°, the pressure level after control is higher than the pressure level before control. This is called spillover. The optimal control forces are chosen so as to minimize the pressure in one particular direction and the pressure in other directions is not taken into account. The particular angles $\theta = 90°$ and 135° are bearing directions of the notches in the directivity pattern of the uncontrolled system. However, the spillover is not greater than 5 dB.

Also shown on Figure 41 are the amplitude and phase of the control forces and of the forces in the mounts for the uncontrolled (u) and controlled (c) system respectively. Figure 9 shows the mounts layout on the plate and their respective number corresponding

to the number of the forces in Figure 41. The forces in the mounts are 3 to 6 times smaller when the system is controlled and this is why the sound pressure is globally reduced. The amplitude of the control forces is comparable to that of the forces in the passive mounts after control, but the phase is different. The contribution of the two sets of forces tend to interact destructively. Moreover, before control, the forces in the mounts are almost symmetrical with respect to the x- and y-axes of the plate and the pairs of mounts (1,5), (2,6), (3,7) and (4,8) are almost in phase and have comparable amplitudes. After control, the symmetry is broken so as to minimize the radiation at 60° and the pairs of mounts (1,5) and (2,6) do no longer vibrate in phase nor have comparable amplitudes. The forces in the mounts have been redistributed so as to reach local minimization in the direction $\theta = 60°$. This example shows that the control forces act in two ways. By reducing the amplitude of the forces in the mounts, they reduce the global level of radiation. By redistributing the forces in the mounts, they produce a local (selected) minimum.

The radiation is minimized in one direction only with eight control forces. This means that the system is underdetermined. The algorithm used here is therefore the one derived by Nelson et al [46] and explained in section 6.7. In that section, we discussed the value of the parameter β which acts as a balance between minimizing the sound pressure radiated and the amplitude of the control forces. Here, β is chosen so as to obtain maximum pressure reduction in the direction $\theta = 60°$. It is chosen as small as possible, but still large enough so that the matrix $\left[[C][C]^{T^*} + \beta[I]\right]$ be invertible (see section II.6.7.). A good way to ensure that this will occur is to chose β as a function of the minimum of the matrix $[C][C]^{T^*}$. In all the simulations performed, β was taken as 10^{-16} times this maximum value. The control effort is minimized, which means that the control forces are chosen so that their amplitude is as small as possible.

Now, the influence of the number of active mounts in the system on the control efficiency is studied. Figures 42 and 43 display the controlled and uncontrolled radiation of the system with respectively 6 and 4 mounts, for an excitation frequency of 242 Hz, resonance frequency of the mode (2,2). The corresponding mounts layout are show on Figures 8 and 7. The two systems undergo the same disturbance as in the case of Figure 41. The comparison of these three figures shows that the control is more easily achieved with a higher number of mounts since the control effort is considerably smaller for the 8-mount system. For a large number of mounts, the control is very directive (achieved principally in the direction $\theta = 60°$) whereas it is global for fewer mounts. A large number of control forces enable to redistribute the forces on the radiating structure in order to minimize the desired quantity only. A small number of control forces will result in a global reduction by destructive interaction with the forces in the passive mounts. This is why the amplitude of the control forces will be higher for a small number of active-passive mounts.

Figures 44 and 45 show the directivity pattern of the plate-cylinder system controlled in the directions $\theta = 60°$ and $\theta = 90°$ respectively, for a frequency of excitation of 516 Hz, corresponding to the resonance of both modes (4,5) and (5,4). Figures 46 and 47 show the modal decomposition of the sound pressure radiated by the plate-cylinder systems first uncontrolled, then controlled at the points of coordinates , and respectively.

Figures 46 and 47 show that the radiation of the uncontrolled plate-cylinder system is mainly due to the contribution of the modes (2,1) which resonates at 468 Hz, and (5,4) which resonates at 516 Hz. After control in the direction $\theta = 60°$, the contribution of the mode (5,4) increases in the same time that the contribution of the mode (2,1) decreases. The controlled radiation is also characteristic of the modes having a longitudinal mode number $m = 5$, with a main lobe in the mid-plane direction and two notches at

$\theta = 60°$ and 120°. In contrast, when the control is achieved at $\theta = 90°$, the mode (5,4) ceases to contribute to the radiation and the radiation pattern is of a dipole type. The control effort is very low in both cases (as compared to that of Figures 41 through 43, for example) and the forces in the mounts are very slightly changed by the control. The global radiation level is not changed significantly, but the radiation pattern is totally different. The control forces have favored one of the contributing modes to achieve control in the desired direction by redistributing the amplitude of the forces in the active-passive mounts instead of reducing globally the level of sound pressure as in the case of Figures 41 through 43. At 516 Hz, two modes contribute to the radiation whereas at 242 Hz, the mode (2,2) is strongly dominant and the mode(1,4) contributes for a small part to the radiation. Therefore, when a single mode dominates the radiation, applying control will yield total radiation control and the control effort will be larger.

In some other cases, there is only one mode contributing significantly to the radiation. For example, at 87 Hz, which is the resonance frequency of the mode (1,2), minimizing in the mid-plane direction yields to global and total control over the sound field, Figure 48. No even longitudinal mode (characterized by a notch at $\theta = 90°$) has its resonance frequency close enough to 87 Hz to obtain a mode restructuration as for the previous cases at 516 Hz. The modes having a resonance close to 87 Hz are the modes (1,1) and (1,3) which also have a maximum of radiation in the mid-plane direction.

3.2. Control of the radiation in several directions

In this section, the radiation of the coupled plate-cylinder system is control in several directions of the radiating half-plane. As discussed in section II.6.2, the cost function is now the sum of the pressures at the points of coordinates $\left(R, \theta_p, \phi = 0\right)$ where $p = 1...P$,

and P is the number of directions where the pressure will be minimized. The distance R is still chosen so as to be in the far-field.

Figure 49 shows the radiation of the coupled plate-cylinder system first uncontrolled, and then controlled in the two directions $\theta = 50°$ and $\theta = 130°$. The control leads to a global reduction of the pressure level, whereas control in one direction, Figures 44 and 45, lead to a very directive reduction. The forces in the mounts are not significantly changed. The control effort is not a lot higher than for the minimization in one direction only, Figure 44, but yields a much more satisfactory result.

Figure 50 shows the radiation with control in the three directions $\theta = 37°$, $\theta = 90°$ and $\theta = 143°$. The control seems less efficient than in the previous case since the overall reduction is lower, although the control effort is higher. In fact, minimizing the pressure in the mid-plane direction cancels the whole contribution of the mode (5,4), thus the control effort is high. This shows that the choice of the direction(s) of minimization has a dramatic influence on the efficiency of the control.

Figure 51 shows the radiation of the same coupled plate-cylinder system excited at 516 Hz with control in the four directions $\theta = 30°$, $\theta = 70°$, $\theta = 110°$ and $\theta = 150°$. This case yields a global and total reduction of the sound pressure field. The control forces and the forces in the passive mounts after control are almost of equal magnitude but opposed phase, and therefore they cancel each other. No force is transmitted to the cylinder, and thus the disturbance does not create any radiation from the cylindrical shell. The control effort is higher than in the other cases, but is still low (0.3755 N) compared to the amplitude of the disturbance (10 N).

The same four directions of control lead to a global reduction of the sound field at 1020 Hz (off-resonance), Figure 52. The control effort is very low since the uncontrolled radiation level is low as well. The forces in the passive mounts undergo very little change when then control is applied.

Other simulations show that the radiation can be totally controlled for any frequency by minimizing the pressure in four directions, but that the control effort required to achieve the global control is much higher when a single mode contributes mainly to the radiation. When several modes contribute to the radiation, the dynamics of the system after control are altered so that the modes phases are changed (in term of radiation) and the modes interact destructively. When one mode only contributes significantly to the radiation, the boundary conditions of the structure are changed, which requires considerably less effort.

3.3. Active Vibration Control

The results obtained with the Active Structural Acoustic Control (ASAC) approaches will here be contrasted to those of Active Vibration Control (AVC), as defined in the introductory part of section II.6.1. In the latter case the radial displacement of the radiating structure is minimized at selected points. In the following simulations, the displacement of the cylindrical shell is minimized at the location of the mounts which are the only points on the structure to undergo an excitation. Since the passive mounts and the control forces are collocated to form the active-passive mounts, the displacement of the whole cylinder and thus its acoustic radiation in the far-field are expected to be, if not canceled, dramatically reduced. A trivial solution to the vibration isolation problem is to

cancel the vibrations by the mean of control forces having equal amplitudes as the forces in the passive mounts, but opposed phase.

First, the ability of ASAC and AVC to perform the control of the radiation from the coupled plate-cylinder system will be compared, then we will discuss the control effort required by each approach to perform the control. Since the Active Vibration Control reduces the vibrations in the structure, and therefore performs a global control of the radiation, it should be contrasted to an Active Structural Acoustic Control approach that minimizes the pressure field globally as well. This is why the performance of AVC at the location of the active-passive mounts will be contrasted to ASAC in several directions of the radiating space as defined in section III.3.2.

Since the exact collocation of the passive-mounts and of the control forces is practically impossible to achieve, we will also discuss the case where the control forces are slightly apart from the passive mounts. The error in the collocation of the active-passive mounts is defined as

$$e_c = \frac{d_a}{2\pi a} \times 100 \tag{99}$$

where d_a is the offset of the mounts.

All the simulations in this section apply to a coupled plate-cylinder system with 8 mounts, excited by a point force disturbance located at the point of coordinates $(x = L_p/10, y = w_p/10)$ on the plate.

At 303 Hz, resonance frequency of the mode (3,3), the Active Vibration Control at the point of attachment of the mounts on the cylinder, Figure 53, and the Active Structural Acoustic Control in the four directions $\theta = 30°$, $\theta = 70°$, $\theta = 110°$ and $\theta = 150°$, Figure 54, give both a global and total control of the radiation from the coupled plate-

cylinder system in the far-field. The two control approaches lead to the same control forces distribution and therefore to the same result. The control effort is also the same in both cases. However, if the control forces and the passive mounts are not collocated, i.e. the offset of control forces with respect to the passive mounts in the direction of the z-axis of the cylinder is d_a=0.01m and e_c=0.2%, the AVC, Figure 55, yields a global but not total reduction of the pressure field. The overall reduction is approximately 12 dB. In the case of ASAC, the offset of the control forces does not yield any change in the control performances, and the radiated pressure is canceled. If e_c=0.5%, Figure 56, the AVC efficiency is even more impaired and the global reduction is only 6 to 10 dB. The control effort is not significantly changed by the delocation of the control forces. If e_c=2%, which is high but still realistic, the control yield spillover in most of the pressure field, Figure 57.

This shows that the efficiency of AVC is comparable to that of ASAC -in term of radiated pressure reduction- only when the control forces and the passive mounts are exactly collocated.

AVC for collocated active-passive mounts, Figure 58, and ASAC in four directions, Figure 59 give the exact same result in term of sound pressure reduction an in term of control effort at 242 Hz, the resonance frequency of the mode (2,2). When e_c=0.2%, Figure 60, or e_c=0.5%, Figure 61, the AVC does not yield total pressure control. However, the pressure after control is very low, and an overall reduction of 40 or 30 dB is achieved, the control effort remaining the same as for the collocated mounts.

At 180 Hz, the resonance frequency of the mode (1,1), the AVC for collocated active-passive mounts, Figure 62, and the ASAC, Figure 63, also give the same results. The delocation, as in the previous case, has little effect on the control efficiency as shown in Figure 64, for e_c=0.2%. The global pressure reduction is 40 dB. When the frequency is

low, the offset becomes smaller compared to the wavelength and the effect of the offset is reduced.

Off-resonance, at 495 Hz, AVC for collocated mounts, Figure 65, and ASAC, Figure 66, achieve the same overall radiation reduction, and now the delocation of the control forces has a lot less influence on the AVC efficiency. Even if e_c=1%, Figure 67, the pressure reduction is total. Moreover, the control effort is decreased as compared to the collocated case. The control forces do no longer need to have the same amplitude as the forces in the passive mounts in order to perform the control. However, if the distance between the passive mounts and the control forces is as large as 0.13m and e_c=3%, Figure 68, the control efficiency is highly impaired. The sound pressure is only reduced by 10 dB locally.

Finally, the Active Vibration Control and the Active Structural Acoustic Control have two major differences :

- the Active Vibration Control is highly sensitive to whether the control forces and the passive components of the mounts are exactly collocated or not. The further apart these components are, the more the control efficiency is impaired.
- the Active Vibration Control yields only global radiation over the complete radiating plane, whereas the different approaches of the Active Structural Acoustic Control can minimize the pressure in selected directions or in selected areas of the radiated pressure field.

3.4. Parallel and opposed active mounts

In this section, two different kind of active-passive mounts will be compared : the parallel active-passive mount and the opposed active-passive mount as defined in

section 1.3. In the first case, the active control forces act both on the raft and on the cylinder whereas they act only on the cylinder in the second case. The two configurations are shown in Figure 4.

Figures 69 through 88 show the behavior of these two methods for different kind of active control, i.e. control in one or several directions of radiation and control of the displacements at the location of the mounts. In this section the coupled plate-cylinder system has 8 active passive mounts and is excited by a point force disturbance located at the point of coordinates $(x = L_p/10, y = w_p/10)$ on the plate.

Figures 69 and 70 show the radiation of the two systems at 242 Hz, the resonance frequency of the mode (2,2). In both cases, the radiation is controlled in the direction $\theta = 110°$, but the opposed system requires more control effort. The control in two directions, Figures 71 and 72 or three directions, Figures 73 and 74 show the same behavior.

Off-resonance, at 350 Hz, Figures 75 and 76, the opposed system does not require more control effort than the parallel system to perform the control in the direction $\theta = 103°$. The only difference between the results of the two cases is a small variation in the amplitude and phase of the forces in the two systems. When Active Vibration Control (see section 3.3.) is applied to the displacement at the location of the mounts, Figures 77 and 78, the opposed system requires slightly less control effort than the parallel system. The amplitude and phase of the control forces are different for the two system although they perform the control with the same efficiency.

On resonance, at 516 Hz the performance of the opposed system is now comparable to that of the parallel system. The control efficiency is the same and so is the control effort for the control in the direction $\theta = 90°$, Figures 79 and 80. As for the off-resonance case, the control of the displacement at the mounts location, Figures 81 and 82, requires less

effort with the opposed system. In fact, several modes are contributing to the radiation at 516 Hz (recall the modal decomposition of Figures 46 and 47) as for the off-resonance cases ; therefore the system, at this frequency, behaves like the off-resonance case.

At low frequency, 180 Hz, resonance frequency of the mode (1,1), the two systems have comparable performances in term of control efficiency and control effort for minimization of the sound pressure in the direction $\theta = 90°$, Figures 83 and 84. The opposed system requires more control effort than the parallel system (3.212 N as compared to 3.204 N) for minimization of the radiation in the four directions $\theta = 30°$, $\theta = 70°$, $\theta = 110°$ and $\theta = 150°$, Figures 85 and 86. However, this difference is very small compared to on-resonance cases at higher frequencies (Figures 69 and 70 or 71 and 72, for example).

Off-resonance, at low frequency (220 Hz), the control in one direction ($\theta = 112°$), Figures 87 and 88, or in four directions ($\theta = 30°$, $\theta = 70°$, $\theta = 110°$ and $\theta = 150°$), Figures 89 and 90, give approximately the same results for the parallel and the opposed active-passive mounts configurations.

These results are consistent with the analysis of Nelson et al. [35]. They compared the performances of parallel and opposed passive-active isolator on a simple two-degree of freedom model. Results showed that the opposed active-passive mounts performances compared well to those of the parallel mounts off-resonance and at low frequencies, but required much more control effort on-resonance. Simulations on the coupled plate-cylinder system showed that control using opposed mounts was as efficient as control using parallel mounts off-resonance (350 Hz and 495 Hz) and at low frequencies (180 Hz and 220 Hz), but had larger control forces on-resonance (242 Hz).

3.5. Control of the radiation by minimization of radiating components associated with circumferential modes

This section presents simulations of the radiation of the coupled plate-cylinder system in the far-field when the pressure sound radiated is controlled by minimizing the radiating components associated with circumferential modes. This approach was defined in section II.6.5.

The cost function is calculated as the sum of the contributions of all the modes of circumferential order $n_1, n_2, \ldots n_N$ which contribute the most to the radiation in the direction θ, i.e. the modes which have a high radiation efficiency. The cost function can take in account one or several circumferential modes n.

The coupled plate-cylinder system has 8 active passive mounts and is excited by a point force disturbance located at the point of coordinates $(x = L_p/10, y = w_p/10)$ on the plate.

At 516 Hz, resonance frequency of the modes (5,4) and (4,5), two modes contribute significantly to the radiation when the system is not controlled as shown in Figure 91 : the mode (2,1) and the mode (5,4). The bar graph shows the modal decomposition of the pressure radiated by the system in a selected direction θ, first for the uncontrolled system, then for the system controlled minimizing selected components. Minimizing the contribution of components associated with the circumferential mode number of order 1 to the acoustic pressure radiated in the direction $\theta = 60°$ cancels the contribution of the mode (2,1). The corresponding radiation plot is shown in Figure 92. This plots show the radiation of the system before and after control of the selected components, which are designated by their associated circumferential mode number n. The dash-dotted line indicates the direction θ of pressure minimization. The plot is similar to that obtained

when all the components were minimized in that direction, Figure 44. The modal decomposition of Figures 46 and 47 showed that the contribution of the mode (2,1) was significantly reduced. If the contribution of the components associated with the circumferential mode number of order 4 is minimized, Figure 91 shows that the contribution of mode (5,4) is significantly reduced and Figure 93 shows the corresponding radiation plot. Again, the plot is similar to that obtained when all the components were minimized in the direction $\theta = 90°$, Figure 45, and the modal decomposition of Figures 46 and 47 showed that the contribution of the mode (5,4) was canceled after control.

This shows that there are different ways of controlling selected modes. They can be canceled using selected components in the evaluation of the cost function. They can also be controlled by minimizing the pressure field in a direction corresponding to a maximum contribution from this particular mode.

Finally, minimizing both components of order 1 and 4 yield total radiation control (not shown).

At 180 Hz, resonance frequency of the mode (1,1), the radiation is dominated by the modes (1,1) and (2,3) as shown by the modal decomposition of Figure 94. When the contribution of components of order $n = 1$ is minimized, Figure 95, the radiation is not very significantly reduced globally. However, the modal decomposition has changed as shown in Figure 94. The mode (1,1) has been reduced by 30 dB. The longitudinal modes of order $m = 1$ do no longer radiate whereas those with longitudinal modes of order $m = 2$ radiate more than before control. Minimizing the contribution of components of order $n = 3$, Figure 96, does not yield to significant change in the radiation level, but changes the modal distribution. In this case, the longitudinal modes of order $m = 1$ radiate more than before control. Finally, minimizing both components corresponding to $n = 1$ and $n = 3$,

Figure 97, yields almost total control of the radiation from the coupled plate-cylinder system in the far-field.

Minimizing selected components does not necessarily yield significant reduction in the radiation level. However, minimizing simultaneously all the components contributing significantly to the radiation ensures total control.

The radiation at 242 Hz, resonance frequency of the mode (2,2), has a main contribution from this mode but also a significant contribution from modes (1,4), (2,3) and (3,4) as seen in Figure 98. Minimizing components of order n=2, Figure 99, or $n=3$, Figure 100, yield significant global control of the pressure field, but minimizing components of order $n=4$, Figure 101, does not yield any reduction of the radiation. However, minimizing the contribution of the modes n=2 and $n=3$ simultaneously, Figure 102 does not yield total control. Total control is obtained only for minimization of the contribution from the three modes n=2, $n=3$ and $n=4$.

As in the case of radiation at 180 Hz, even if the minimization of the components associated with $n=4$ seem to yield no reduction, they must be included in the cost function in order to get total control of the pressure radiated.

Modal decomposition of the radiation from the system excited off-resonance at 495 Hz, Figure 103, shows a dominant mode (2,1) and also contribution from the mode (2,6). This figure also shows that minimizing the contribution of the modes of circumferential order $n=1$ in the direction $\theta=83°$ yield almost total control of all the modes. However, Figure 104 shows that the radiation is only canceled in that particular direction and not over the whole pressure field. In Figure 105, the component of order $n=6$ is minimized. The control yields global reduction. Minimization of the cost function evaluated with both modes of circumferential order $n=1$ and $n=6$ yields total control of the radiation from the structure.

Finally, minimizing the pressure radiated in the far-field by selected components associated with circumferential mode numbers is a good way to ensure total radiation control over the pressure field. However, it requires knowledge of which modes contribute significantly to the radiation. As discussed in section II.6.5., evaluating the derivative of Hankel function in Equation (73) for the pressure radiated in the far-field enables one to see which circumferential modes are likely to radiate significantly. Modal decomposition of the radiation shows the relative amplitude of the modes. However, it is possible that the calculations could be computed in a direction where a major radiating mode has a notch, and thus give no information about the contribution of this particular mode. Nevertheless, once the significant modes are identified, this approach provides good global control, both on and off-resonance, and for any frequency.

Chapter IV

Conclusions

The purpose of this work was to show that control of the acoustic radiation from a coupled plate-cylinder system using active-passive mounts is theoretically feasible. A mathematical description for the sound pressure radiated by the system in the far-field was derived for a point force applied to the transmitting structure (the rigid plate). The pressure at selected points of the sound field was given primarily as a function of the disturbance on the plate and the control forces in the active-passive mounts.

The coupling was first studied by varying the parameters having an influence on the transmission of vibrations from the transmitting structure to the receiving structure (the cylinder), i.e. the location of the active-passive mounts on the two structures, the number of the mounts and the location of the disturbance on the transmitting structure. Significant results were found and discussed :

- The larger the number of active-passive mounts between the two structures, the more cylinder modes are excited for a given disturbance.
- The coupling with the plate was shown to yield a high level of radiation off-resonance, whereas the radiation of an uncoupled cylinder has high peaks on-resonance and a low level of radiation off-resonance.
- The location of the mounts both on the plate and on the cylindrical shell has a dramatic influence on the radiation from the latter structure since some configurations will favor the excitation of particular modes.

- The location of the disturbance on the plate has an influence on the global level of radiation. A disturbance close to the center of the plate will yield a relatively low radiated pressure level, whereas a disturbance close to the edges of the plate will yield higher radiation level. Also, changing the location yields a change in the directivity pattern by placing more energy in some particular mounts and thus exciting some regions of the cylindrical shell more than others.

The characteristics of the different components of the system where then discussed along with their influence on the cylindrical shell radiation, showing that :

- The lighter the transmitting structure, the more the system radiates. However, the weight of the plate does not have any influence on the directivity pattern.
- The stiffness of the passive component in the mounts has an effect on the radiation level. The stiffer the mounts, the higher the radiation level.
- Increasing the damping ratio in the mounts yields a global reduction of the sound pressure level at low frequencies. At higher frequencies, however, the radiation is increased. Therefore, the passive isolation technique has a limited range of application.
- Different thickness ratio of the cylindrical shell yield different radiation patterns. The resonance frequencies are changed and also the modes do not appear in the same order ; thinner shells having a lower fundamental frequency.

Finally, different control approaches were compared in terms of the attenuation of the acoustic field as well as in terms of the control effort. It was found that :

- The control effort is lower when a large number of mounts is used to control the radiation, and also directive control can be enhanced more accurately.

- Active Structural Acoustic Control (ASAC) approaches give good results in terms of reducing the radiation. Total pressure control can be achieved in one selected direction θ of the sound field using the control forces in the active-passive mounts. However, this approach often yields spillover in other uncontrolled regions of the pressure field.
- Control of the radiation in several directions yields good results. When control is performed in a large number of directions, the pressure field is totally minimized.
- Control of the radiation by minimization of radiating components associated with circumferential modes yield good results. This approach enables to obtain total control by minimizing all the modes that radiate significantly. However, it requires that these mode be identified (either by modal decomposition of the radiation or by inspecting the Hankel derivative in the relation for the pressure in the far-field) in order to perform the control.
- The Active Vibration Control (AVC) approach gives results comparable to those of ASAC when the control forces and the passive components of the mounts are perfectly collocated. In that particular case, it yields total control over the pressure field. However, if the control forces are applied at a slightly different location than that of the passive mounts, the results of ASAC are almost unchanged whereas AVC yield global but not total control. In other words, the overall controlled sound pressure level is reduced. The performances of AVC are therefore highly dependent on the active-passive mounts collocation. Moreover, the AVC approach does not allow to perform easily directional control of the radiation whereas ASAC does.
- Parallel and opposed active-passive mounts configuration yield comparable results off-resonance, but the latter requires a much higher control effort than the

former to control the radiation when the cylinder is driven on-resonance. At low frequency, however, the opposed configuration gives slightly better results.

Finally, the Active Structural Acoustic Control approach is to be preferred to the Active Vibration Control approach in our case because the quantity to be minimized is the pressure in the far-field, and also directional control is a very efficient mean of controlling the radiation. Moreover, the active-passive mounts cannot be strictly collocated in practice. The parallel active-passive mounts configuration is also more suitable than the opposed configuration since it will require less effort.

Chapter V

Recommended Future Work

The following investigations could be interesting extensions of this work :

- This study considered a system composed of a rigid plate mounted inside a cylinder of finite length. Considering an elastic plate would be very interesting since it would allow a more complicated type of coupling where the resonance frequencies of the coupled system could be different from the resonance frequencies of the cylindrical shell.
- The active-passive mounts were considered to apply only vertical forces (in the direction of the z-axis of the plate coordinate system, Figure 2). Considering all the possible forces and moments at the two ends of each active-passive (as in [1]) mounts would yield more realistic results.

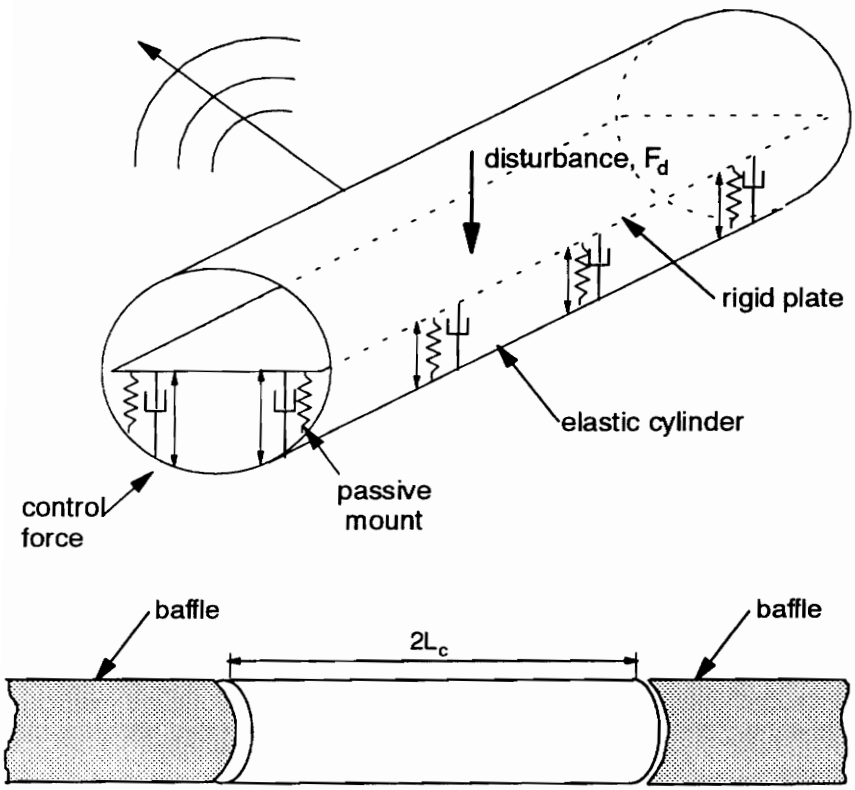

Figure 1 : Coupled raft-cylinder system

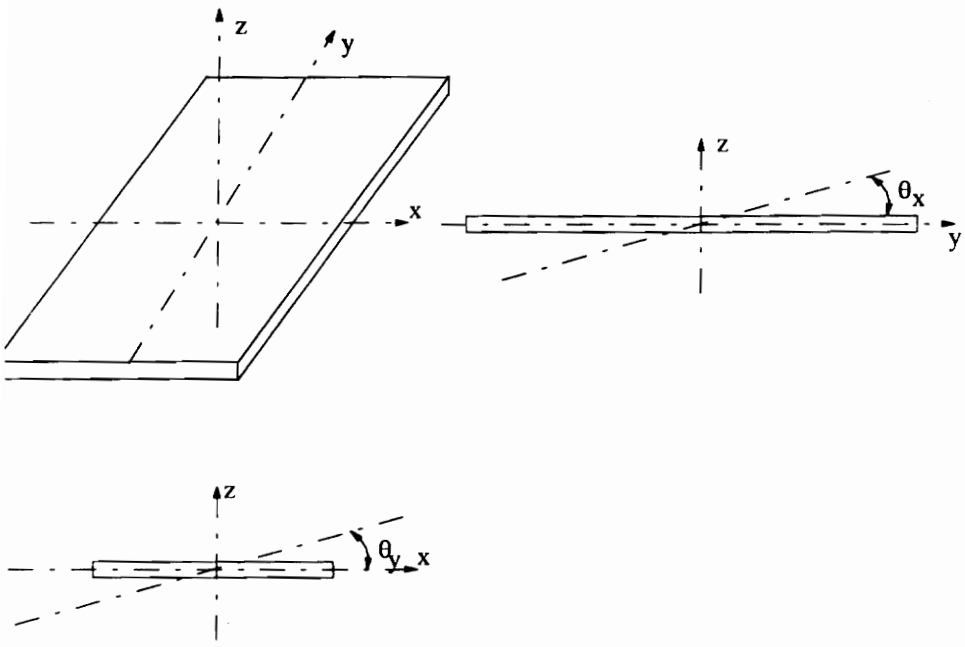

Figure 2 : Coordinate system of the plate

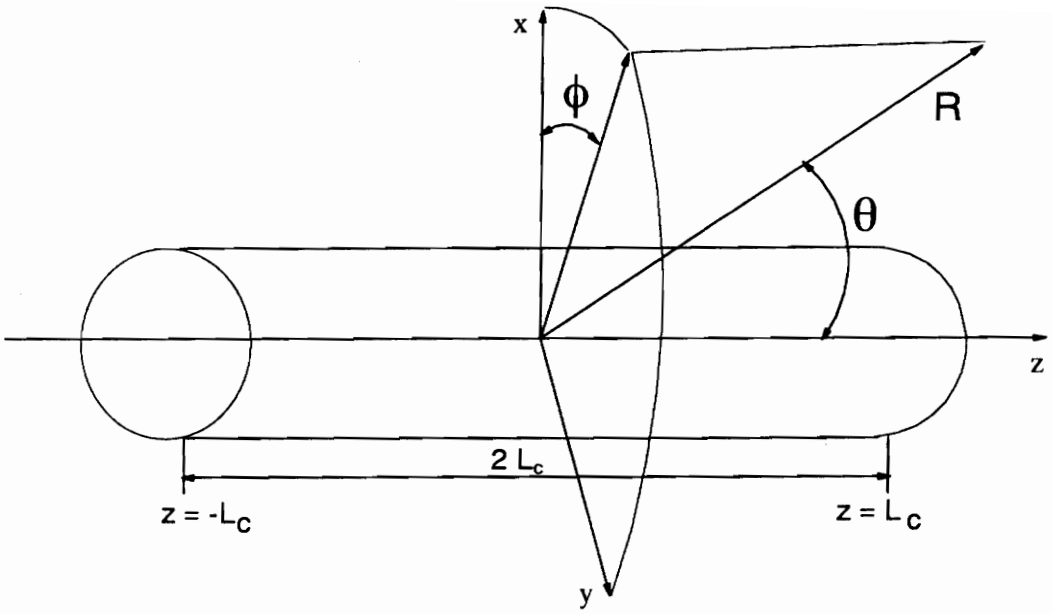

Figure 3 : Coordinate system of the cylinder

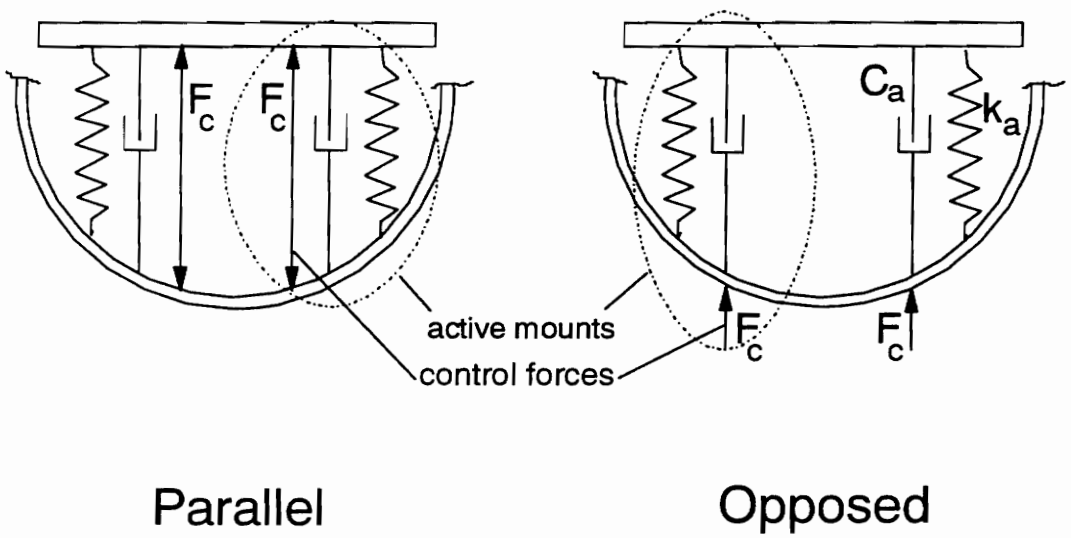

Figure 4 : Parallel and opposed active-passive mounts configurations

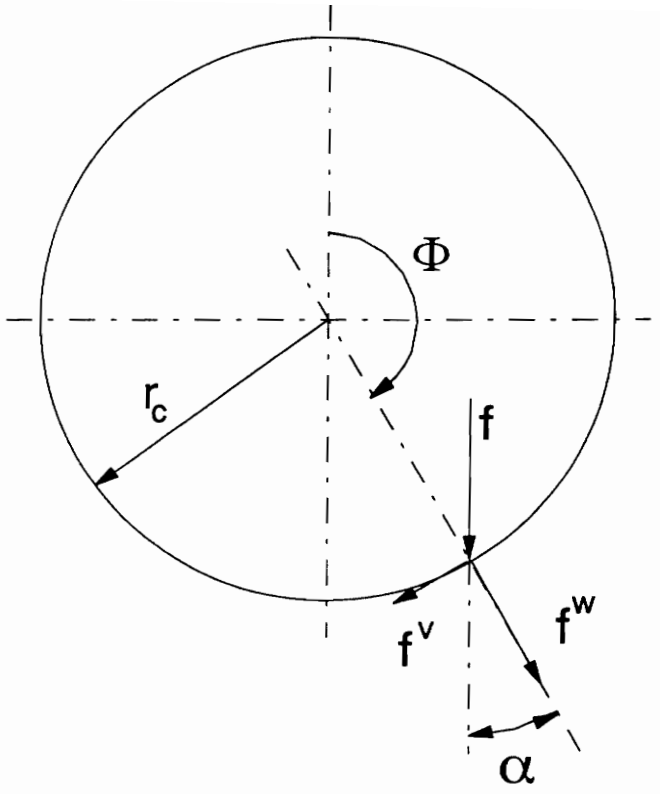

Figure 5 : Forces in the mounts : tangential and radial components

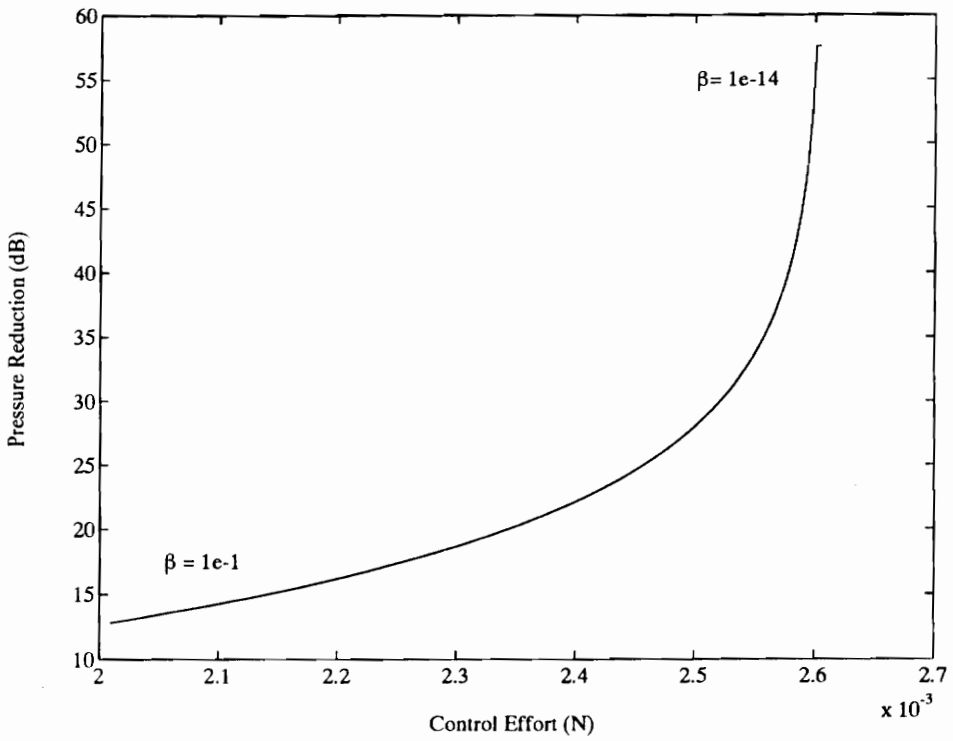

Figure 6 : Influence of the parameter β on the control efficiency and on the control effort.

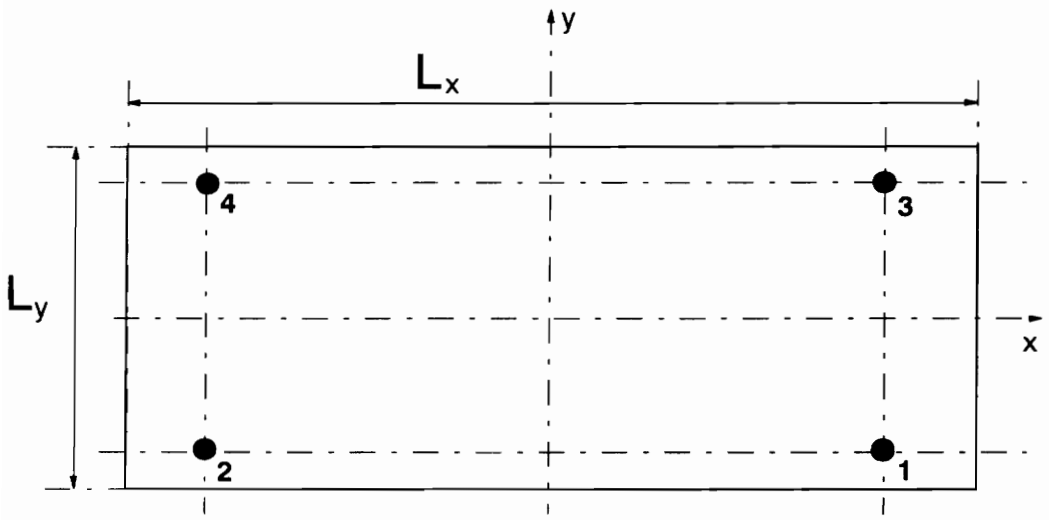

Figure 7 : Location of the mounts on the plate for the 4 mount system

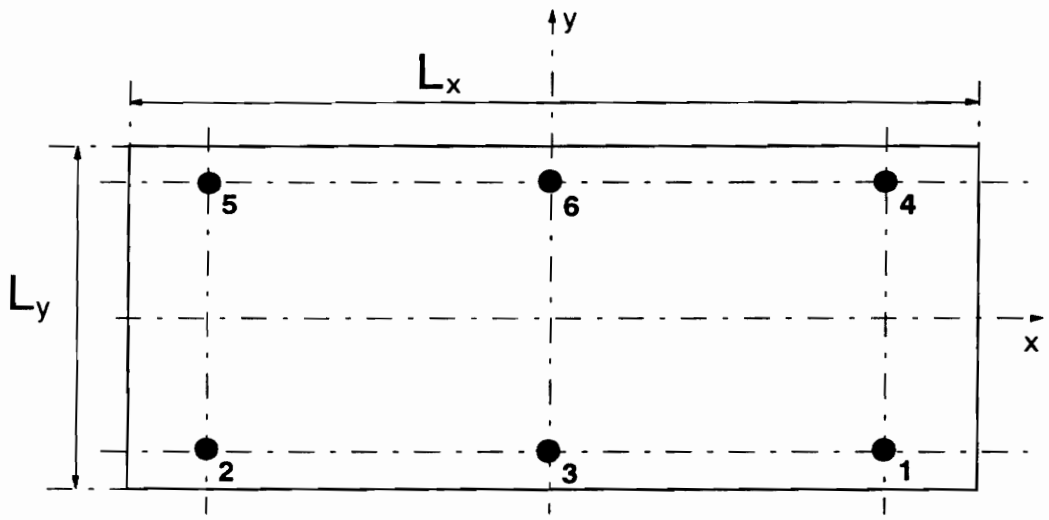

Figure 8 : Location of the mounts on the plate for the 6 mount system

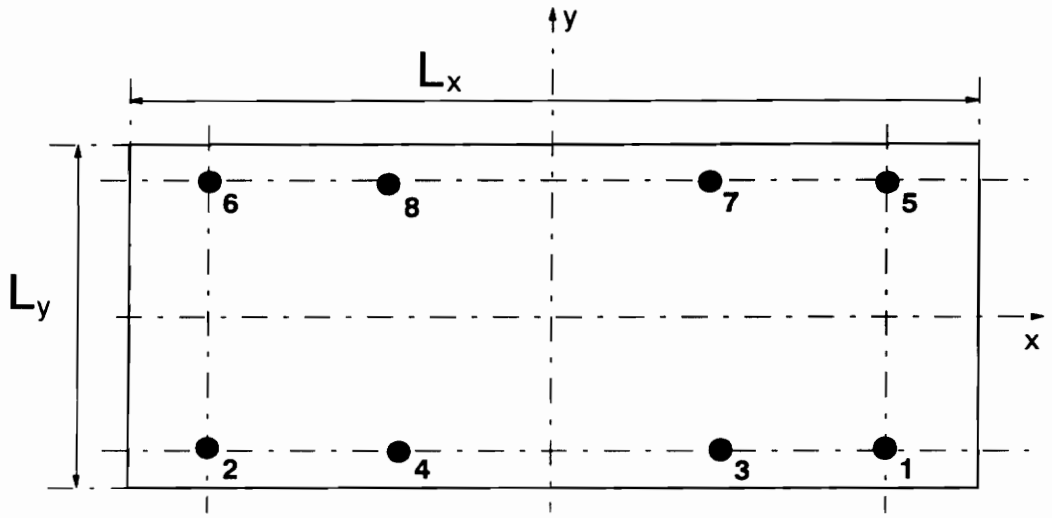

Figure 9 : Location of the mounts on the plate for the 8 mount system

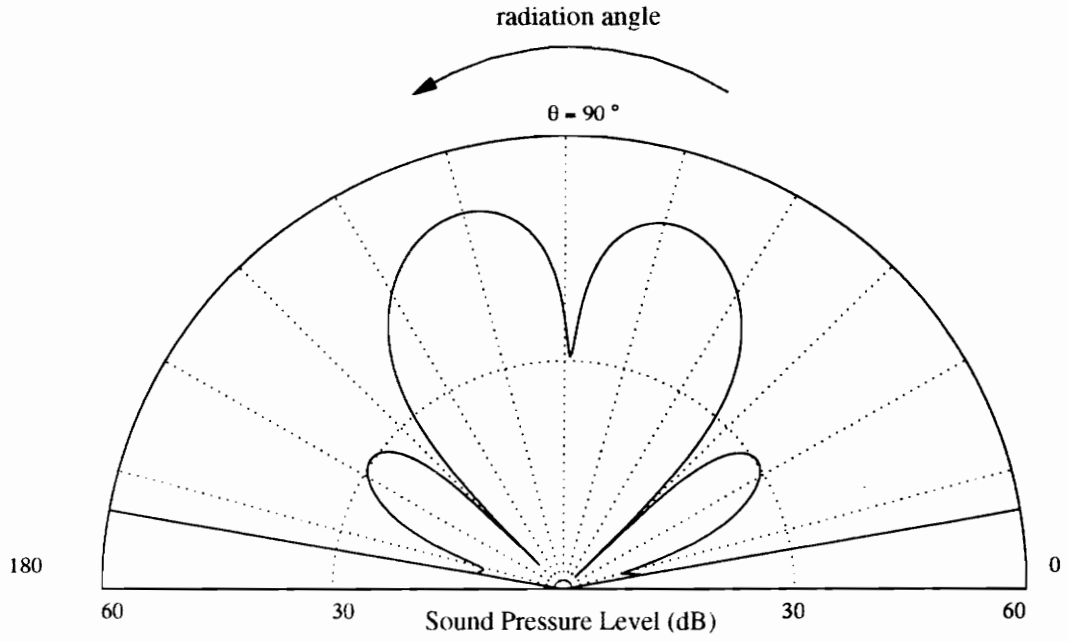

Figure 10 : Radiation of the coupled system with 8 mounts, at 242 Hz

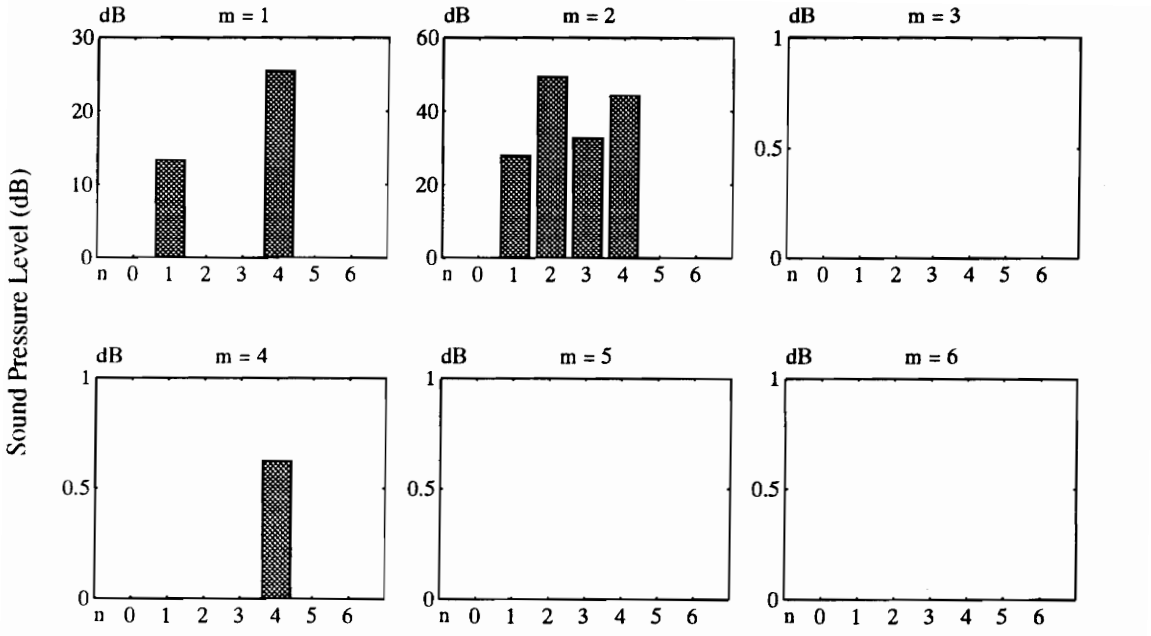

Figure 11 : Modal decomposition of the coupled system with 8 mounts at 242 Hz in the direction $\theta = 70°$

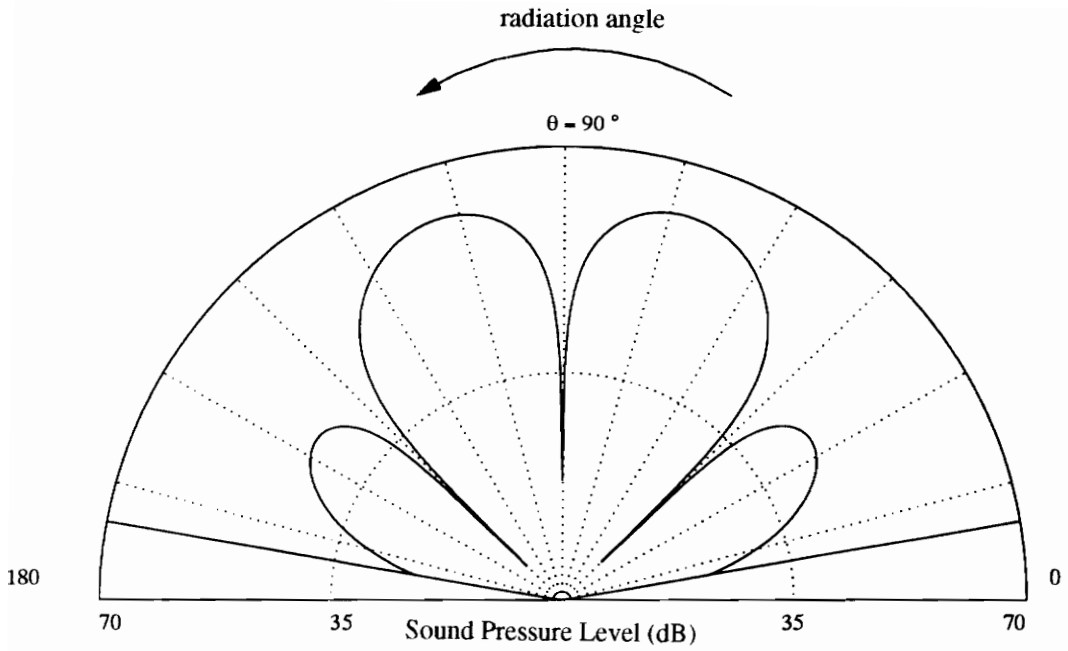

Figure 12 : Radiation of the coupled system with 6 mounts, at 242 Hz

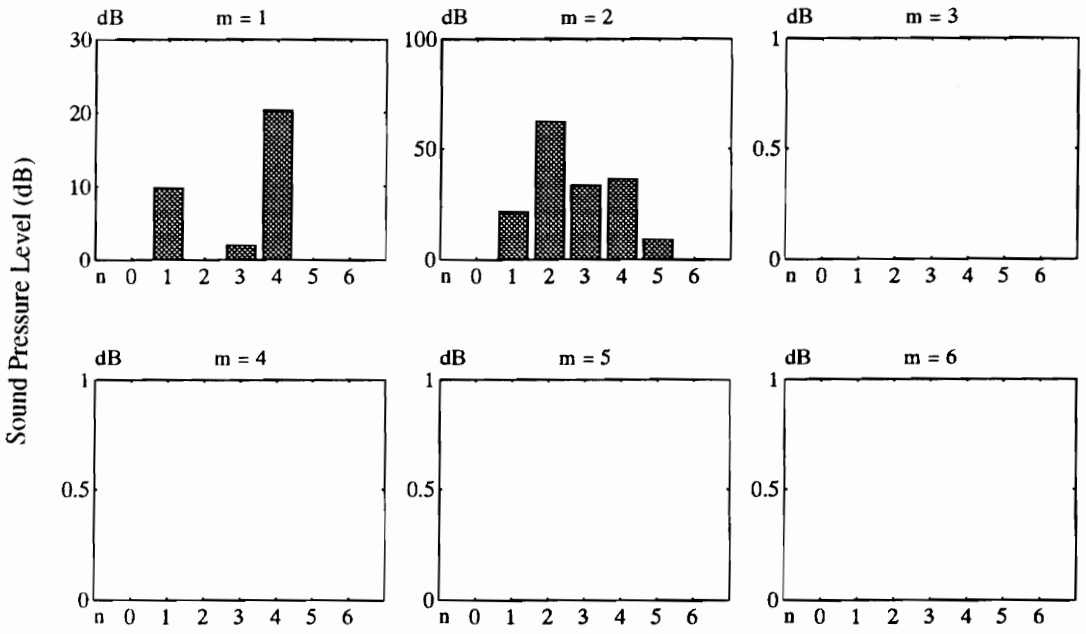

Figure 13 : Modal decomposition of the coupled system with 6 mounts at 242 Hz in the direction $\theta = 70°$

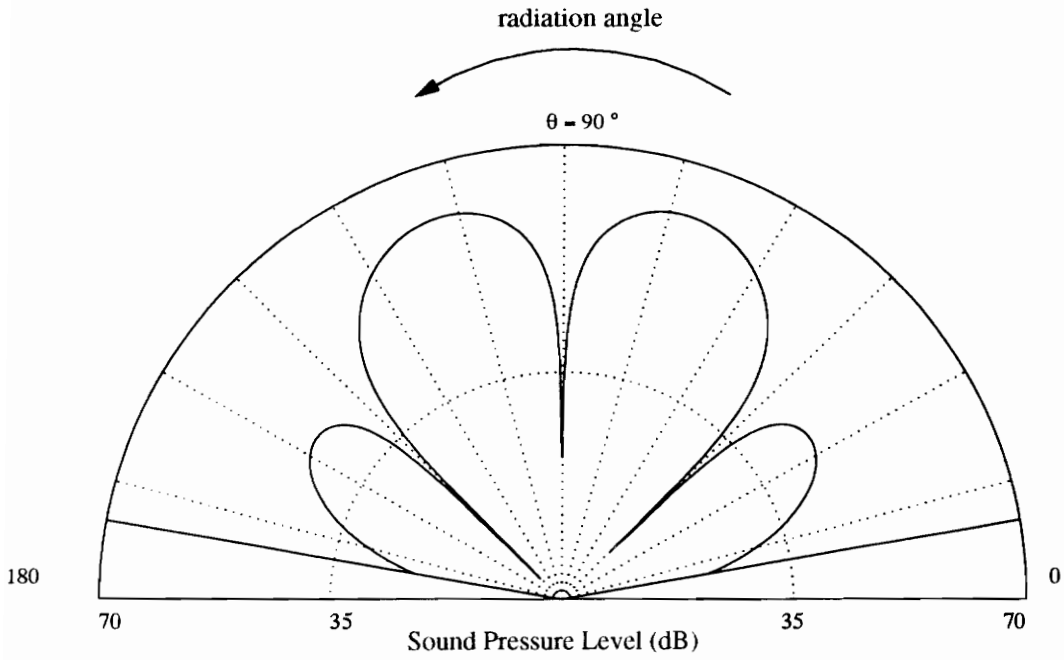

Figure 14 : Radiation of the coupled system with 4 mounts, at 242 Hz

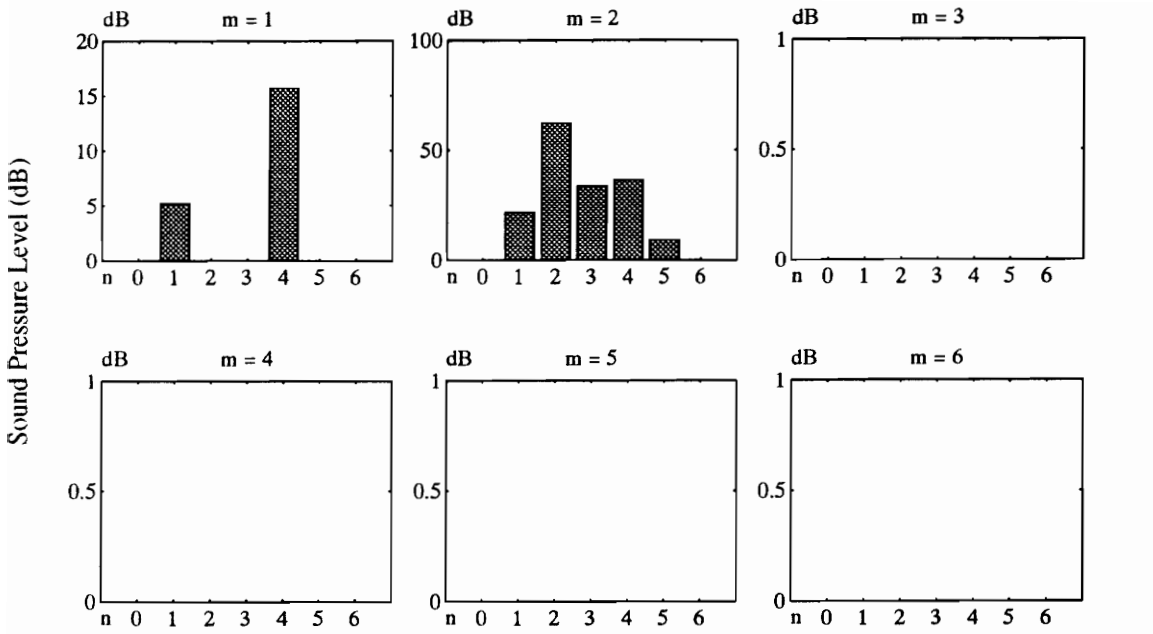

Figure 15 : Modal decomposition of the coupled system with 4 mounts at 242 Hz in the direction $\theta = 70°$

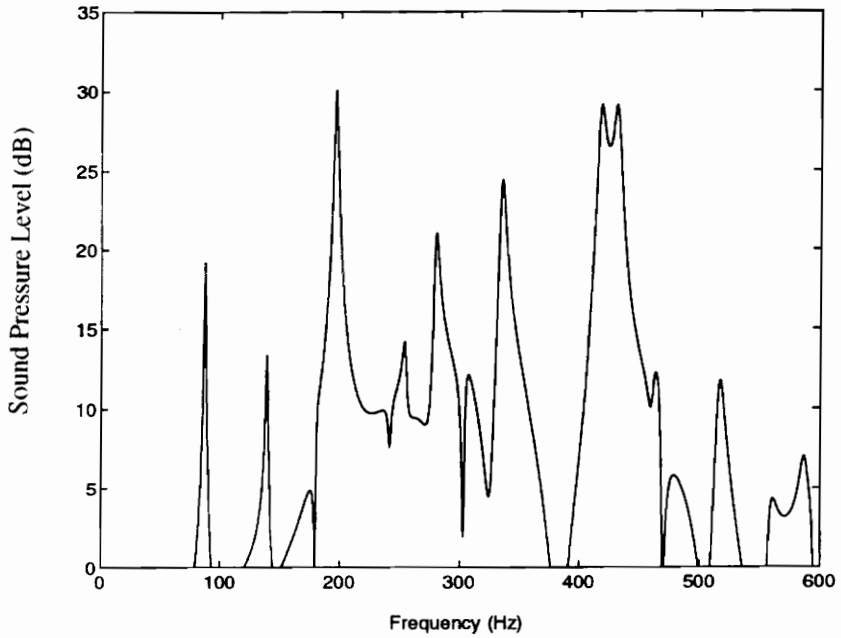

Figure 16: Sound pressure levels radiated by the cylinder at $\theta = 45°$

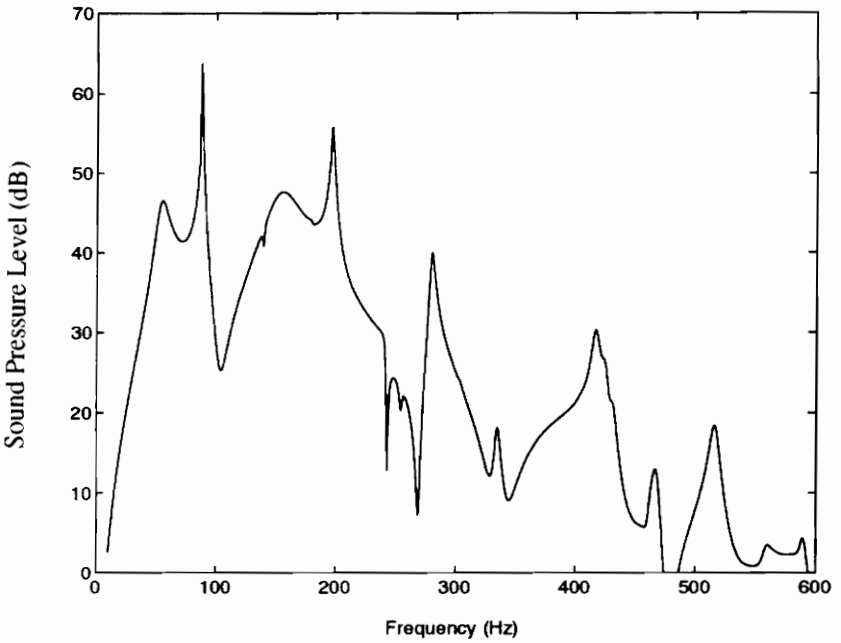

Figure 17: Sound pressure levels radiated by the coupled plate-cylinder system at $\theta = 45°$

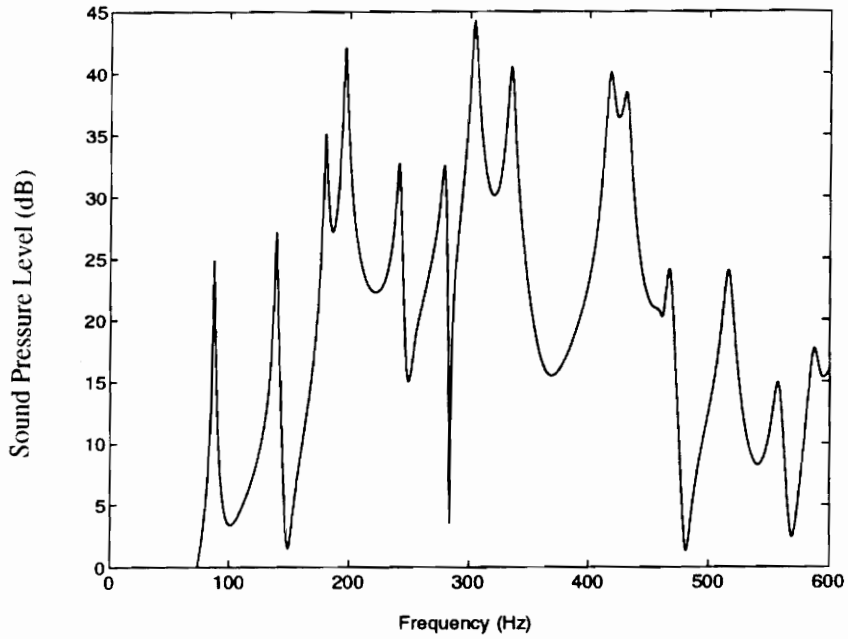

Figure 18 : Sound pressure levels radiated by the cylinder at $\theta = 60°$

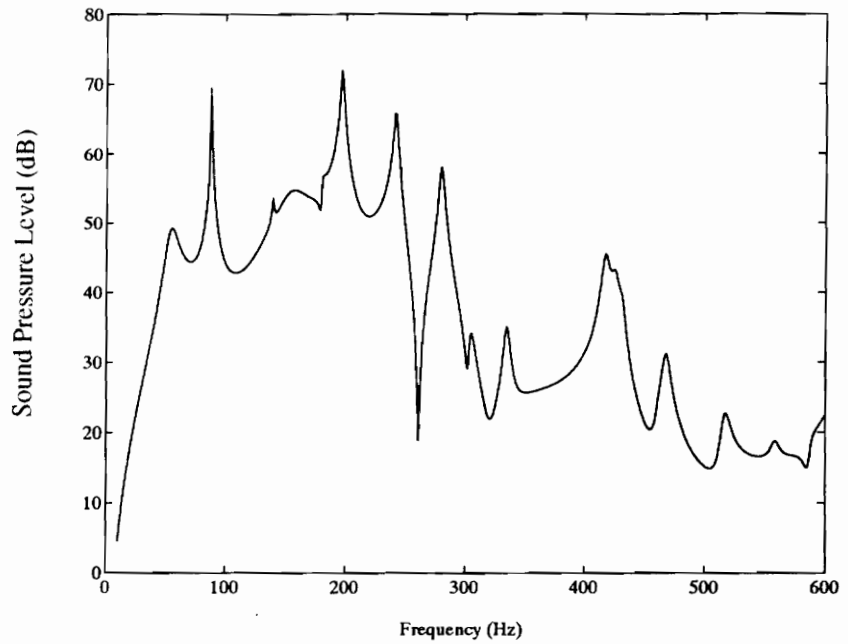

Figure 19 : Sound pressure levels radiated by the coupled plate-cylinder system at $\theta = 60°$

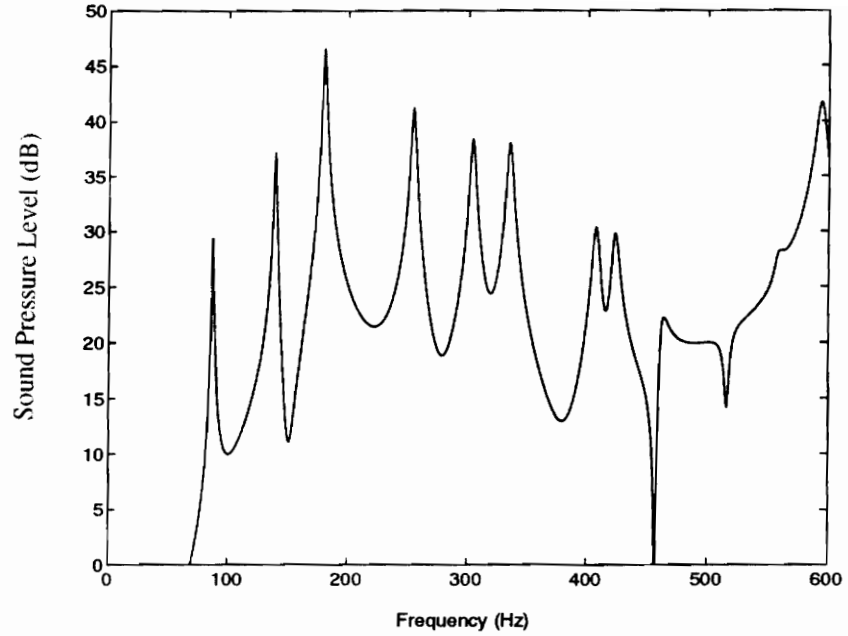

Figure 20 : Sound pressure levels radiated by the cylinder at $\theta = 90°$

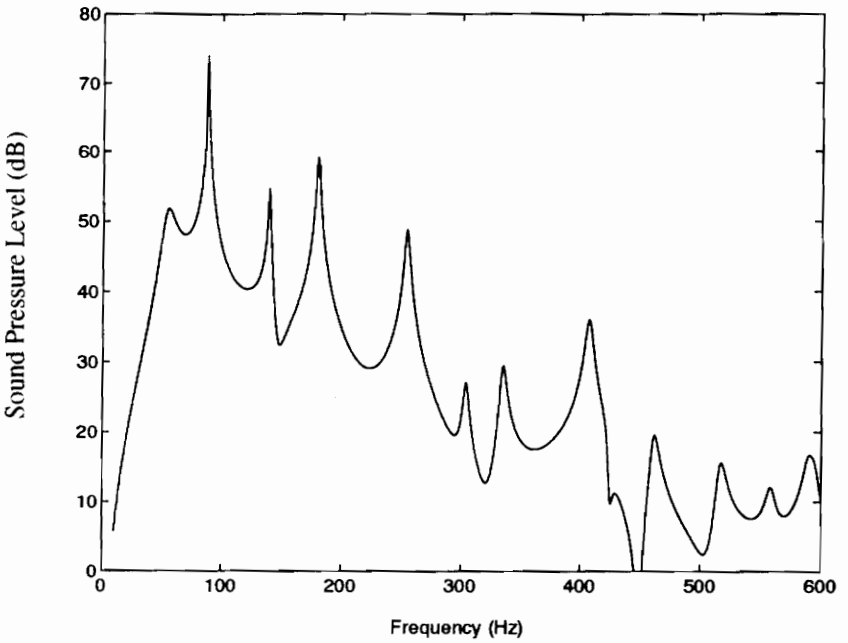

Figure 21 : Sound pressure levels radiated by the coupled plate-cylinder system at $\theta = 90°$

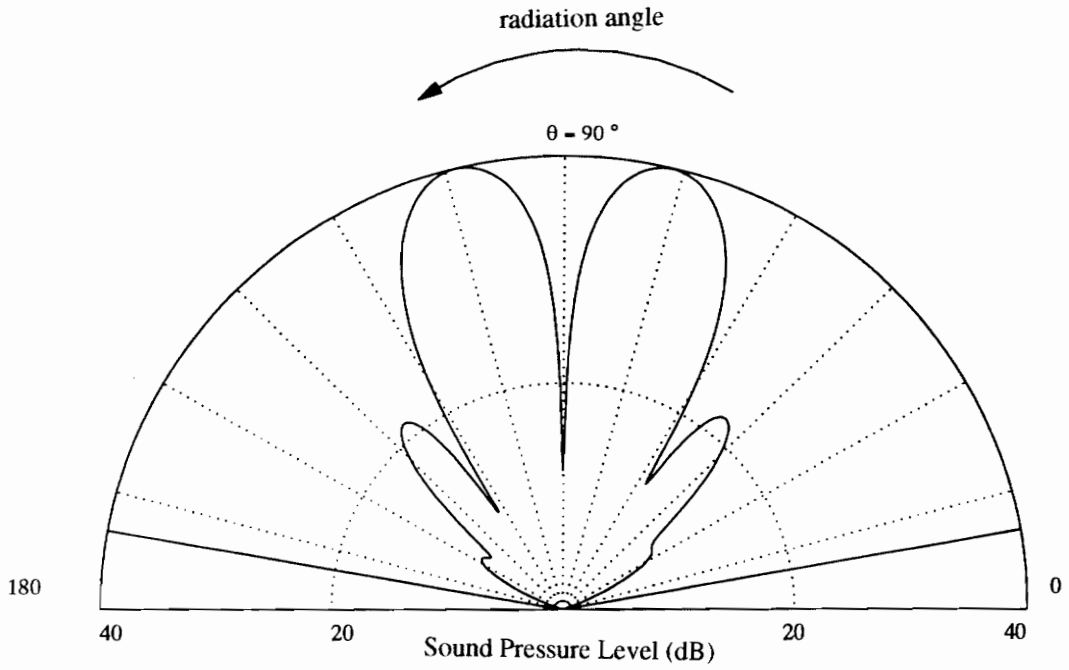

Figure 22 : Radiation of the system with 6 mounts (layout A) at 303 Hz

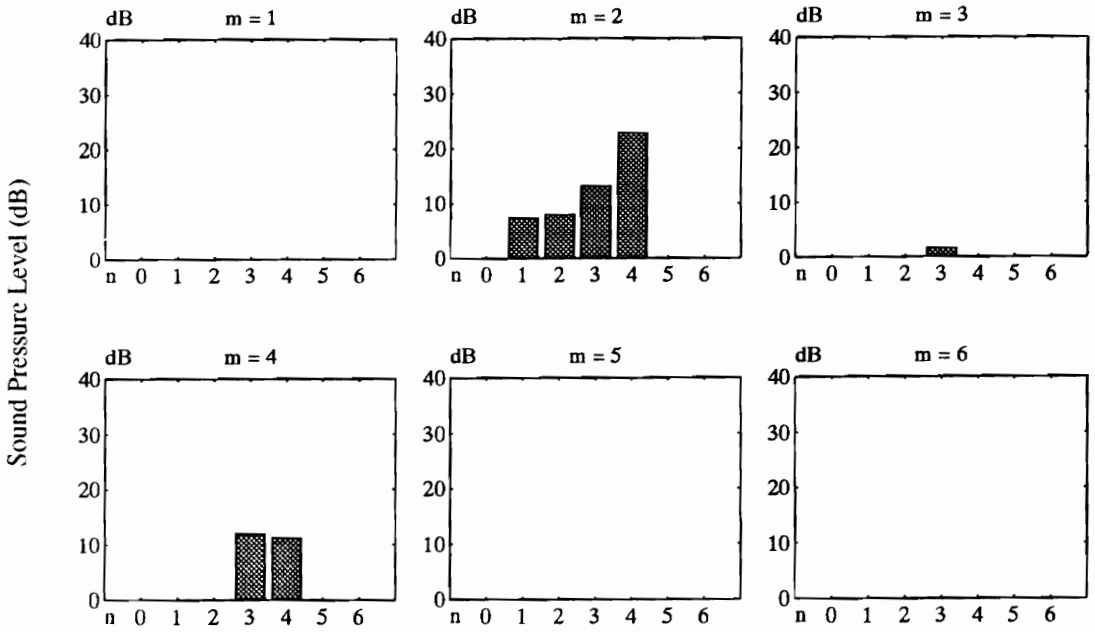

Figure 23 : Modal decomposition of the system with 6 mounts (layout A) at 303 Hz, in the direction $\theta = 120°$

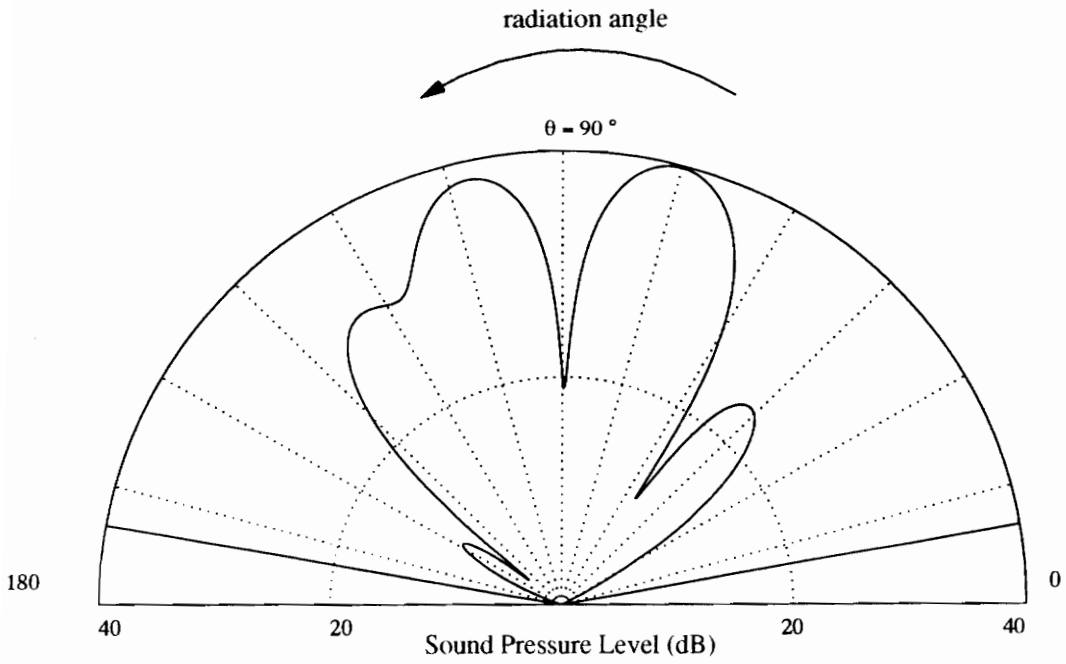

Figure 24 : Radiation of the system with 6 mounts (layout B), at 303 Hz

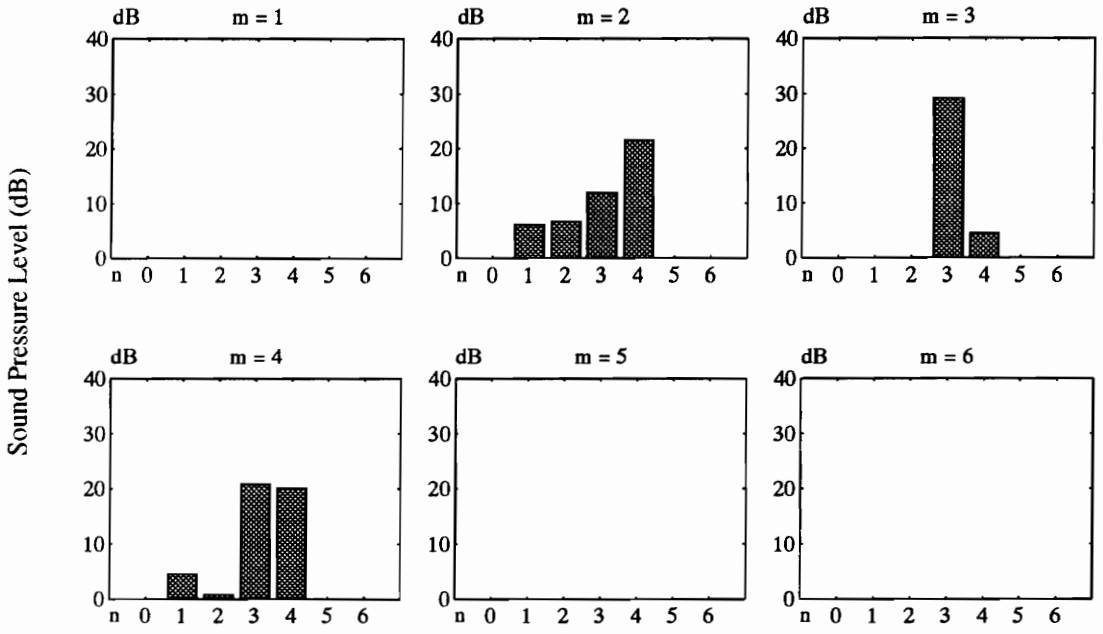

Figure 25 : Modal decomposition of the system with 6 mounts (layout B) at 303 Hz, in the direction $\theta = 120°$

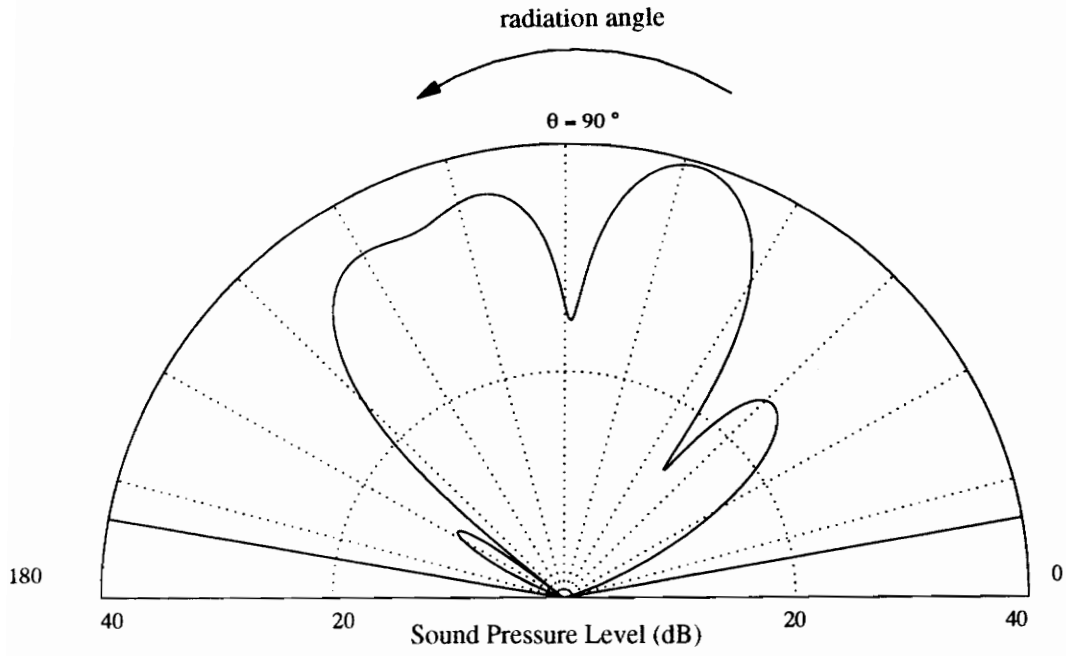

Figure 26 : Radiation of the system with 6 mounts (layout C), at 303 Hz

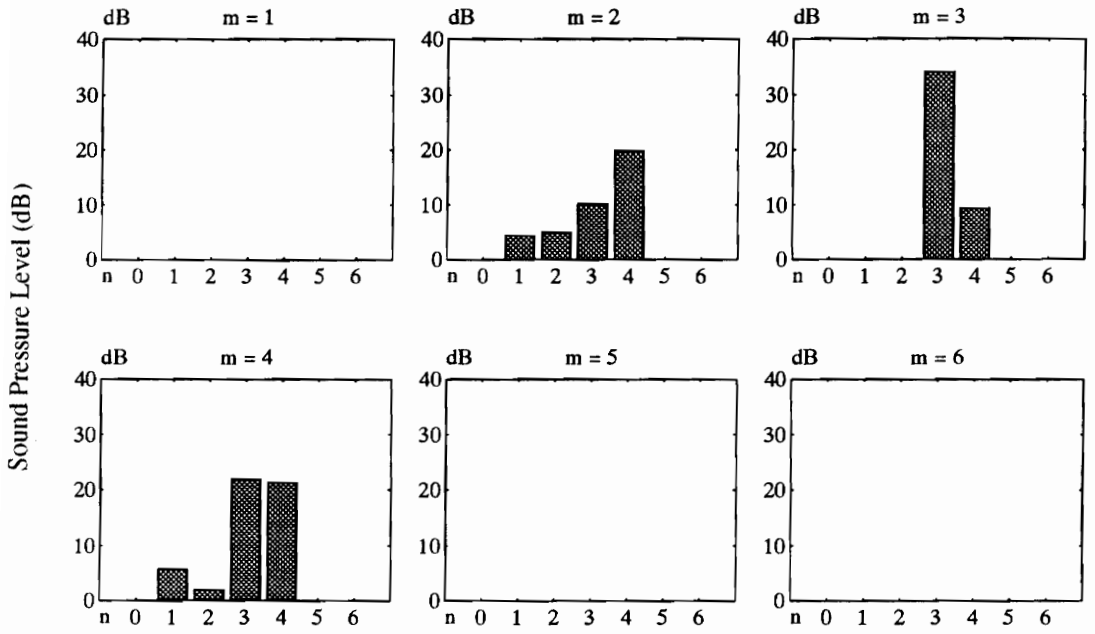

Figure 27 : Modal decomposition of the system with 6 mounts (layout C) at 303 Hz, in the direction $\theta = 120°$

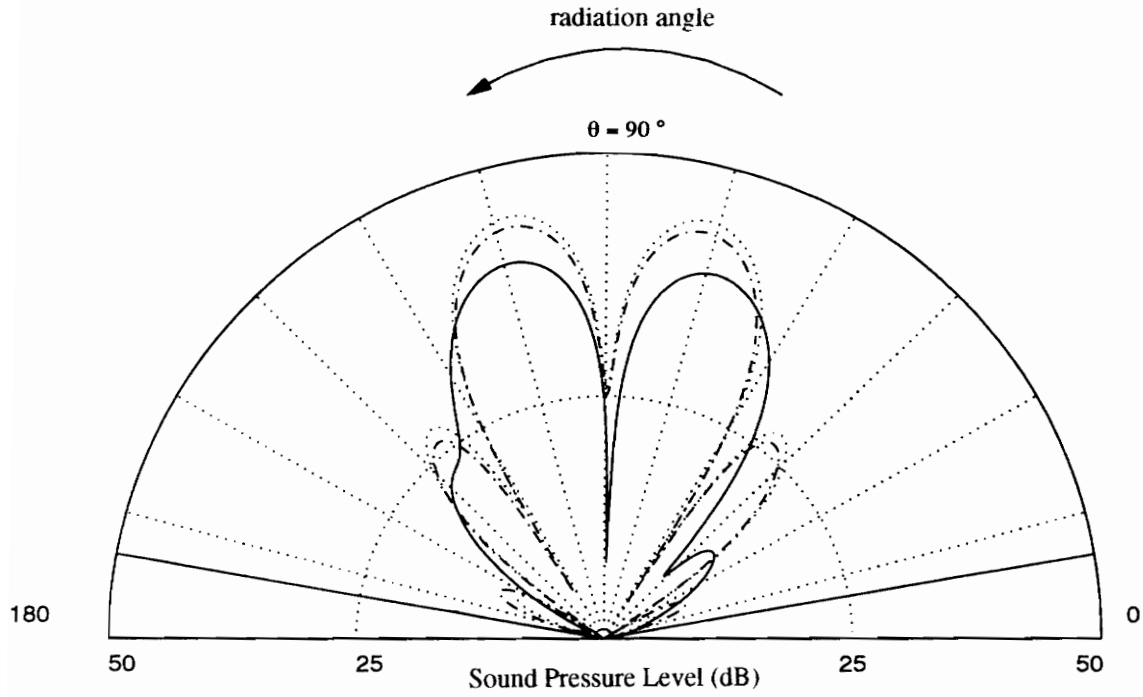

Figure 28 : Influence of the circumferential coordinate of the mounts location at 303 Hz : $\phi = 2\pi / 3$ -----, $\phi = 3\pi / 4$ ·····, $\phi = 4\pi / 5$ -·-·-

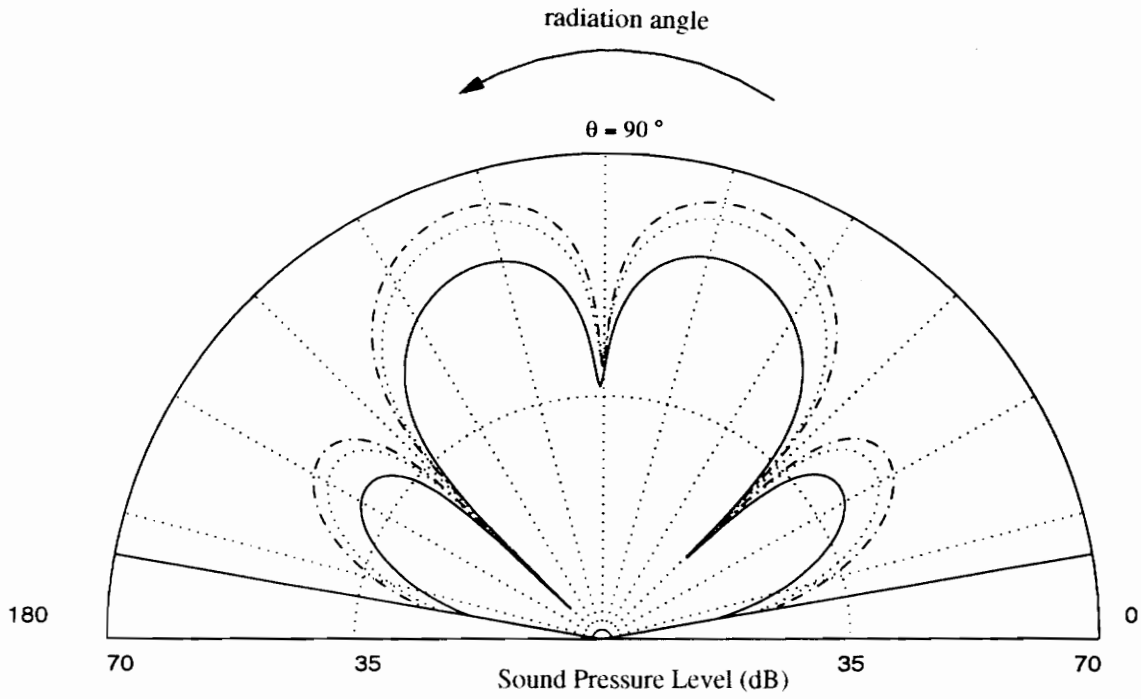

Figure 29 : Influence of the circumferential coordinate of the mounts location at 242 Hz : $\phi = 2\pi / 3$ -----, $\phi = 3\pi / 4$ ·····, $\phi = 4\pi / 5$ -·-·-

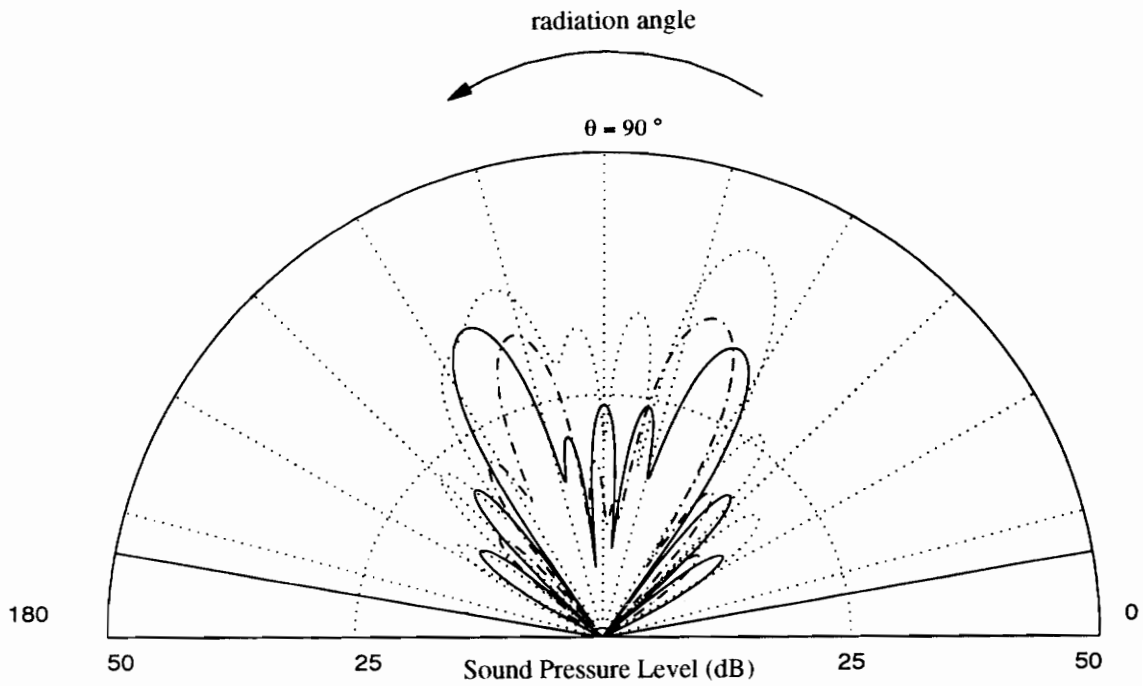

Figure 30 : Influence of the circumferential coordinate of the mounts location at 516 Hz : $\phi = 2\pi / 3$ -----, $\phi = 3\pi / 4$ ·····, $\phi = 4\pi / 5$ -·-·-·

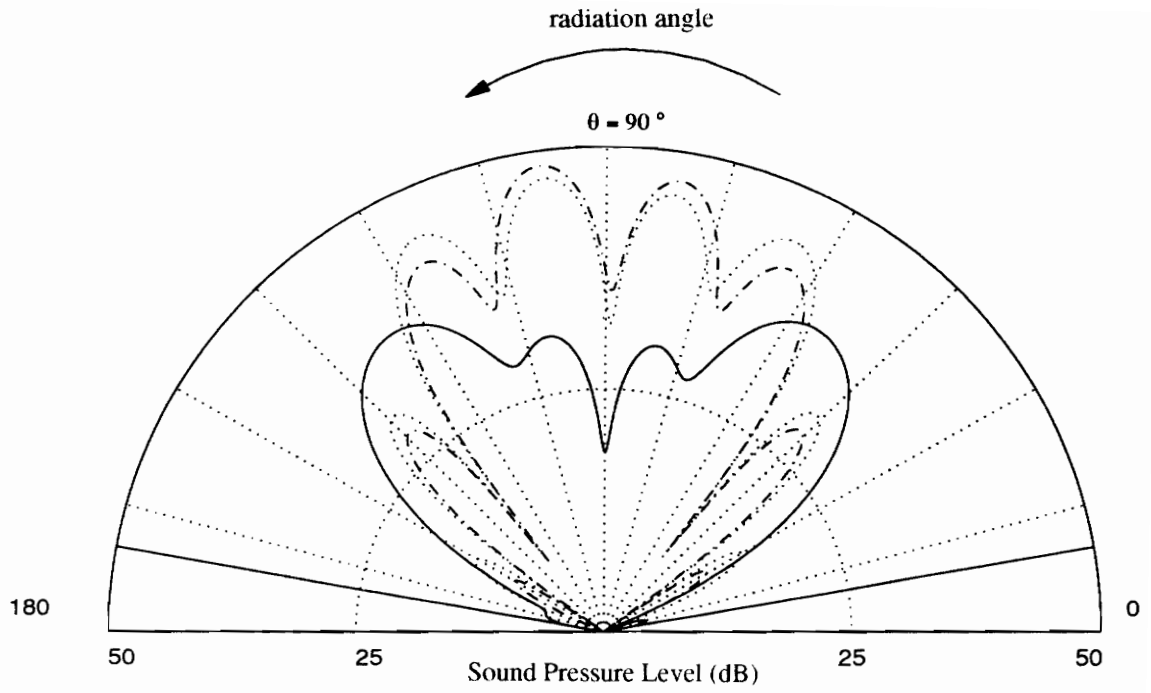

Figure 31 : Influence of the circumferential coordinate of the mounts location at 420 Hz : $\phi = 2\pi / 3$ -----, $\phi = 3\pi / 4$ ·····, $\phi = 4\pi / 5$ -·-·-

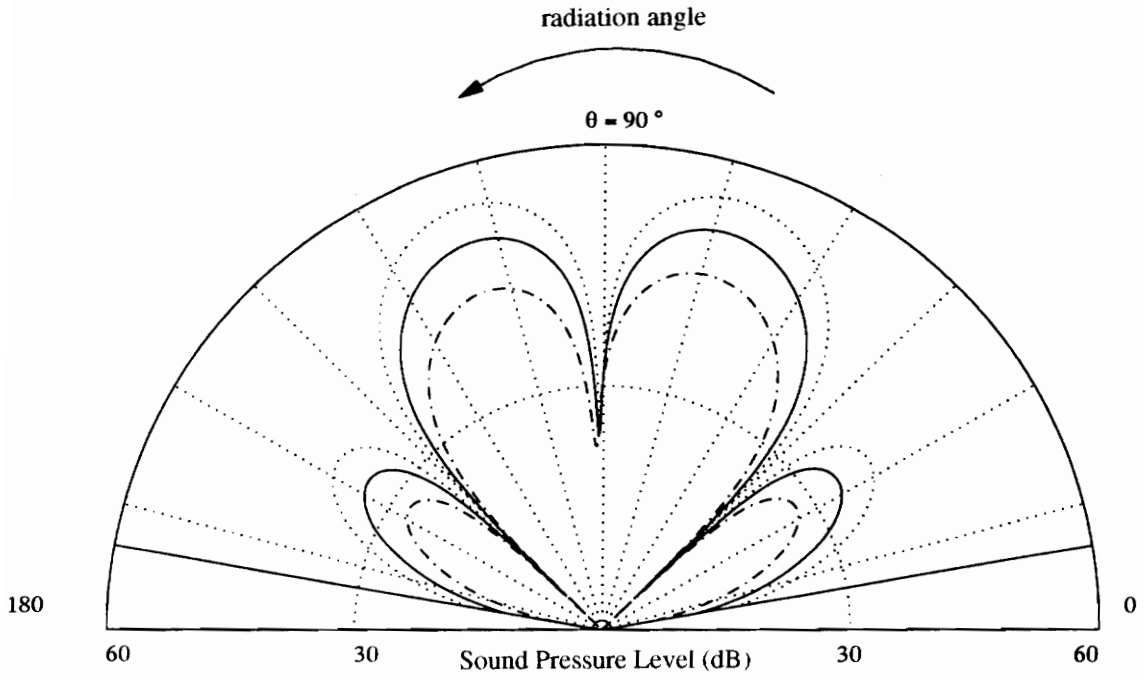

Figure 32 : Influence of the location of the disturbance on the plate at 242 Hz :

$(x, y) = (L_c / 3, w_c / 3)$ -----, $(L_c / 5, w_c / 5)$ ·····, $(L_c / 10, w_c / 10)$ -·-·-

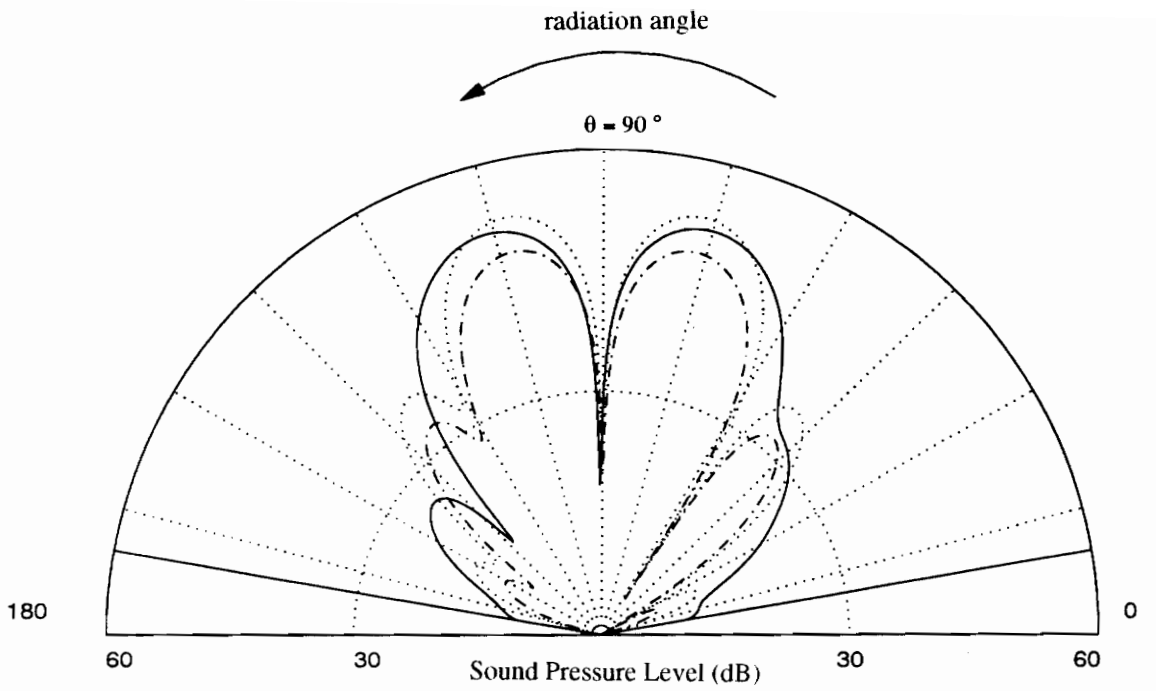

Figure 33 : Influence of the location of the disturbance on the plate at 303 Hz:

$(x, y) = (-L_c / 3, w_c / 3)$ -----, $(L_c / 3, w_c / 3)$ ·····, $(L_c / 5, w_c / 5)$ -·-·-

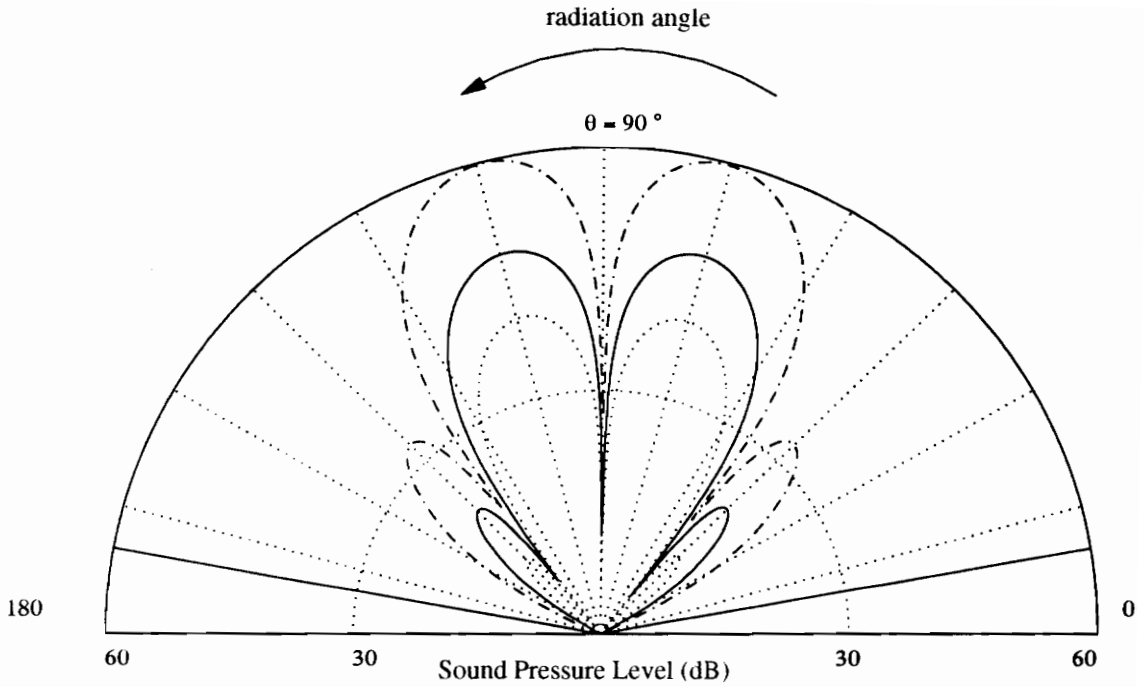

Figure 34 : Influence of the thickness of the raft at 280 Hz:

h_c =.002 -----, 004·····, .001·-·-·-

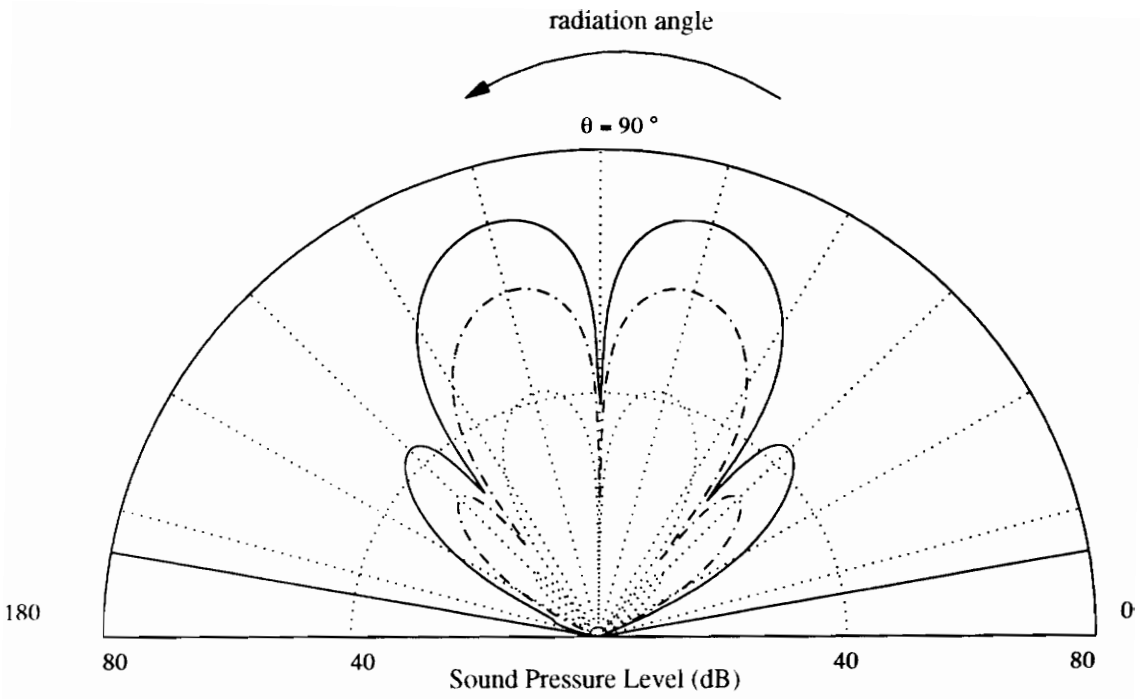

Figure 35 : Influence of the stiffness in the passive mounts at 280 Hz:

K_a =1e6 -----, 1e5 ·····, 5e5 -·-·-

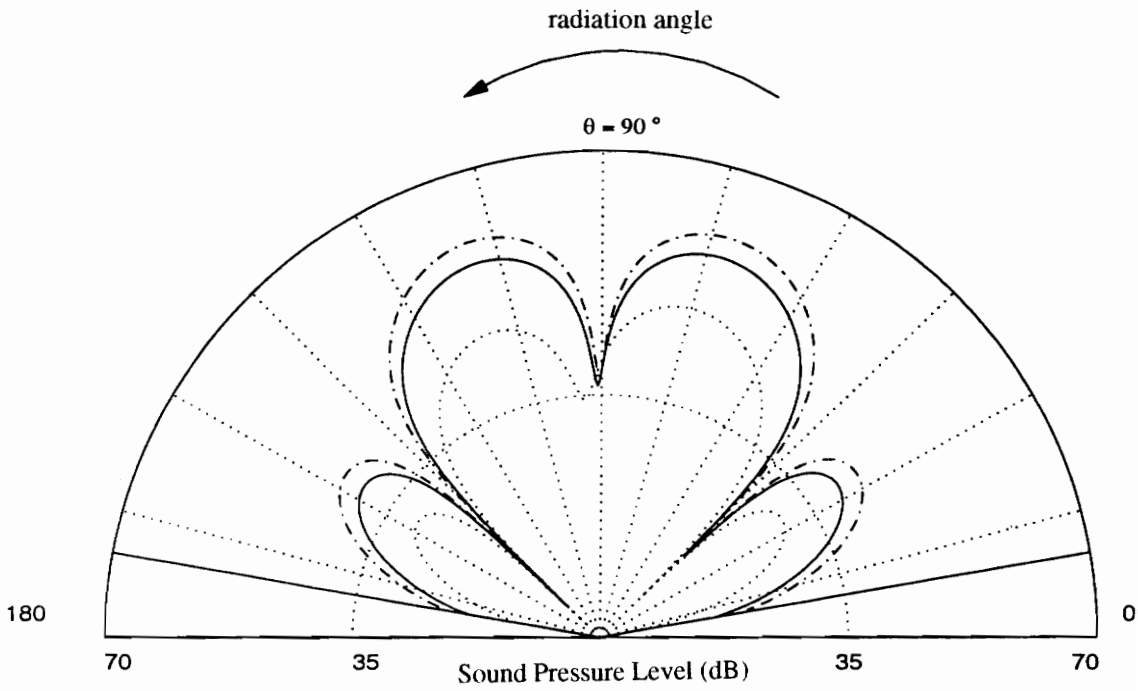

Figure 36 : Influence of the damping ratio at 242 Hz:

η=.1521 -----, η=.7603 ·····, η=.07603 -·-·-·

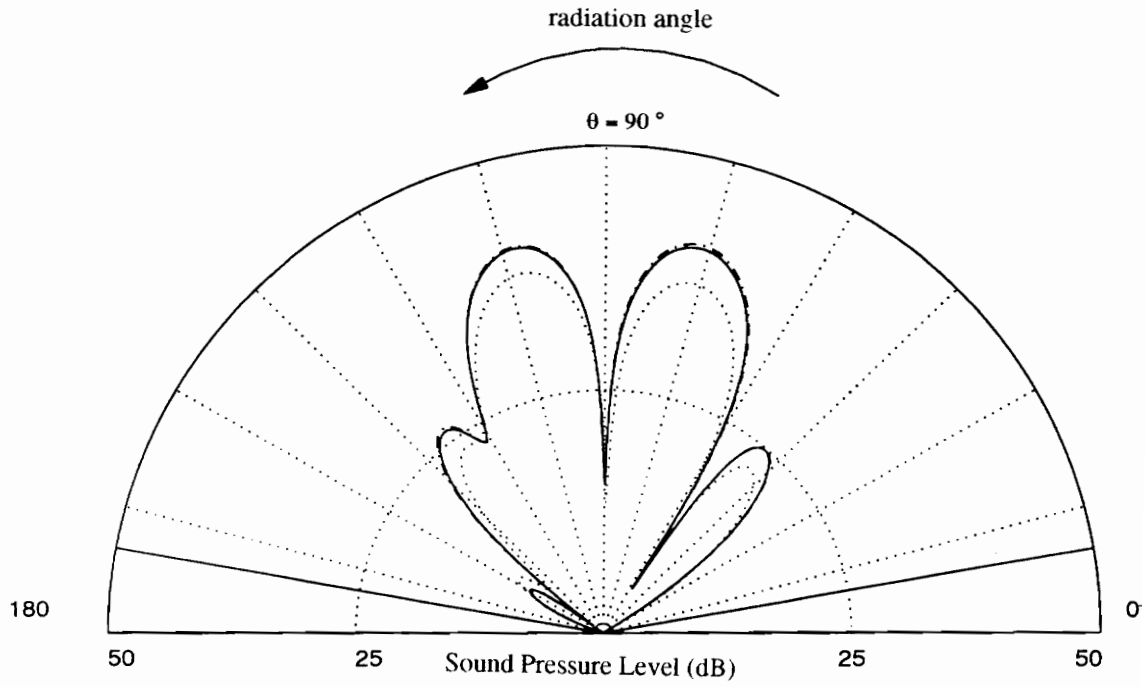

Figure 37 : Influence of the damping ratio at 303 Hz

η=.1904 -----, η=.9519 ·····, η=.09519 -·-·-

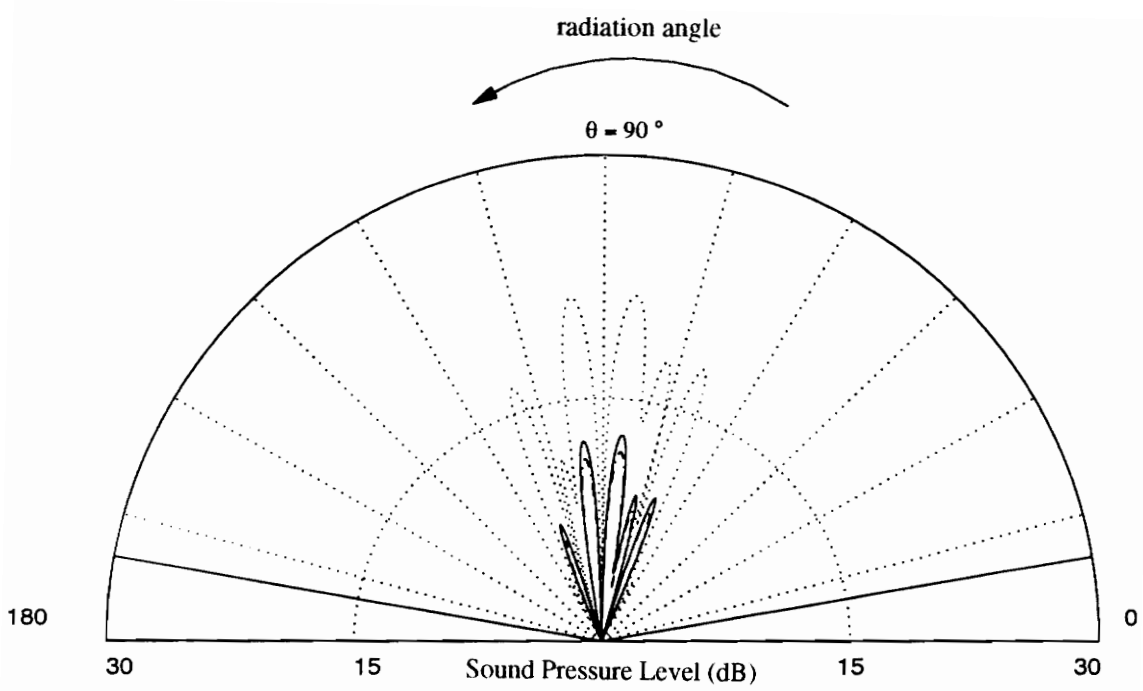

Figure 38 : Influence of the damping ratio at 1020 Hz

η=.6409 -----, η=3.204 ·····, η=.3204 -·-·-

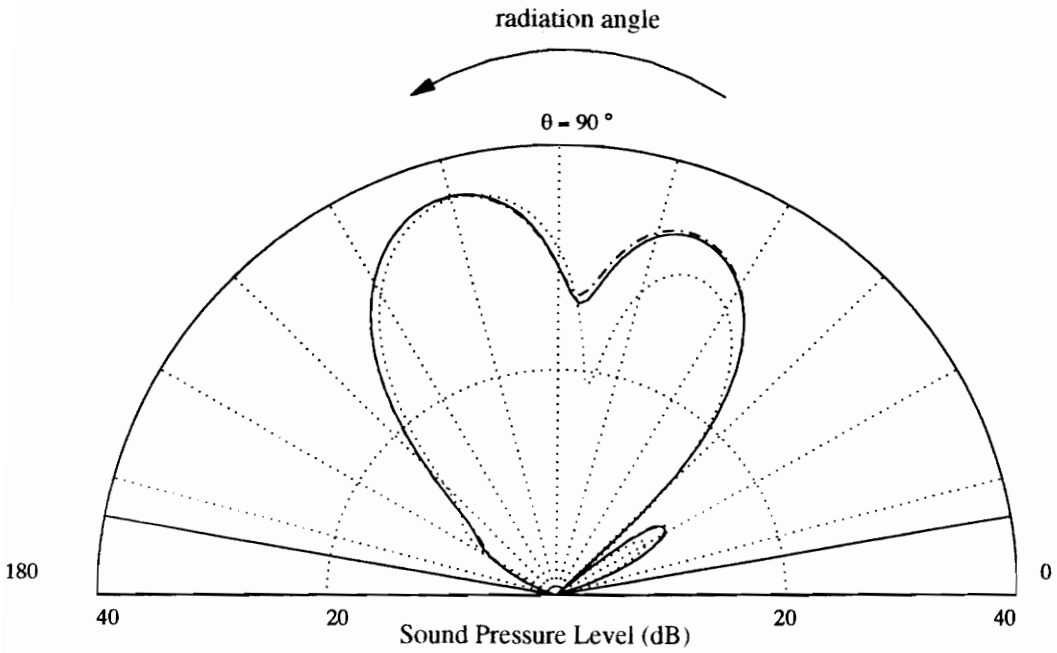

Figure 39 : Influence of the damping ratio at 220 Hz

η=.1382 -----, η=.6912 ·····, η=.06912 -·-·-

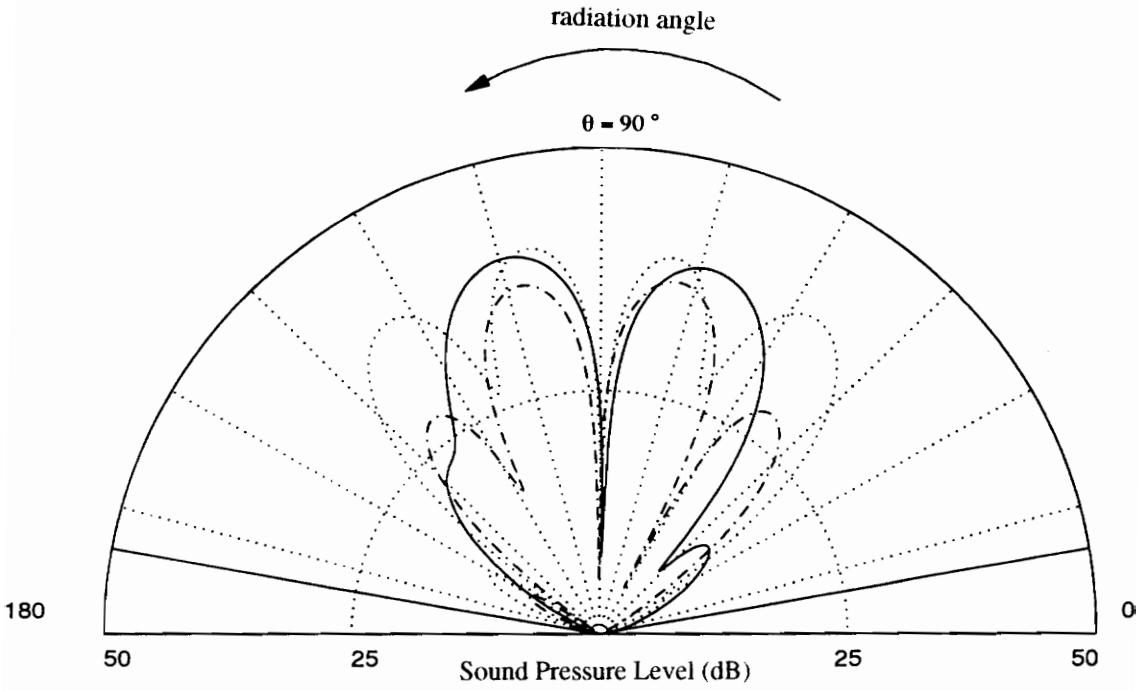

Figure 40 : Influence of the thickness ratio at 303 Hz

h_c / r_c=.005 -----, h_c / r_c=.003 ·····, h_c / r_c=.004 -·-·-

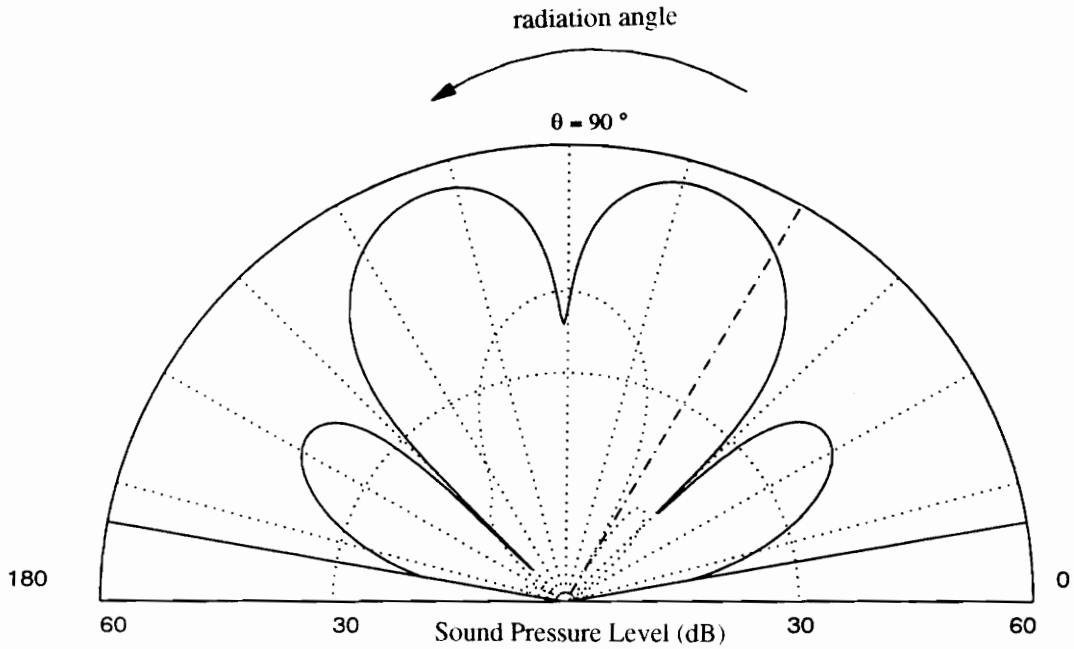

Frequency:

242

Effort:

0.8293

#	F. control:		F. mounts (u):		F. mounts (c):	
1	0.3136	(-4.111)	1.803	(-0.07883)	0.3611	(1.461)
2	0.2657	(2.052)	1.876	(-0.4565)	0.3858	(-23.67)
3	0.3068	(-6.521)	0.9425	(0.1028)	0.3281	(1.995)
4	0.2736	(3.197)	1.032	(-0.7741)	0.394	(9.175)
5	0.2745	(2.186)	1.783	(-0.1612)	0.2189	(1.383)
6	0.3247	(-4.113)	1.842	(-0.3943)	0.2771	(-2.918)
7	0.3068	(-6.521)	0.9425	(0.1028)	0.3281	(1.995)
8	0.2736	(3.197)	1.032	(-0.7741)	0.394	(9.175)

Figure 41 : Radiation of the system with 8 mounts at 242 Hz: no control -----, control at $\theta = 60°$ ------

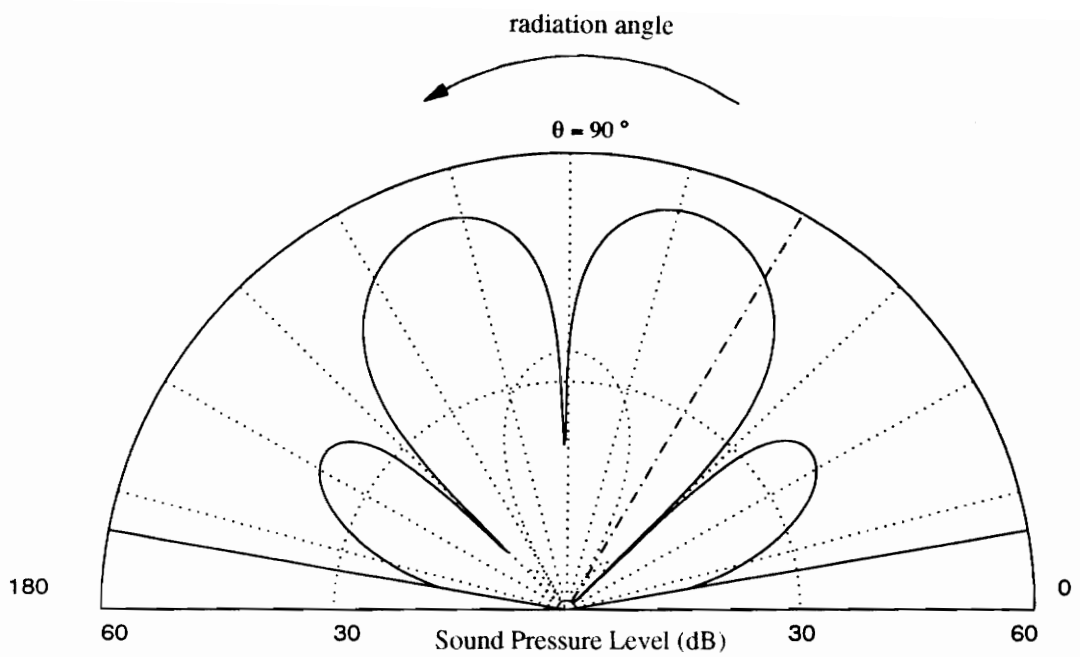

Frequency:	#	F. control:		F. mounts (u):		F. mounts (c):	
	1	0.3629	(-2.705)	2	(0.6038)	0.5809	(1.182)
242	2	0.6862	(1.277)	1.53	(0.4008)	0.287	(-1.528)
Effort:	3	0.4751	(5.022)	0.3431	(5.373)	0.3628	(3.258)
	4	0.6822	(1.427)	1.928	(0.5863)	0.4313	(1.267)
1.294	5	0.3909	(-2.23)	1.584	(0.4413)	0.2864	(-0.5064)
	6	0.4771	(2.692)	0.2494	(5.374)	0.2363	(87.94)

Figure 42 : Radiation of the system with 6 mounts at 242 Hz: no control -----, control at $\theta = 60°$ ------

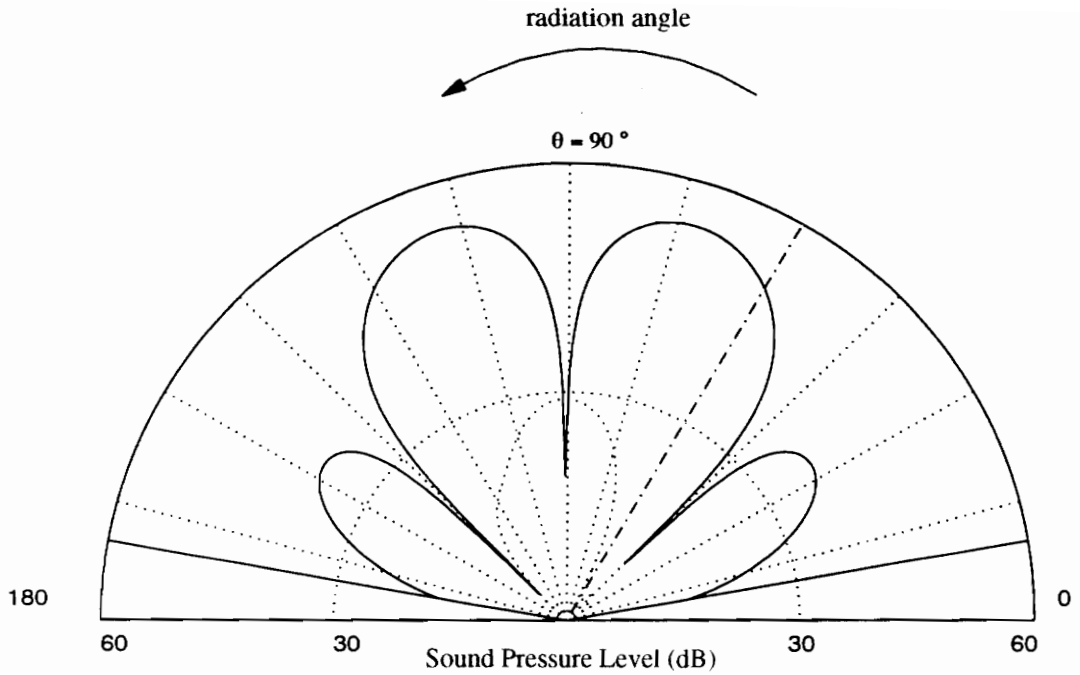

Frequency:	#	F. control:		F. mounts (u):		F. mounts (c):	
242	1	0.4989	(-2.682)	1.984	(0.6022)	0.6684	(1.018)
	2	0.9402	(1.174)	1.543	(0.4075)	0.2938	(-0.7465)
Effort:	3	0.9375	(1.293)	1.916	(0.5847)	0.5001	(1.119)
1.516	4	0.5353	(-2.258)	1.595	(0.4459)	0.3658	(-0.1756)

Figure 43 : Radiation of the system with 4 mounts at 242 Hz: no control -----, control at $\theta = 60°$ -·-·-

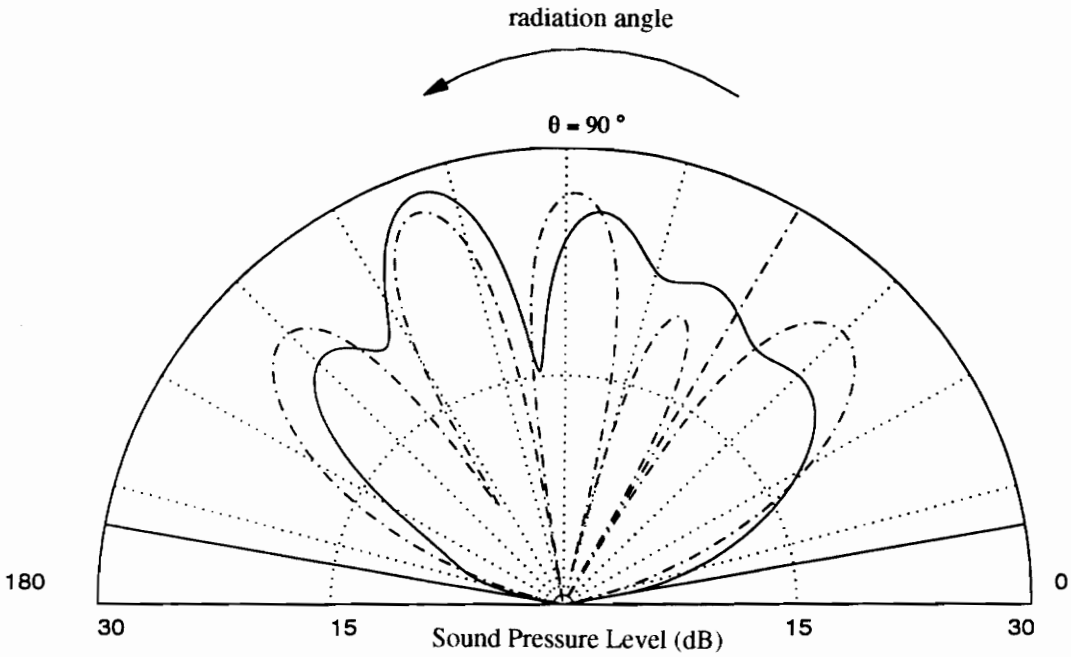

Frequency:	#	F. control:		F. mounts (u):		F. mounts (c):	
516	1	0.02476	(-15.99)	0.2044	(2.383)	0.2076	(2.335)
	2	0.1313	(0.6723)	0.06192	(1.886)	0.05755	(1.844)
Effort:	3	0.08318	(3.089)	0.1379	(2.427)	0.14	(2.295)
	4	0.06131	(2.658)	0.009333	(-1.851)	0.01308	(-3.048)
0.2335	5	0.05206	(10.37)	0.1826	(2.36)	0.1802	(2.448)
	6	0.1123	(0.4513)	0.08352	(2.049)	0.08509	(1.833)
	7	0.08318	(3.089)	0.1379	(2.427)	0.14	(2.295)
	8	0.06131	(2.658)	0.009333	(-1.851)	0.01308	(-3.048)

Figure 44 : Radiation of the system with 8 mounts at 516 Hz: no control -----, control at $\theta = 60°$ ------

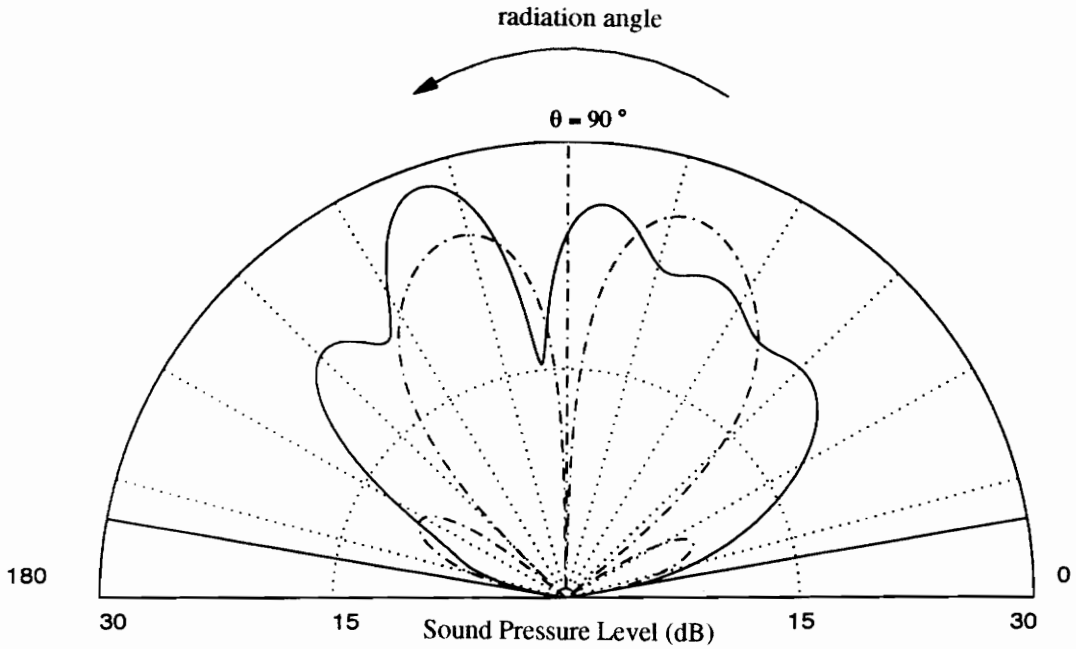

Frequency:

516

Effort:

0.1648

#	F. control:		F. mounts (u):		F. mounts (c):	
1	0.07901	(3.235)	0.2044	(2.383)	0.2084	(2.252)
2	0.07883	(3.103)	0.06192	(1.886)	0.06247	(1.914)
3	0.02351	(1.252)	0.1379	(2.427)	0.1413	(2.324)
4	0.0225	(1.214)	0.009333	(-1.851)	0.009921	(-2.362)
5	0.07928	(3.276)	0.1826	(2.36)	0.1867	(2.218)
6	0.07921	(3.141)	0.08352	(2.049)	0.08417	(2.069)
7	0.02351	(1.252)	0.1379	(2.427)	0.1413	(2.324)
8	0.0225	(1.214)	0.009333	(-1.851)	0.009921	(-2.362)

Figure 45 : Radiation of the system with 8 mounts at 516 Hz: no control -----, control at $\theta = 90°$ -.-.-

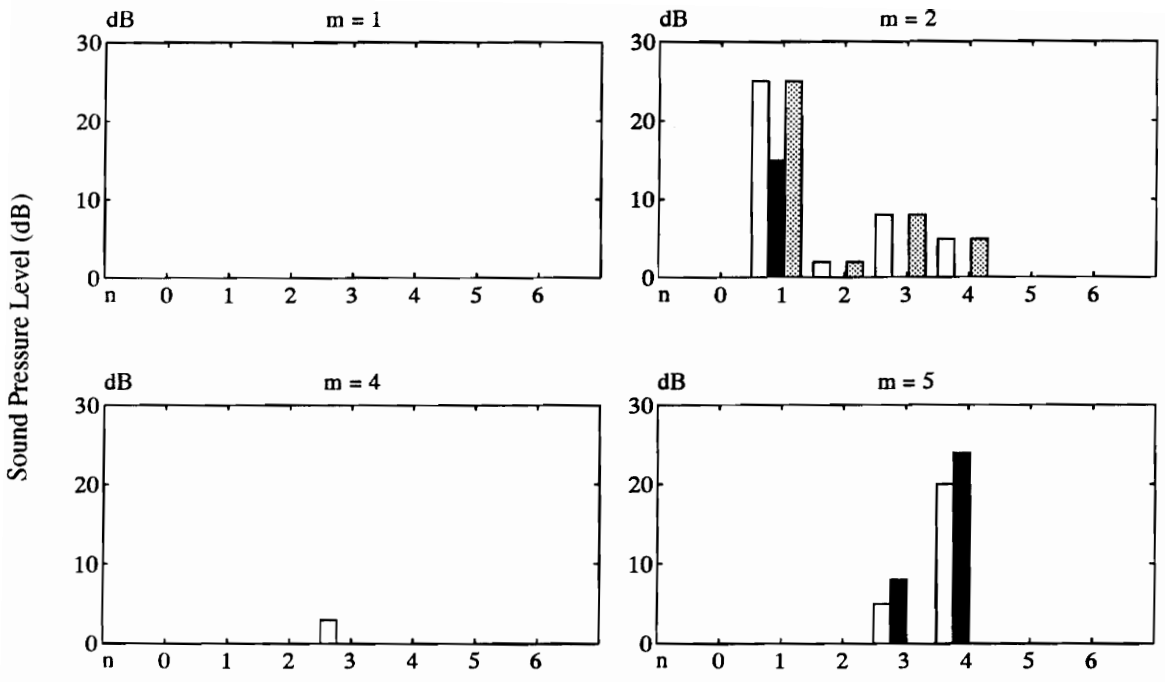

Figure 46 : Modal decomposition of the sound pressure radiated by the system at the point of coordinates $(R = 10\text{m}, \theta = 122°, \phi = 0)$

□ no control , ■ control at $\theta = 60°$, ▨ control at $\theta = 90°$

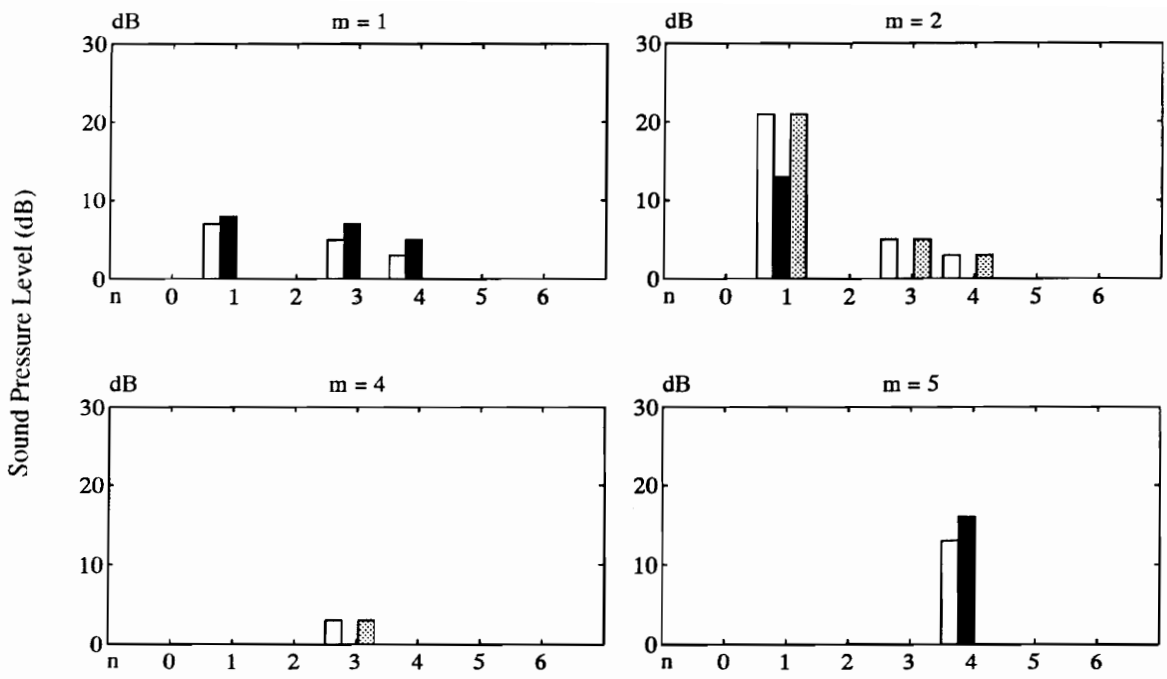

Figure 47 : Modal decomposition of the sound pressure radiated by the system at the point of coordinates $(R = 10\text{m}, \theta = 98°, \phi = 0)$.

□ no control , ■ control at $\theta = 60°$, ▨ control at $\theta = 90°$

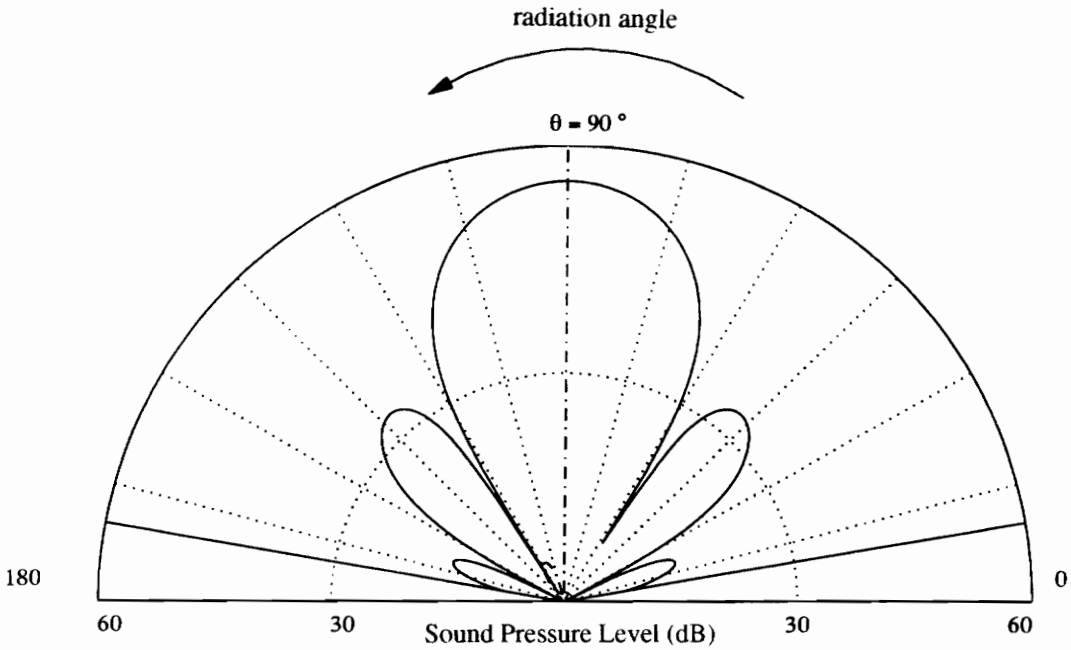

Frequency:
87
Effort:
1.058

#	F. control:		F. mounts (u):		F. mounts (c):	
1	0.5841	(-4.37)	2.354	(-4.274)	1.383	(-9.188)
2	0.1162	(-2.057)	1.344	(-3.48)	0.6392	(-4.026)
3	0.4423	(-4.859)	2.19	(-4.884)	1.305	(-13.66)
4	0.09594	(201.3)	1.685	(-4.496)	0.9331	(-8.782)
5	0.5841	(-4.372)	1.39	(7.532)	2.259	(-7.31)
6	0.1162	(-2.054)	2.408	(10.03)	3.011	(-10.26)
7	0.4423	(-4.859)	2.19	(-4.884)	1.305	(-13.66)
8	0.09594	(201.3)	1.685	(-4.496)	0.9331	(-8.782)

Figure 48 : Control of the radiation at 87 Hz in one direction, $\theta = 90°$

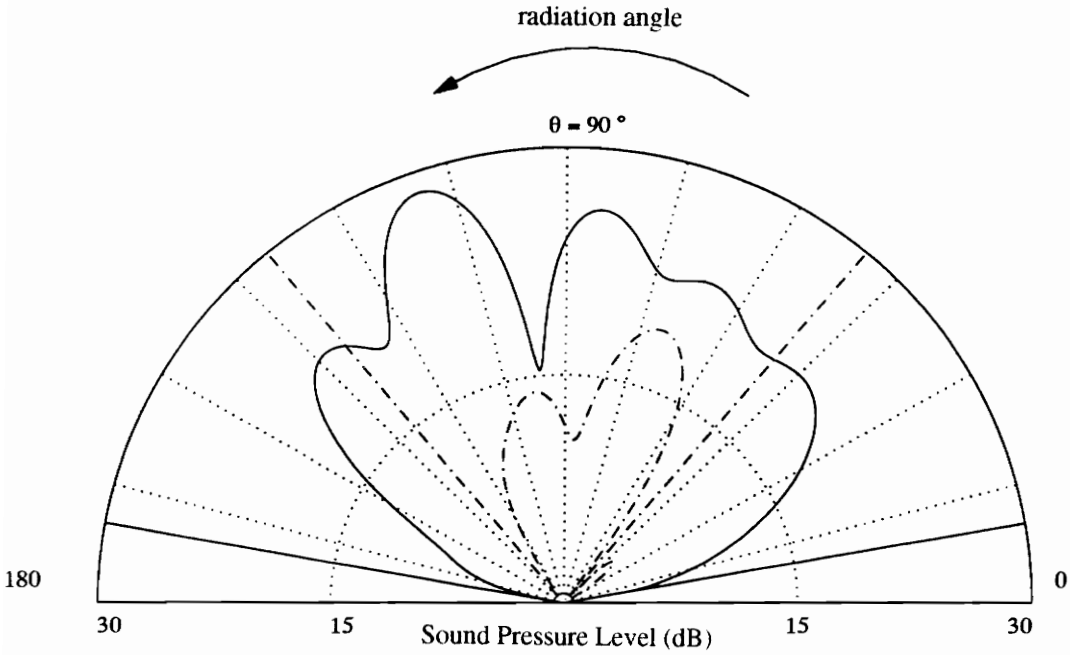

Frequency:
516
Effort:
0.2744

#	F. control:		F. mounts (u):		F. mounts (c):	
1	0.1148	(1.371)	0.2044	(2.383)	0.2065	(2.256)
2	0.01253	(1.524)	0.06192	(1.886)	0.05606	(2.044)
3	0.1021	(4.093)	0.1379	(2.427)	0.1409	(2.209)
4	0.1022	(3.311)	0.009333	(-1.851)	0.01411	(-6.06)
5	0.1373	(1.747)	0.1826	(2.36)	0.1788	(2.302)
6	0.0376	(5.047)	0.08352	(2.049)	0.08388	(2.044)
7	0.1021	(4.093)	0.1379	(2.427)	0.1409	(2.209)
8	0.1022	(3.311)	0.009333	(-1.851)	0.01411	(-6.06)

Figure 49 : Control of the radiation at 516 Hz in two directions

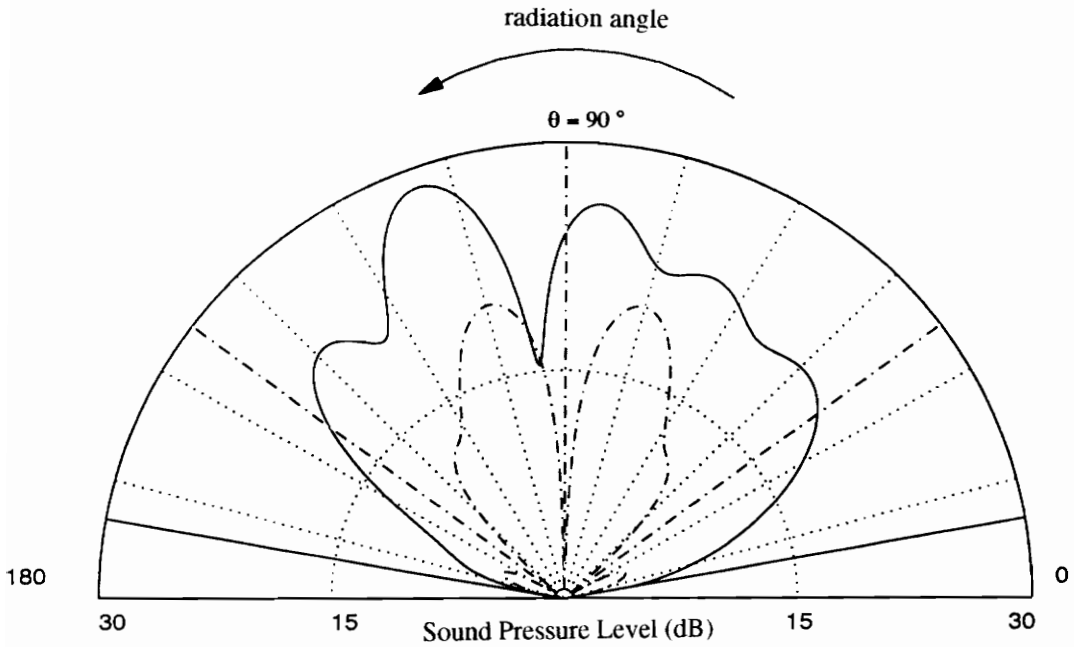

Frequency:	#	F. control:		F. mounts (u):		F. mounts (c):	
516	1	0.1328	(1.255)	0.2061	(2.558)	0.2198	(2.245)
	2	0.04088	(0.2213)	0.06123	(1.855)	0.06353	(1.725)
Effort:	3	0.1439	(-18.44)	0.1394	(2.737)	0.1501	(2.336)
	4	0.08169	(-0.04267)	0.005661	(-6.121)	0.008463	(-3.768)
0.3161	5	0.1545	(1.6)	0.1844	(2.553)	0.1918	(2.277)
	6	0.04488	(-0.4501)	0.08283	(2.025)	0.09148	(1.828)
	7	0.1439	(-18.44)	0.1394	(2.737)	0.1501	(2.336)
	8	0.08169	(-0.04267)	0.005661	(-6.121)	0.008463	(-3.768)

Figure 50 : Control of the radiation at 516 Hz in three directions

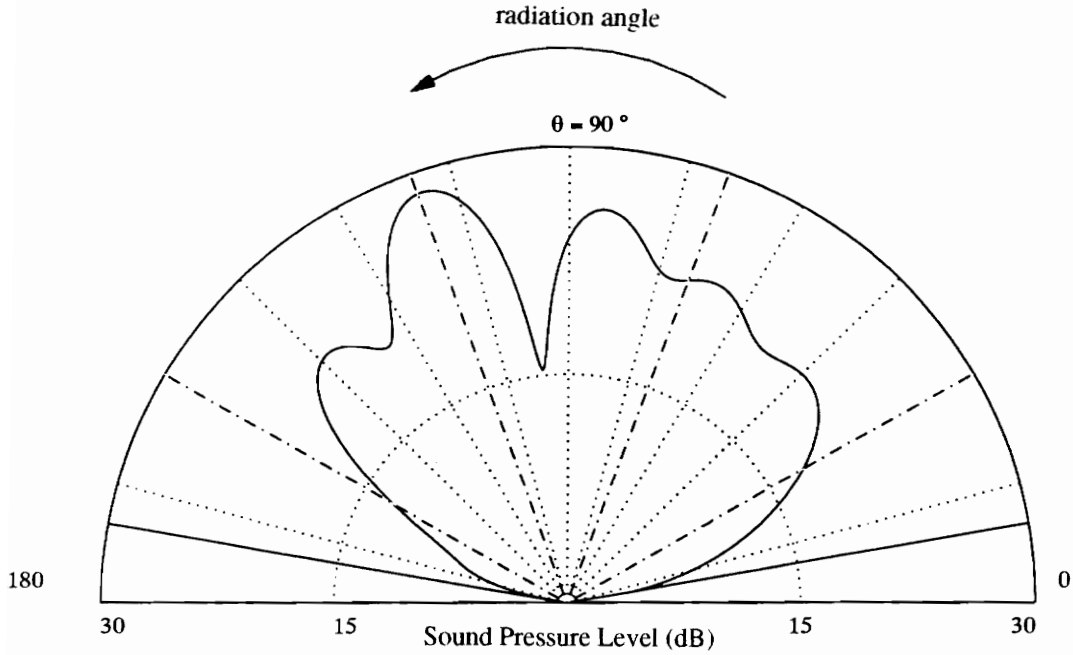

Frequency:

516

Effort:

0.3755

#	F. control:		F. mounts (a):		F. mounts (c):	
1	0.1814	(1.884)	0.2044	(2.383)	0.2188	(2.102)
2	0.09801	(2.422)	0.06192	(1.886)	0.06038	(1.842)
3	0.1492	(2.085)	0.1379	(2.427)	0.1492	(2.085)
4	0.01436	(-5.017)	0.009333	(-1.851)	0.01436	(-5.017)
5	0.2244	(2.38)	0.1826	(2.36)	0.1865	(2.173)
6	0.05668	(1.22)	0.08352	(2.049)	0.09275	(1.827)
7	0.1492	(2.085)	0.1379	(2.427)	0.1492	(2.085)
8	0.01436	(-5.017)	0.009333	(-1.851)	0.01436	(-5.017)

Figure 51 : Control of the radiation at 516 Hz in four directions

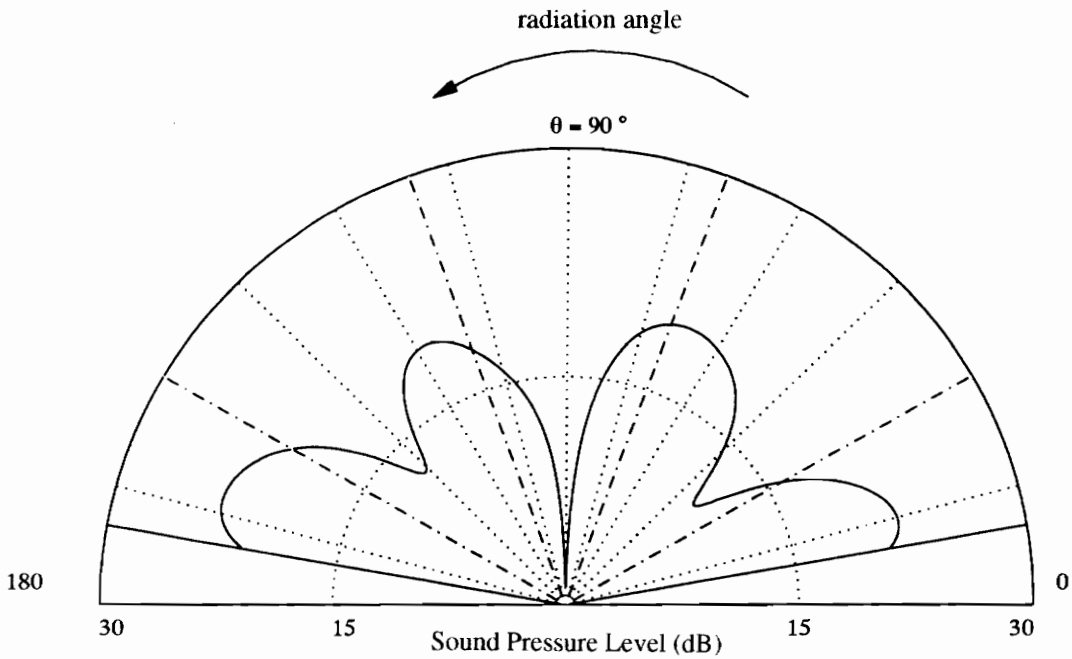

Frequency:
1020
Effort:
0.09015

#	F. control:		F. mounts (a):		F. mounts (c):	
1	0.0487	(1.375)	0.05184	(1.46)	0.05291	(1.411)
2	0.01612	(1.398)	0.01197	(1.279)	0.01193	(1.255)
3	0.03659	(1.441)	0.03583	(1.486)	0.03659	(1.441)
4	0.004344	(1.665)	0.004042	(1.919)	0.004344	(1.665)
5	0.05082	(1.463)	0.04614	(1.457)	0.0466	(1.428)
6	0.01409	(1.127)	0.01766	(1.342)	0.01824	(1.267)
7	0.03659	(1.441)	0.03583	(1.486)	0.03659	(1.441)
8	0.004344	(1.665)	0.004042	(1.919)	0.004344	(1.665)

Figure 52 : Control of the radiation at 1020 Hz in four directions

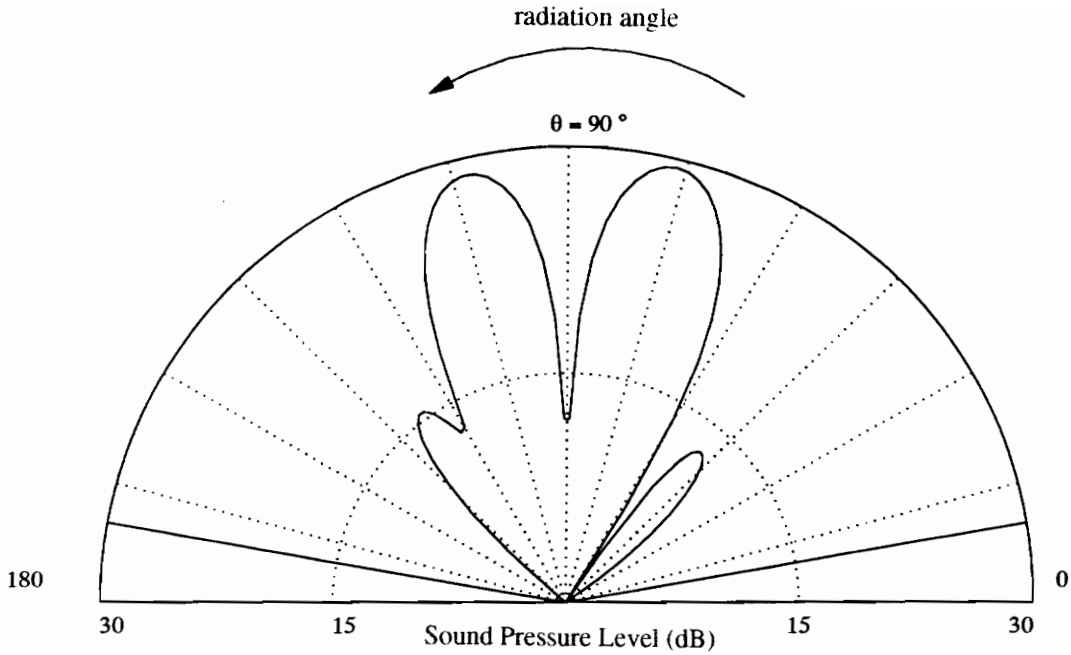

Frequency:	#	F. control:		F. mounts (u):		F. mounts (c):	
303	1	0.263	(2.721)	0.3158	(3.775)	0.3521	(3.252)
	2	0.1921	(3.804)	0.109	(2.832)	0.1028	(2.555)
Effort:	3	0.2385	(3.428)	0.2096	(4.05)	0.2385	(3.428)
	4	0.01294	(-4.208)	0.007696	(0.07717)	0.01294	(-4.208)
0.6111	5	0.384	(3.925)	0.2834	(3.749)	0.2939	(3.445)
	6	0.07616	(1.296)	0.1412	(3.079)	0.1611	(2.6)
	7	0.2385	(3.428)	0.2096	(4.05)	0.2385	(3.428)
	8	0.01294	(-4.208)	0.007696	(0.07717)	0.01294	(-4.208)

Figure 53 : Active Vibration Control at the location of the mounts at 303 Hz

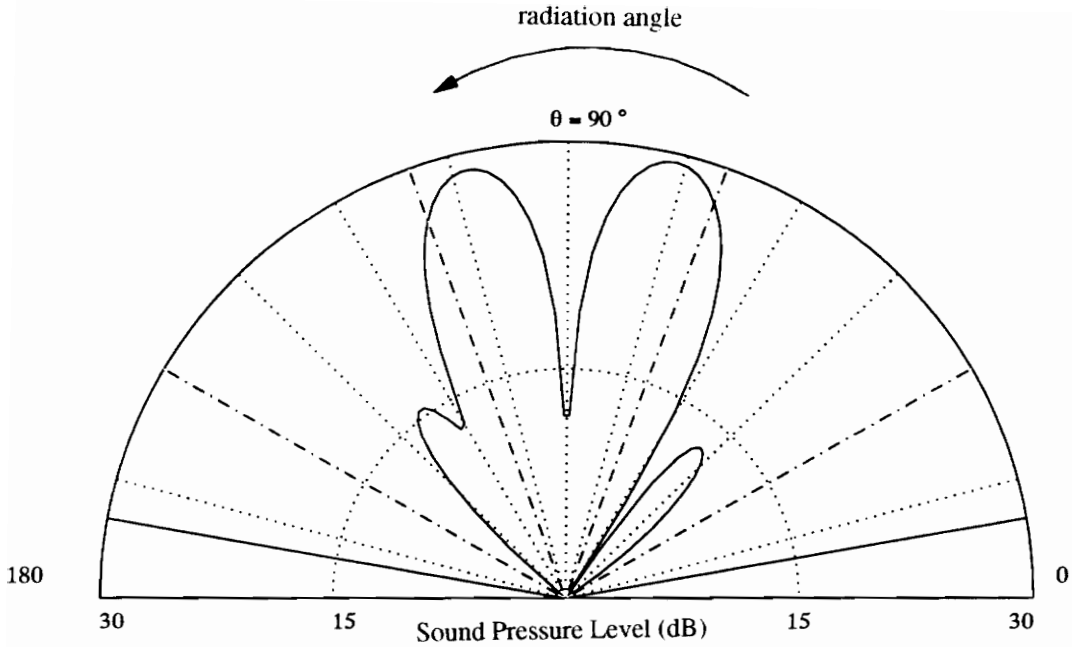

Frequency:

303

Effort:

0.611

#	F. control:		F. mounts (u):		F. mounts (c):	
1	0.2629	(2.721)	0.3158	(3.775)	0.3521	(3.252)
2	0.1922	(3.804)	0.109	(2.832)	0.1028	(2.555)
3	0.2385	(3.428)	0.2096	(4.05)	0.2385	(3.428)
4	0.01291	(-4.193)	0.007696	(0.07717)	0.01294	(-4.209)
5	0.3839	(3.925)	0.2834	(3.749)	0.2939	(3.446)
6	0.07617	(1.296)	0.1412	(3.079)	0.1611	(2.6)
7	0.2385	(3.428)	0.2096	(4.05)	0.2385	(3.428)
8	0.01291	(-4.193)	0.007696	(0.07717)	0.01294	(-4.209)

Figure 54 : Active Structural Acoustic Control in four directions at 303 Hz

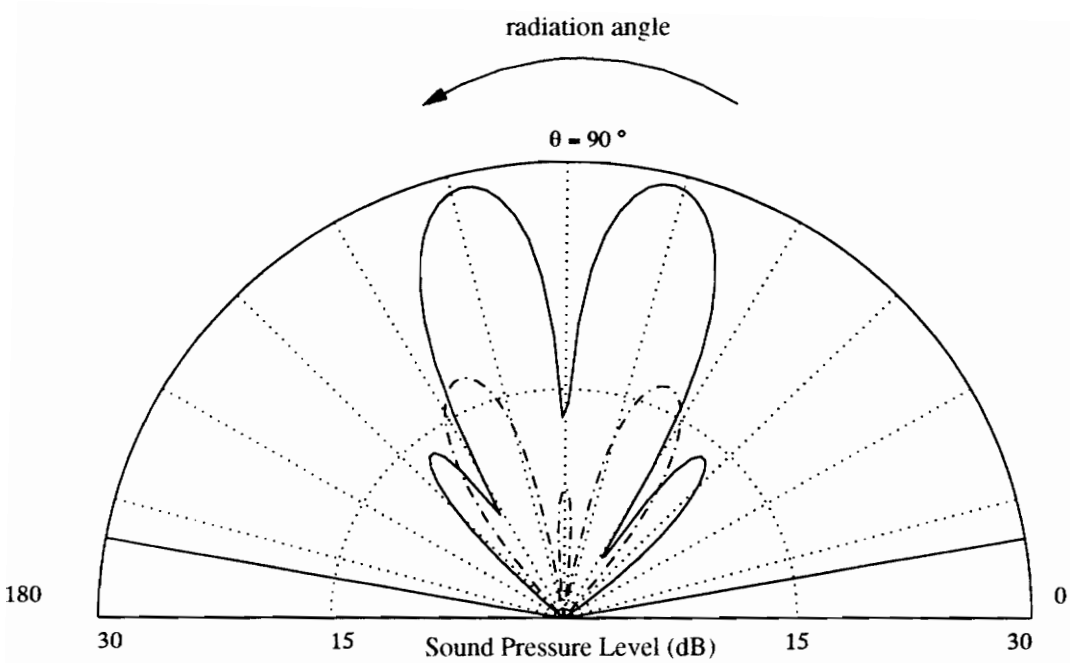

Frequency:
303
Effort:
0.6086

#	F. control:		F. mounts (a):		F. mounts (c):	
1	0.2542	(2.706)	0.3158	(3.775)	0.3532	(3.245)
2	0.19	(3.788)	0.109	(2.832)	0.104	(2.547)
3	0.2494	(3.416)	0.2096	(4.05)	0.239	(3.422)
4	0.01145	(-2.683)	0.007696	(0.07717)	0.01242	(-3.634)
5	0.3731	(3.927)	0.2834	(3.749)	0.2952	(3.434)
6	0.07605	(1.308)	0.1412	(3.079)	0.1622	(2.593)
7	0.2494	(3.416)	0.2096	(4.05)	0.239	(3.422)
8	0.01145	(-2.683)	0.007696	(0.07717)	0.01242	(-3.634)

Figure 55 : Active Vibration Control close to the location of the mounts (0.2% error) at 303 Hz

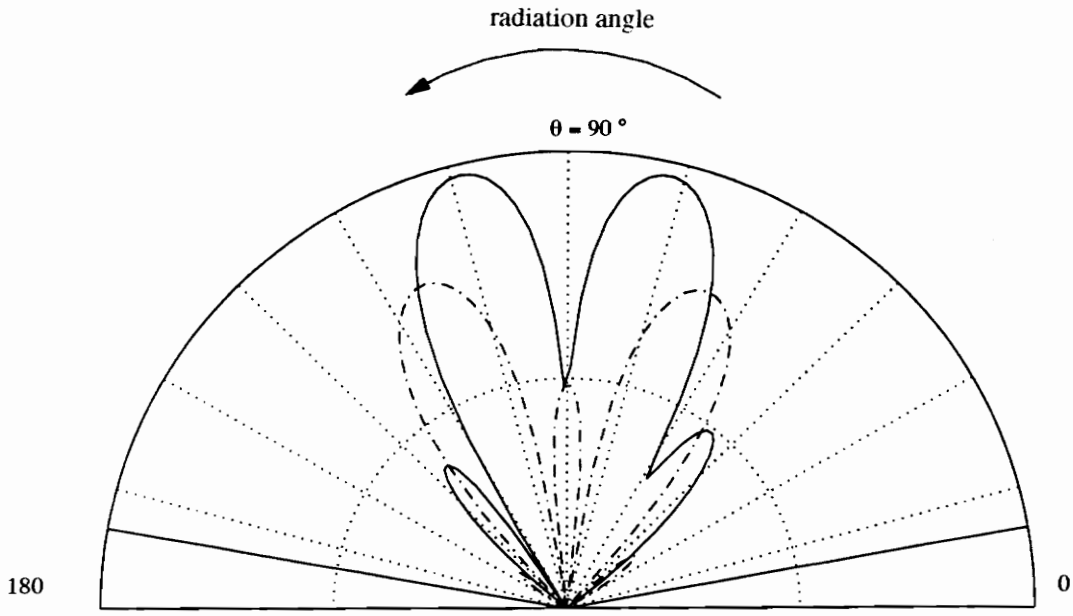

Frequency:
303
Effort:
0.607

#	F. control:		F. mounts (u):		F. mounts (c):	
1	0.2455	(2.689)	0.3158	(3.775)	0.3542	(3.237)
2	0.1881	(3.774)	0.109	(2.832)	0.1053	(2.538)
3	0.2603	(3.405)	0.2096	(4.05)	0.2394	(3.417)
4	0.01035	(-1.837)	0.007696	(0.07717)	0.01192	(-3.16)
5	0.3624	(3.931)	0.2834	(3.749)	0.2964	(3.423)
6	0.07586	(1.317)	0.1412	(3.079)	0.1632	(2.587)
7	0.2603	(3.405)	0.2096	(4.05)	0.2394	(3.417)
8	0.01035	(-1.837)	0.007696	(0.07717)	0.01192	(-3.16)

Figure 56 : Active Vibration Control close to the location of the mounts (0.5% error) at 303 Hz

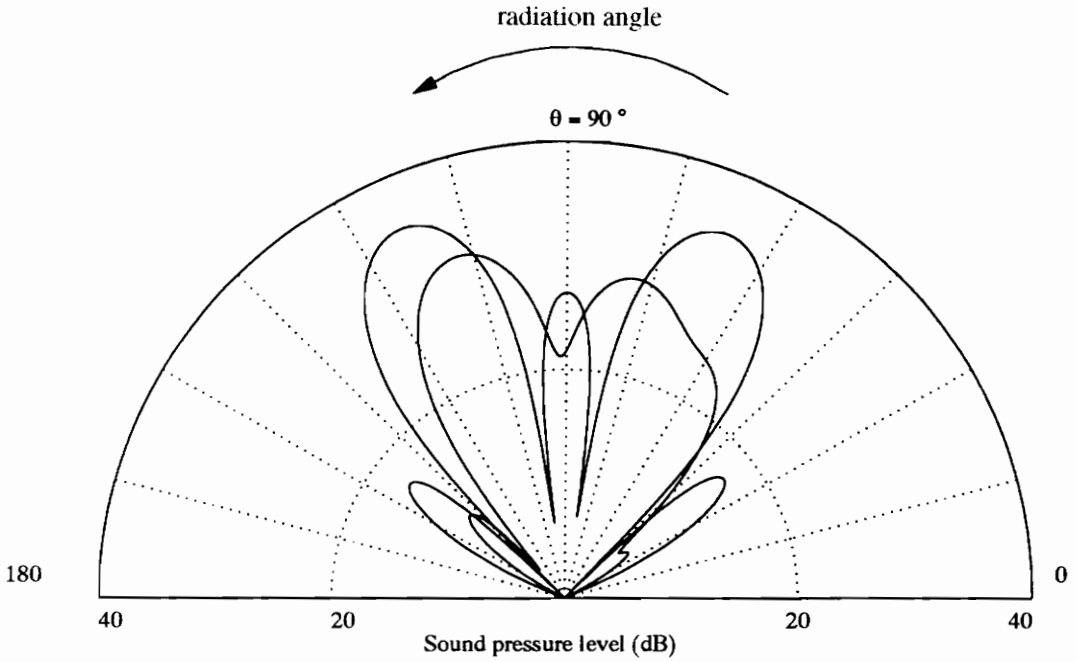

Frequency:	#	F. control:		F. mounts (u):		F. mounts (c):	
303	1	0.1802	(2.507)	0.3155	(3.779)	0.3597	(3.192)
	2	0.1747	(3.88)	0.1088	(2.836)	0.112	(2.48)
Effort:	3	0.3413	(3.309)	0.2095	(4.052)	0.2419	(3.382)
	4	0.01957	(0.8522)	0.007699	(0.08113)	0.009747	(-1.523)
0.6232	5	0.2959	(4.099)	0.2831	(3.753)	0.3031	(3.355)
	6	0.06389	(1.191)	0.141	(3.083)	0.1687	(2.546)
	7	0.3413	(3.309)	0.2095	(4.052)	0.2419	(3.382)
	8	0.01957	(0.8522)	0.007699	(0.08113)	0.009747	(-1.523)

Figure 57 : Active Vibration Control close to the location of the mounts (2% error) at 303 Hz

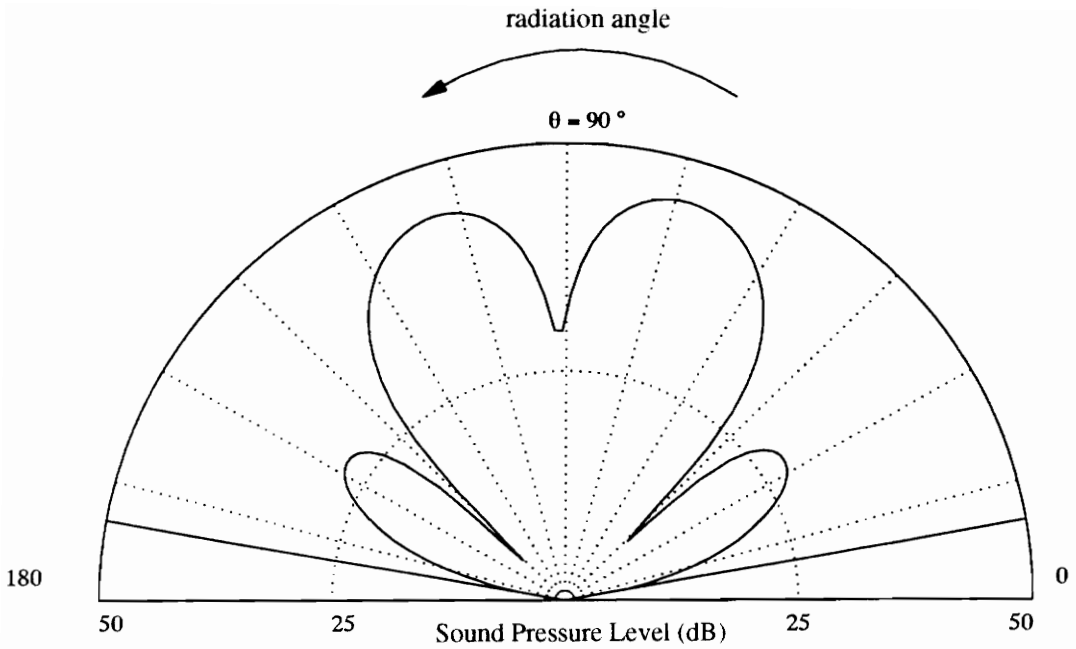

Frequency:	#	F. control:		F. mounts (a):		F. mounts (c):	
242	1	0.3557	(1.599)	0.6271	(7.164)	0.672	(2.618)
	2	0.5289	(3.768)	0.2799	(15.7)	0.2045	(1.909)
Effort:	3	0.4535	(2.937)	0.4005	(8.043)	0.4535	(2.937)
	4	0.02819	(-1.39)	0.05571	(-4.062)	0.0282	(-1.39)
1.257	5	0.8641	(3.577)	0.5706	(7.749)	0.5352	(2.878)
	6	0.1174	(-0.2086)	0.3361	(11.34)	0.3413	(2.037)
	7	0.4535	(2.937)	0.4005	(8.043)	0.4535	(2.937)
	8	0.02819	(-1.39)	0.05571	(-4.062)	0.0282	(-1.39)

Figure 58 : Active Vibration Control at the location of the mounts at 242 Hz

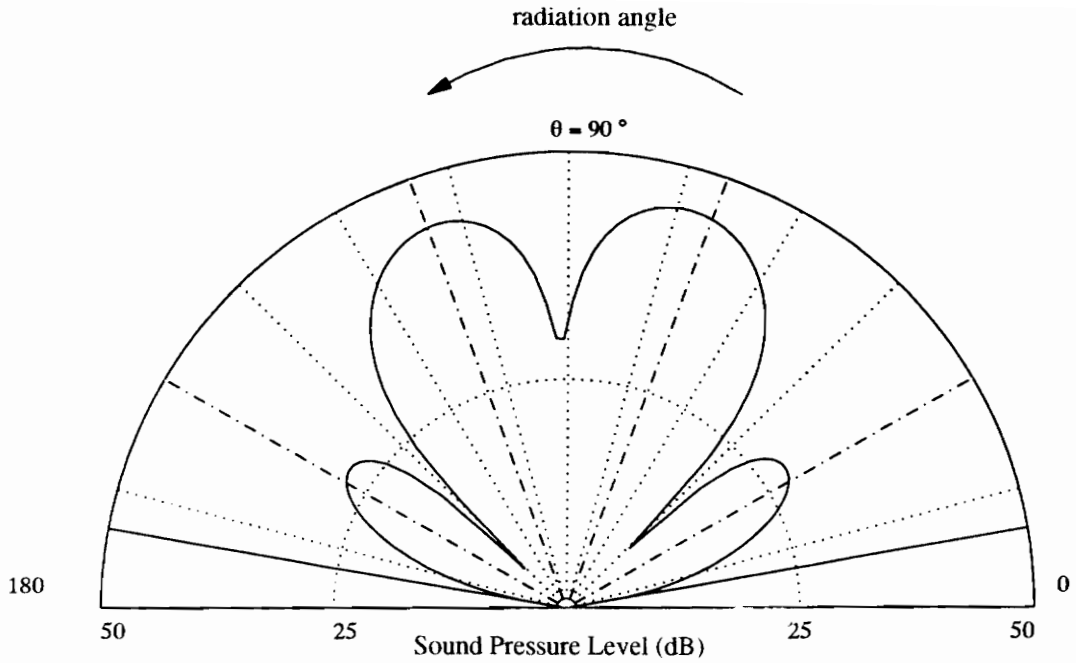

Frequency:	#	F. control:		F. mounts (u):		F. mounts (c):	
242	1	0.3557	(1.601)	0.6271	(7.164)	0.6719	(2.618)
	2	0.5287	(3.762)	0.2799	(15.7)	0.2044	(1.908)
Effort:	3	0.4534	(2.935)	0.4005	(8.043)	0.4535	(2.937)
	4	0.02807	(-1.385)	0.05571	(-4.062)	0.02822	(-1.391)
1.257	5	0.8641	(3.58)	0.5706	(7.749)	0.5352	(2.877)
	6	0.1175	(-0.2095)	0.3361	(11.34)	0.3413	(2.037)
	7	0.4534	(2.935)	0.4005	(8.043)	0.4535	(2.937)
	8	0.02807	(-1.385)	0.05571	(-4.062)	0.02822	(-1.391)

Figure 59 : Active Structural Acoustic Control in four directions at 242 Hz

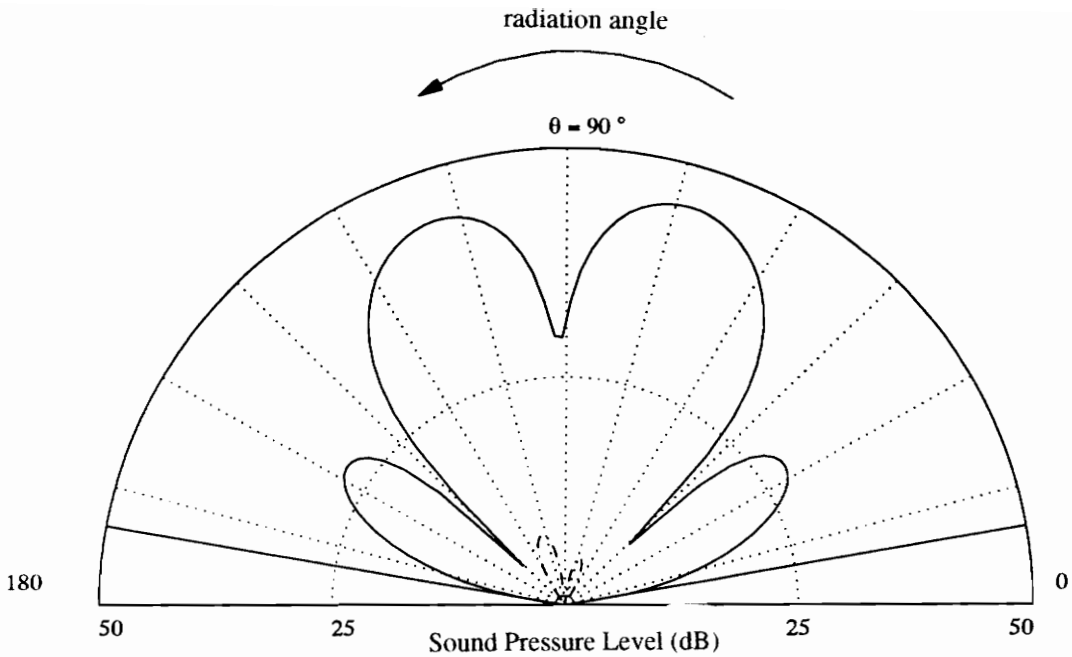

Frequency:	#	F. control:		F. mounts (u):		F. mounts (c):	
242	1	0.3427	(1.569)	0.6271	(7.164)	0.6764	(2.604)
	2	0.5285	(3.753)	0.2799	(15.7)	0.209	(1.907)
Effort:	3	0.4753	(2.91)	0.4005	(8.043)	0.4557	(2.925)
	4	0.02676	(-0.9322)	0.05571	(-4.062)	0.02722	(-1.192)
1.258	5	0.8471	(3.595)	0.5706	(7.749)	0.5397	(2.86)
	6	0.1169	(-0.1787)	0.3361	(11.34)	0.3458	(2.031)
	7	0.4753	(2.91)	0.4005	(8.043)	0.4557	(2.925)
	8	0.02676	(-0.9322)	0.05571	(-4.062)	0.02722	(-1.192)

Figure 60 : Active Vibration Control close to the location of the mounts (0.2% error) at 242 Hz

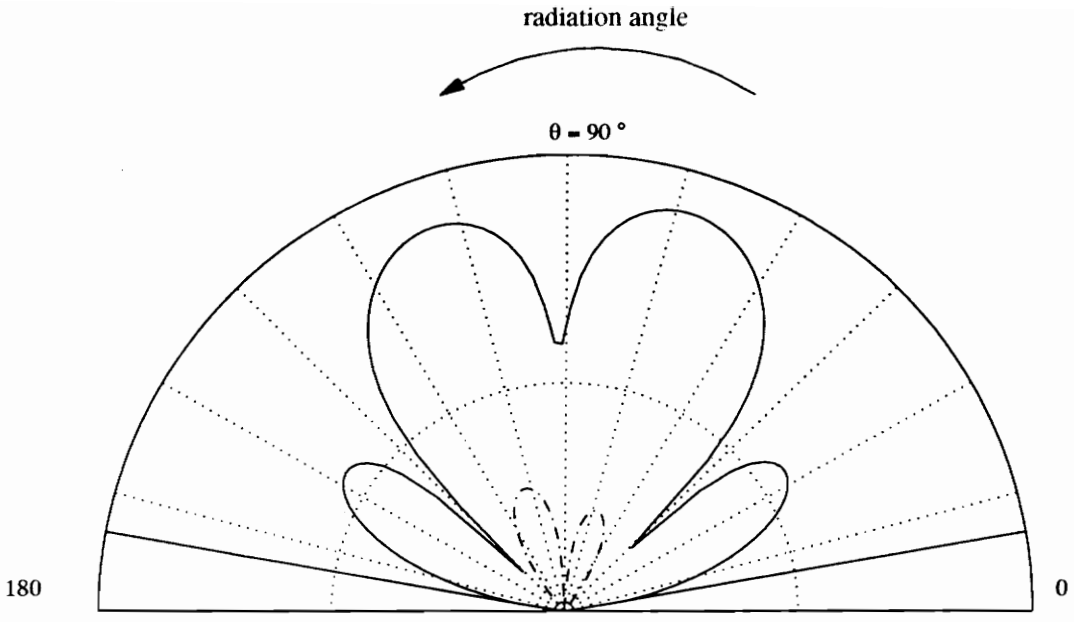

Frequency:

242

Effort:

1.259

#	F. control:		F. mounts (a):		F. mounts (c):	
1	0.3292	(1.536)	0.6271	(7.164)	0.6807	(2.591)
2	0.5285	(3.741)	0.2799	(15.7)	0.2135	(1.905)
3	0.497	(2.884)	0.4005	(8.043)	0.4578	(2.913)
4	0.02655	(-0.6115)	0.05571	(-4.062)	0.02643	(-1.018)
5	0.8301	(3.616)	0.5706	(7.749)	0.544	(2.843)
6	0.1165	(-0.1522)	0.3361	(11.34)	0.3502	(2.025)
7	0.497	(2.884)	0.4005	(8.043)	0.4578	(2.913)
8	0.02655	(-0.6115)	0.05571	(-4.062)	0.02643	(-1.018)

Figure 61 : Active Vibration Control close to the location of the mounts (0.5% error) at 242 Hz

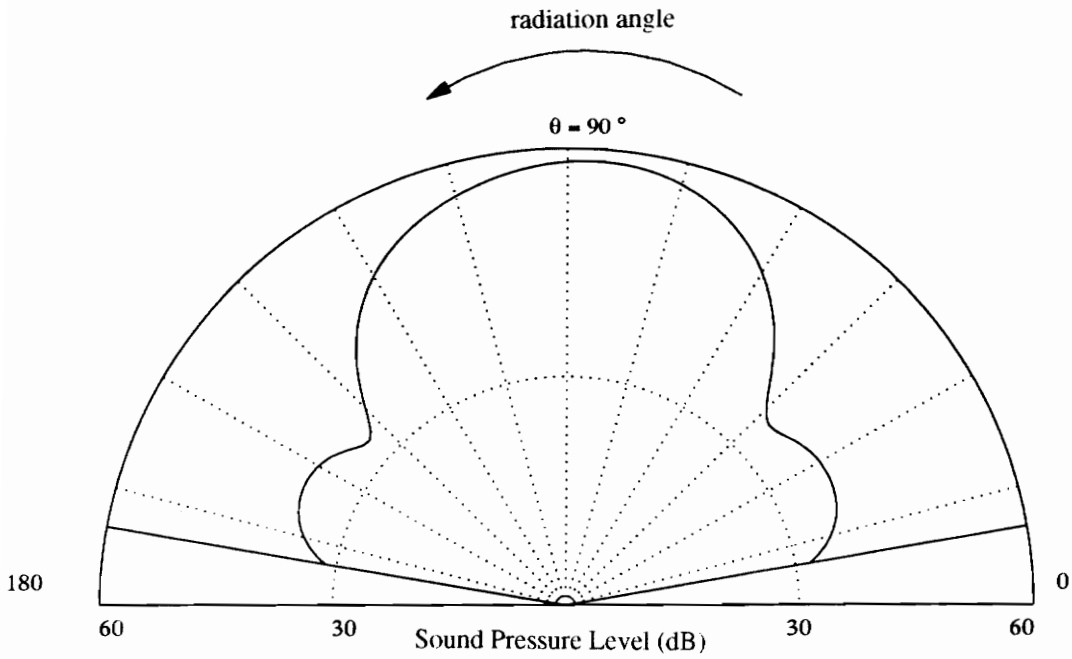

Frequency:	#	F. control:		F. mounts (a):		F. mounts (c):	
180	1	1.196	(-2.37)	3.558	(0.3294)	0.5355	(0.4849)
	2	0.8751	(2.356)	3.277	(0.2481)	0.5794	(-2.945)
Effort:	3	0.4479	(0.9654)	1.877	(0.5035)	0.4479	(0.9654)
	4	0.4744	(-50.96)	1.615	(0.1967)	0.4744	(-50.97)
3.026	5	1.614	(2.154)	3.485	(0.3195)	0.3805	(0.4871)
	6	1.872	(-5.698)	3.332	(0.2666)	0.575	(-1.453)
	7	0.4479	(0.9654)	1.877	(0.5035)	0.4479	(0.9654)
	8	0.4744	(-50.96)	1.615	(0.1967)	0.4744	(-50.97)

Figure 62 : Active Vibration Control at the location of the mounts at 180 Hz

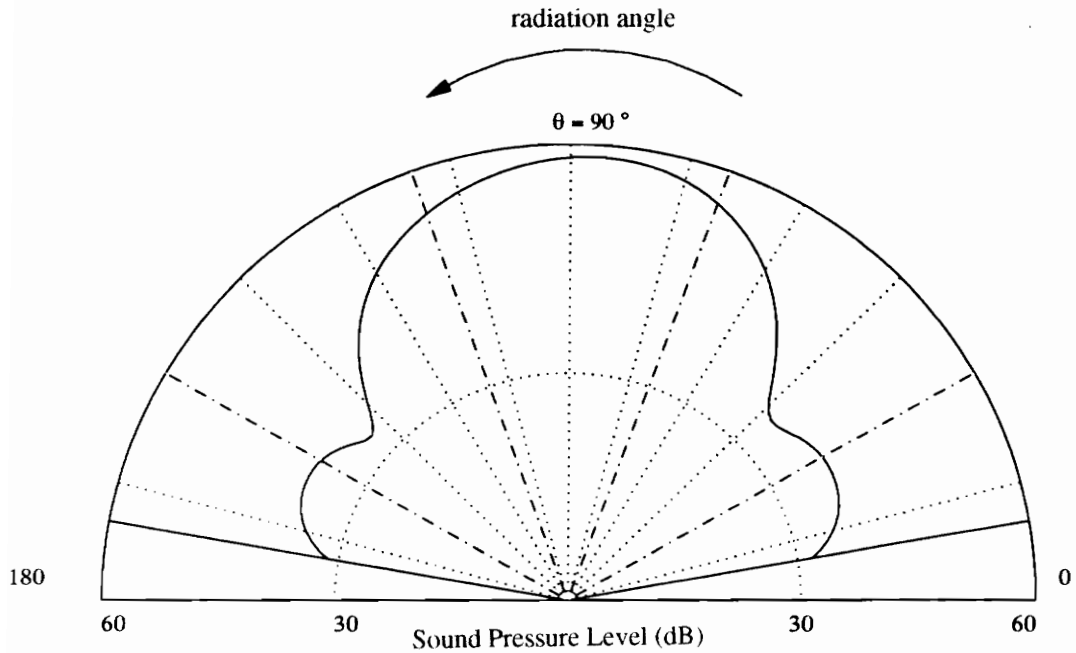

Frequency:	#	F. control:		F. mounts (u):		F. mounts (c):	
180	1	1.194	(-2.37)	3.558	(0.3294)	0.5355	(0.4856)
	2	0.873	(2.356)	3.277	(0.2481)	0.5792	(-2.946)
Effort:	3	0.4476	(0.9634)	1.877	(0.5035)	0.4479	(0.9663)
	4	0.4732	(-48.55)	1.615	(0.1967)	0.4744	(-51.26)
3.024	5	1.614	(2.156)	3.485	(0.3195)	0.3805	(0.4878)
	6	1.872	(-5.713)	3.332	(0.2666)	0.5747	(-1.453)
	7	0.4476	(0.9634)	1.877	(0.5035)	0.4479	(0.9663)
	8	0.4732	(-48.55)	1.615	(0.1967)	0.4744	(-51.26)

Figure 63 : Active Structural Acoustic Control in four directions at 180 Hz

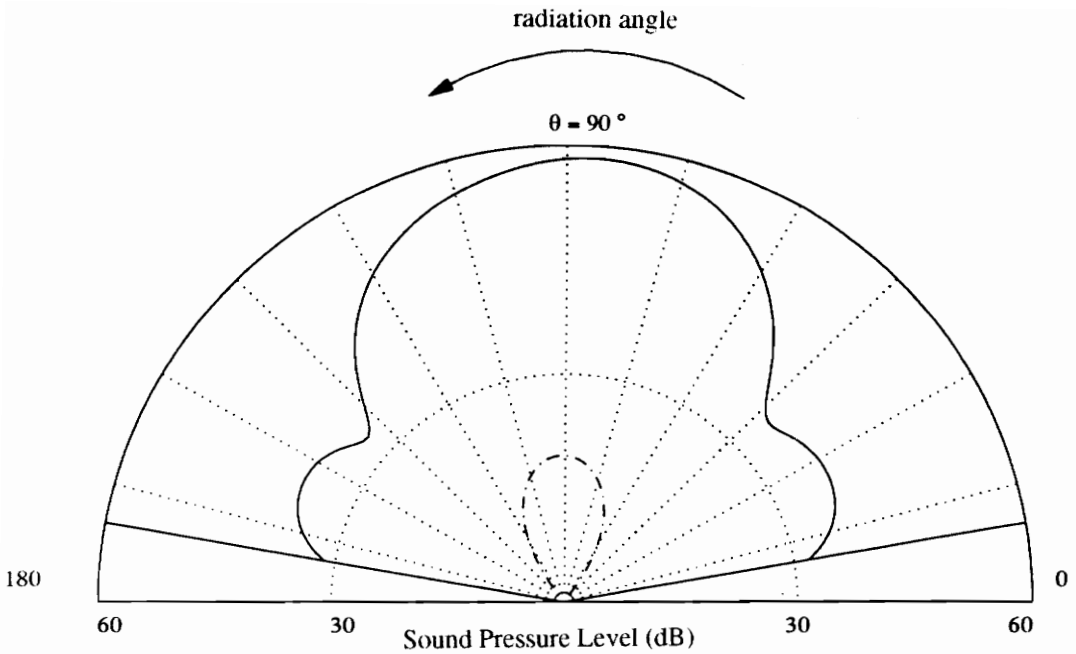

Frequency:	#	F. control:		F. mounts (a):		F. mounts (c):	
180	1	1.226	(-2.453)	3.558	(0.3294)	0.5393	(0.4522)
	2	0.8983	(2.34)	3.277	(0.2481)	0.5891	(-2.848)
Effort:	3	0.4643	(0.9211)	1.877	(0.5035)	0.4469	(0.9296)
	4	0.4968	(-29.6)	1.615	(0.1967)	0.4773	(-36.6)
3.054	5	1.605	(2.161)	3.485	(0.3195)	0.3843	(0.4515)
	6	1.875	(-5.585)	3.332	(0.2666)	0.5894	(-1.437)
	7	0.4643	(0.9211)	1.877	(0.5035)	0.4469	(0.9296)
	8	0.4968	(-29.6)	1.615	(0.1967)	0.4773	(-36.6)

Figure 64 : Active Vibration Control close to the location of the mounts (0.2% error) at 180 Hz

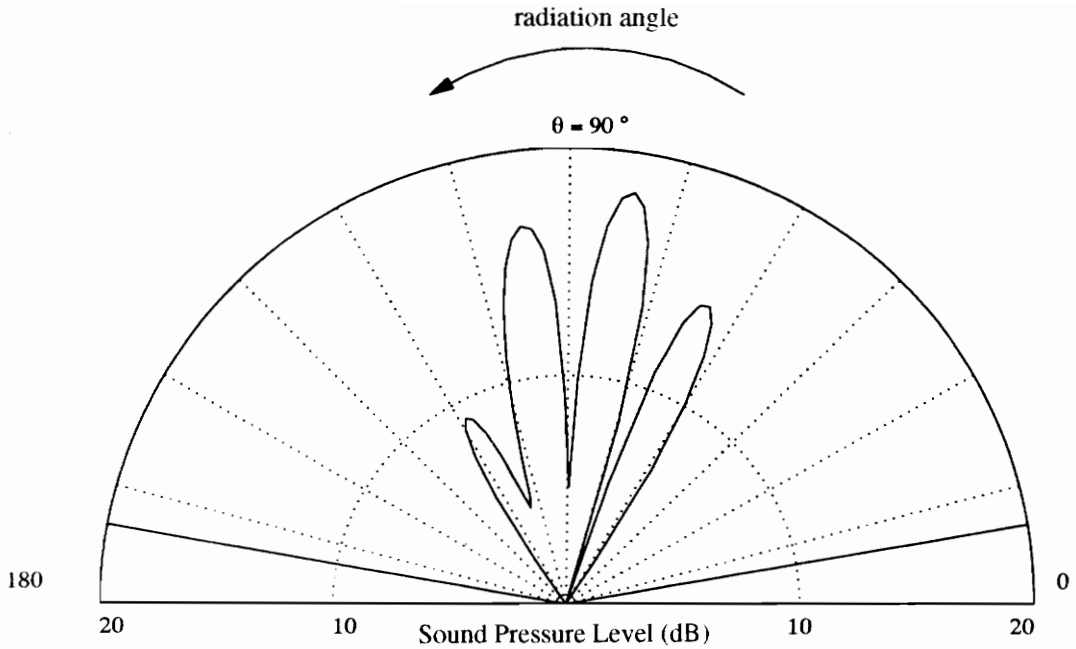

Frequency:
495
Effort:
0.1812

#	F. control:		F. mounts (a):		F. mounts (c):	
1	0.09439	(2.628)	0.1019	(2.9)	0.1063	(2.752)
2	0.03778	(2.808)	0.02575	(2.456)	0.02592	(2.397)
3	0.07323	(2.794)	0.06979	(2.964)	0.07323	(2.794)
4	0.007207	(4.508)	0.006079	(6.405)	0.007207	(4.508)
5	0.1044	(2.933)	0.09081	(2.893)	0.09248	(2.814)
6	0.02799	(1.987)	0.03681	(2.594)	0.03972	(2.4)
7	0.07323	(2.794)	0.06979	(2.964)	0.07323	(2.794)
8	0.007207	(4.508)	0.006079	(6.405)	0.007207	(4.508)

Figure 65 : Active Vibration Control at the location of the mounts at 495 Hz

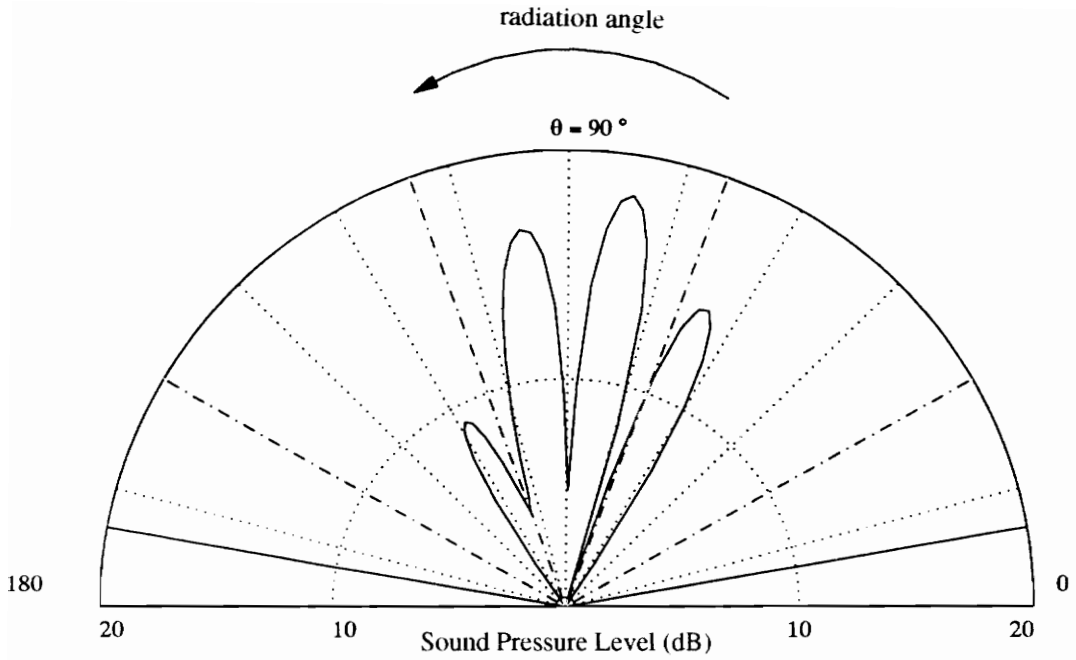

Frequency:
495
Effort:
0.1812

#	F. control:		F. mounts (a):		F. mounts (c):	
1	0.09438	(2.628)	0.1019	(2.9)	0.1063	(2.752)
2	0.03776	(2.808)	0.02575	(2.456)	0.02592	(2.396)
3	0.07323	(2.794)	0.06979	(2.964)	0.07323	(2.794)
4	0.007203	(4.509)	0.006079	(6.405)	0.007206	(4.508)
5	0.1044	(2.933)	0.09081	(2.893)	0.09248	(2.814)
6	0.02798	(1.986)	0.03681	(2.594)	0.03972	(2.4)
7	0.07323	(2.794)	0.06979	(2.964)	0.07323	(2.794)
8	0.007203	(4.509)	0.006079	(6.405)	0.007206	(4.508)

Figure 66 : Active Structural Acoustic Control in four directions at 495 Hz

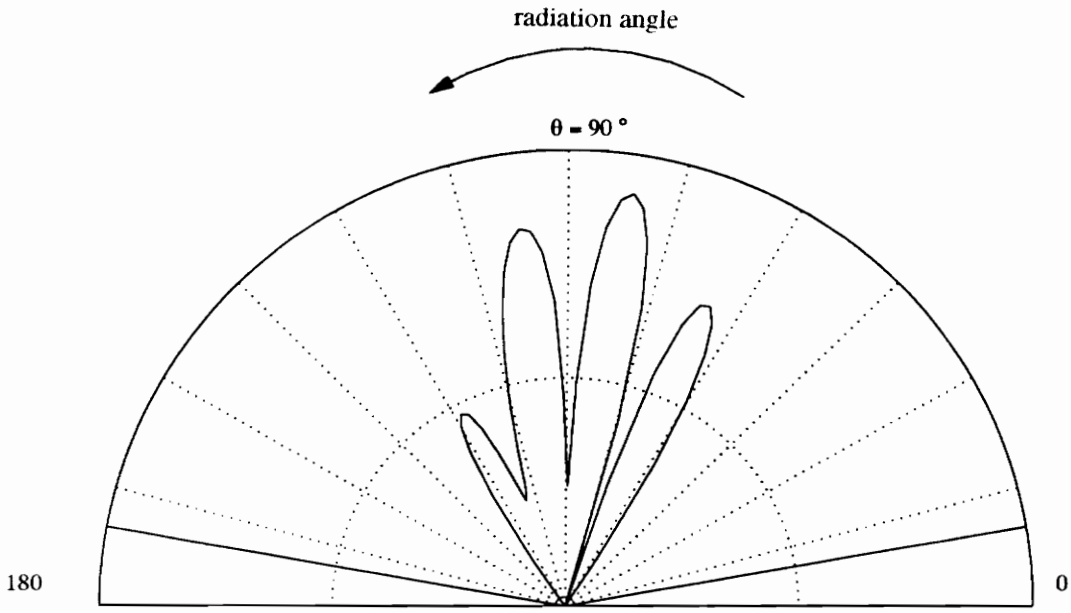

Frequency:
495
Effort:
0.1797

#	F. control:		F. mounts (u):		F. mounts (c):	
1	0.09108	(2.6)	0.1019	(2.9)	0.1063	(2.75)
2	0.03718	(2.722)	0.02575	(2.456)	0.02604	(2.39)
3	0.07609	(2.794)	0.06979	(2.964)	0.07325	(2.792)
4	0.007269	(4.649)	0.006079	(6.405)	0.007137	(4.585)
5	0.1008	(2.904)	0.09081	(2.893)	0.0926	(2.811)
6	0.02773	(1.935)	0.03681	(2.594)	0.0398	(2.396)
7	0.07609	(2.794)	0.06979	(2.964)	0.07325	(2.792)
8	0.007269	(4.649)	0.006079	(6.405)	0.007137	(4.585)

Figure 67 : Active Vibration Control close to the location of the mounts (1% error) at 495 Hz

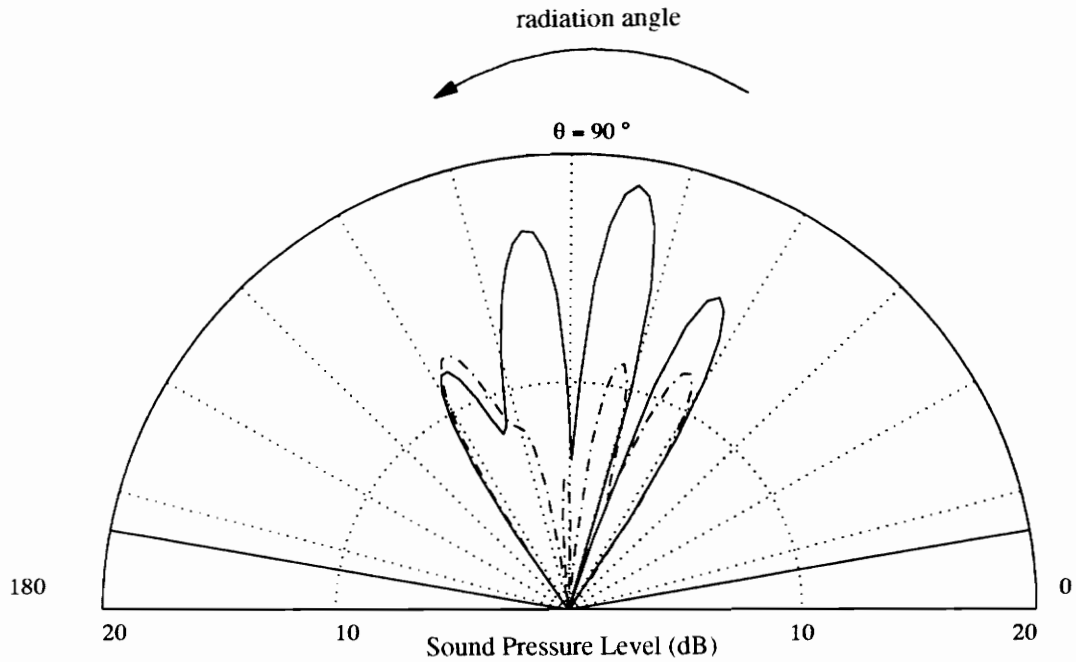

Frequency:

495

Effort:

0.1649

#	F. control:		F. mounts (m):		F. mounts (c):	
1	0.0369	(2.356)	0.1019	(2.9)	0.1064	(2.761)
2	0.04845	(2.226)	0.02575	(2.456)	0.02721	(2.347)
3	0.09949	(2.954)	0.06979	(2.964)	0.07302	(2.812)
4	0.003618	(-0.5844)	0.006079	(6.405)	0.00633	(6.035)
5	0.04457	(2.906)	0.09081	(2.893)	0.09316	(2.816)
6	0.04108	(1.822)	0.03681	(2.594)	0.04048	(2.377)
7	0.09949	(2.954)	0.06979	(2.964)	0.07302	(2.812)
8	0.003618	(-0.5844)	0.006079	(6.405)	0.00633	(6.035)

Figure 68 : Active Vibration Control close to the location of the mounts (3% error) at 495 Hz

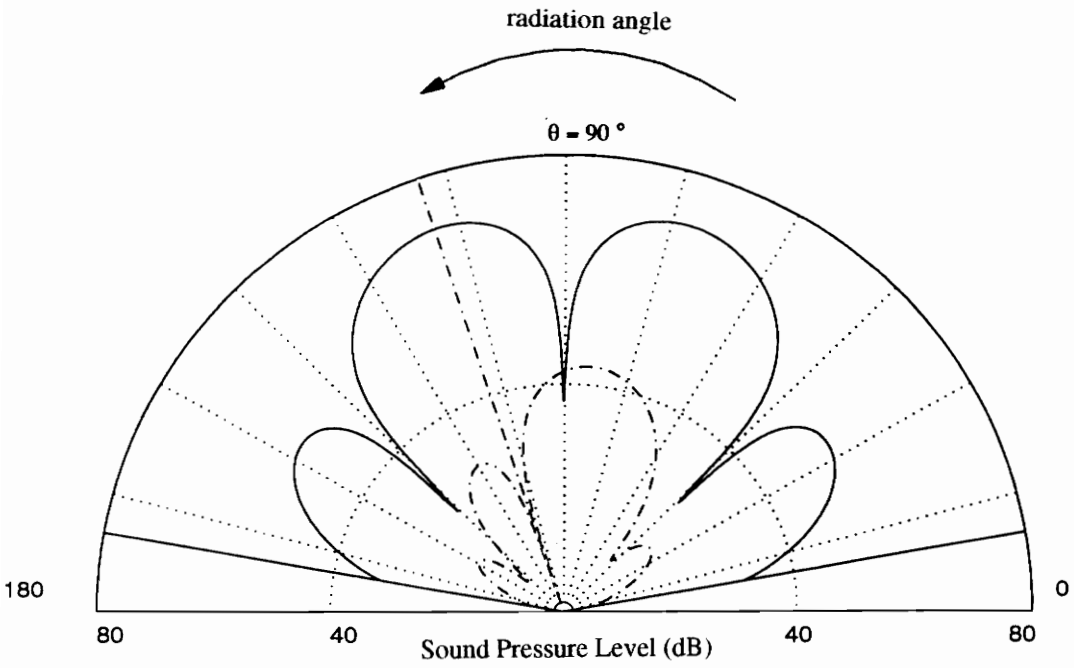

Frequency:	#	F. control:		F. mounts (u):		F. mounts (c):	
242	1	0.5218	(-4.121)	8.896	(-0.1223)	0.5071	(1.193)
	2	0.4694	(3.318)	8.933	(-0.1412)	0.2894	(-2.078)
Effort:	3	0.5023	(-6.596)	4.464	(-0.1167)	0.4201	(1.713)
	4	0.4691	(4.857)	4.475	(-0.2216)	0.297	(-25.1)
1.386	5	0.4634	(3.45)	8.891	(-0.1267)	0.3609	(1.157)
	6	0.5187	(-3.886)	8.927	(-0.1382)	0.2506	(-0.6787)
	7	0.5023	(-6.596)	4.464	(-0.1167)	0.4201	(1.713)
	8	0.4691	(4.857)	4.475	(-0.2216)	0.297	(-25.1)

Figure 69 : Parallel system with 8 mounts, 242 Hz, control at $\theta = 132°$

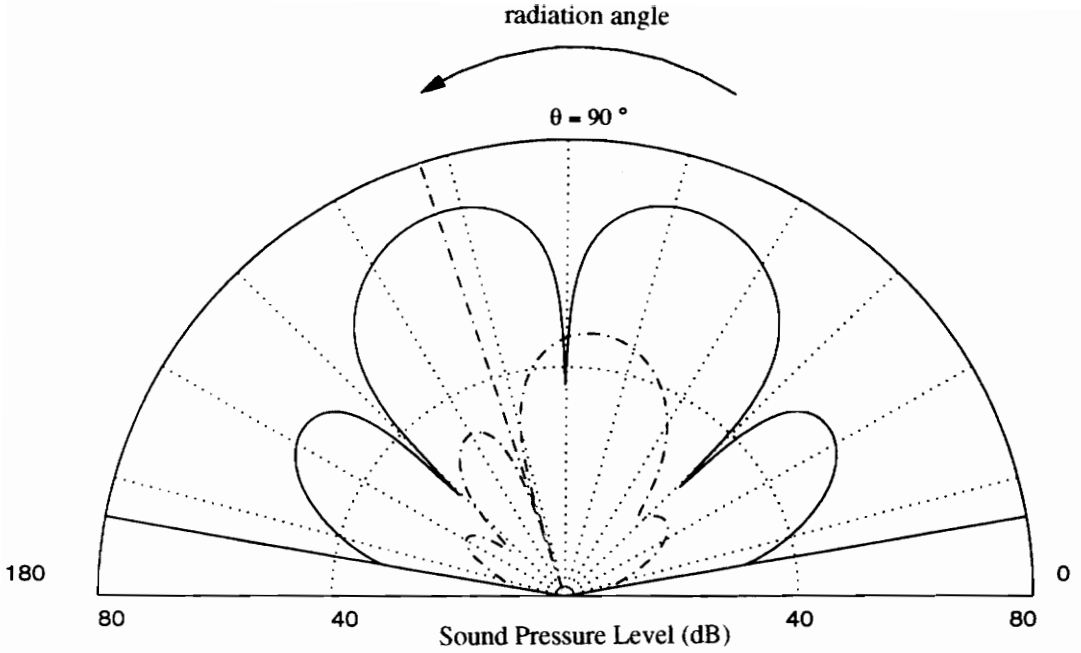

Frequency:
242
Effort:
3.565

#	F. control:		F. mounts (u):		F. mounts (c):	
1	1.465	(-1.181)	8.896	(-0.1223)	1.211	(0.05717)
2	1.212	(0.8516)	8.933	(-0.1412)	0.8192	(-0.3866)
3	1.264	(-1.855)	4.464	(-0.1167)	0.771	(0.3007)
4	1.099	(1.283)	4.475	(-0.2216)	0.3282	(-0.5402)
5	1.162	(0.8722)	8.891	(-0.1267)	0.8606	(0.09276)
6	1.46	(-1.107)	8.927	(-0.1382)	1.157	(-0.2728)
7	1.264	(-1.855)	4.464	(-0.1167)	0.771	(0.3007)
8	1.099	(1.283)	4.475	(-0.2216)	0.3282	(-0.5402)

Figure 70 : Opposed system with 8 mounts, 242 Hz, control at $\theta = 132°$

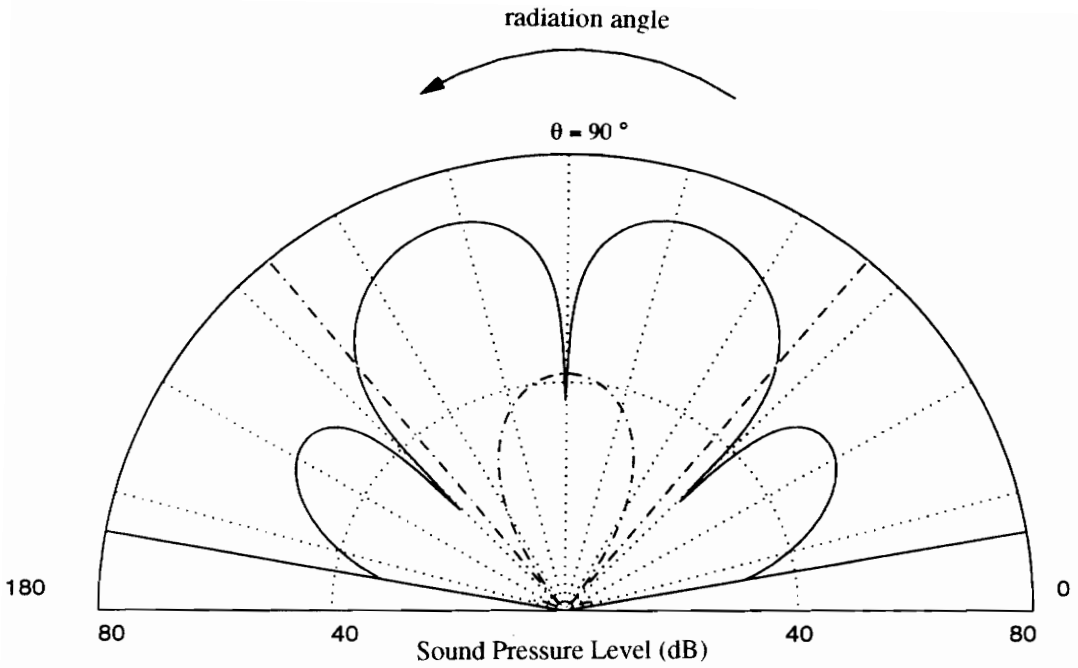

Frequency:

242

Effort:

1.854

#	F. control:		F. mounts (u):		F. mounts (c):	
1	1.301	(-1.359)	8.896	(-0.1223)	0.4122	(0.4522)
2	0.9326	(-3.377)	8.933	(-0.1412)	0.4136	(-5.623)
3	0.294	(-2.952)	4.464	(-0.1167)	0.3516	(0.8557)
4	0.2392	(0.8852)	4.475	(-0.2216)	0.3518	(7.742)
5	0.5673	(0.5426)	8.891	(-0.1267)	0.2735	(0.3727)
6	0.5166	(5.354)	8.927	(-0.1382)	0.3817	(-1.71)
7	0.294	(-2.952)	4.464	(-0.1167)	0.3516	(0.8557)
8	0.2392	(0.8852)	4.475	(-0.2216)	0.3518	(7.742)

Figure 71 : Parallel system with 8 mounts, 242 Hz, control in 2 directions

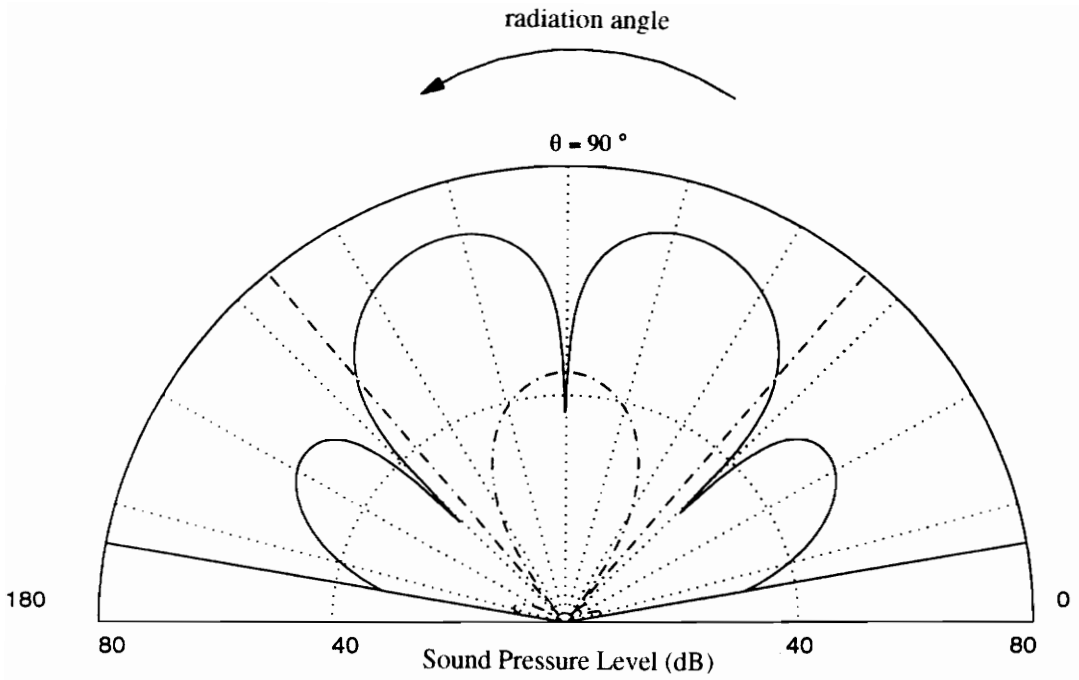

Frequency:	#	F. control:		F. mounts (u):		F. mounts (c):	
242	1	2.699	(-0.7882)	8.896	(-0.1223)	1.459	(-0.1955)
	2	1.664	(1.855)	8.933	(-0.1412)	0.9212	(-0.6335)
Effort:	3	1.038	(-0.8643)	4.464	(-0.1167)	0.897	(-0.002067)
	4	0.7324	(0.5228)	4.475	(-0.2216)	0.3277	(-1.046)
4.108	5	1.446	(0.2546)	8.891	(-0.1267)	1.007	(-0.193)
	6	1.226	(-1.34)	8.927	(-0.1382)	1.35	(-0.4596)
	7	1.038	(-0.8643)	4.464	(-0.1167)	0.897	(-0.002067)
	8	0.7324	(0.5228)	4.475	(-0.2216)	0.3277	(-1.046)

Figure 72 : Opposed system with 8 mounts, 242 Hz, control in 2 directions

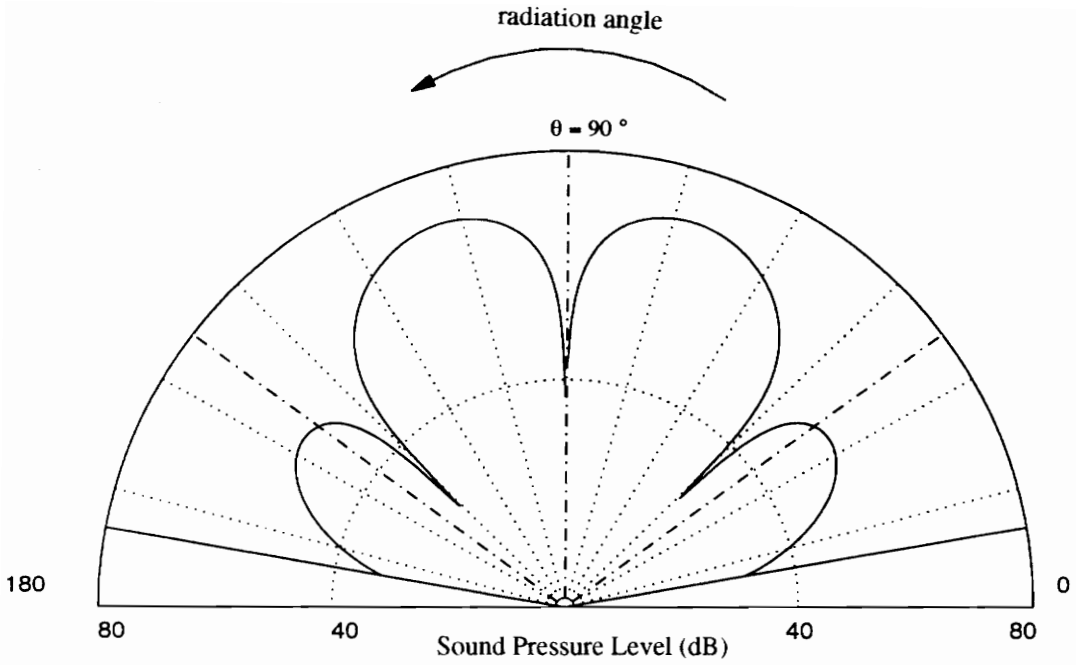

Frequency:	#	F. control:		F. mounts (u):		F. mounts (c):	
242	1	1.358	(-2.364)	8.896	(-0.1223)	0.5723	(-0.1838)
	2	0.455	(1.209)	8.933	(-0.1412)	0.858	(-4.833)
Effort:	3	0.438	(0.305)	4.464	(-0.1167)	0.4081	(0.3442)
	4	0.6133	(-396.6)	4.475	(-0.2216)	0.6091	(17.14)
3.033	5	1.271	(1.573)	8.891	(-0.1267)	0.409	(-0.1302)
	6	2.098	(-8.858)	8.927	(-0.1382)	0.9462	(-2.417)
	7	0.438	(0.305)	4.464	(-0.1167)	0.4081	(0.3442)
	8	0.6133	(-396.6)	4.475	(-0.2216)	0.6091	(17.14)

Figure 73 : Parallel system with 8 mounts, 242 Hz, control in 3 directions

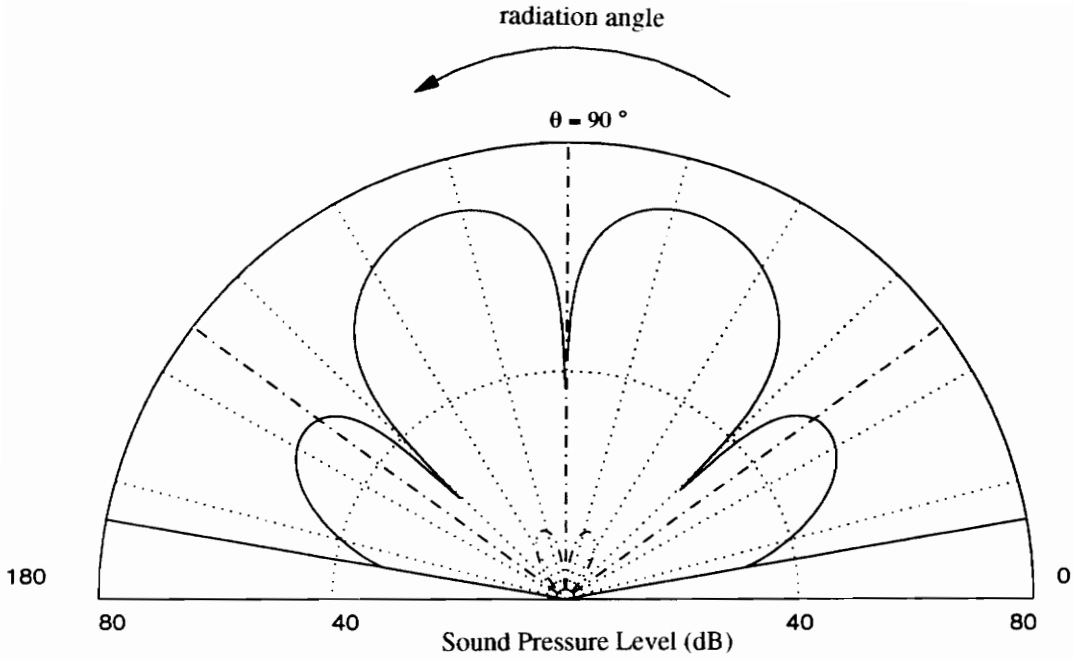

Frequency:	#	F. control:		F. mounts (u):		F. mounts (c):	
242	1	2.567	(-0.7698)	8.896	(-0.1223)	1.927	(-0.2833)
	2	1.296	(0.4668)	8.933	(-0.1412)	1.385	(-0.8544)
Effort:	3	1.288	(-0.1444)	4.464	(-0.1167)	1.144	(-0.09255)
	4	0.7375	(-1.529)	4.475	(-0.2216)	0.6045	(-2.16)
5.071	5	1.988	(0.6045)	8.891	(-0.1267)	1.333	(-0.2433)
	6	3.015	(-1.111)	8.927	(-0.1382)	1.951	(-0.6116)
	7	1.288	(-0.1444)	4.464	(-0.1167)	1.144	(-0.09255)
	8	0.7375	(-1.529)	4.475	(-0.2216)	0.6045	(-2.16)

Figure 74 : Opposed system with 8 mounts, 242 Hz, control in 3 directions

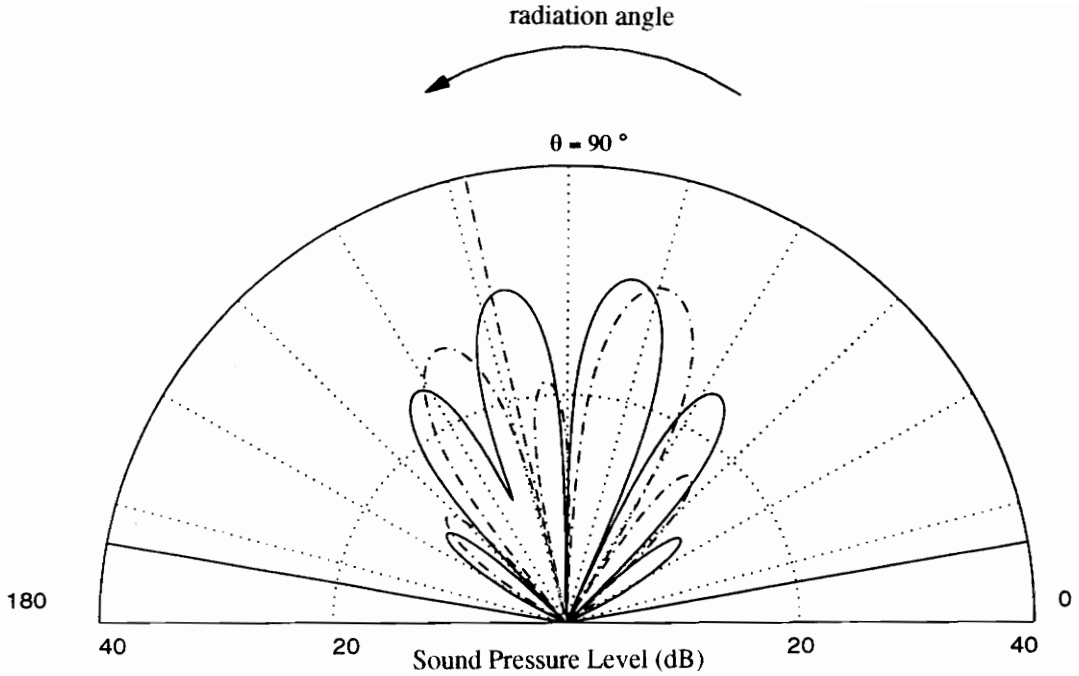

Frequency:
350
Effort:
0.71

#	F. control:		F. mounts (u):		F. mounts (c):	
1	0.2944	(0.8976)	0.5847	(3.208)	0.5698	(3.631)
2	0.2148	(-2.203)	0.3813	(3.092)	0.3513	(4.041)
3	0.09779	(-0.1934)	0.3438	(3.487)	0.3391	(3.847)
4	0.3206	(1.344)	0.141	(2.932)	0.122	(4.261)
5	0.3532	(1.23)	0.5127	(3.197)	0.4795	(3.876)
6	0.1475	(-1.304)	0.4532	(3.163)	0.4416	(3.747)
7	0.09779	(-0.1934)	0.3438	(3.487)	0.3391	(3.847)
8	0.3206	(1.344)	0.141	(2.932)	0.122	(4.261)

Figure 75 : Parallel system with 8 mounts, 350 Hz, control at $\theta = 103°$

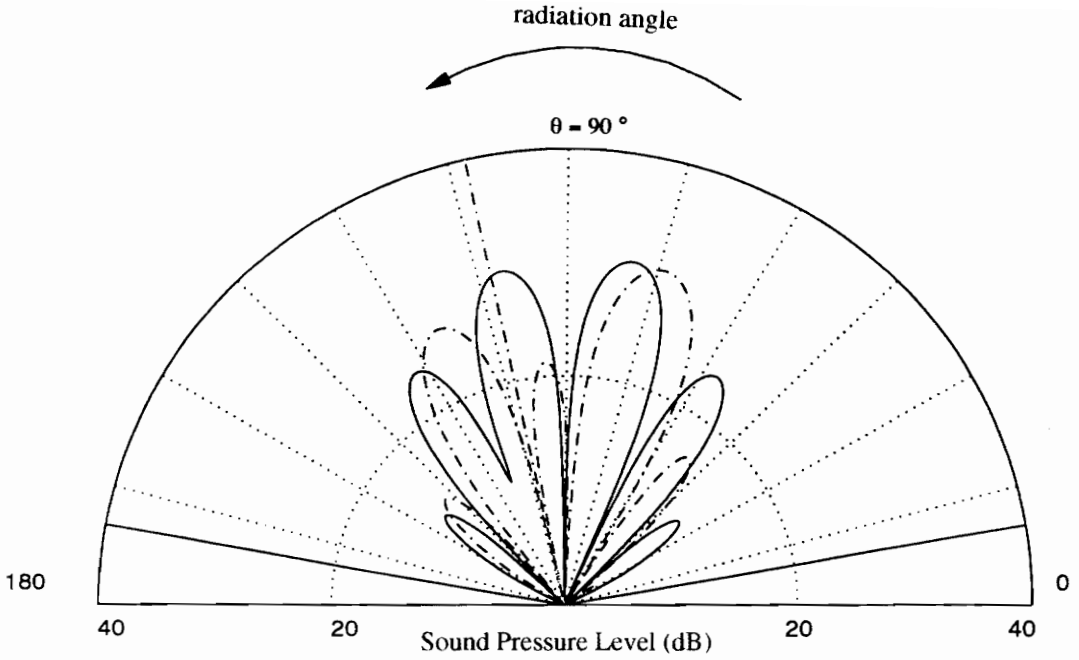

Frequency:
350
Effort:
0.71

#	F. control:		F. mounts (u):		F. mounts (c):	
1	0.2944	(0.8977)	0.5847	(3.208)	0.5698	(3.632)
2	0.2148	(-2.203)	0.3813	(3.092)	0.3513	(4.041)
3	0.09777	(-0.1939)	0.3438	(3.487)	0.3392	(3.844)
4	0.3206	(1.344)	0.141	(2.932)	0.122	(4.258)
5	0.3532	(1.23)	0.5127	(3.197)	0.4795	(3.877)
6	0.1475	(-1.304)	0.4532	(3.163)	0.4416	(3.747)
7	0.09777	(-0.1939)	0.3438	(3.487)	0.3392	(3.844)
8	0.3206	(1.344)	0.141	(2.932)	0.122	(4.258)

Figure 76 : Opposed system with 8 mounts, 350 Hz, control at $\theta = 103°$

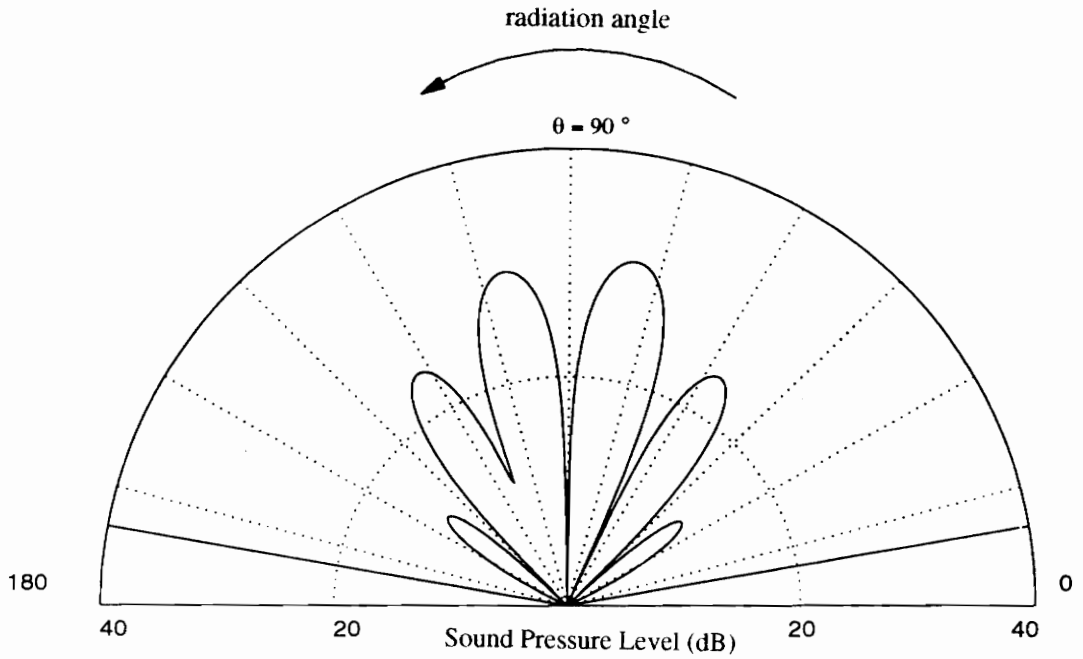

Frequency:
350
Effort:
1.143

#	F. control:		F. mounts (u):		F. mounts (c):	
1	0.4745	(2.619)	0.5847	(3.208)	0.6154	(2.963)
2	0.5023	(3.61)	0.3813	(3.092)	0.3604	(3.123)
3	0.3714	(3.158)	0.3438	(3.487)	0.3714	(3.158)
4	0.1165	(3.184)	0.141	(2.932)	0.1165	(3.184)
5	0.6447	(3.461)	0.5127	(3.197)	0.5026	(3.163)
6	0.333	(2.405)	0.4532	(3.163)	0.4732	(2.947)
7	0.3714	(3.158)	0.3438	(3.487)	0.3714	(3.158)
8	0.1165	(3.184)	0.141	(2.932)	0.1165	(3.184)

Figure 77: Parallel system with 8 mounts, 350 Hz, control of the displacement at the location of the mounts

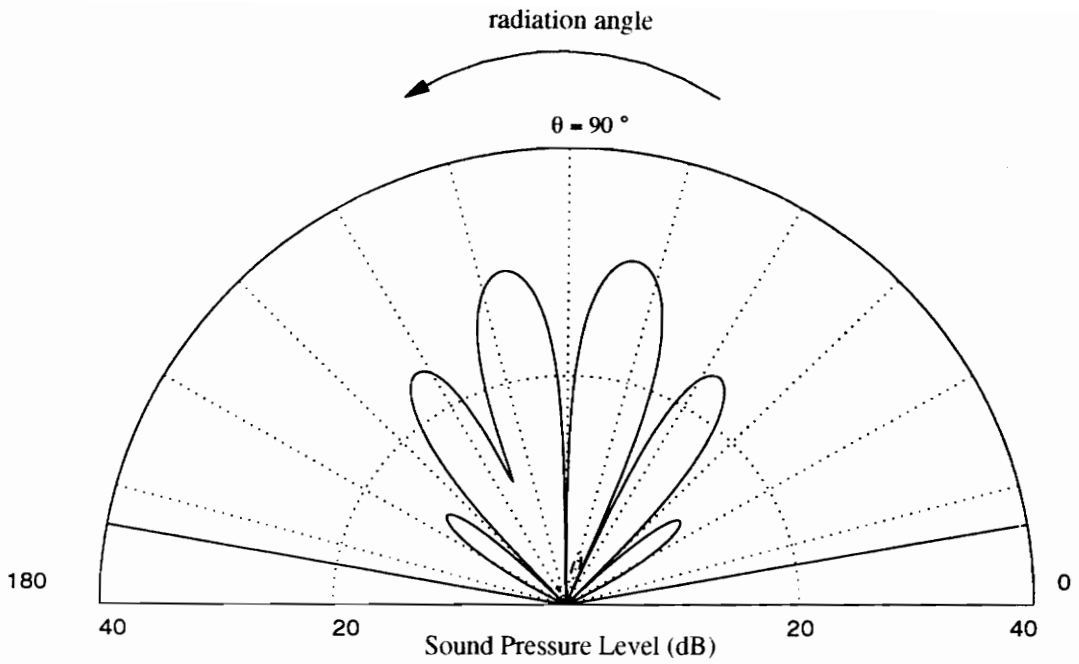

Frequency: 350

Effort: 1.107

#	F. control:		F. mounts (u):		F. mounts (c):	
1	0.5487	(3.202)	0.5847	(3.208)	0.6239	(2.999)
2	0.4175	(3.127)	0.3813	(3.092)	0.3707	(3.156)
3	0.3432	(3.487)	0.3438	(3.487)	0.3752	(3.205)
4	0.1401	(2.935)	0.141	(2.932)	0.1221	(3.216)
5	0.5487	(3.202)	0.5127	(3.197)	0.5115	(3.201)
6	0.4175	(3.127)	0.4532	(3.163)	0.4832	(2.981)
7	0.3432	(3.487)	0.3438	(3.487)	0.3752	(3.205)
8	0.1401	(2.935)	0.141	(2.932)	0.1221	(3.216)

Figure 78: Opposed system with 8 mounts, 350 Hz, control of the displacement at the location of the mounts

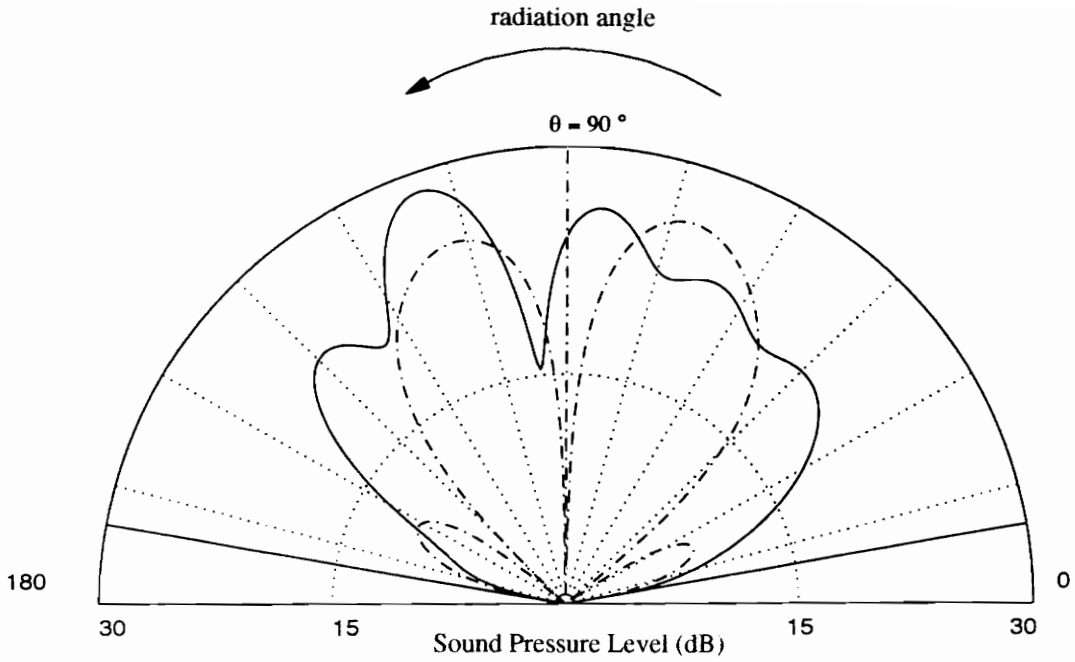

Frequency:	#	F. control:		F. mounts (u):		F. mounts (c):	
516	1	0.08057	(3.67)	0.2061	(2.558)	0.2104	(2.412)
	2	0.08051	(3.501)	0.06123	(1.855)	0.06175	(1.884)
Effort:	3	0.02393	(1.344)	0.1394	(2.737)	0.1429	(2.611)
	4	0.02291	(1.302)	0.005661	(-6.121)	0.006512	(-18.32)
0.168	5	0.08086	(3.721)	0.1844	(2.553)	0.1886	(2.394)
	6	0.0808	(3.548)	0.08283	(2.025)	0.08345	(2.046)
	7	0.02393	(1.344)	0.1394	(2.737)	0.1429	(2.611)
	8	0.02291	(1.302)	0.005661	(-6.121)	0.006512	(-18.32)

Figure 79 : Parallel system with 8 mounts, 516 Hz, control in 1 direction, $\theta = 90°$

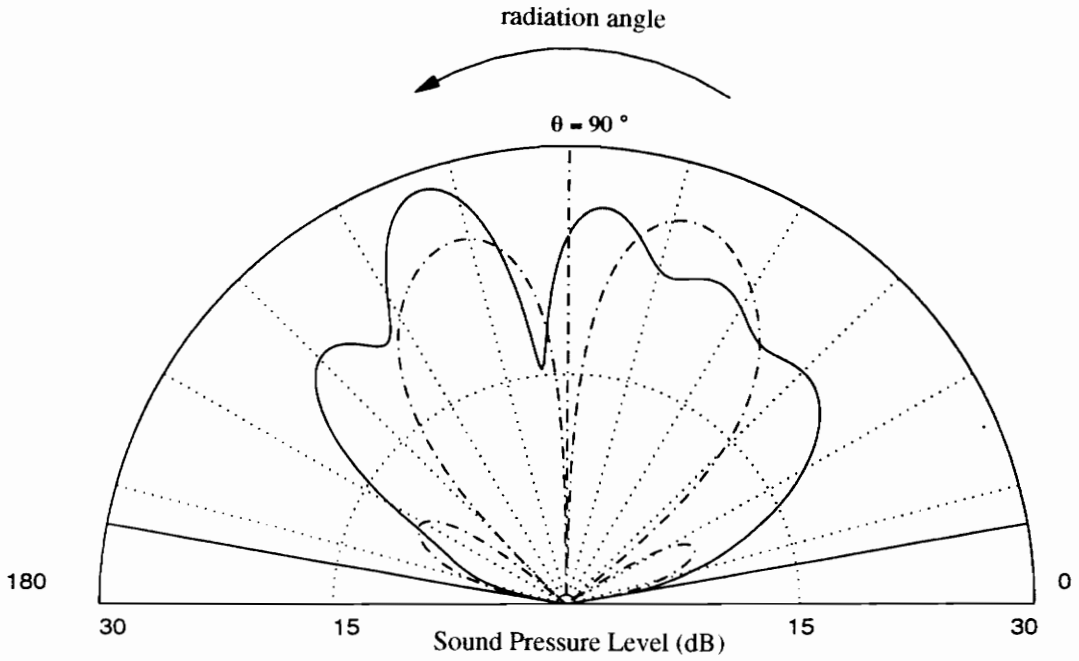

Frequency:
516
Effort:
0.1679

#	F. control:		F. mounts (u):		F. mounts (c):	
1	0.08052	(3.661)	0.2061	(2.558)	0.2103	(2.41)
2	0.08045	(3.496)	0.06123	(1.855)	0.06177	(1.885)
3	0.02396	(1.341)	0.1394	(2.737)	0.1428	(2.609)
4	0.02293	(1.299)	0.005661	(-6.121)	0.006557	(-17.94)
5	0.08081	(3.713)	0.1844	(2.553)	0.1885	(2.391)
6	0.08073	(3.544)	0.08283	(2.025)	0.08348	(2.047)
7	0.02396	(1.341)	0.1394	(2.737)	0.1428	(2.609)
8	0.02293	(1.299)	0.005661	(-6.121)	0.006557	(-17.94)

Figure 80 : Opposed system with 8 mounts, 516 Hz, control in 1 direction, $\theta = 90°$

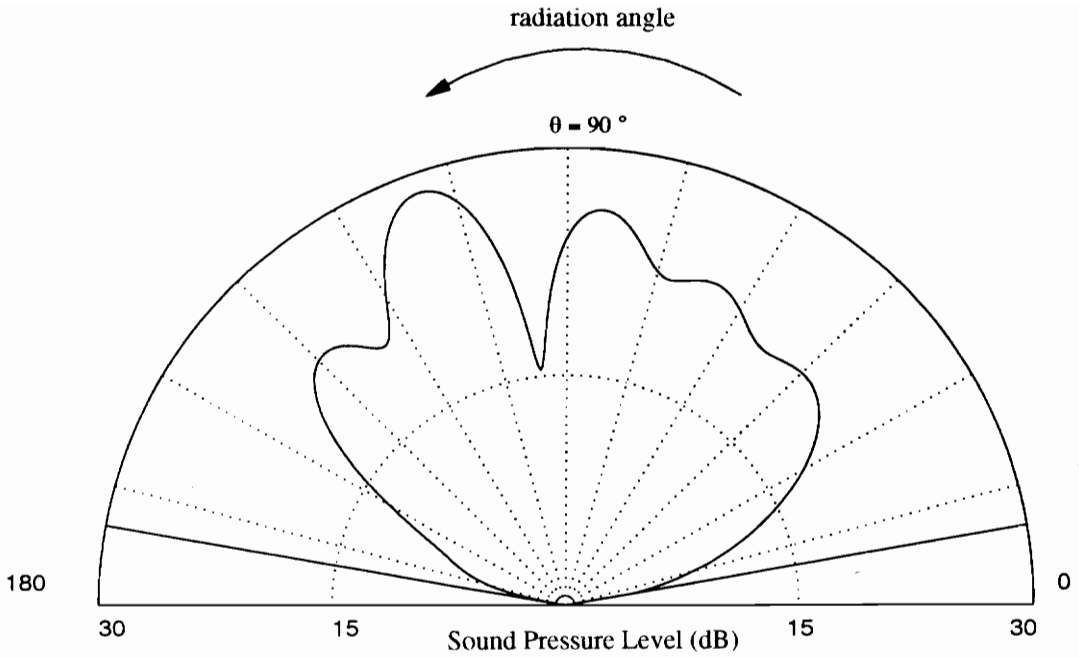

Frequency:
516
Effort:
0.3784

#	F. control:		F. mounts (u):		F. mounts (c):	
1	0.183	(2.015)	0.2061	(2.558)	0.2208	(2.244)
2	0.09736	(2.423)	0.06123	(1.855)	0.05959	(1.798)
3	0.1508	(2.317)	0.1394	(2.737)	0.1508	(2.317)
4	0.01148	(22.16)	0.005661	(-6.121)	0.01148	(22.16)
5	0.2266	(2.556)	0.1844	(2.553)	0.1884	(2.34)
6	0.0561	(1.178)	0.08283	(2.025)	0.09213	(1.814)
7	0.1508	(2.317)	0.1394	(2.737)	0.1508	(2.317)
8	0.01148	(22.16)	0.005661	(-6.121)	0.01148	(22.16)

Figure 81 : Parallel system with 8 mounts, 516 Hz, control of the displacement at the location of the mounts

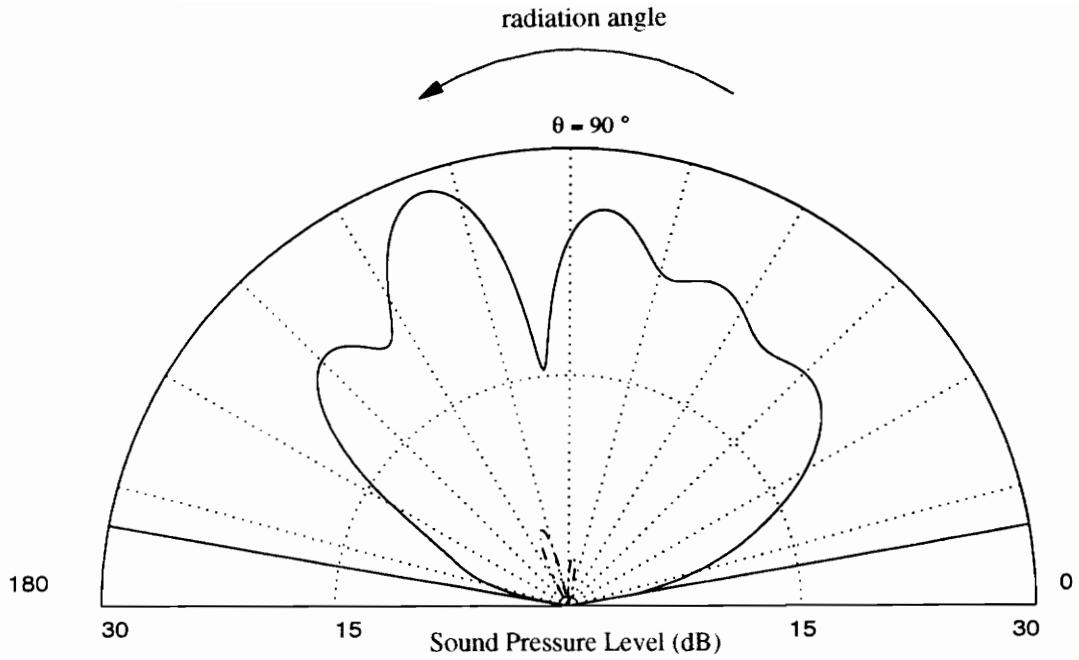

Frequency:
516
Effort:
0.353

#	F. control:		F. mounts (u):		F. mounts (c):	
1	0.1944	(2.461)	0.2061	(2.558)	0.2226	(2.278)
2	0.07237	(1.964)	0.06123	(1.855)	0.06222	(1.841)
3	0.1386	(2.574)	0.1394	(2.737)	0.1514	(2.353)
4	0.007399	(-2.571)	0.005661	(-6.121)	0.01005	(-67.73)
5	0.1944	(2.461)	0.1844	(2.553)	0.1906	(2.365)
6	0.07237	(1.964)	0.08283	(2.025)	0.09429	(1.862)
7	0.1386	(2.574)	0.1394	(2.737)	0.1514	(2.353)
8	0.007399	(-2.571)	0.005661	(-6.121)	0.01005	(-67.73)

Figure 82 : Opposed system with 8 mounts, 516 Hz, control of the displacement at the location of the mounts

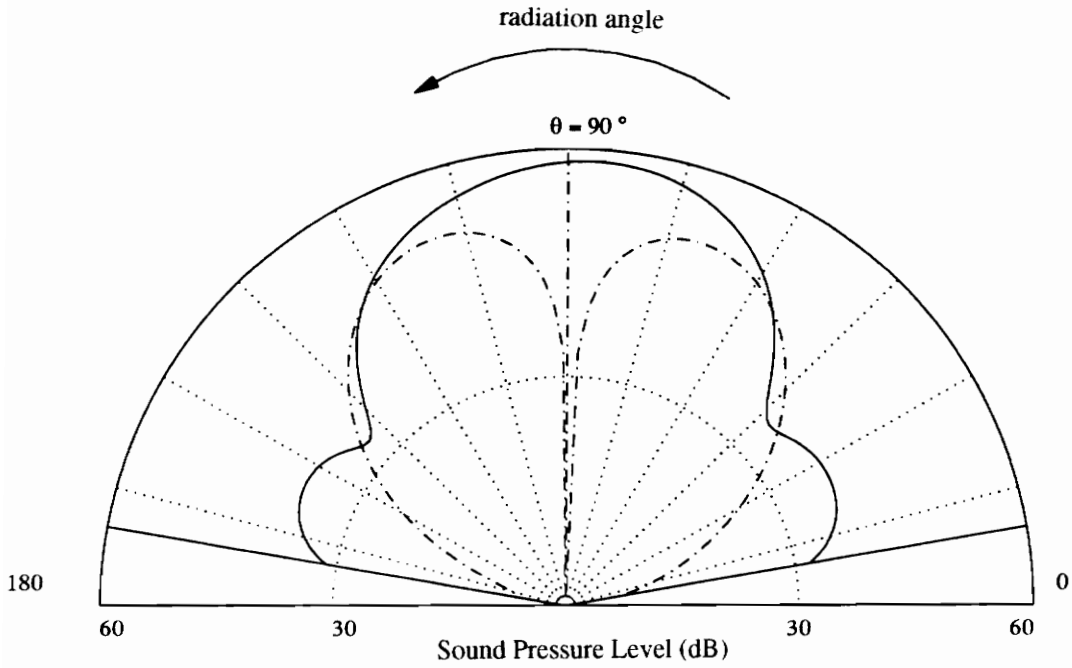

Frequency:	#	F. control:		F. mounts (u):		F. mounts (c):	
180	1	0.2481	(3.916)	3.558	(0.3294)	5.179	(0.2412)
	2	0.4455	(7.958)	3.277	(0.2481)	4.732	(0.2017)
Effort:	3	0.4076	(5.202)	1.877	(0.5035)	2.742	(0.378)
	4	0.5068	(6.752)	1.615	(0.1967)	2.298	(0.1868)
1.173	5	0.2559	(3.327)	3.485	(0.3195)	5.112	(0.2383)
	6	0.4518	(6.531)	3.332	(0.2666)	4.787	(0.2087)
	7	0.4076	(5.202)	1.877	(0.5035)	2.742	(0.378)
	8	0.5068	(6.752)	1.615	(0.1967)	2.298	(0.1868)

Figure 83 : Parallel system with 8 mounts, 180 Hz, control in the direction $\theta = 90°$

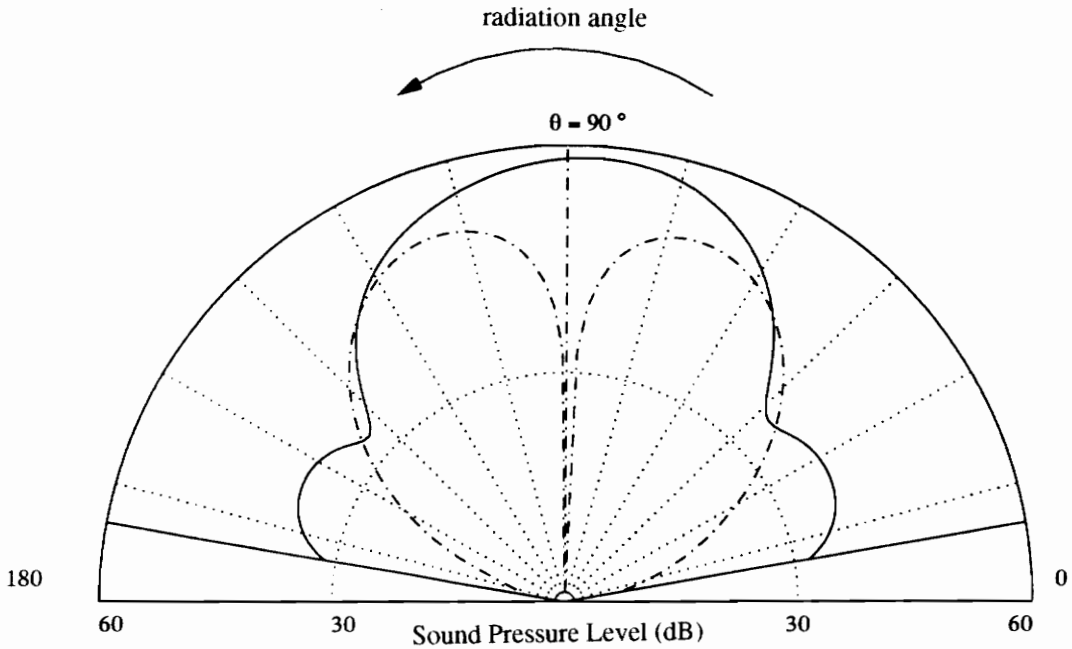

Frequency:

180

Effort:

1.16

#	F. control:		F. mounts (a):		F. mounts (c):	
1	0.2548	(2.49)	3.558	(0.3294)	5.048	(0.2566)
2	0.4373	(7.409)	3.277	(0.2481)	4.543	(0.2239)
3	0.4057	(3.804)	1.877	(0.5035)	2.684	(0.4025)
4	0.4985	(5.786)	1.615	(0.1967)	2.179	(0.2263)
5	0.2612	(2.246)	3.485	(0.3195)	4.971	(0.2546)
6	0.4411	(6.197)	3.332	(0.2666)	4.609	(0.2296)
7	0.4057	(3.804)	1.877	(0.5035)	2.684	(0.4025)
8	0.4985	(5.786)	1.615	(0.1967)	2.179	(0.2263)

Figure 84 : Opposed system with 8 mounts, 180 Hz, control in the direction $\theta = 90°$

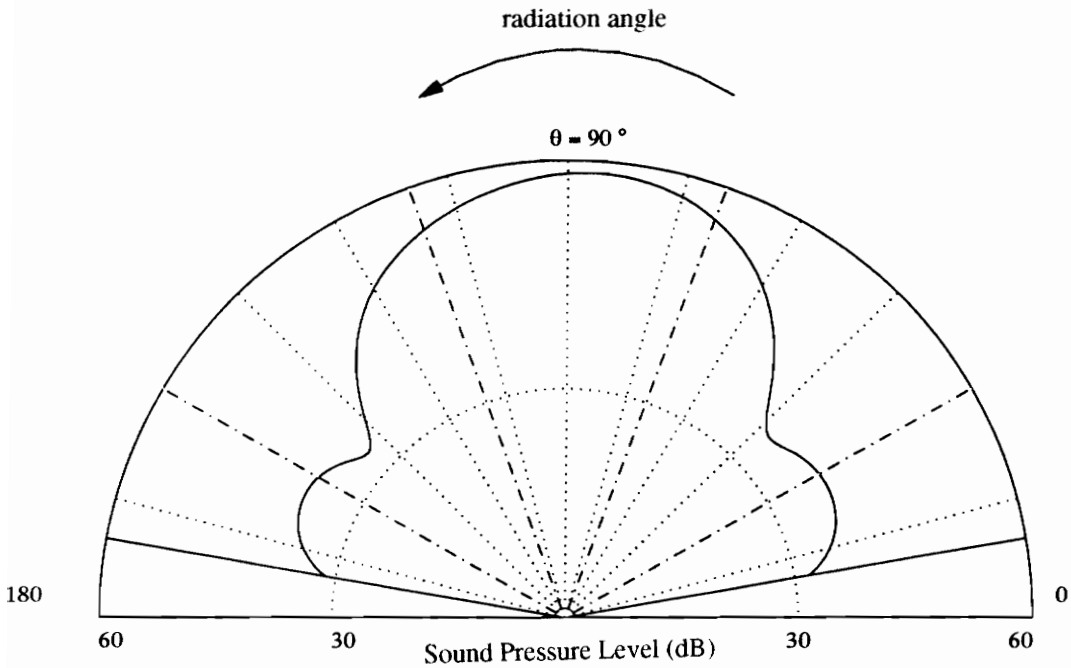

Frequency:	#	F. control:		F. mounts (u):		F. mounts (c):	
180	1	1.194	(-2.37)	3.558	(0.3294)	0.5355	(0.4856)
	2	0.873	(2.356)	3.277	(0.2481)	0.5792	(-2.946)
Effort:	3	0.4476	(0.9634)	1.877	(0.5035)	0.4479	(0.9663)
	4	0.4732	(-48.55)	1.615	(0.1967)	0.4744	(-51.26)
3.024	5	1.614	(2.156)	3.485	(0.3195)	0.3805	(0.4878)
	6	1.872	(-5.713)	3.332	(0.2666)	0.5747	(-1.453)
	7	0.4476	(0.9634)	1.877	(0.5035)	0.4479	(0.9663)
	8	0.4732	(-48.55)	1.615	(0.1967)	0.4744	(-51.26)

Figure 85 : Parallel system with 8 mounts, 180 Hz, control in four directions

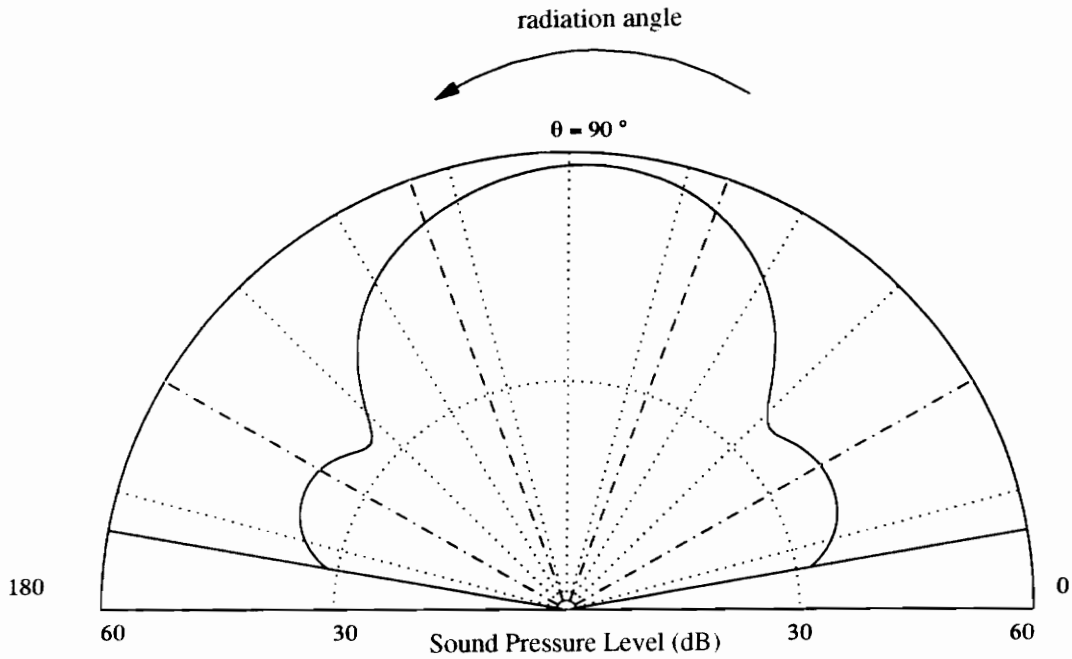

Frequency:	#	F. control:		F. mounts (u):		F. mounts (c):	
180	1	1.218	(-3.637)	3.558	(0.3294)	0.6239	(0.4415)
	2	1.083	(1.415)	3.277	(0.2481)	0.5486	(-2.285)
Effort:	3	0.5057	(0.803)	1.877	(0.5035)	0.5061	(0.8048)
	4	0.4367	(-17.38)	1.615	(0.1967)	0.4379	(-17.86)
3.212	5	1.791	(1.396)	3.485	(0.3195)	0.4421	(0.4446)
	6	1.887	(-25.63)	3.332	(0.2666)	0.5706	(-1.101)
	7	0.5057	(0.803)	1.877	(0.5035)	0.5061	(0.8048)
	8	0.4367	(-17.38)	1.615	(0.1967)	0.4379	(-17.86)

Figure 86 : Opposed system with 8 mounts, 180 Hz, control in four directions

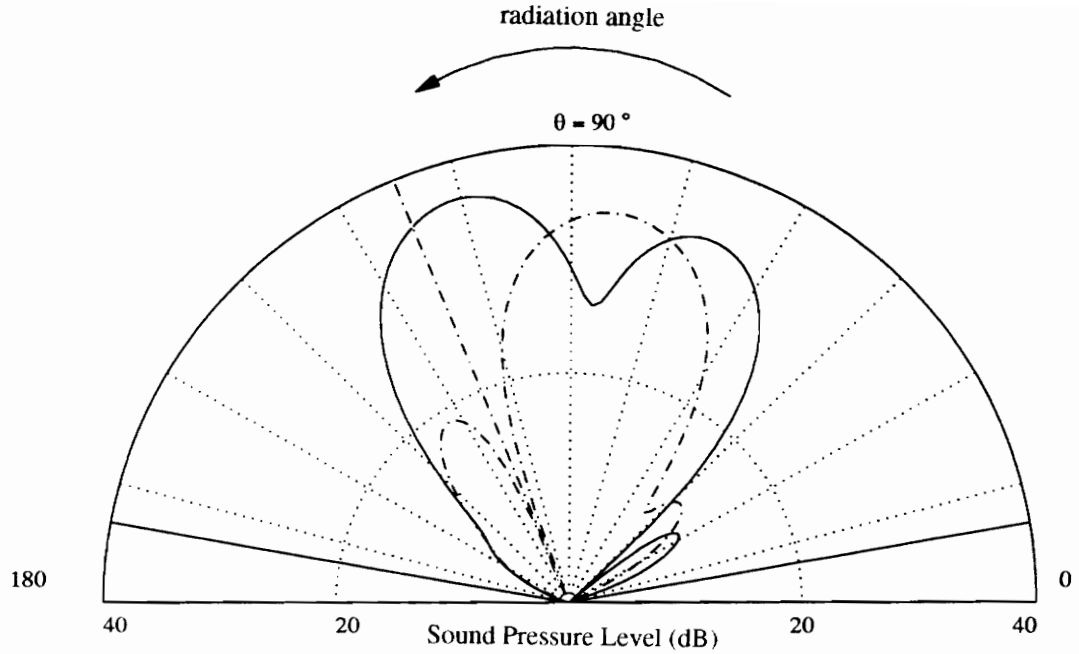

Frequency:
220
Effort:
1.248

#	F. control:		F. mounts (a):		F. mounts (c):	
1	0.0809	(2.706)	0.9135	(2.577)	0.5858	(10.01)
2	0.6583	(1.443)	0.4936	(2.023)	0.107	(-2.28)
3	0.01533	(1.041)	0.5638	(3.169)	0.4165	(7.87)
4	0.4754	(1.665)	0.1476	(1.366)	0.08613	(1.598)
5	0.7646	(5.16)	0.8414	(2.551)	0.4436	(-26.33)
6	0.2823	(-0.477)	0.5644	(2.159)	0.2395	(9.077)
7	0.01533	(1.041)	0.5638	(3.169)	0.4165	(7.87)
8	0.4754	(1.665)	0.1476	(1.366)	0.08613	(1.598)

Figure 87 : Parallel system with 8 mounts, 220 Hz, control in the direction $\theta = 112°$

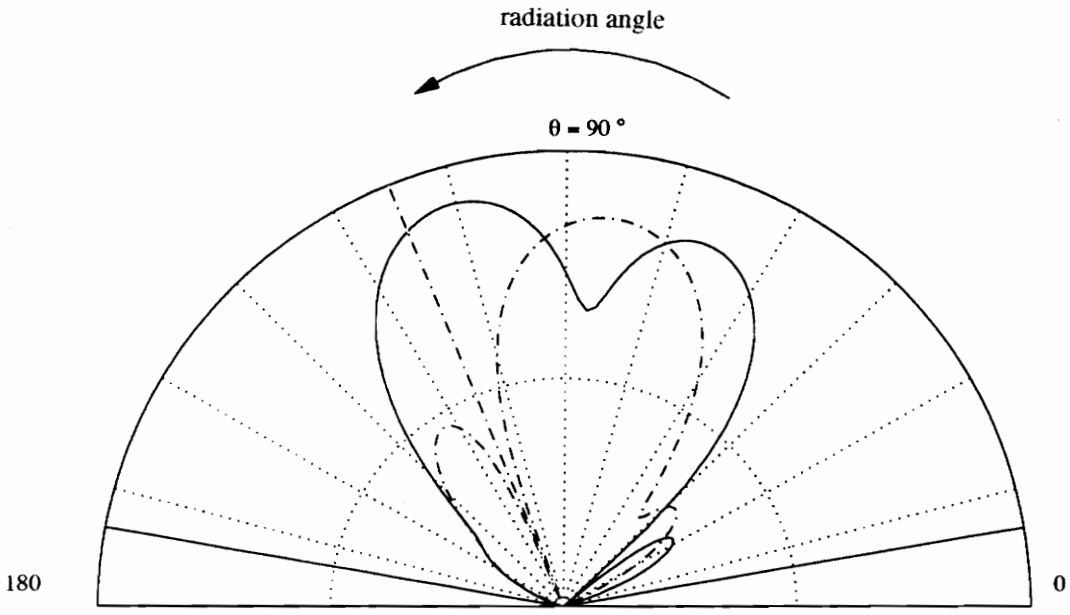

Frequency:	#	F. control:		F. mounts (u):		F. mounts (c):	
220	1	0.08684	(2.829)	0.9135	(2.577)	0.5927	(9.486)
	2	0.663	(1.431)	0.4936	(2.023)	0.1106	(-2.557)
Effort:	3	0.01967	(1.435)	0.5638	(3.169)	0.4209	(7.617)
	4	0.4775	(1.648)	0.1476	(1.366)	0.08309	(1.598)
1.256	5	0.7704	(5.133)	0.8414	(2.551)	0.4492	(-31.93)
	6	0.2846	(-0.4573)	0.5644	(2.159)	0.2458	(8.182)
	7	0.01967	(1.435)	0.5638	(3.169)	0.4209	(7.617)
	8	0.4775	(1.648)	0.1476	(1.366)	0.08309	(1.598)

Figure 88 : Opposed system with 8 mounts, 220 Hz, control in the direction $\theta = 112°$

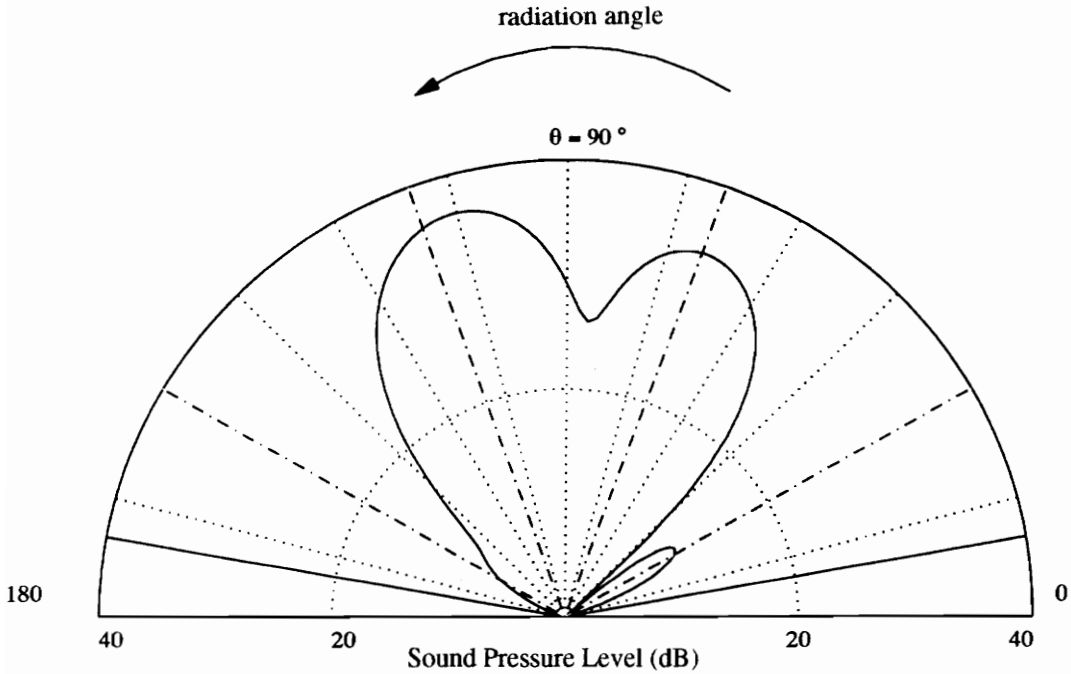

Frequency:
220
Effort:
1.776

#	F. control:		F. mounts (u):		F. mounts (c):	
1	0.3142	(0.6184)	0.9135	(2.577)	0.8479	(2.068)
2	0.8265	(3.379)	0.4936	(2.023)	0.234	(1.255)
3	0.5799	(2.423)	0.5638	(3.169)	0.5799	(2.423)
4	0.06475	(-2.066)	0.1476	(1.366)	0.06476	(-2.067)
5	1.262	(3.035)	0.8414	(2.551)	0.6539	(2.308)
6	0.3124	(-1.457)	0.5644	(2.159)	0.4259	(1.502)
7	0.5799	(2.423)	0.5638	(3.169)	0.5799	(2.423)
8	0.06475	(-2.066)	0.1476	(1.366)	0.06476	(-2.067)

Figure 89 : Parallel system with 8 mounts, 220 Hz, control in four directions

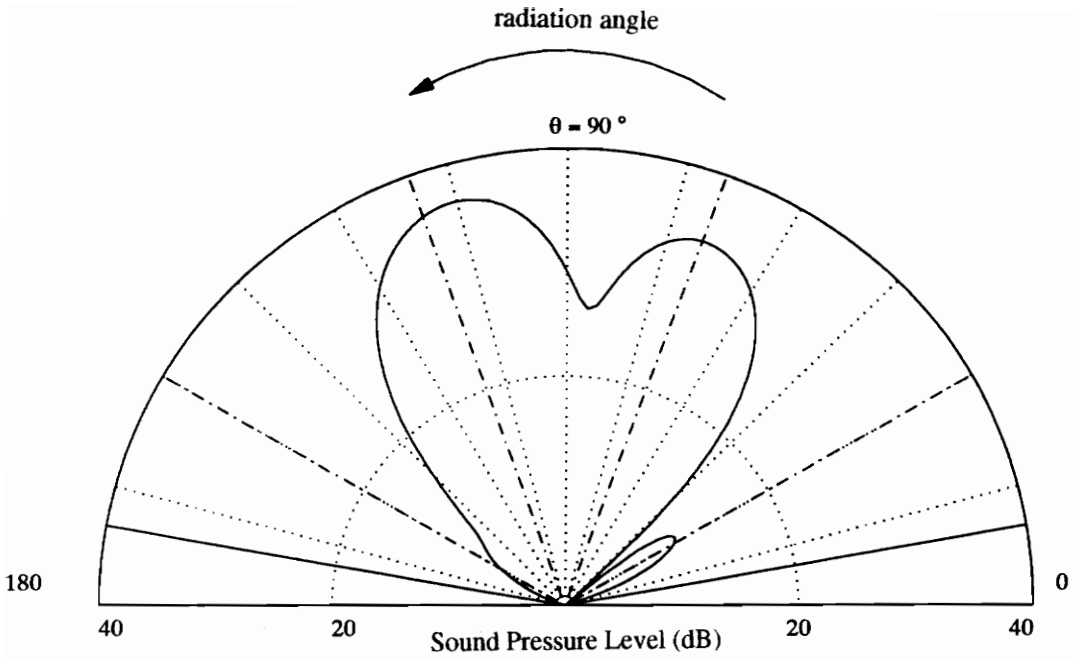

Frequency:

220

Effort:

1.779

#	F. control:		F. mounts (u):		F. mounts (c):	
1	0.3199	(0.6449)	0.9135	(2.577)	0.8535	(2.066)
2	0.8279	(3.362)	0.4936	(2.023)	0.2378	(1.274)
3	0.5832	(2.423)	0.5638	(3.169)	0.5832	(2.423)
4	0.06308	(-1.972)	0.1476	(1.366)	0.06309	(-1.973)
5	1.264	(3.021)	0.8414	(2.551)	0.6584	(2.309)
6	0.3064	(-1.403)	0.5644	(2.159)	0.431	(1.512)
7	0.5832	(2.423)	0.5638	(3.169)	0.5832	(2.423)
8	0.06308	(-1.972)	0.1476	(1.366)	0.06309	(-1.973)

Figure 90 : Opposed system with 8 mounts, 220 Hz, control in four directions

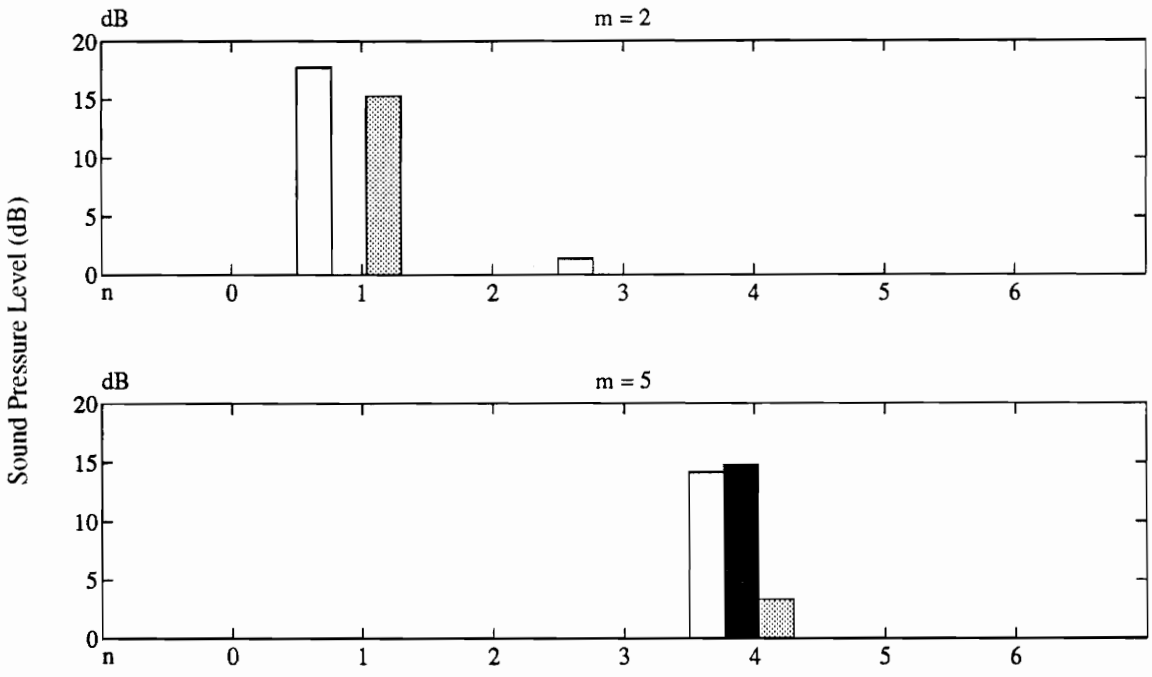

Figure 91 : System with 8 mounts, 516 Hz, modal decomposition of the pressure in the direction $\theta = 83°$

□ no control , ■ n=1 , ▨ n=4

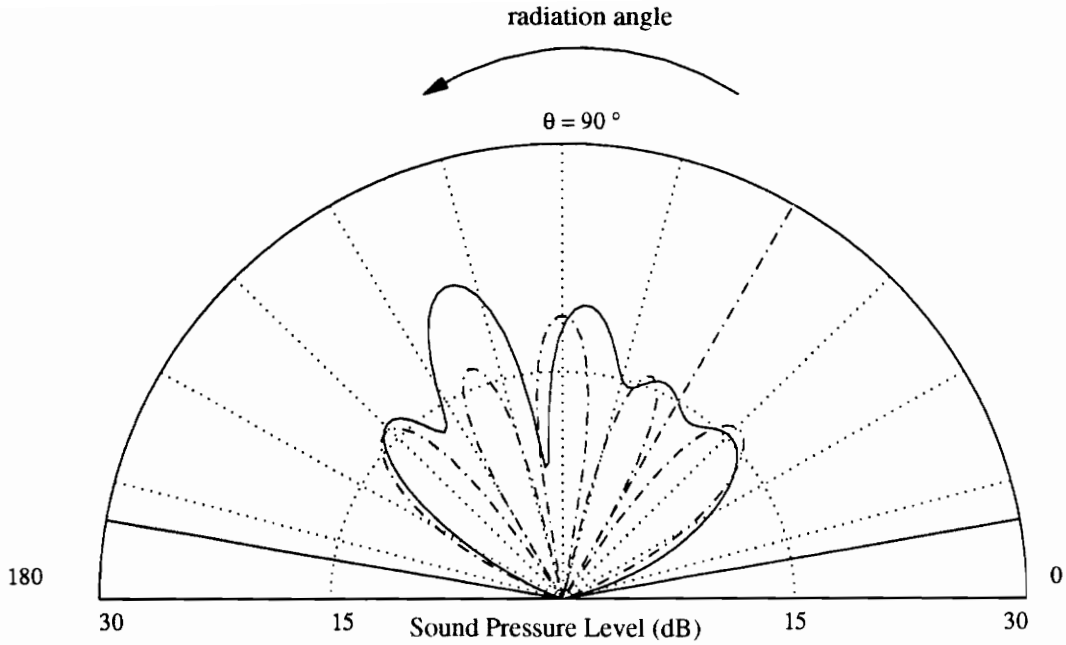

Frequency:
516
Effort:
0.1273

#	F. control:		F. mounts (u):		F. mounts (c):	
1	0.04944	(1.541)	0.09379	(2.899)	0.09435	(2.869)
2	0.05885	(6.124)	0.02333	(2.304)	0.02213	(2.36)
3	0.03047	(6.645)	0.06446	(3.025)	0.065	(2.845)
4	0.03662	(1.617)	0.005497	(3.013)	0.006903	(3.905)
5	0.05634	(1.839)	0.08362	(2.905)	0.08211	(2.956)
6	0.05094	(5.272)	0.03348	(2.454)	0.0344	(2.374)
7	0.03047	(6.645)	0.06446	(3.025)	0.065	(2.845)
8	0.03662	(1.617)	0.005497	(3.013)	0.006903	(3.905)

Figure 92 : System with 8 mounts, 516 Hz, minimization of components associated with n=1

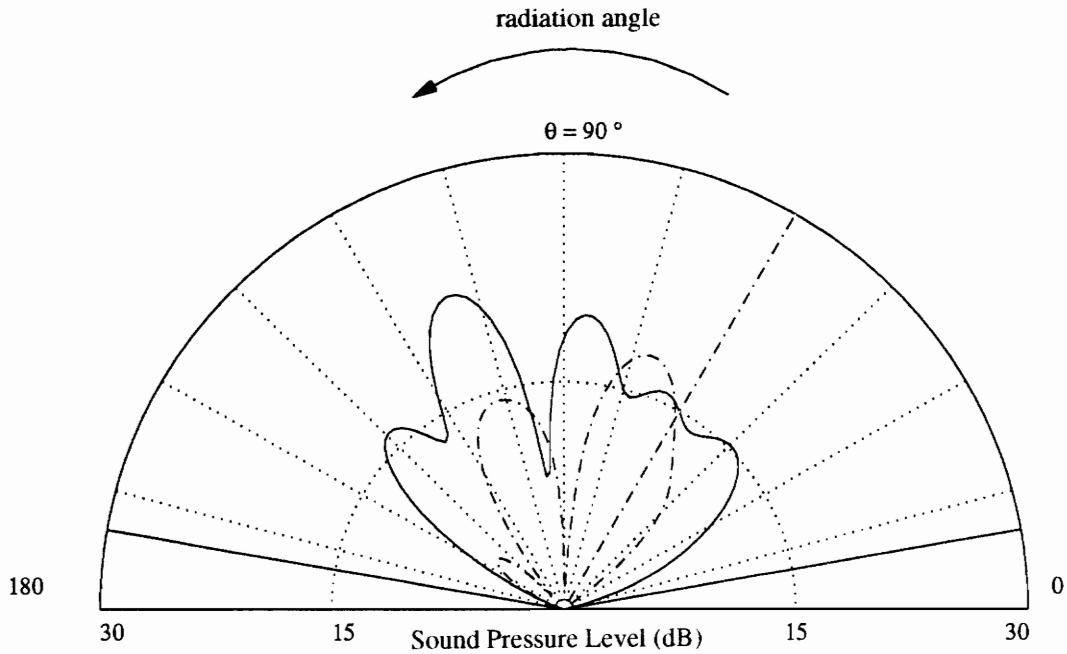

Frequency:
516
Effort:
0.1029

#	F. control:		F. mounts (u):		F. mounts (c):	
1	0.05089	(5.165)	0.09379	(2.899)	0.0946	(2.726)
2	0.03916	(6.534)	0.02333	(2.304)	0.02299	(2.414)
3	0.02885	(1.503)	0.06446	(3.025)	0.06519	(2.849)
4	0.01313	(-7.115)	0.005497	(3.013)	0.006324	(3.404)
5	0.05271	(5.359)	0.08362	(2.905)	0.08395	(2.728)
6	0.041	(6.853)	0.03348	(2.454)	0.03364	(2.507)
7	0.02885	(1.503)	0.06446	(3.025)	0.06519	(2.849)
8	0.01313	(-7.115)	0.005497	(3.013)	0.006324	(3.404)

Figure 93 : System with 8 mounts, 516 Hz, minimization of components associated with n=4

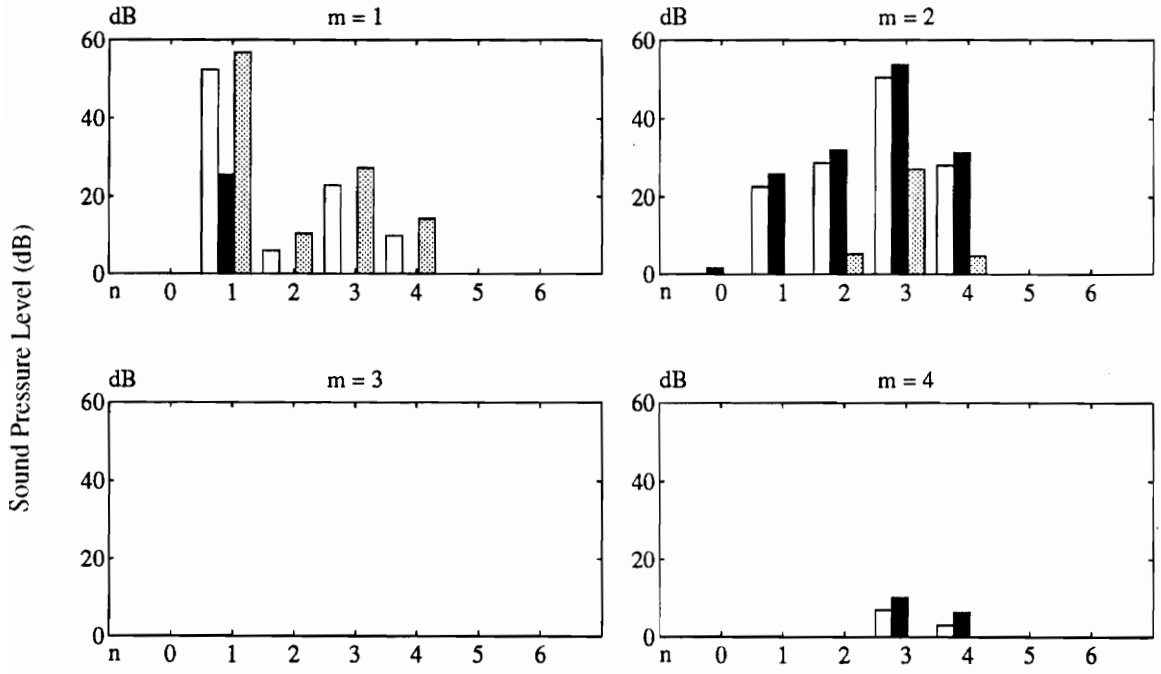

Figure 94 : System with 8 mounts, 180 Hz, modal decomposition of the pressure in the direction $\theta = 83°$

□ no control , ■ n=1 , ▨ n=3

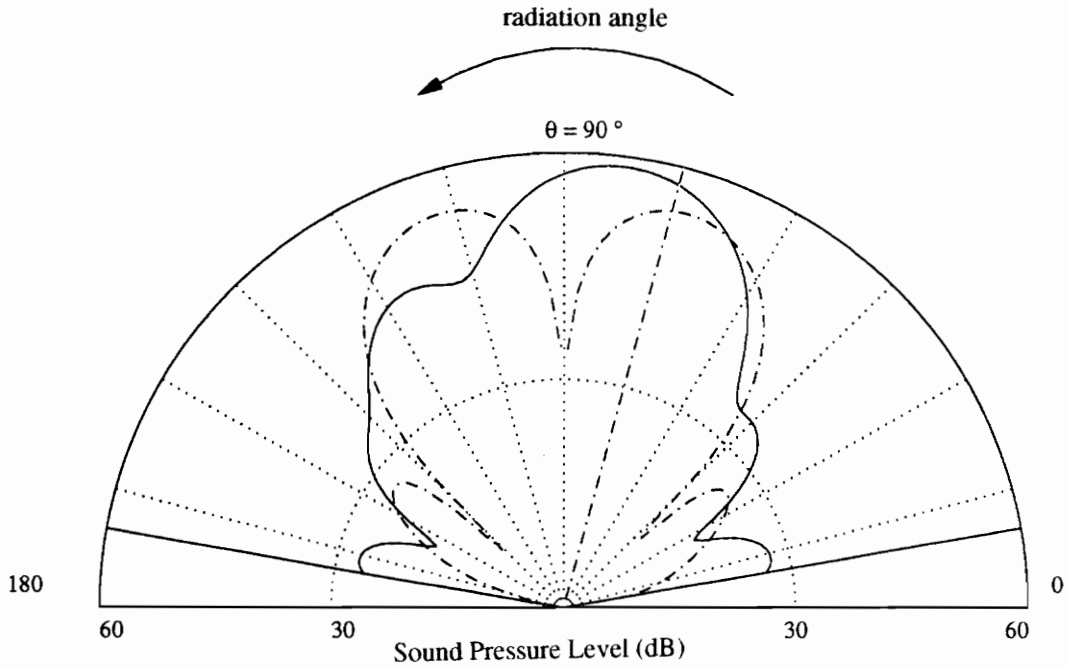

Frequency:
180
Effort:
1.146

#	F. control:		F. mounts (u):		F. mounts (c):	
1	0.2441	(4.531)	3.558	(0.3294)	5.169	(0.2445)
2	0.4392	(9.67)	3.277	(0.2481)	4.72	(0.2064)
3	0.3985	(6.077)	1.877	(0.5035)	2.737	(0.3842)
4	0.497	(8.054)	1.615	(0.1967)	2.292	(0.1962)
5	0.2435	(3.209)	3.485	(0.3195)	5.101	(0.2417)
6	0.4359	(6.546)	3.332	(0.2666)	4.776	(0.2131)
7	0.3985	(6.077)	1.877	(0.5035)	2.737	(0.3842)
8	0.497	(8.054)	1.615	(0.1967)	2.292	(0.1962)

Figure 95 : System with 8 mounts, 180 Hz, minimization of components associated with n=1

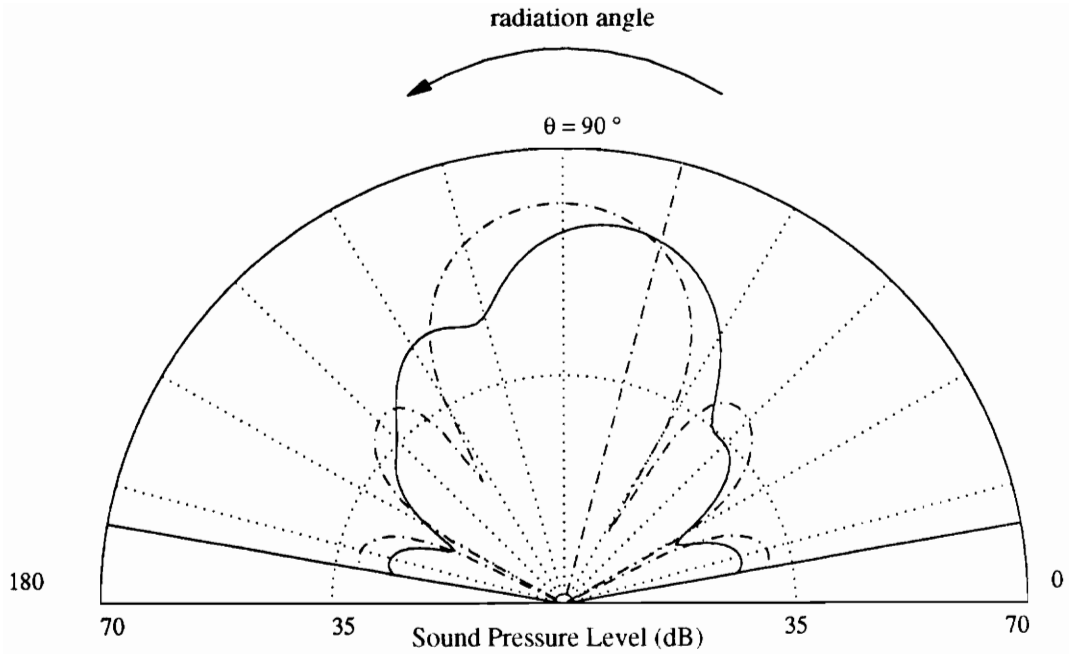

Frequency:
180
Effort:
1.484

#	F. control:		F. mounts (u):		F. mounts (c):	
1	0.4489	(-4.287)	3.558	(0.3294)	0.4046	(-3.11)
2	0.5803	(3.895)	3.277	(0.2481)	0.2312	(2.204)
3	0.4592	(-7.679)	1.877	(0.5035)	0.3518	(-4.145)
4	0.5495	(5.357)	1.615	(0.1967)	0.2561	(8.595)
5	0.6235	(4.696)	3.485	(0.3195)	0.3007	(-1.405)
6	0.4983	(-4.058)	3.332	(0.2666)	0.08176	(1.724)
7	0.4592	(-7.679)	1.877	(0.5035)	0.3518	(-4.145)
8	0.5495	(5.357)	1.615	(0.1967)	0.2561	(8.595)

Figure 96 : System with 8 mounts, 180 Hz, minimization of components associated with n=3

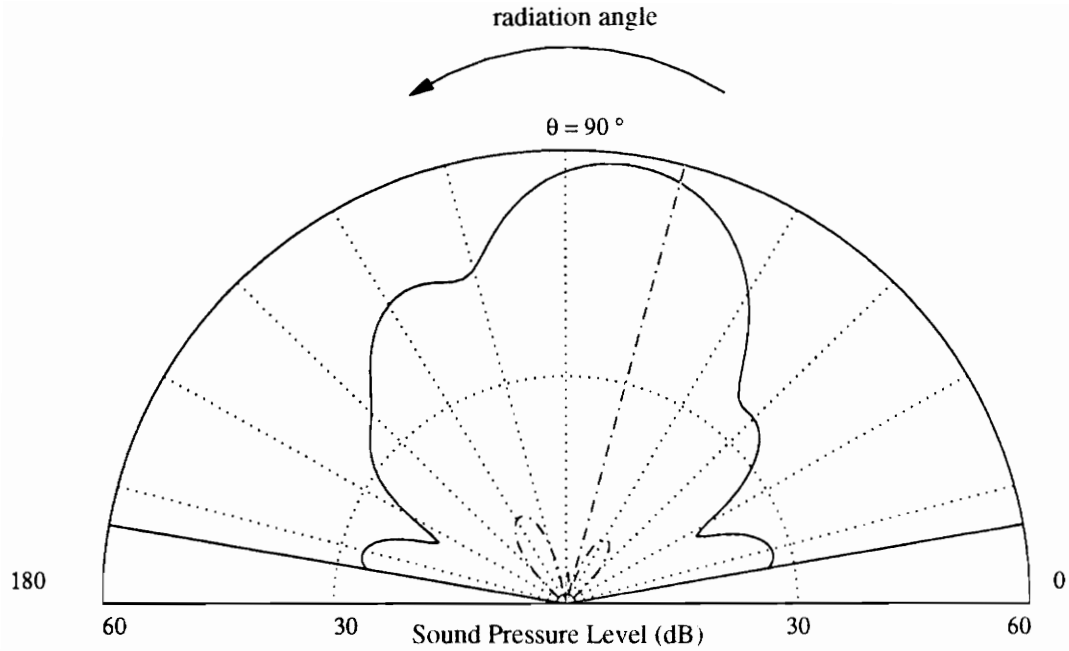

Frequency:
180
Effort:
2.711

#	F. control:		F. mounts (u):		F. mounts (c):	
1	0.4337	(-0.9215)	3.558	(0.3294)	0.5158	(0.7873)
2	0.1703	(0.5693)	3.277	(0.2481)	0.535	(-4.122)
3	0.2625	(0.1101)	1.877	(0.5035)	0.464	(1.329)
4	0.1004	(-2.499)	1.615	(0.1967)	0.475	(34.66)
5	1.779	(2.671)	3.485	(0.3195)	0.367	(0.7861)
6	1.951	(-15.6)	3.332	(0.2666)	0.4838	(-1.749)
7	0.2625	(0.1101)	1.877	(0.5035)	0.464	(1.329)
8	0.1004	(-2.499)	1.615	(0.1967)	0.475	(34.66)

Figure 97 : System with 8 mounts, 180 Hz, minimization of components associated with n=1 & 3

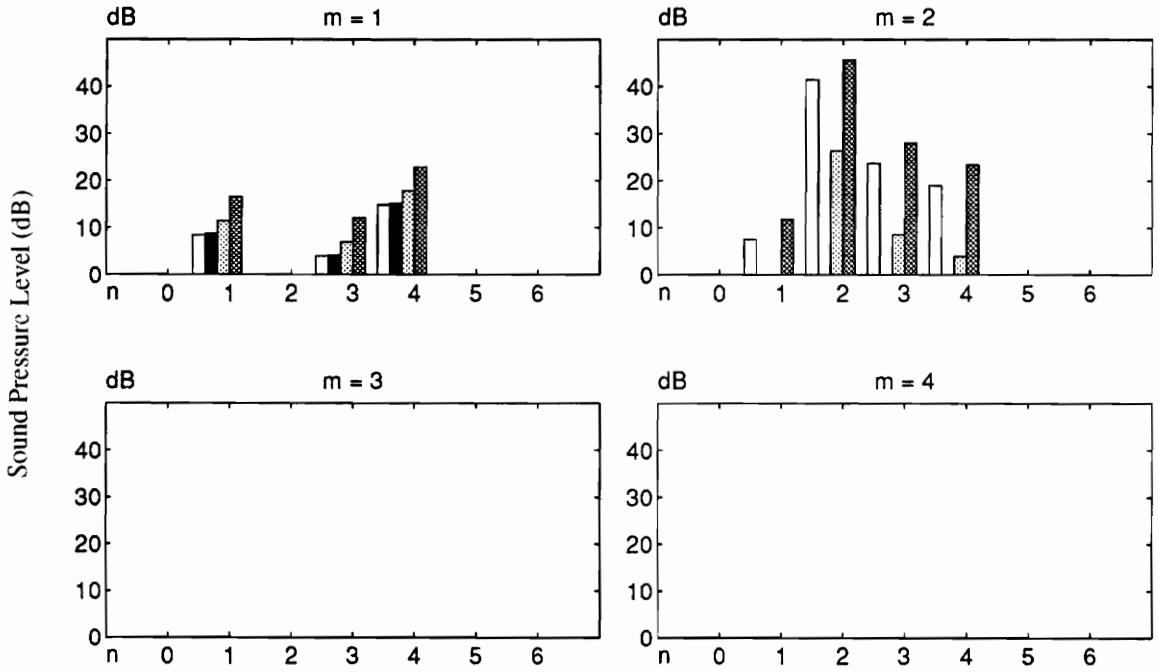

Figure 98 : System with 8 mounts, 242 Hz, modal decomposition of the pressure in the direction $\theta = 83°$

□ no control , ■ n=2 , ▨ n=3 , ▨ n=4

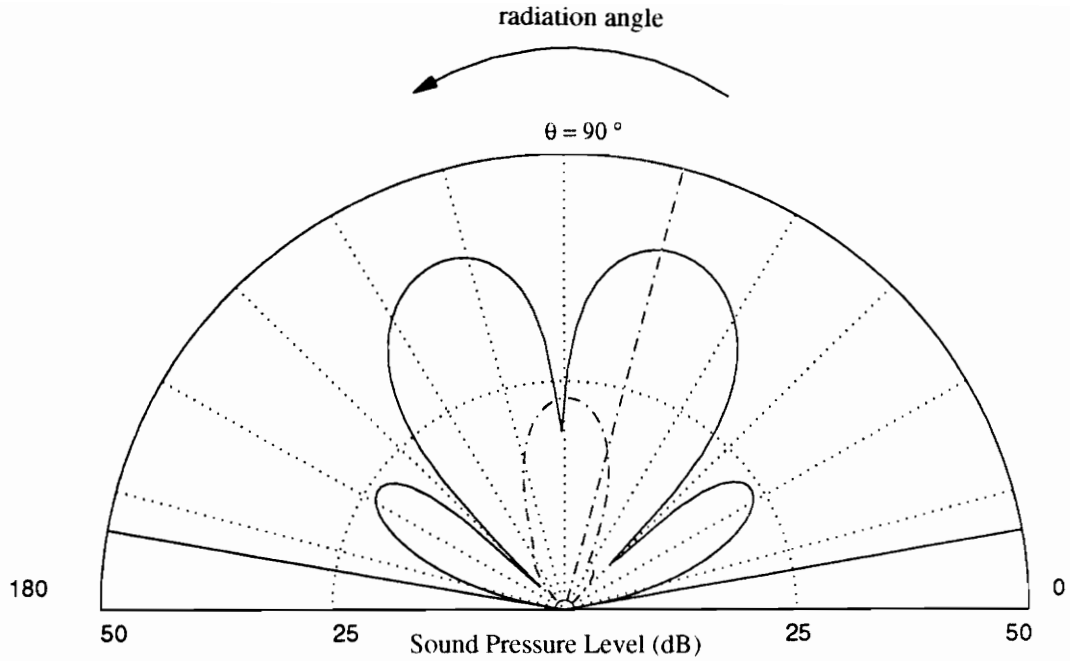

Frequency:	#	F. control:	
242	1	0.2574	(7.685)
	2	0.262	(7.975)
Effort:	3	0.1687	(7.672)
	4	0.1729	(8.092)
0.6217	5	0.2574	(7.685)
	6	0.262	(7.975)
	7	0.1687	(7.672)
	8	0.1729	(8.092)

Figure 99 : System with 8 mounts, 242 Hz, minimization of components associated with n=2

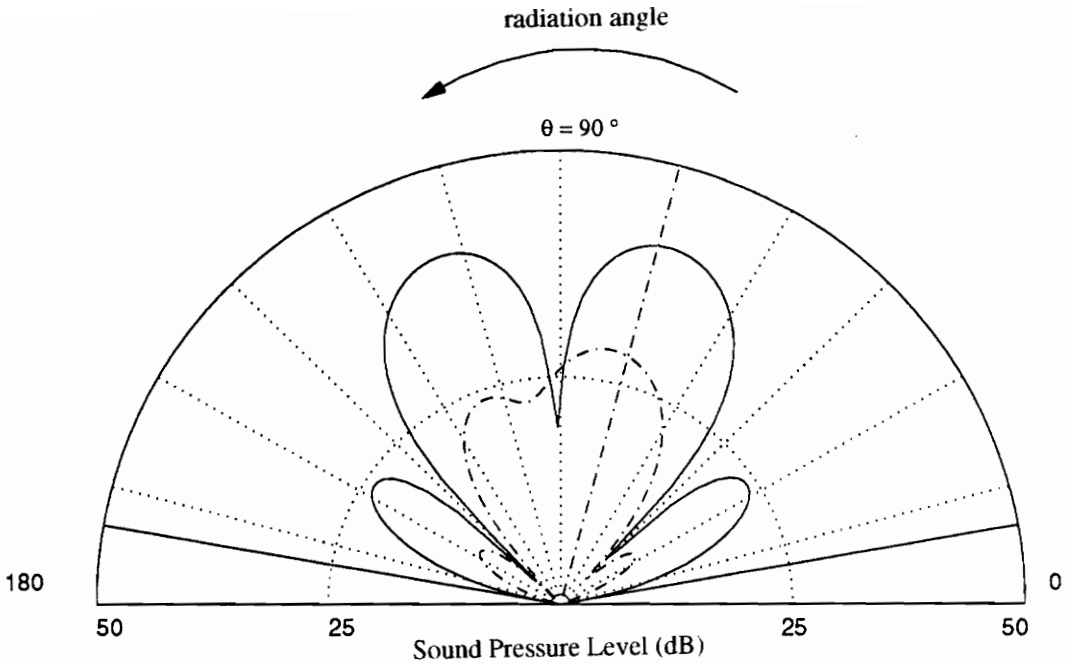

Frequency:	#	F. control:	
242	1	0.2395	(2.636)
	2	0.2449	(-2.549)
Effort:	3	0.1633	(2.857)
	4	0.163	(-2.71)
0.5842	5	0.2395	(2.636)
	6	0.2449	(-2.549)
	7	0.1633	(2.857)
	8	0.163	(-2.71)

Figure 100 : System with 8 mounts, 242 Hz, minimization of components associated with n=3

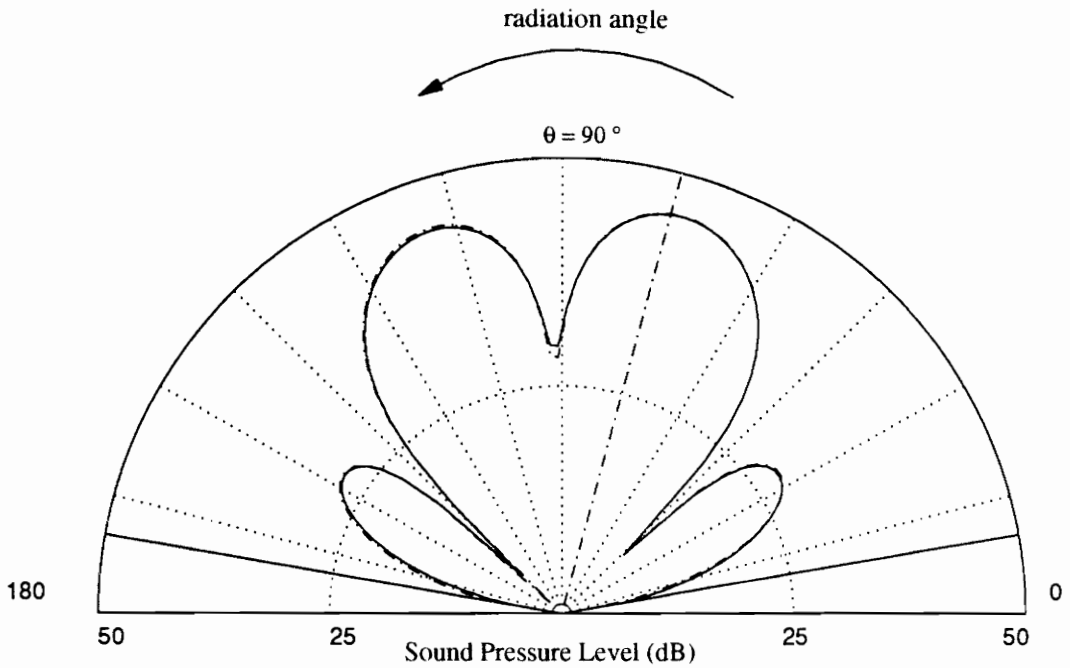

Frequency:
242
Effort:
0.5765

#	F. control:		F. mounts (u):		F. mounts (c):	
1	0.1523	(1.133)	0.6271	(7.164)	0.6908	(2.703)
2	0.2224	(-0.1006)	0.2799	(15.7)	0.3149	(2.19)
3	0.2071	(0.7467)	0.4005	(8.043)	0.4414	(3.272)
4	0.2407	(0.1395)	0.05571	(-4.062)	0.06583	(1.498)
5	0.1904	(11.11)	0.5706	(7.749)	0.6227	(2.504)
6	0.1475	(0.3846)	0.3361	(11.34)	0.3819	(2.623)
7	0.2071	(0.7467)	0.4005	(8.043)	0.4414	(3.272)
8	0.2407	(0.1395)	0.05571	(-4.062)	0.06583	(1.498)

Figure 101 : System with 8 mounts, 242 Hz, minimization of components associated with n=4

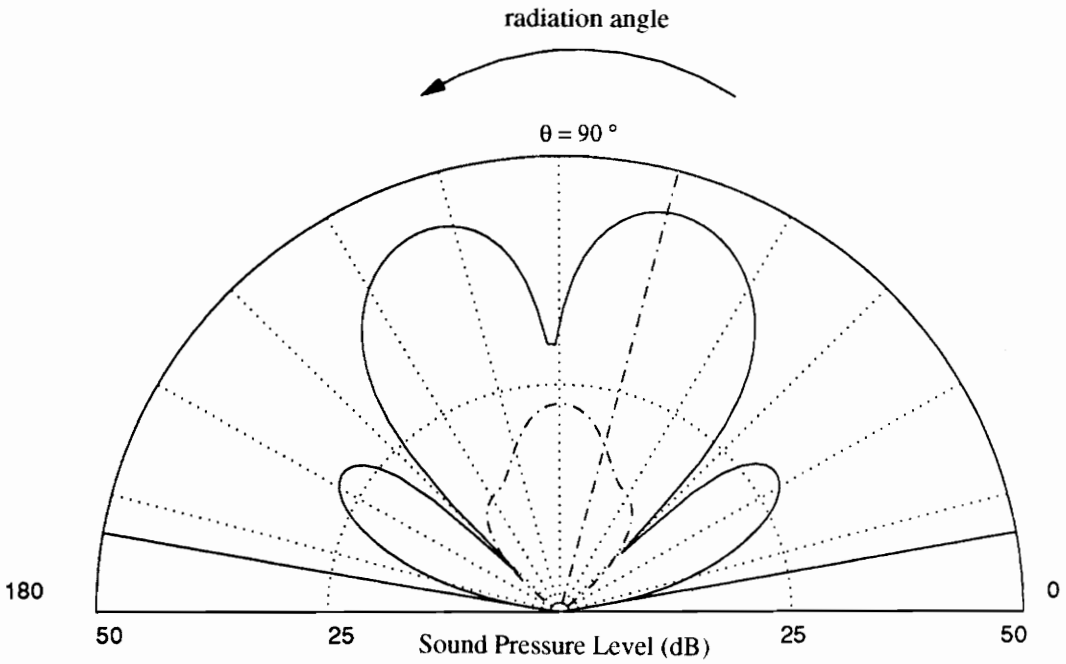

Frequency:
242
Effort:
1.086

#	F. control:		F. mounts (u):		F. mounts (c):	
1	0.4415	(2.292)	0.6271	(7.164)	0.5745	(2.963)
2	0.2142	(3.245)	0.2799	(15.7)	0.1346	(1.93)
3	0.2054	(2.284)	0.4005	(8.043)	0.399	(3.268)
4	0.2308	(6.78)	0.05571	(-4.062)	0.04912	(-13.7)
5	0.8379	(3.943)	0.5706	(7.749)	0.4541	(3.247)
6	0.2145	(-3.569)	0.3361	(11.34)	0.2549	(2.187)
7	0.2054	(2.284)	0.4005	(8.043)	0.399	(3.268)
8	0.2308	(6.78)	0.05571	(-4.062)	0.04912	(-13.7)

Figure 102 : System with 8 mounts, 242 Hz, minimization of components associated with n=2 & 3

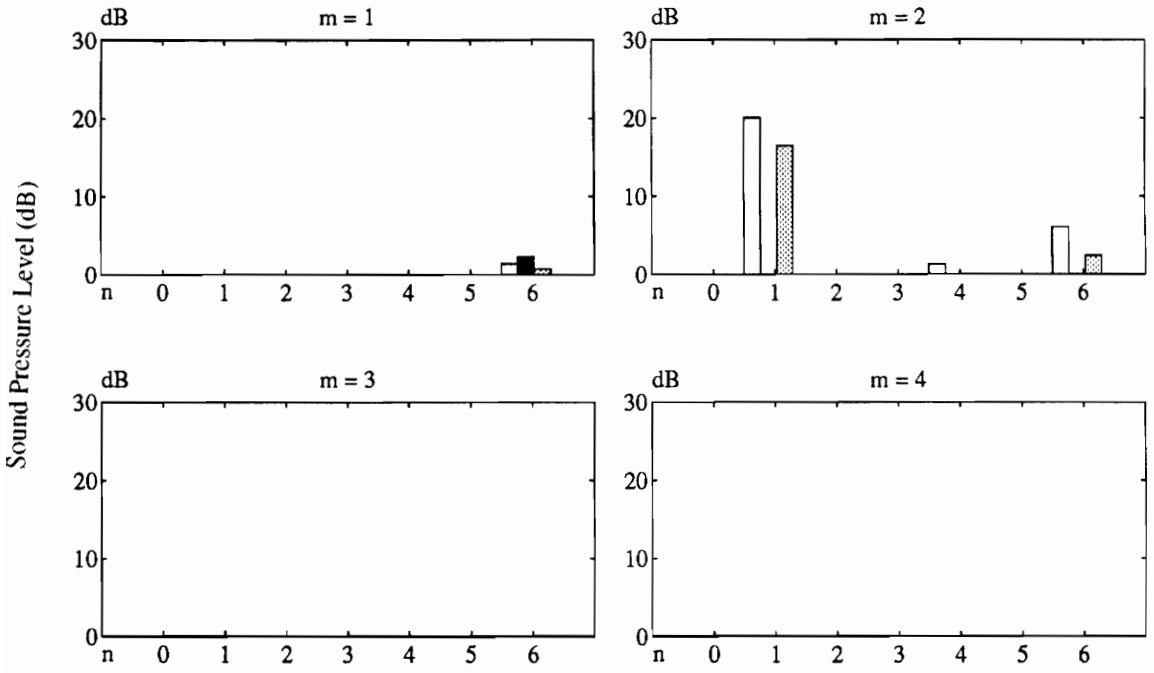

Figure 103 : System with 8 mounts, 495 Hz, modal decomposition of the pressure in the direction $\theta = 83°$

□ no control , ■ n=1 , ▨ n=6

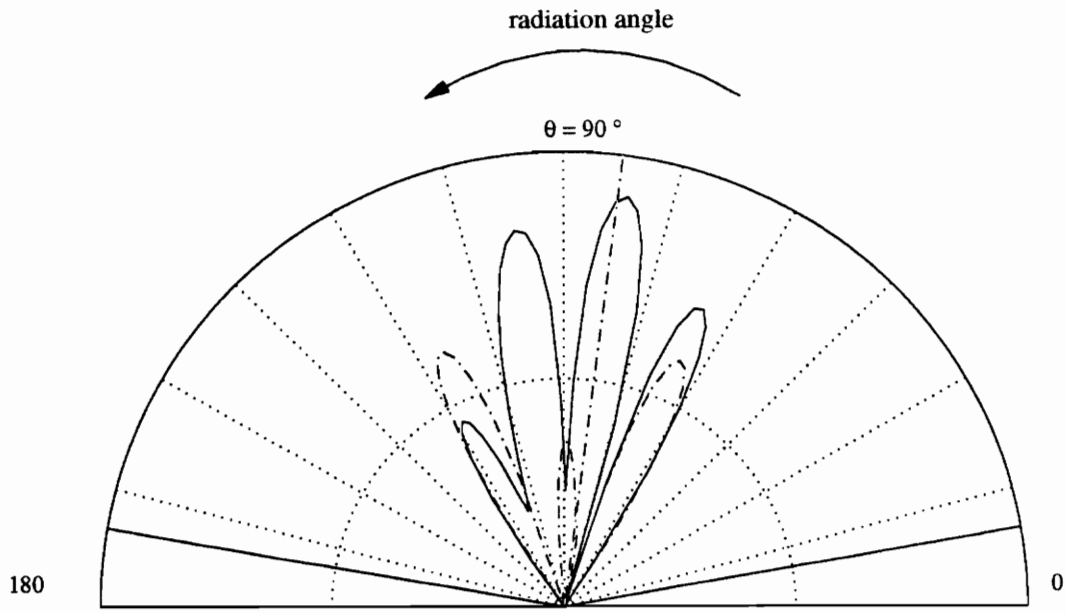

Frequency:
495
Effort:
0.1399

#	F. control:		F. mounts (u):		F. mounts (c):	
1	0.05292	(2.348)	0.1019	(2.9)	0.1026	(2.832)
2	0.0632	(5.034)	0.02575	(2.456)	0.02407	(2.461)
3	0.03367	(2.176)	0.06979	(2.964)	0.07068	(2.876)
4	0.04348	(5.37)	0.006079	(6.405)	0.007482	(4.421)
5	0.06182	(2.888)	0.09081	(2.893)	0.08898	(2.888)
6	0.0538	(4.074)	0.03681	(2.594)	0.0377	(2.485)
7	0.03367	(2.176)	0.06979	(2.964)	0.07068	(2.876)
8	0.04348	(5.37)	0.006079	(6.405)	0.007482	(4.421)

Figure 104 : System with 8 mounts, 495 Hz, minimization of components associated with n=1

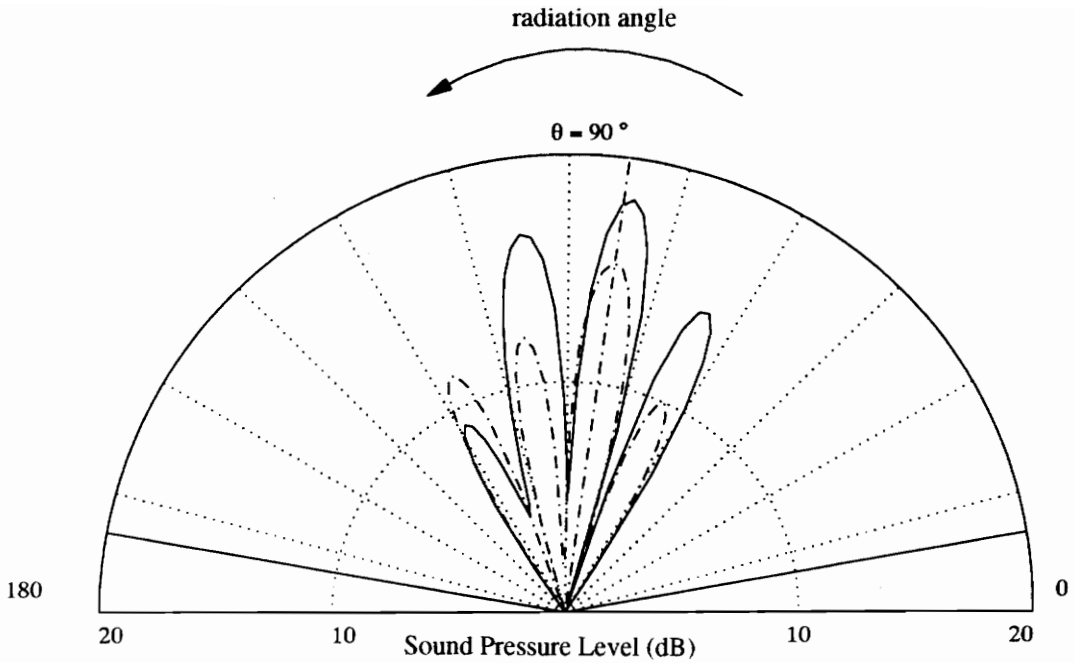

Frequency:
495
Effort:
0.12

#	F. control:		F. mounts (n):		F. mounts (c):	
1	0.03891	(3.273)	0.1019	(2.9)	0.1033	(2.661)
2	0.04474	(-0.9484)	0.02575	(2.456)	0.02549	(1.978)
3	0.04166	(0.9251)	0.06979	(2.964)	0.07098	(2.734)
4	0.04517	(-0.3028)	0.006079	(6.405)	0.006943	(13.55)
5	0.04273	(5.319)	0.09081	(2.893)	0.09071	(2.584)
6	0.03894	(-0.8969)	0.03681	(2.594)	0.03795	(2.314)
7	0.04166	(0.9251)	0.06979	(2.964)	0.07098	(2.734)
8	0.04517	(-0.3028)	0.006079	(6.405)	0.006943	(13.55)

Figure 105 : System with 8 mounts, 495 Hz, minimization of components associated with n=6

Tables

Table 1: Specifications of the rigid plate

L_x	2 m
L_y	1.1 m
h_p	0.002 m
E_p	19.2e10 N/m^2
ν_p	0.3
η_p	1.5 %
ρ_p	7800 kg/m^3

Table 2 : Specifications of the elastic cylinder

r_c	0.7 m
h_c / r_c	0.05
L_c	1 m
E_c	19.2e10 N/m^2
ν_c	0.3
η_c	1.5 %
ρ_c	7 800 kg/m^3

L_c is the half-length of the cylinder. The cylinder has a large radius compared to its length.

The thickness of the shell is defined by the ratio h_c / r_c and the value 0.05 sets the limits of application of the thin shell theory.

Note: the damping of the structure is included in Young's modulus $\overline{E}_c = E_c(1+j\eta_c)$, where η_c is the structural damping in the cylindrical shell.

Table 3: Natural frequencies (Hz) of the cylinder

		$n=0$			$n=1$	
m	$\Omega_{mn}^{(1)}$	$\Omega_{mn}^{(2)}$	$\Omega_{mn}^{(3)}$	$\Omega_{mn}^{(1)}$	$\Omega_{mn}^{(2)}$	$\Omega_{mn}^{(3)}$
1	384.6	609.1	1204	179.9	906.3	1733
2	769.3	1030	1424	467.7	1235	1956
3	1103	1154	1997	708.6	1514	2373
4	1119	1539	2630	870.6	1793	2907
5	1128	1923	3273	968.5	2107	3492
6	1138	2308	3919	1031	2449	4100

		$n=2$			$n=3$	
m	$\Omega_{mn}^{(1)}$	$\Omega_{mn}^{(2)}$	$\Omega_{mn}^{(3)}$	$\Omega_{mn}^{(1)}$	$\Omega_{mn}^{(2)}$	$\Omega_{mn}^{(3)}$
1	87.09	1484	2704	139.2	2146	3789
2	241.5	1686	2888	196.3	2276	3934
3	422.6	1932	3192	303.9	2462	4172
4	587	2195	3597	431.2	2683	4493
5	722.5	2475	4075	558.2	2930	4882
6	831.2	2775	4601	676.9	3198	5325

Table 3: Natural frequencies (Hz) of the cylinder

	$n=4$			$n=5$		
m	$\Omega_{mn}^{(1)}$	$\Omega_{mn}^{(2)}$	$\Omega_{mn}^{(3)}$	$\Omega_{mn}^{(1)}$	$\Omega_{mn}^{(2)}$	$\Omega_{mn}^{(3)}$
1	254.3	2831	4916	407	3522	6063
2	279.8	2923	5034	425.3	3593	6162
3	334.9	3065	5227	461	3706	6324
4	417.2	3246	5490	516.3	3855	6545
5	516.3	3457	5814	589.8	4035	6821
6	622.9	3692	6191	677.3	4240	7146

	$n=6$		
m	$\Omega_{mn}^{(1)}$	$\Omega_{mn}^{(2)}$	$\Omega_{mn}^{(3)}$
1	594.5	4217	7222
2	610.9	4275	7306
3	640.4	4368	7445
4	684.5	4493	7635
5	743.8	4647	7874
6	817.2	4827	8158

Note : $\Omega_{mn}^{(1)}$, $\Omega_{mn}^{(2)}$ and $\Omega_{mn}^{(3)}$ are the three resonance frequencies for each mode (m,n)

Table 4 : Sorted natural frequencies (Hz) of the cylinder

Frequency	m	n	Frequency	m	n
87	1	2	587	4	2
139	1	3	590	5	5
180	1	1	594	1	6
196	2	3	609	1	0
242	2	2	611	2	6
254	1	4	623	6	4
280	2	4	640	3	6
304	3	3	677	6	3
335	3	4	677	6	5
385	1	0	685	4	6
407	1	5	709	3	1
417	4	4	723	5	2
423	3	2	732	7	4
425	2	5	744	5	6
431	4	3	769	2	0
461	3	5	775	7	5
468	2	1	786	7	3
516	5	4	816	1	7
516	4	5	817	6	6
558	5	3	831	6	2

Table 4 : Sorted natural frequencies (Hz) of the cylinder

Frequency	m	n	Frequency	m	n
832	2	7	950	9	4
841	8	4	952	5	7
859	3	7	968	5	1
871	4	1	985	9	3
880	8	5	990	9	5
888	8	3	998	8	2
899	4	7	1000	8	6
903	7	6	1017	6	7
906	1	1	1030	2	0
920	7	2	1031	6	1

Table 5 : Coordinates of the points of attachment of the 8 active-passive mounts on the cylinder

ϕ	z1	z2	z3	z4
$2\pi/3$	$-0.9\times L_c$	$-0.4\times L_c$	$0.4\times L_c$	$0.9\times L_c$
$-2\pi/3$	$-0.9 * L$	$-0.4\times L_c$	$0.4\times L_c$	$0.9 * L$

Table 6 : Coordinates of the points of attachment of the 8 active-passive mounts on the plate

y	x1	x2	x3	x4
$-0.45\times w_p$	$-0.9\times L_p$	$-0.4\times L_p$	$0.4\times L_p$	$0.9\times L_p$
$0.45\times w_p$	$-0.9 * L$	$-0.4\times L_p$	$0.4\times L_p$	$0.9 * L$

Table 7 : Specifications of the passive mounts

K_a	10^6 N/m
C_a	10^2 N.s

Except where notified, the system has 8 active-passive mounts attached to the plate and to the cylinder as described in Tables 5 and 6:

Table 8: Configurations of the 6-mount system

Configuration A:

ϕ	z_1	z_2	z_3
$2\pi/3$	$-0.9\times L_c$	0	$0.9\times L_c$
$-2\pi/3$	$-0.9\times L_c$	0	$0.9\times L_c$

Configuration B:

ϕ	z_1	z_2	z_3
$2\pi/3$	$-L_c/3$	0	$L_c/3$
$-2\pi/3$	$-L_c/3$	0	$L_c/3$

Configuration C:

ϕ	z_1	z_2	z_3
$2\pi/3$	$-L_c/4$	0	$L_c/4$
$-2\pi/3$	$-L_c/4$	0	$L_c/4$

were ϕ is the circumferential coordinate and z_1, z_2 and z_3 the longitudinal coordinates of the points of attachment of the active-passive mounts on the cylinder.

Table 9: Cut-off frequencies of the circumferential modes

n	f_c (Hz)
2	45.2
3	130.0
4	245.0
5	390.0
6	561.5

These frequencies are the cut-off frequencies of the circumferential modes in the case of an infinite cylinder. They give a rough estimation of whether the circumferential mode is propagating or not in the finite-length structure. The modes $n = 0$ and $n = 1$ propagate for all frequencies.

References

[1] J. PAN, C.H. HANSEN, "Power transmission from a vibrating source through an intermediate flexible panel to a flexible cylinder", ASME Journal of Vibration and Acoustics,

[2] G.E. WARNAKA, "Active Attenuation of Noise - The State of the Art", Noise Control Engineering, **18**(3), 100-100, 1982

[3] G.E. WARNAKA, "Applications for Active Noise Control", Proceedings of Noise-Con, 399-404, 1987

[4] J.E. FFOWCS-WILLIAMS, "Anti-Sound", Proceedings of the Royal Society of London A395, 63-68, 1984

[5] B. CHAPLIN, "Anti-Noise - The Essex Breakthrough", Chartered Mechanical Engineering, 41-47, 1983

[6] P. LUEG, "Process of Silencing Sound Oscillations", U.S. Patent No. 2043416, 1936

[7] H.L. OLSON and E.G. MAY, "Electronic Sound Absorber", Journal of the Acoustical Society of America, **25**(6), 1130-1136, 1953

[8] W. B. CONOVER, "Recent Contributions to Transformer Audible Noise Control", AIEE Transactions, Applications and Industry, **74**(D), 77-86, 1955

[9] W. B. CONOVER, "Fighting Noise with Noise", Noise Control, 2(1), 78-82, 1956

[10] S. ONADA and K. KIDO, "Automatic Control of Stationnary Noise by Means of Directivity Synthesis", 6th International Congress on Acoustics, Tokyo, Japan, 1986

[11] M. JESSEL and G.A. MANGIANTE, "Active Absorbers in an Air Duct", Journal of Sound and Vibration, **27**(3), 411-436, 1973

[12] S.J. ELLIOTT and P.A. NELSON, "The active Control of Sound", Electronic and Communication Engineering Journal, august 1990

[13] S.J. ELLIOTT, P.A. NELSON, I.M. STOTHERS and C.C. BOUCHER, "In Flight Experiments on Active Control of Propeller-Induced Cabin Noises", Journal of Sound and Vibration, **140**, 219-238, 1990

[14] C.R. FULLER and J.D. JONES, "Experiments of Reduction of Propeller Induced Interior Noise by Active Control of Cylinder Vibration", Journal of Sound and Vibration, **112**(2), 389-395, 1987

[15] J.D. JONES and C.R. FULLER, "Active Control of Sound Fields in Elastic Cylinders by Vibrational Inputs", Proceedings of Noise-Con, 413-418, 1987

[16] J.D. JONES and C.R. FULLER, "Active Control of Sound Fields in Elastic Cylinders by Multicontrol Forces", AIAA Journal, **27**(6), 845-852, 1989

[17] C.R. FULLER, "Active Control of Sound Transmission/Radiation from Elastic Plates by Vibration Inputs : I. Analysis", Journal of Sound and Vibration, **136**(1), 1-15, 1990

[18] C. GUIGOU and C.R. FULLER,"Active Control of Sound Radiation from a Simply Supported Beam", Journal of the Acoustical Society of America, **93**(5), 2716-2725, 1993

[19] J. PAN, S.D. SNYDER, C.H. HANSEN and C.R. FULLER, "Active Control of Far-field Sound Radiated by a Rectangular Panel - a General Analysis", Journal of the Acoustical Society of America, **91**(4), 2056-2066, 1992

[20] C. R. FULLER, R. A. BURDISSO, "A Wavenumber Domain Approach to the Active Control of Structure-borne Sound", Journal of Sound and Vibration, **148**(2), 355-360, (1991)

[21] R.L. CLARK and C.R. FULLER, "Active Structural Acoustic Control with Adaptive Structures Including Wavenumber Considerations", Journal of Intelligent Material Systems and Structures, **3**(2), 296-315, 1992

[22] R.L. CLARK and C.R. FULLER, "Control of Sound Radiation with Adaptive Structures", First U.S. Japan Conference on Adaptive Structures, Maui, Hawai, Technomic Press, Eds B.K. Wada, J.L. Fanson and K. Miura, 227-245, 1990

[23] R.L. CLARK and C.R. FULLER, "Experiments on Active Control of Structurally Radiated Sound Using Multiple Piezoceramic Actuators", Journal of the Acoustical Society of America, **91**(6), 3313-3320, 1992

[24] S. LEFEBVRE, "Active Control of Interior noise using Piezoelectric Actuators in a Large-Scale Composite Fuselage Model", M.S. Thesis, Virginia Polytechnic and State University, Blacksburg, Va, 1991

[25] A.W. LEISSA, "Vibration of Shells", NASA SP-288, 1973

[26] S.B. ABLER and R.J. SILCOX, "Experimental Evaluation of Active Noise Control in a Thin-walled Cylinder", Proceedings of Noise-Con, 341-346, 1987

[27] A.J. BULLMORE, P.A. NELSON and S.J. ELLIOTT, "Active Minimization of Acoustic Potential Energy in Harmonically Excited Cylindrical Enclosed Sound Fields", AIAA-86, 1958- , 1986

[28] R.L. CLARK and C.R. FULLER, "Active Control of Structurally Radiated Sound from an Enclosed Finite Cylinder", 2nd Conference on Recent Advances in Active Control of Sound and Vibration, Blacksburg, VA, 380-402, 1993

[29] H. SUMALI, "Demonstration of Active Structural Acoustic Control of Cylinder", M.S. Thesis, Virginia Polytechnic and State University, Blacksburg, Va, 1992

[30] H.L. LESTER and C.R. FULLER, "Active Control of Propeller Induced Noise Fields Inside a Flexible Cylinder", AIAA paper No 86-1857, 1986

[31] R.J. SILCOX, H.C. LESTER and S.B. ABLER, "Evalutation of Active Noise Control in a cylindrical shell", J Vib Acoust Stress REliab Des, **111**(3), 337-342, 1989

[32] C.R. FULLER, "Structural Influence of the Cabin Floor on Sound Transmission into an Aircraft - Analytical Investigations", AIAA, **24**(10), oct 1987

[33] J.D. JONES and C.R. FULLER, "Influence of a Floor on Sound Transmission into an Aircraft Fuselage Model", Journal of Aircraft, **25**(10), 882-889, 1988

[34] A.H. VON FLOTOW, "An Expository Review of Active Control of Machinery Mounts", Proceedings of the 27th Conference on Decision and Control, Austin, Texas, 2029-2032, 1988

[35] P. A. NELSON, M. D. JENKINS, S. J. ELLIOT, "Active Isolation of Periodic Vibrations", NOISE-CON 87, June 8-10, Pennsylvania State University State College, Pennsylvania.

[36] A. LEFEBVRE, C. GUIGOU and C.R. FULLER, "Experiments on Active Isolation Using Distributed PVDF Error Sensors", Journal of Sound and Vibration, **155**(1), 177-184, 1992

[37] C. GUIGOU, C.R. FULLER and P.R. WAGSTAFF, "Active Isolation of Vibration with Adaptive Structures", submitted to the Journal of the Acoustical Society of America, 1992

[38] J. PAN, C.H. HANSEN, "Total Power Flow from a vibrating rigid body to a thin panel through two active Isolators", Journal of the Acoustical Society of America, **92**, 895-907 (1992)

[39] J. PAN, C.H. HANSEN, "Active Control of Power Flow from a vibrating rigid body to a flexible panel through two active Isolators", Journal of the Acoustical Society of America, **93**(4), Pt.1, 1947-1953 (April 1993)

[40] L. MEIROVITCH, "Elements of Vibration Analysis", New-York, Mc Graw-Hill, 2d edition, 1986

[41] L. MEIROVITCH, "Analytical Methods in Vibrations", Macmillan, 1962

[42] M. C. JUNGER, D. FEIT, "Sound Structures and Their Interaction", Boston: MIT Press, 1986

[43] LAMB, "Hydrodynamics", 1945

[44] E.T. COPSON, "Asymptotic Expansions", Cambridge, 1965

[45] S. J. ELLIOTT, I. M. STOTHERS and P. A. NELSON, "A multiple error LMS algorithm and its application to the active control of sound and vibration", IEEE Transaction on Acoustic Speach and Signal Processing, **ASSP -35** (10), 1423-1434, 1987

[46] S. J. ELLIOTT, C. C. BOUCHER and P. A. NELSON, "The behavior of a multiple channel active control system", IEEE Transactions on Signal Processing, **40** (5), 10411052, (1992)

[47] "PC-Matlab User's Guide", The MathWorks Inc., 1989

[48] F. FAHY, "Sound and Structural Vibration : Radiation, Transmission and Response", Orlando, Academic Press, 308p, 1985

[49] S. LORD RAYLEIGH, "The theory of Sound", New-York, Dover, 2d edition, 1945

[50] L. CREMER, M. HEKLAND and E.E. UNGARD, "Structure Borne Sound", Berlin, Springer-Verlag, 1974

[51] P.M.MORSE, "Vibration and Sound", York, Mc Graw-Hill, 2d edition, 1948

[52] P.M.MORSE and K.U. INGARD, "Theoretical Acoustics", Princeton University Press, 1948

[53] A.E.H. LOVE, "The Mathematical Theory of Elasticity", New-York, Dover publications, 643p, 1944

[54] S. TIMOSHENKO, "Vibrations problems in Engineering", New-York, D. Van Nostrand Company Inc., 3rd edition, 468p, 1955

Appendix 1

Orthogonality conditions of cylinder modes

The two integrations (with respect to z and ϕ) can be performed separately since they are totally independent.

First, for the integration with respect to ϕ:

$$\int_{-\pi}^{\pi} \cos(n\phi)\cos(q\phi)d\phi = 0 \text{ if } n \neq p$$

$$= \int_{-\pi}^{\pi} \cos^2(n\phi)d\phi = \int_{-\pi}^{\pi} \frac{\cos(2n\phi)+1}{2}d\phi = \pi \text{ if } (n = p) \neq 0 \quad (100)$$

$$= 2\pi \text{ if } n = p = 0$$

which can be written in the following form:

$$\frac{\varepsilon_n}{2\pi}\int_{-\pi}^{\pi} \cos(n\phi)\cos(q\phi)d\phi = \delta_{nq} \text{ with } \varepsilon_0 = 1 \text{ and } \varepsilon_{n\neq 0} = 2 \quad (101)$$

The same kind of derivation shows that:

$$\frac{1}{\pi}\int_{-\pi}^{\pi} \sin(n\phi)\sin(q\phi)d\phi = \delta_{nq} \quad (102)$$

Now, for the integration with respect to z:

$$\int_{-L_c}^{L_c} \cos\left[k_m(z+L_c)\right]\cos\left[k_p(z+L_c)\right]dz = 0 \text{ if } m \neq p$$

$$= \int_{-L_c}^{L_c} \cos^2\left[k_m(z+L_c)\right]dz = \frac{1}{2}\int_{-L_c}^{L_c} 1+\cos\left(\frac{m\pi}{2L_c}(z+L_c)\right)dz$$

$$= \frac{1}{2}\left[z+\frac{2L_c}{m\pi}\sin\left(\frac{m\pi}{2L_c}(z+L_c)\right)\right]_{-L_c}^{L_c} = L_c \text{ if } m = p \tag{103}$$

Similarly,

$$\int_{-L_c}^{L_c} \sin\left[k_m(z+L_c)\right]\sin\left[k_p(z+L_c)\right]dz = L_c \tag{104}$$

Finally, the result of the double integral is:

$$\begin{cases} \dfrac{\varepsilon_n}{2\pi}\dfrac{1}{L_c}\displaystyle\int_{-\pi}^{\pi}\int_{-L_c}^{L_c} \cos(n\phi)\cos\left[k_m(z+L_c)\right]\cos(q\phi)\cos\left[k_p(z+L_c)\right]d\phi dz = \delta_{nq}\delta_{mp} \\ \dfrac{\varepsilon_n}{\pi}\dfrac{1}{L_c}\displaystyle\int_{-\pi}^{\pi}\int_{-L_c}^{L_c} \sin(n\phi)\sin\left[k_m(z+L_c)\right]\sin(q\phi)\sin\left[k_p(z+L_c)\right]d\phi dz = \delta_{nq}\delta_{mp} \\ \dfrac{\varepsilon_n}{2\pi}\dfrac{1}{L_c}\displaystyle\int_{-\pi}^{\pi}\int_{-L_c}^{L_c} \cos(n\phi)\sin\left[k_m(z+L_c)\right]\cos(q\phi)\sin\left[k_p(z+L_c)\right]d\phi dz = \delta_{nq}\delta_{mp} \end{cases} \tag{105}$$

Appendix 2

Hankel function derivative and large-argument asymptotic value

The large-argument asymptotic value gives:

$$H_n^{(1)}(x) = \left(\frac{2}{\pi x}\right)^{\frac{1}{2}} (-j)^n e^{\left(jx - j\frac{\pi}{4}\right)} \quad \text{for } x >> n^2 + 1 \tag{106}$$

therefore

$$H_n^{(1)}\left[\left(k_0{}^2 - \gamma^2\right)^{\frac{1}{2}} r\right] = \left(\frac{2}{\left(k_0{}^2 - \gamma^2\right)^{\frac{1}{2}} r}\right)^{\frac{1}{2}} (-j)^n e^{-j\frac{\pi}{4}} e^{j\left(k_0{}^2 - \gamma^2\right)^{\frac{1}{2}} r} \tag{107}$$

The derivative of Hankel function is evaluated as follow:

For $n \neq 0$,

$$\begin{aligned} H_n^{(1)}(x) &= J_n(x) + jY_n(x) \\ H_n^{(1)'}(x) &= J_n'(x) + jY_n'(x) \\ &= \frac{1}{2}\left[J_{n-1}(x) - J_{n+1}(x)\right] + j\frac{1}{2}\left[Y_{n-1}(x) - Y_{n+1}(x)\right] \\ &= \frac{1}{2}\left[J_{n-1}(x) + jY_{n-1}(x)\right] - \frac{1}{2}\left[J_{n+1}(x) + jY_{n+1}(x)\right] \\ &= \frac{1}{2}\left[H_{n-1}^{(1)}(x) - H_{n+1}^{(1)}(x)\right] \end{aligned} \tag{108}$$

where $J_n(x)$ and $Y_n(x)$ are Bessel's function of first and second kind respectively.

For $n = 0$,

$$H_0^{(1)}(x) = \frac{1}{2}\left[H_{-1}^{(1)}(x) - H_1^{(1)}(x)\right] = \frac{1}{2}\left[-H_1^{(1)}(x) - H_1^{(1)}(x)\right] = -H_1^{(1)}(x) \qquad (109)$$

Appendix 3

Stationary phase approximation

Starting from the expression of the pressure in spherical coordinates,

$$p(R,\theta,\phi)=\frac{\rho\omega^2}{\left(2\pi^3 R\sin\theta\right)^{\frac{1}{2}}}\sum_{m=0}^{\infty}\sum_{n=0}^{\infty}\psi_{mn}(\phi)(-j)^n e^{j\frac{\pi}{4}}\int_{-\infty}^{\infty}\frac{e^{j\gamma R\cos\theta}e^{i\left(k_0{}^2-\gamma^2\right)^{\frac{1}{2}}R\sin\theta}\tilde{\xi}_m(\gamma)}{\left(k_0{}^2-\gamma^2\right)^{\frac{3}{4}}H_n^{(1)'}\left[\left(k_0{}^2-\gamma^2\right)^{\frac{1}{2}}r_c\right]}d\gamma \quad (110)$$

Separating the modulus and the phase, the pressure integral can be written

$$I=\int_{-\infty}^{\infty}\Phi(\gamma)e^{\Psi(\gamma)}d\gamma \quad (111)$$

$$\Phi(\gamma)=\frac{\tilde{\xi}_m(\gamma)}{\left(k_0{}^2-\gamma^2\right)^{\frac{3}{4}}H_n^{(1)'}\left[\left(k_0{}^2-\gamma^2\right)^{\frac{1}{2}}r_c\right]} \quad (112)$$

$$\Psi(\gamma)=R\left[\left(k_0{}^2-\gamma^2\right)^{\frac{1}{2}}\sin\theta+\gamma\cos\theta\right] \quad (113)$$

The derivative of the phase is

$$\frac{d}{d\gamma}\Psi(\gamma) = R\left[\frac{-\gamma\sin\theta}{\left(k_0{}^2-\gamma^2\right)^{\frac{1}{2}}}+\cos\theta\right] \qquad (114)$$
$$= 0 \quad \text{for} \quad \gamma = \bar{\gamma} = k_0\cos\theta$$

The second derivative is

$$\frac{d^2}{d\gamma^2}\Psi(\gamma) = -R\sin\theta\left[\frac{1}{\left(k_0{}^2-\gamma^2\right)^{\frac{1}{2}}}+\frac{\gamma^2}{\left(k_0{}^2-\gamma^2\right)^{\frac{3}{2}}}\right] \qquad (115)$$

$$\frac{d^2}{d\gamma^2}\Psi(k_0\cos\theta) = -R\sin\theta\left[\frac{1}{k_0\sin\theta}+\frac{k_0{}^2\cos^2\theta}{k_0{}^3\sin^3\theta}\right] = -R\left[\frac{1}{k_0}+\frac{\cos^2\theta}{k_0\sin^2\theta}\right] = -\frac{R}{k_0\sin^2\theta} \qquad (116)$$

$$\Phi(k_0\cos\theta) = \frac{\tilde{\xi}_m(k_0\cos\theta)}{(k_0\sin\theta)^{\frac{3}{4}}H_n^{(1)'}[k_0\sin\theta r_c]} \qquad (117)$$

The stationary-phase approximation is:

$$I = \frac{(2\pi)^{\frac{1}{2}}\Phi(\bar{\gamma})e^{\pm j\frac{\pi}{4}+j\Psi(\bar{\gamma})}}{\left|\frac{d^2\Psi(\bar{\gamma})}{d\gamma^2}\right|^{\frac{1}{2}}} = \frac{(2\pi)^{\frac{1}{2}}\tilde{\xi}_m(k_0\cos\theta)e^{-j\frac{\pi}{4}+jRk_0}}{(k_0\sin\theta)^{\frac{3}{2}}H_n^{(1)'}[k_0\sin\theta r_c]\left[\frac{R}{k_0\sin^2\theta}\right]^{\frac{1}{2}}} \qquad (118)$$
$$= \frac{(2\pi)^{\frac{1}{2}}\tilde{\xi}_m(k_0\cos\theta)e^{j\left(k_0R-\frac{\pi}{4}\right)}}{k_0(\sin\theta)^{\frac{1}{2}}H_n^{(1)'}[k_0\sin\theta r_c]R^{\frac{1}{2}}}$$

since the second derivative of the phase is negative, $-\pi/4$ is to be used in the approximation formula above.

Finally,

$$p(R,\theta,\phi)=\frac{\rho\omega^2}{\pi Rk\sin\theta}\sum_{m=0}^{\infty}\sum_{n=0}^{\infty}\psi_{mn}(\phi)(-j)^n\frac{\tilde{\xi}_m(k\cos\theta)e^{j\left(kR-\frac{\pi}{2}\right)}}{H_n^{(1)'}\left[kr_c\sin\theta\right]} \tag{119}$$

Vita

Eric was born on July 9th, 1970 in Laon, France. He grew up in Marle with his two brothers and his two sisters. At this time, all he knew about the United States was the far-west and John Wayne riding his horse, and he never thought he would once come to "l'Amérique". He entered the University of Technology of Compiegne in 1988 where he started a degree in Mechanical Engineering. In 1990, he went to Glasgow, in Scotland, for 5 months as an exchange student. There he learnt "a wee bit" of English : enough to read a book on advanced vibrations, but at the end of his stay, he still had trouble with the Scottish accent when getting a beer in a pub. Back in France, his British friends made fun of his Scottish accent. In 1992, he landed in the United States, his briefcase full of French cheese, to attend school at Virginia Tech. He was taken to the mountains of Virginia by a Greyhound bus. Had the driver spoken Japanese, it would have been the same ; later on, he learned it was called the Southern accent. When the bus dropped his travel companions and him in a desolated tractor shop (the Greyhound bus station), they thought of going back. But Blacksburg turned out to be better than it had seemed first. Then, Eric first met his advisor. Having trouble with the Australian accent, he naively thought he could rely on his notes, but unfortunately his advisor's handwriting didn't make more sense either. After completing his Master of Science, he now understands the "Aussie" language as well as "l'Américain", but still, he has no idea of what the car mechanics says when he goes to the shop. Eric is now headed to Israel to do his military service as a research assistant at the University of the Negev. He was told that everybody speaks English in Israel, but from what he learned, he thinks he will be better off learning Hebrew.